Biopacemaking: New Targets and New Mechanisms

A thesis submitted to The University of Manchester for the degree of Doctor of Philosophy in the Faculty of Medical and Human Sciences

2016

Dr Moinuddin Choudhury

School of Medicine

Table of contents

Word count 46,637

List of tables

List of figures

List of abbreviations

Ad	Adenovirus
AAV	Adeno-associated virus
Ad5	Human adenovirus serotype 5
AF	Atrial fibrillation
ANOVA	Analysis of variance
AP	Action potential
AV	Atrioventricular
AVN	Atrioventricular node
bp	Base pairs
bpm	Beats per minute
cAMP	Adenosine 3’,5’-cyclic monophosphate
CAR	Coxsackie/adenovirus receptor
Cav	Caveolin
CICR	Calcium induced calcium release
CCS	Cardiac conduction system
CPE	Cytopathological effect
cRT	Corrected recovery time
CT	Crista terminalis
Ct	Threshold cycle
Cx	Connexin
DD	Diastolic depolarization
DMEM	Dulbecco’s modified Eagle’s medium
DMSO	Dimethyl sulfoxide
ECG	Electrocardiogram
EDTA	Ethylenediaminetetraacetic acid
FBS	Foetal bovine solution
FO	Fossa ovalis
GFP	Green fluorescent protein
HCN	Hyperpolarization-activated cyclic nucleotide-gated
hMSCs	Human mesenchymal stem cells

iPSCs	Induced pluripotent stem cells
IU	Infectious units
IVC	Inferior vena cava
Kb	Kilobases
LCR	Local Ca^{2+} release
LV	Left ventricle
MDP	Maximum diastolic potential
MEM	Minimum essential medium
MOI	Multiplicity of infection
mRNA	Messenger ribonucleic acid
NCX	Sodium calcium exchanger
OCT	Optimum cutting temperature
PBS	Phosphate buffered saline
pfu	Plaque forming units
RA	Right atrium
RAA	Right atrial appendage
RAd	Recombinant adenovirus
RT-qPCR	Real time quantitative polymerase chain reaction
RYR	Ryanodine receptor
SAN	Sinoatrial node
SAP	Subsidiary atrial pacemaker
SERCA	Sarco/endoplasmic reticulum Ca^{2+}-ATPase
SND	Sinus node dysfunction
SOCC	Store operated calcium channel
SR	Sarcoplasmic reticulum
SV	Sinus venosus
SVC	Superior vena cava
Tbx	Tbox transcription factor
TV	Tricuspid valve

Abstract

Dr Moinuddin Choudhury
Submission for the degree of Doctor of Philosophy, The University of Manchester

Biopacemaking: New Targets and New Mechanisms
June 2016

BACKGROUND: Biopacemaking is the attempt to replicate sinoatrial node (SAN)-like pacemaker activity in other areas of the heart by manipulating genes involved in pacemaking. Application of this could emulate the electronic pacemaker without the need for implantation of permanent hardware, or directly repair dysfunctional SAN tissue in human disease. We upregulated the transcription factors Tbx18, Tbx3 and the membrane ion exchanger NCX1 in bradycardic subsidiary atrial pacemaker (SAP) tissue which we used as a model of SAN dysfunction. We aimed to show that one or more of these gene targets could improve pacemaker function and alter the molecular character of SAP tissue and thus could potentially be used for the repair of dysfunctional SAN tissue.

METHODS: SAP tissue was isolated from the right atria of rats and kept beating in culture at 37°C for 48 hours. Recombinant adenoviruses were injected into SAP preparations to upregulate Tbx18, Tbx3 and NCX1 individually. Beating rate, overdrive suppression and pharmacological response to I_f blockade and β-adrenergic stimulation were measured along with molecular changes in pacemaker and atrial genes and proteins using RT-qPCR and immunohistochemistry.

RESULTS: Tbx18 upregulation significantly increased SAP beating rate after 48 hours of culture (a final rate of 141 ± 9 bpm in uninfected SAP tissue versus 215 ± 16 bpm in Ad-Tbx18 infected SAP tissue, $p<0.01$). It induced upregulation of HCN2 ($p<0.01$) and RYR2 ($p<0.05$), downregulation of HCN4 ($p<0.05$) and no change HCN1, Tbx3, $K_v1.5$, $K_{ir}2.1$, $Na_v1.5$, NCX1, Cx43, Cx45, $Ca_v1.2$ or $Ca_v3.1$. There was also no change in overdrive suppression and no change in response to pharmacology. No increase in beating rate was seen with either Tbx3 or NCX1 upregulation. Tbx3 preparations induced downregulation of the atrial genes $K_{ir}2.1$ ($p<0.01$) and $Na_v1.5$ ($p<0.05$), along with HCN1 ($p<0.05$), HCN4 ($p<0.01$), Tbx18 ($p<0.05$) and NCX1 ($p<0.01$), upregulated Cx43 ($p<0.05$) and showed no change in Cx45, RYR2, $K_v1.5$. NCX1 preparations demonstrated reduced overdrive suppression ($p<0.05$).

CONCLUSION: Tbx18 showed the most potential for biopacemaking in SAP tissue, however both Tbx3 and NCX1 could be applied as secondary targets to fine tune biopacemaker function. Future work would focus on applying these targets to dysfunctional SAN tissue in larger animals.

Declaration

No portion of the work referred to in the thesis has been submitted in support of an application for another degree or qualification of this or any other university or institute of learning.

Copyright statement

Acknowledgements

The last few years working on this project have been some of the best years of my career to date. Up until now, like all other medical doctors, I've been attempting to climb the career ladder, gaining experience and sitting exams. There are rewards that come from interacting with patients and colleagues, there is satisfaction in learning your craft and clinical decisions can be based upon pre-determined guidelines which provide reassurance.

The world of research was a culture shock. Suddenly there were no guidelines and now creativity was encouraged. There was a goal in the form of a hypothesis or a concept, but no well-trodden path towards it. We became explorers and not just on the annual lab hike through the peak district! Our scientific journey would require determination in the face of recurrent failure, imagination to solve new problems and patience to work diligently.

These are all qualities that I saw within my supervisors Mark Boyett, Gwilym Morris, Halina Dobrzynski and Paul Kingston. Especially I came to greatly respect Mark's vast knowledge and humility, Gwilym's intellect and ambition, Halina's passion for knowledge and infectious enthusiasm and Paul's skill for bringing about new forms of viral life and his eye for fine detail. I need to also thank everyone in the lab who taught me their skills: Joseph Yanni, Xue Cai, Andrew Atkinson, Sunil Logantha, Alicia D'Souza, Salik Kakar, Louise Miller, Heiko Schneider, Zoltan Borbas and Ian Temple. Not forgetting my wife and family who have been incredibly supportive, allowing me to work late into many evenings.

Now I go back to clinical work to follow guidelines once again. I will miss the academic life mainly because of the people I met but also the unique atmosphere I experienced heavy with the sense of new ideas being created and new knowledge being discovered. I look forward to the time when I might discover it again another time.

The author

Qualifications

2012 MRCP(UK)

2006 MBChB

2003 BSc(Hons) 2.1 – Neurosciences (Intercalated Degree)

Prizes, awards and distinctions

2015 Young Investigator Award Runner-Up – British Cardiovascular Society

2012 BHF clinical research fellowship grant

2005 MBChB module distinction – "Primary Care, Public Health and Psychiatry"

2004 1st class final BSc dissertation – "Deep Brain Stimulation in Parkinson's Disease"

2003 MBChB module distinction – "The Ethics of Cloning"

Publications

- **Choudhury M**, et al. Biology of the sinus node and its disease. Arrhythmia & Electrophysiology Review. 2015;4(1):28–34
- Morris GM, **Choudhury M**, et al. Characterization of a right atrial subsidiary pacemaker and acceleration of the pacing rate by HCN over-expression. Cardiovasc Res. 2013;100(1):160-9

Abstracts/Posters

- **Choudhury M**, et al. Tbx18 Overexpression Improves Function and Alters Gene Expression in Bradycardic Subsidiary Right Atrial Pacemaker Tissue. Europace, 2015; 17: iii205 [European Heart Rhythm Association "Cardiostim" Poster]
- **Choudhury M**, et al. Functional and molecular comparison of subsidiary right atrial pacemaker tissue to the sinoatrial node. Circulation, 2013; 128: A13052 [American Heart Association Poster]

Oral presentations

- **Choudhury M**, et al. YIA1 TBX18 Biopacemaking Improves Beating Rate and Alters Gene Expression in Bradycardic Subsidiary Right Atrial Pacemaker Tissue. Heart, 2015;101:Suppl 4 A121-A123

1. INTRODUCTION

The sinoatrial node (SAN) is the natural pacemaker of the heart and has been studied in detail for over 100 years. In the second century the Greek philosopher and physiologist Claudius Galen observed the heart to continue beating independently when excised from the body.[1] It was not until the nineteenth century that the British physiologist Walter Gaskell demonstrated the myogenic origin of the heartbeat, tracing its contractile sequence to the 'sinus venosus' (SV) in the superior right atrium (RA).[1, 2] In 1906, from a rented cottage in Kent turned laboratory, the Scottish anthropologist Sir Arthur Keith and his medical student Martin Flack microscopically identified remnants of "primitive fibres" within the SV with similar features to atrioventricular (AV) conduction tissue described earlier that year by Sunao Tawara.[3, 4] Keith concluded that the primitive structure in the sinus venosus must be the origin of the cardiac impulse and was subsequently credited for having discovered the SAN.[4] Since then, the SAN's histology, molecular features and electrophysiology have been extensively examined and today we continue to add detail to our understanding of the mechanisms involved in SAN automaticity and function.

SAN dysfunction (SND) is seen in human disease causing it to beat too slowly or miss beats. SND is also known as sick sinus syndrome, prevalent in 0.03% of the UK population. SND can lead to dizziness, loss of consciousness and collapse.[5] Currently this condition is treated by implanting an electronic pacemaker under the skin and feeding wires into the heart. The prospect is often slightly daunting initially for the patient. However since their invention over 50 years ago, these devices have improved in their reliability, safety, cost and size. They are the only effective treatment for SND to date the latest data suggesting around 40,000 new pacemakers being fitted in the UK per year, about 20% of which were for SND.[6]

Nonetheless, electronic pacemakers still harbour several inherent drawbacks. These include the need for indwelling hardware, the need to periodically replace generators via further invasive procedures, strong magnetic fields must be avoided, they are unresponsive to the autonomic nervous system and thus have a limited response to

demands from exercise and emotion, and there is a small risk during implantation of causing significant bleeding, serious infection or puncturing the lung. Infection can necessitate the need for system extraction which can be complex and dangerous once embedded over time. Furthermore, non-physiological pacing via the right ventricular apex long-term has been associated with ventricular dyssynchrony and cardiomyopathy.[7]

In the last 15 years, the concept of 'biopacemaking' has arisen. Through advances in our knowledge of the molecular biology of the SAN and developments in gene therapy, we can now employ techniques such as the injection of engineered viruses into cardiac muscle to transduce pacemaker genes and create ectopic SAN-like pacemaker tissue anywhere in the heart. Thus we have the potential to emulate the electronic pacemaker without the need for implantation of an external energy source or wires, whilst also being sensitive to the autonomic nervous system.[8, 9] There is also potential to repair dysfunctional pacemaker tissue by reverse engineering molecular abnormalities that occur in SND. However, biopacemaker research is still in its infancy and there are many challenges remaining including the search for the right gene targets, the best location for a biopacemaker and safe methods of delivery. The ideal biopacemaker should be robust, reliable, have similar physiological functional parameters to the SAN and respond to autonomic regulation. Once these challenges have been overcome, the biopacemaker could become a viable alternative therapeutic option to the electronic pacemaker.

1.1 Embryonic development of the sinoatrial node

In mammals, the initial heart tube forms from two regions of the lateral plate mesoderm during the gastrulation stage of embryonic development.[10] A caudal pool of progenitor cells remain which continue to extend both poles of the heart tube.[11] All cells in this primary myocardium are poorly differentiated and display slow automatic sinusoidal electrical activity.[12] As the heart chambers develop, most cells differentiate and proliferate quickly into atrial and ventricular 'working myocardium'. They express high conductance gap junctions and ion channels, increased numbers of mitochondria and sarcomere components. This leads to rapid impulse propagation but loss of automaticity.[10]

Three discrete areas do not differentiate into working myocardium. These are the SV, the AV canal and the outflow tract (figure 1).[12] Instead these areas retain their primary character with slow automatic electrical activity. A dominating rhythm arises from the SV.[13] The development of a conduction pathway via fast working myocardium interrupted by these slow primary tissues will eventually give rise to a recognisable electrocardiogram (ECG) and this basic pathway is conserved in all vertebrates with multi-chambered hearts.[12] Higher vertebrate animals go on to develop a more complex SAN within the SV and atrioventricular node (AVN) within the AV canal. Different species develop these to different extents, for example larger animals have evolved more defined systems.[10]

The differential developmental lineage of the cardiac conduction system (CCS) and working myocardium is directed by specific genes. *Nkx2-5* is a homeobox gene (homeobox genes are a family of genes that direct early structural embryonic development) that drives working myocardial development. By day 10.5 of embryonic development in mice *Nkx2-5* is apparent in working myocardium, but absent from the sinus horns developing from the SV.[14] *Nkx2-5* is thought to activate working myocardial genes such as *Nppa* and the high conductance gap junctions Connexin (Cx) 40 amongst others.[14] *Nkx2-5* also represses genes specific to CCS development such as the transcription factor *Tbx3* and the pacemaker ion channel gene *Hcn4* limiting the border of the developing CCS.[14] Conversely *Tbx3* present in the developing CCS represses *Nppa* and *Cx40*, the downstream atrial genes of *Nkx2-5*, and so the CCS and working myocardium become mutually exclusive with a defined border.[14, 15]

Transgenic mice were used to investigate the interactions of *Nkx2-5* and *Tbx3.* In one study *Nkx2-5* deficient mice died at day 10, they failed to initiate chamber development, *Nppa* and *Cx40* were not activated, and there was marked ectopic expression of *Tbx3* and *Hcn4* throughout the heart tube.[14] *Tbx3* deficient mice died between day 11 and 13, but interestingly at day 11.5 a junction between *Nkx2-5/Nppa/Cx40* positive and negative myocardium still formed at the SV, along with a SAN-like structure with *Hcn4* present, suggesting that *Tbx3* is not required for initial definition but for later fine tuning of the CCS gene program.[14]

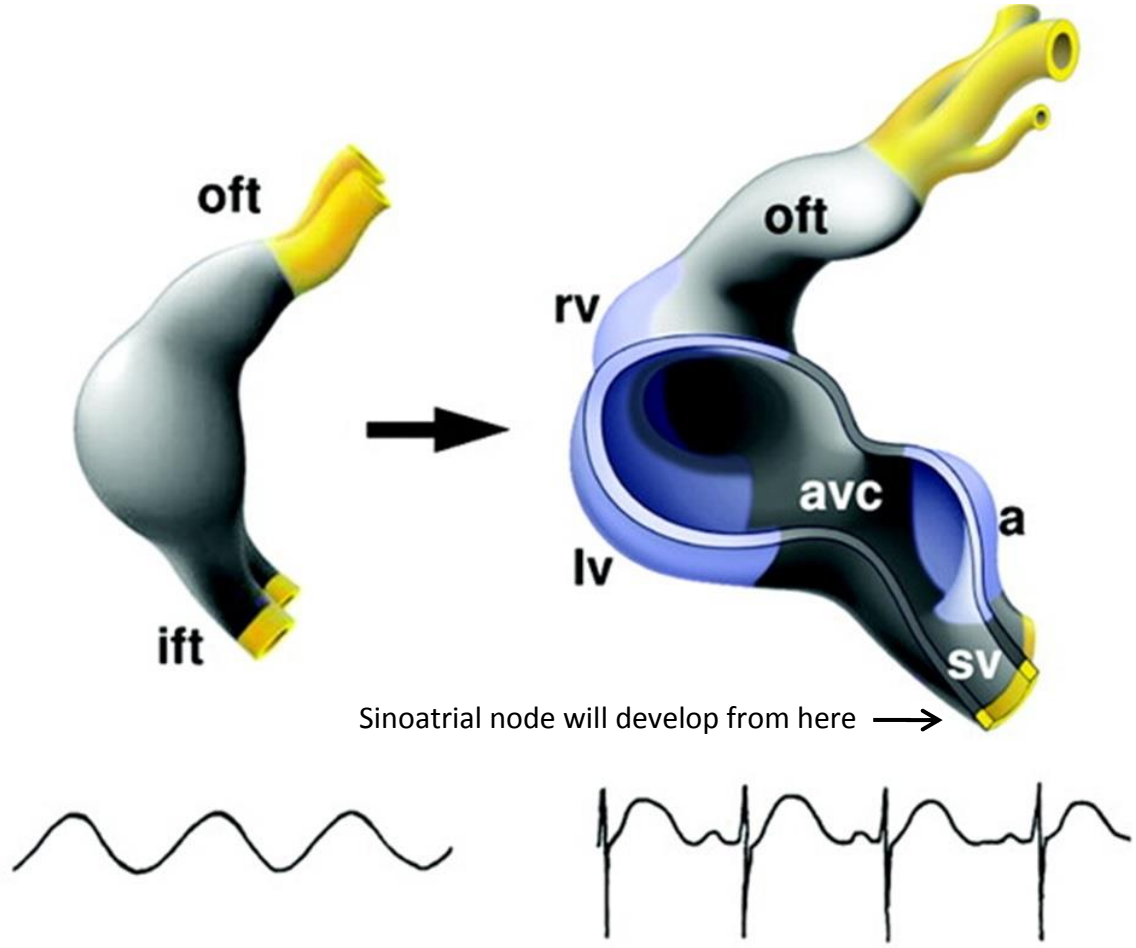

Figure 1. Embryogenesis of the SAN

Diagram illustrating the embryonic development of conduction tissue in mammals. The sinus venosus, atrioventricular canal and outflow tract (grey) retain primary characteristics with pacemaking capability, whilst the rest of the tube (purple) differentiates into working myocardium, expands quickly forming the chambers of the heart and loses its inherent automaticity in the process. The SAN develops from the sinus venosus. oft, outflow tract; ift, inflow tract; rv, right ventricle; lv, left ventricle; avc, atrioventricular canal; sv, sinus venosus; a, atrium. Adapted from Christoffels et al, 2010.[10]

In transgenic mice that expressed *Tbx3* ectopically throughout the heart, chamber formation became dysfunctional, *Nppa* and *Cx40* expression was repressed, however *Hcn4* was not yet activated.[14]

Another study examined transgenic mice deficient in *Tbx3.*[16] Again, deficiency did not prevent the SAN from forming and *Hcn4* was still expressed, but the SAN was significantly smaller than in wild type mice. At day 12.5 in *Tbx3* deficient embryos, *Nppa* and *Cx40* remained inactivated in the developing SAN, presumed to be because *Nkx2-5* was not yet present in this region, but another atrial gap junction gene *Cx43* did encroach upon the SAN border. However, by day 13.5 *Nppa*, *Cx40* and *Cx43* were all now being expressed in the SAN. In addition, the atrial Na^+ channel $Na_v1.5$ (expressed by the gene *Scn5a*) normally absent from the SAN was also ectopically induced in *Tbx3* deficient mice.[16]

The same group also examined mice ectopically expressing *Tbx3*.[16] They showed downregulation of the working myocardial genes *Nppa*, *Cx40*, *Cx43* along with $Na_v1.5$ and the atrial K^+ channel $K_{ir}2.1$. They also saw upregulation of pacemaker genes for *Hcn1*, *Hcn2* and *Hcn4* along with the SAN T-type Ca^{2+} channel $Ca_v3.1$.[16] They then used an '*αMhc'* line of transgenic mouse that expressed *Tbx3* ectopically but for a shorter period in early embryogenesis prior to and during chamber differentiation. These mice again demonstrated downregulation of *Nppa* and *Cx40*, but this time *Hcn4* was not affected. They concluded that *Tbx3* functioned as a repressor of the atrial gene program, but that the eventual promotion of pacemaker genes such as *Hcn4* was via an indirect pathway.[16]

A homeobox gene called *Shox2* has been described, seen to be restricted to the SV in the embryonic mouse heart.[17, 18] *Shox2* is seen to be expressed from day 8.5 and remains consistently specific to the developing SAN at day 12.5. The function of *Shox2* was examined using *Shox2* deficient mice.[18] Null mutation of *Shox2* was lethal due to severe hypoplasia of the developing SV, atrial malformation and severe bradycardia between day 11.5 and 12.5.[18] By day 11.5 *Shox2* deficiency was associated with upregulation of *Nkx2-5*, *Nppa* and *Cx40*, along with downregulation of *Tbx3* and *Hcn4*.[18] As such, *Shox2* was

purported to function upstream of *Nkx2-5* as its repressor. However, a specific binding site between *Shox2* and *Nkx2-5* was not found suggesting an indirect effect.[18]

Pitx2c is a homeobox gene which directs the differentiation of the left and right sides of the heart.[14] In Pitx2c deficient mice by day 10.5, embryos develop two sets of venous valves and sinus horns, and by day 15.5 a second left-sided SAN develops complete with a nodal artery and typical *Hcn4* positive, *Cx40* negative gene expression.[14] It is therefore suggested that *Pitx2c* acts as a repressor of SAN development, upstream of *Shox2* (figure 2).[14, 18]

Tbx18 is a T-box transcription factor (proteins that direct limb and heart development) that is seen early in the developing SV from day 9.5 in the mouse embryo.[19, 20] As *Nkx2-5* positive myocardium develops, a separate pool of mesenchymal progenitor cells remain at the caudal pole of the heart tube which express *Tbx18* but not *Nkx2-5*.[19] When these cells are isolated and cultured they develop into *Hcn4* positive, *Nkx2-5* negative myocardium.[20] Lineage analysis studying the fate of *Tbx18* positive and *Nkx2-5* positive cells show that they always remain mutually exclusive, with only *Tbx18* expressing cells going on to form the SAN.[19, 20] Furthermore, neither *Nkx2-5* or *Tbx18* deficient mice demonstrated any derepression of the other gene suggesting that both genes are regulated by other upstream factors.[19] *Tbx18* deficient mice fail to form sinus horns from the SV.[20] From day 12.5 early SAN tissue fails to enlarge and the core SAN "head" is malformed.[20] This suggests therefore that *Tbx18* is required for the morphogenesis of the SAN head upon which *Tbx3* later exerts its pacemaker program of genes.[10, 20]

1.2 Structure of the sinoatrial node

In general the SAN is seen as a length of tissue within the posterior wall of the RA, beginning close to where the superior vena cava (SVC) feeds into the RA and extends down beside the crista terminalis (CT) towards the inferior vena cava (IVC) (figure 3).[21] There is variability in the exact location, size and shape of the SAN between humans and smaller mammals.[22]

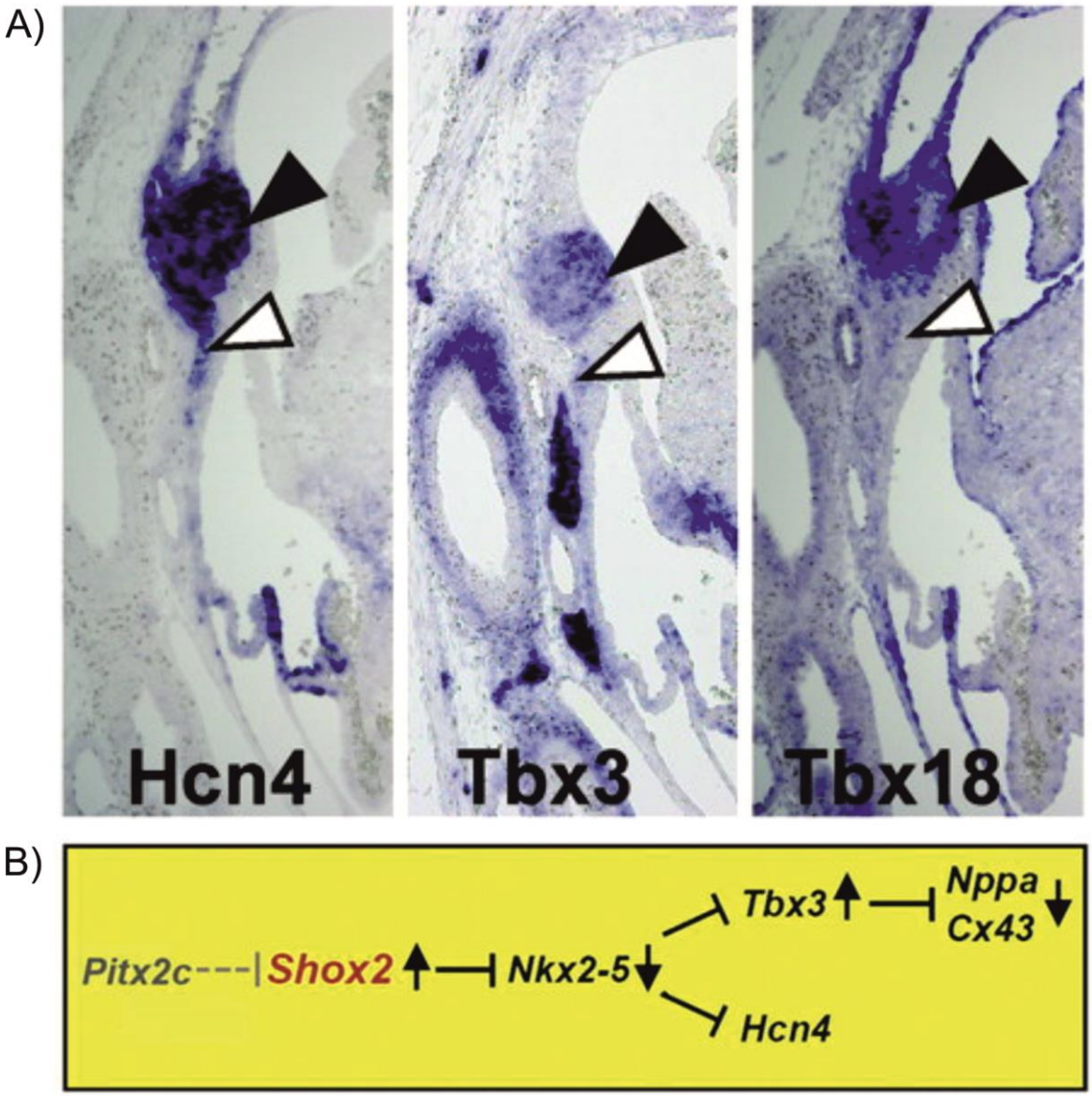

Figure 2. Gene interactions involved in SAN development

Complex interaction of several developmental genes and transcription factors including *Pitx2c*, *Shox2*, *Nkx2-5*, Tbx18 and Tbx3 are required to produce the specialised end phenotype of the cardiac conduction system. A) In situ hybridisation highlights the pattern of co-localization between *Hcn4*, Tbx3 and Tbx18 in transgenic mice within the SAN head (black arrow) and SAN tail (white arrow); B) A purported sequence of gene interactions relating to increasing levels of Shox2 (highlighted red) leading to the suppression of atrial genes and promotion of pacemaker genes as observed in transgenic mice. Tbx18 is not thought to directly be involved in this pathway however has been associated with promotion of Hcn4. Adapted from Weise et al, 2009 and Espinoza-Lewis et al, 2009.[18, 20]

The SAN is much larger than originally thought and structurally more complex than the dot it is often represented by in some texts. The histologically defined human SAN ranges from 8-21.5 mm in length.[21] The main body is crescent-shaped with a thinner tail of tissue extending towards the IVC, positioned 0.1 – 1 mm subepicardially.[21] Groups of nodal cells are bound by basement membrane and densely packed within fibrous connective tissue.[21, 23] In humans there is no discrete outer layer of fibrous tissue insulating the SAN, unlike ventricular parts of the CCS.[21] The proportion of connective tissue is higher in larger animals and up to 70% in humans, increasing with age.[24] Nodal cells are spindle-shaped, pale, small (about 5-10 µm) and relatively 'empty' of myofibrils (actin and myosin chains involved in cell contraction) and sarcoplasmic reticulum (SR) (intracellular networks of membranes storing Ca^{2+}) compared to that of the surrounding muscular tissue.[23] Networks of t-tubules (deep invaginations of the cell membrane that promote co-ordinated intracellular Ca^{2+} release) are also less developed in SAN cells compared to working myocytes.[25]

Towards the edge of the node the border becomes indiscrete and there are several theories for this. There may be intermingling of nodal and atrial muscle cells with a gradual shift in the ratio of nodal to atrial cells (mosaic effect).[26] Interlocking digits of SAN and working myocardial tissue have also been seen.[21] Furthermore, the morphology of the cells themselves may gradually change between nodal and atrial cell types, with intermediate cell types comprising mixed features in between (gradient effect).[23, 26] All three aspects may exist simultaneously. In humans a large "paranodal area" has also been observed inferolaterally to the SAN with mixed features of both SAN and atrial tissue which may play a role in subsidiary pacemaking or propagation of SAN activity into the atrium.[27]

Transitional tissue in the peripheral SAN overcomes the 'source-sink mismatch', the SAN being a source of low amplitude and the atrium being a large sink that might otherwise absorb SAN activity with little effect.

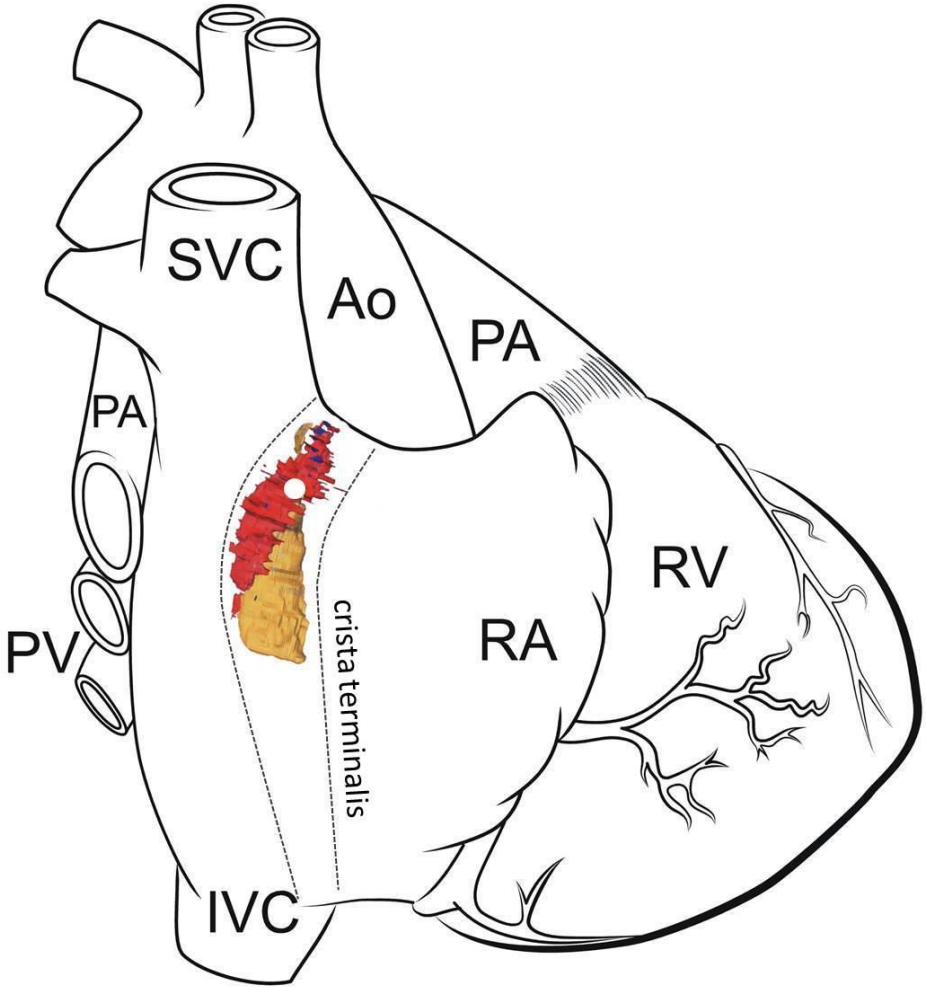

Figure 3. A 3D computer reconstruction of the human SAN

A schematic diagram of the heart, superimposed onto which is a 3D reconstruction of human SAN, the red area representing the SAN and the yellow area representing a paranodal area with intermediate structural features of both SAN and working myocardium. The leading pacemaker is represented by a white spot. Ao, aorta; SVC, superior vena cava; PA, pulmonary artery; PV, pulmonary vein; IVC, inferior vena cava; RA, right atrium; RV, right ventricle. Adapted from Chandler et al, 2011.[27]

The intermediate features of the peripheral SAN allow a gradual amplification of SAN activity to the level needed to drive the atrium. It also forms a complex structure of block zones and exit pathways that direct the delivery of SAN activity to the atrium and prevent suppression of SAN pacemaking by high levels of surrounding atrial hyperpolarization. Superior and inferior exit pathways were demonstrated around the canine SAN using extracellular mapping and ablation of these areas led to SAN exit block.[28] Optical mapping has been used in humans to observe the pattern of propagation of SAN activity into the atrium. The technique has demonstrated exit pathways at superior, middle and inferior levels from the periphery of the SAN breaking through laterally into the CT. It also revealed block zones between these exit pathways as well as medially along the intra-atrial septum.[29] Histology revealed connective, vascular and fat tissue insulating the SAN except for where these exit pathways were demonstrated.[29] However, other work has failed to visualise anatomically defined exit pathways, rather suggesting that they only function as a result of cellular orientation and the molecular structure of the peripheral SAN.[21, 30, 31]

The leading pacemaker tends to come from within the central SAN, although it can be more inferior or even multifocal in some cases. It is also variable between species. This has been seen in isolated hearts using microelectrode recording and optical mapping techniques and *in vivo* using transcatheter endocardial mapping and body surface electrical recordings.[29, 31-33] Spontaneous pacemaking inferiorly in the SAN has been seen to be slower and one theory is that there is a hierarchy of cells arranged with the fastest superiorly and the slowest inferiorly.[34] In addition to a single leading pacemaker changing its beating rate, the leading pacemaker can shift within the SAN to change its rate. For example both sympathetic and vagal stimulation have been shown to cause the leading pacemaker to shift and thus change the beating rate of the SAN.[34-36]

The SAN derives its blood supply from a prominent sinus node artery, which can arise either from the proximal right coronary or left circumflex arteries.[23] It most commonly runs a course through the central SAN down its entire length.[21, 23] In some cases the artery can be eccentric to the body of the SAN and towards the tail of the SAN there is a higher chance that the artery will leave the SAN and deviate towards the endocardium.[21]

1.3 Function of the sinoatrial node

A few years after Keith and Flack described the physical nature of the SAN, electrical recordings using Einthoven's string galvanometer technique in animals confirmed that it was indeed the original source of electrical activity for each heartbeat.[1, 37, 38] In 1949, Sir Alan Hodgkin started to characterise the cardiac action potential (AP) applying intracellular electrode recording and voltage clamp techniques initially developed to record nerve APs. The following 30 years saw many refinements to the mechanistic model of the cardiac AP that we currently understand.[39, 40]

There are 5 phases to a cardiac AP. Phase 0 contains the initial large inward current that depolarizes the cell, causes the 'upstroke' of each AP and leads to cell contraction. During phase 1 those depolarizing ion channels inactivate and there is a transient outward repolarizing current. Phase 2 sees a plateau caused by balanced inward Ca^{2+} and outward K^{+} currents during which muscle contraction is sustained. Phase 3 is when rapid repolarization takes place from K^{+} efflux which will 'reset' the cell back to its baseline potential. Phase 4 is the period between beats when the cell is at its resting potential.

The SAN AP differs in morphology to the working myocardium. The AP in the working myocardium has a fast phase 0 upstroke velocity (>100 V/s), a short phase 2 plateau (around 100 ms) and returns to a stable resting potential (just below -80 mV) in phase 4.[41, 42] Since the resting membrane potential is stable an AP must be triggered by an external stimulus such as depolarization of a neighbouring cell.

In contrast the AP in the SAN has a slower phase 0 upstroke velocity (upto 10 V/s), lower amplitude upstroke, longer phase 2 plateau (around 150 ms) and there is no stable resting potential in phase 4.[31, 41-43] The lack of a stable resting potential is important as its absence allows depolarizing pacemaker currents to be effective during phase 4 (figure 4).

Diastolic depolarization (DD) is another term for phase 4 depolarization caused by pacemaker currents. In SAN cells, DD is triggered when the membrane potential is around

-40 to -65 mV. As such, once phase 3 repolarization fades towards the end of an AP, DD gradually starts to increase the membrane potential once again until the threshold for the next AP is reached. [41, 44] Thus DD is key to closing the cycle between APs and as a result cells will continue to beat automatically.

1.3.1 Diastolic depolarization

There is still debate over the relative dominance of certain molecular mechanisms over others in DD.[45] However the emerging consensus is that there are two interplaying mechanisms both central to DD, the 'membrane clock' and the 'Ca^{2+} clock'.

1.3.1.1 The membrane clock

The membrane clock theory describes the role of several membrane bound ion channels involved in the production of DD early in phase 4, unique to the pacemaker cell AP. The roles of the 'inward rectifier' K^+ current, the 'delayed rectifier' K^+ current and the 'funny' current are discussed below.

1.3.1.1.1 Inward rectifier K^+ current

Working atrial cardiomyocytes have a stable resting membrane potential of just below -80 mV in phase 4 of the AP. This is largely governed by the inward rectifier K^+ current ($I_{K,1}$) which is predominantly generated by the ion channel $K_{ir}2.1$.[46, 47] $I_{K,1}$ does not follow the classic pattern of other voltage-dependent K^+ channels which generate an outward K^+ current at positive membrane potentials, hence it was initially described as 'anomalous rectification'. Rather $I_{K,1}$ starts with a lack of outward current at positive membrane potentials in early phase 3 repolarization, but generates a large outward current towards the final stage of phase 3 causing repolarization to accelerate. However, below the reversal potential of K^+ (at around -90 mV) $I_{K,1}$ instead generates a large inward current which rectifies and stabilises the membrane potential at close to the reversal potential.[48]

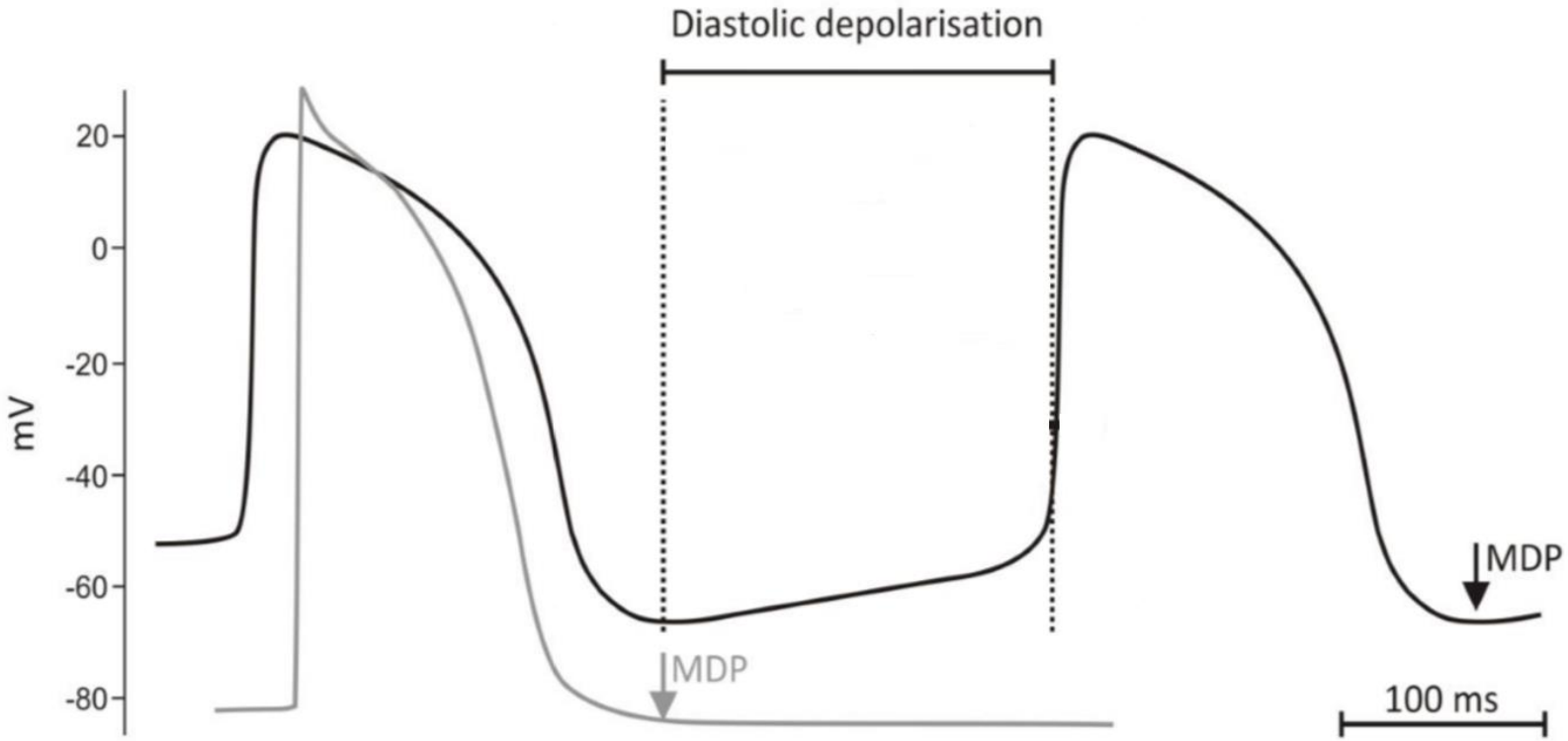

Figure 4. Action potentials from the SAN and from the working atrial myocardium

SAN (black trace) and atrial (grey trace) APs are shown overlapping for comparison. SAN APs demonstrate less negative maximum diastolic potentials (MDP), slower upstroke velocity and longer action potential durations. Adapted from Monfredi et al, 2010.[41]

SAN cardiomyocytes do not have a stable resting potential because they lack $I_{K,1}$ and this allows DD to gradually increase the membrane potential during phase 4 toward the threshold for the next AP.[49] qPCR was used to measure mRNA levels of $K_{ir}2.1$ in human tissue revealing a higher abundance in RA samples compared to the SAN.[47] Immunohistochemistry was used to label $K_{ir}2.1$ protein in the human SAN showing that this channel is expressed in the atrial region but not in the SAN.[50] Additionally, $K_{ir}2.1$ has been overexpressed in transgenic mice linked to an α*MHC* promoter, however expression of this channel in the SAN was repressed suggesting that transcriptional or post-transcriptional inhibition of $K_{ir}2.1$ expression was present in the SAN.[51] Adenoviral expression of a dominant-negative '$K_{ir}2.1AAA$' construct has been used to inhibit $I_{K,1}$ in the guinea pig LV by up to 80%. After 3-4 days, isolated transduced cells demonstrated slow pacemaker activity.[52]

1.3.1.1.2 Delayed rectifier K^+ current

There are three types of delayed rectifier current, ultra-rapid ($I_{K,ur}$), rapid ($I_{K,r}$) and slow ($I_{K,s}$). These are generated by $K_v1.5$, ERG ($K_v11.1$) and K_vLQT1 respectively.[46] They are present in both atrial and SAN tissue but there is heterogeneity in their relative expression regionally and between species.[53, 54] One study showed that in humans there was less $K_v1.5$ and ERG in the SAN compared to the atrium, but another study in the rabbit showed there were similar levels of $K_v1.5$ and more ERG in the SAN versus the atrium.[47 55] However, current density of $I_{K,r}$ and $I_{K,s}$ has been measured in isolated SAN cells from the rabbit showing an increase with cell size, suggesting that smaller central SAN cells have less $I_{K,r}$ and $I_{K,s}$.[53] It was also demonstrated in rabbit SAN tissue that partial blockade of $I_{K,r}$ more easily suppressed spontaneous pacemaker activity in the central SAN than it did in the peripheral SAN.[56]

Overall I_K is therefore thought to be less in the SAN, which has an effect on the speed of repolarization, AP duration (APD) and the maximum diastolic potential (MDP) i.e. the most negative potential at the end of repolarization. A more positive MDP will disinhibit pacemaker potentials early in phase 4 and aid DD. Although less I_K aids DD, blockade of I_K

abolishes pacemaking. This is thought to be because some I_K is still required to repolarize the cell into the range where pacemaker potentials are triggered.[54]

1.3.1.1.3 The 'funny' current

Up until the 1980s it was believed that early DD was caused by the decay of an outward K^+ current termed $I_{K,2,}$ activated during voltage clamp at negative pacemaker potentials in Purkinje fibres. However, the reversal potential for this current was more negative than would be predicted by the Nernst equation for a pure K^+ current. This was initially put down to depletion of extracellular K^+ through sequestration in extracellular clefts.[57, 58] Over a decade later, it was established that high levels of $I_{K,1}$ in Purkinje fibres was confusing the picture. Blockade of $I_{K,1}$ with Ba^{2+} would alter the properties of $I_{K,2}$ to exactly match those of a newer inward mixed cation current called the 'funny' current (I_f) identified in SAN cells where $I_{K,1}$ was absent.[49, 59-61] The fact that I_f was a depolarizing current at negative potentials of -40 to -65 mV as well as the early observation that it was amplified by adrenaline suggested that I_f must be central to the generation of spontaneous and autonomically sensitive pacemaker activity in the heart.[59, 61]

I_f is a mixed Na^+ and K^+ inward current increasingly activated by hyperpolarization below -40 to -45 mV, has a time constant of 2 – 4 s, is small in magnitude (~1pS in single cells), saturates at -100 mV, and has a reversal potential of around -10 to -20 mV.[61, 62] It is therefore gradually activated during ongoing repolarization by $I_{K,r}$, opposing it until $I_{K,r}$ decays and an equilibrium of the two is reached at the MDP. Thereafter, I_f continues to depolarize the cell in early DD and tails off in late DD where Ca^{2+}-dependent mechanisms take over.[61]

The molecular correlate of I_f is the hyperpolarization-activated cyclic nucleotide-gated (HCN) ion channel of which there are four isoforms, HCN1-4.[63] These isoforms are 80 – 90% identical within their transmembrane and cyclic nucleotide binding domains and based on their amino acid sequence are part of the larger K_v superfamily.[46] Differences in the extreme termini of channel subunits account for variations in the channel kinetics and

sensitivity to cyclic nucleotide modulation between isoforms.[63] Each isoform is formed by four subunits aligned on the membrane as a tetramer. Each subunit has six transmembrane domains (S1 – S6), with a positively charged voltage sensor within S4, a pore-forming P-loop between S5 and S6 that has a 'GYG signature sequence' relating to K^+ selectivity, and a long 120 amino acid 3'-5'-cyclic adenosine monophosphate (cAMP) binding domain intracellularly after S6 (figure 5).[63]

Autonomic modulation of HCN channel function via its cAMP binding domain is an important feature that allows the sympathetic and parasympathetic nervous system to control heart rate. Deletion of this cAMP binding domain from HCN channels expressed in *Xenopus* oocytes increased channel activation.[64] The presence of the domain is therefore thought to inhibit pore opening probability through a conformational change in the transmembrane structure, whilst binding of cAMP to the domain acts to relieve this inhibition, shifts the activation curve to more positive voltages and therefore increases I_f.[62, 64] Whereas Ca^{2+}-dependent aspects of the cardiac AP are also affected by cAMP via protein kinase driven phosphorylation, cAMP binds directly to HCN channels providing a mechanism for the sympathetic nervous system to speed up pacemaking without affecting the AP threshold or duration.[62, 65] Acetylcholine released by the parasympathetic nervous system acts to inhibit adenylate cyclase and therefore reduces cAMP production, which reduces I_f and slows pacemaking.[66] Association of HCN channels to other neighbouring proteins can also modulate their function, such as the auxiliary subunit MiRP1, caveolae, β2 adrenoreceptors, membrane phospholipids and protein kinases.[67-72] The high substrate dependence of I_f is one of the reasons why its characterisation has been difficult and varied up until now.[63]

HCN channels 1, 2 and 4 are found in the heart, HCN4 being the most abundant in the SAN in most species. The relative levels of each isoform vary between species, for example in the rabbit SAN HCN4 accounts for >81% of total HCN mRNA and HCN1 for >18%.[73] In dogs, the prevalence of HCN1 was found to be 7% and HCN2 was 8%.[74] HCN1 is seen as the second most prevalent isoform in humans.[47]

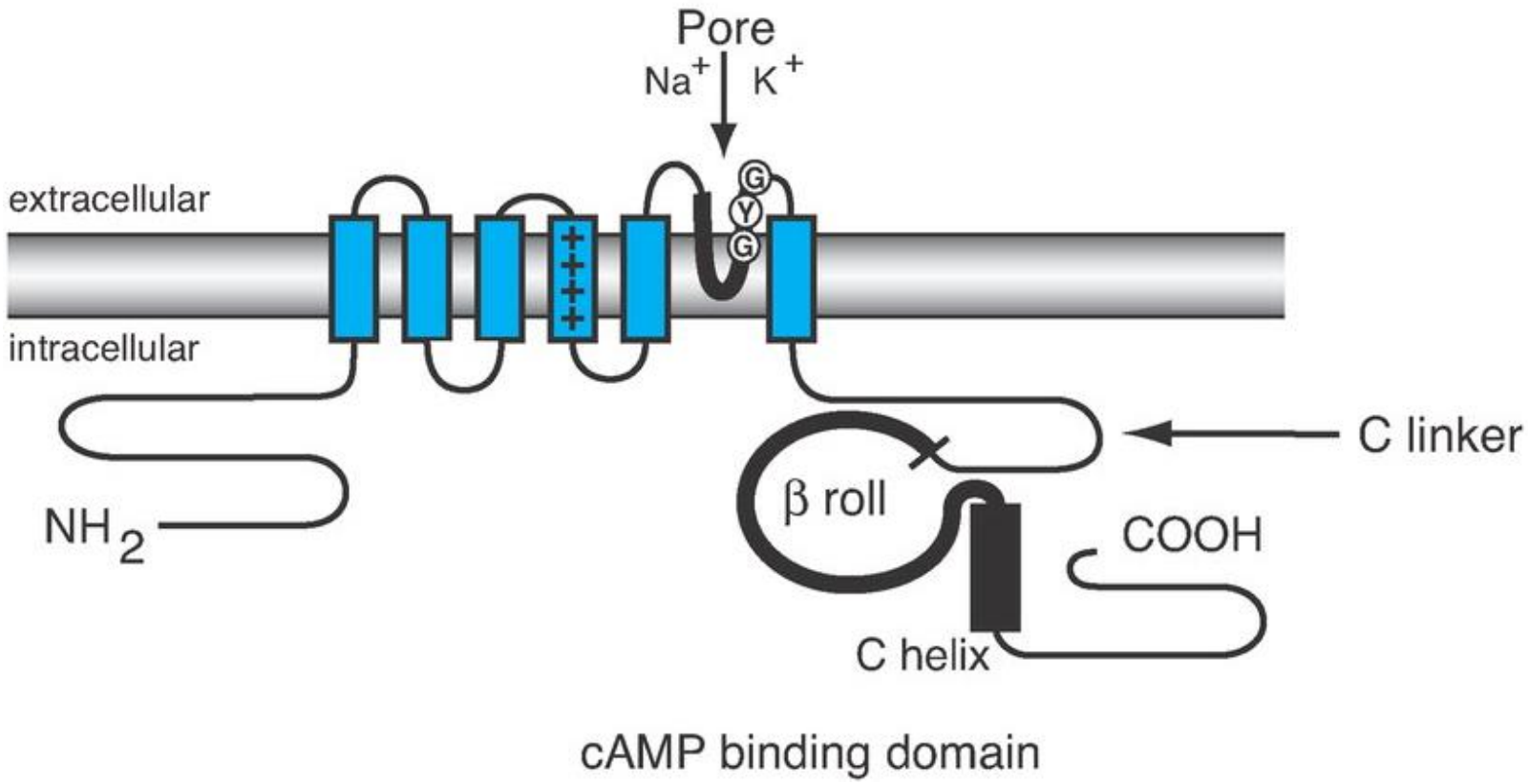

Figure 5. HCN channel structure

Schematic diagram showing the structure of HCN channels within the cell membrane. There are six transmembrane domains (S1-S6) with the channel pore formed between S5 and S6, a positively charged voltage sensor at S4 and a cAMP binding region intracellularly after S6. Taken from Robinson et al, 2003. [63]

The channel kinetics of each isoform varies with HCN1 having the fastest activation time (30 ms) then HCN2 (184 ms) and finally HCN4 (461 ms).[73] Sensitivity of channel function to cAMP binding also varies with HCN2 displaying the greatest.[73]

Native HCN channels are thought to form heteromeric combinations of each isoform, similar to other K^+ channels.[63] HCN1 and HCN2 channel isoforms expressed individually in *Xenopus* oocytes form homomeric channels and demonstrate I_f with differing characteristics to native I_f. However, if both are expressed they show evidence of heteromeric channel formation with characteristics closer to native I_f.[75, 76] Heteromerization of HCN channels therefore only adds to their functional diversity.

Several lines of evidence suggest that I_f is central to SAN pacemaking. Firstly HCN4 can be used as a marker for pacemaker tissue. Immunofluorescence, mRNA data and measurement of I_f density all suggest a high concentration of HCN4 in the SAN but not in surrounding tissue.[47, 54, 77] I_f is associated with the regional gain and loss of automaticity during cardiac development, for example foetal ventricular myocytes initially express I_f and contract spontaneously but both gradually disappear with a similar time course.[78-80] Furthermore, the transcription factor Tbx3 involved in SAN development promotes expression of HCN4.[16]

Pharmacological evidence of the central role of I_f to pacemaking comes from the specific I_f blocker ivabradine, and there is clinical evidence for its use in lowering heart rate in heart failure and ischaemic heart disease.[81-83] One criticism is that ivabradine does not abolish pacemaking and so cannot be a critical mechanism in pacemaking. However, low doses of ivabradine were used to block I_f more specifically and even at higher doses I_f blockade is at maximum ~60%.[84] So although ivabradine does not abolish pacemaking, full and specific blockade of I_f is not yet possible.

Finally, genetic screening of families with seemingly inherited bradycardia has revealed several mutations associated with HCN channels. When these mutant channels were expressed in single cells, they were associated with a negative shift in channel activation, insensitivity to an increase in cAMP, or problems with channel synthesis and trafficking.

[85-87] These mutations demonstrate that normal HCN channel function is required to maintain heart rate.

1.3.1.2 The Ca^{2+} clock

Although there is still debate about whether the membrane or the Ca^{2+} clock is the dominant mechanism for production of automaticity in pacemaker cells, it is now agreed that intracellular Ca^{2+} cycling plays an important role as part of a 'coupled clock'.[45] There are links between both mechanisms which mutually entrain them to each other, and their dual presence creates redundancy and robustness whereby if one mechanism fails pacemaking vital for survival can still continue (figures 6 and 7).

1.3.1.2.1 T-type Ca^{2+} current

Following I_f in early DD, the first Ca^{2+} current is the inward T-type (transient type) Ca^{2+} membrane current ($I_{Ca,T}$) which occurs midway through phase 4 of the AP. It can be measured when the larger overlapping L-type (long-lasting type) Ca^{2+} current ($I_{Ca,L}$) is blocked using nifedipine.[88] $I_{Ca,T}$ is mediated by voltage-gated $Ca_v3.1$ and $Ca_v3.2$ channels that are opened at low voltages of around -50 to -60 mV.[49, 88, 89] These channels are made up of an α_1 subunit which has four transmembrane domains that control pore selectivity to Ca^{2+}, and a β_{1b} subunit that improves membrane trafficking and current.[90, 91] They have a rapid inactivation pattern regulated by a 'ball and chain'-like mechanism located on the C-terminus.[92]

These channels are expressed at a much higher level within the SAN than the working myocardium and accordingly the resulting current is around ten times as dense in the SAN.[47, 88] Single channel conductance is small however at about 8.5 pS.[88] The current overall is therefore relatively low amplitude and moreover expression does vary between species, with human SAN cells expressing $Ca_v3.1$, and mice and guinea-pig SAN cells displaying more $I_{Ca,T}$ than rabbit and porcine SAN cells.[47, 93]

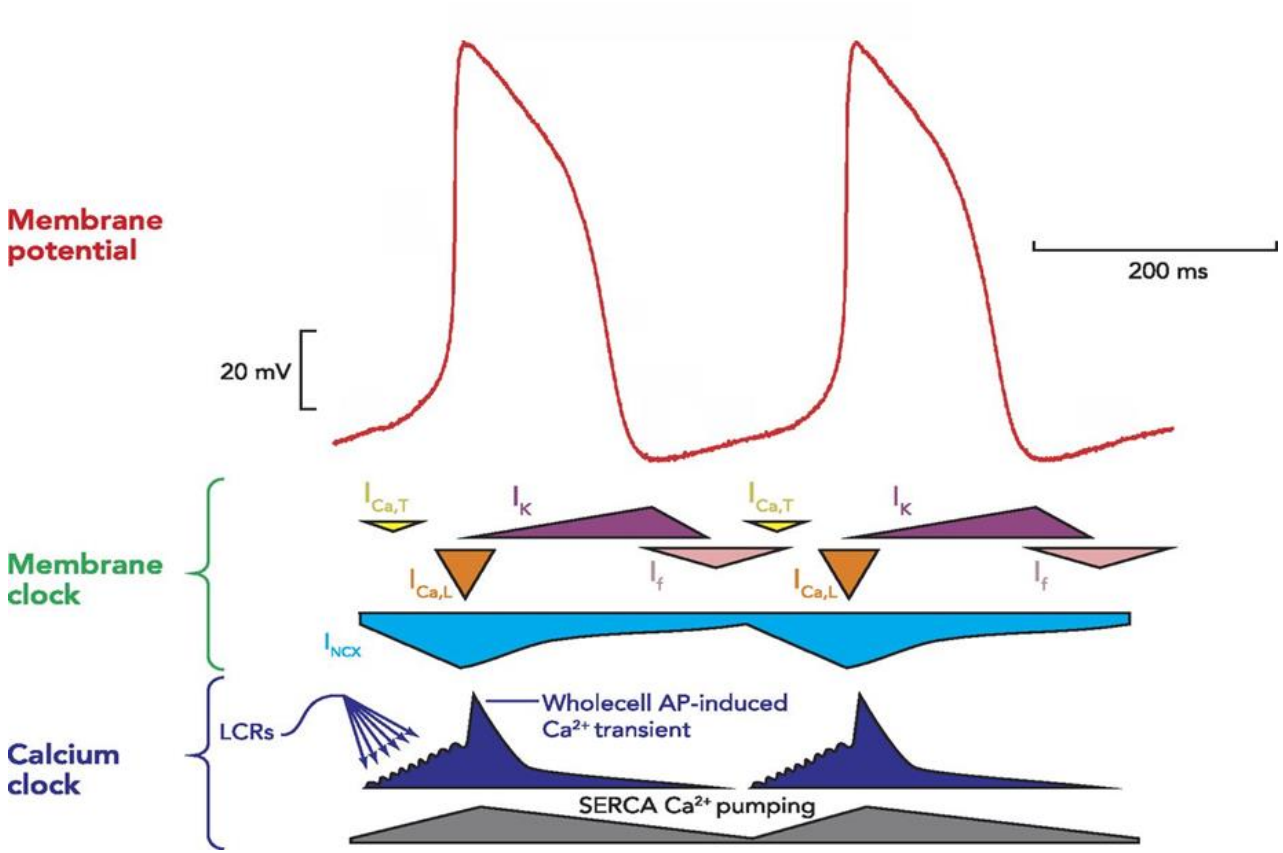

Figure 6. Summary of the timing of pacemaker currents during the SAN action potential

SAN APs (red trace) are shown above the timing of inward and outward currents of the membrane clock and intracellular Ca^{2+} release from the SR as part of the Ca^{2+} clock. LCRs, local Ca^{2+} releases. Adapted from Monfredi et al, 2013. [94]

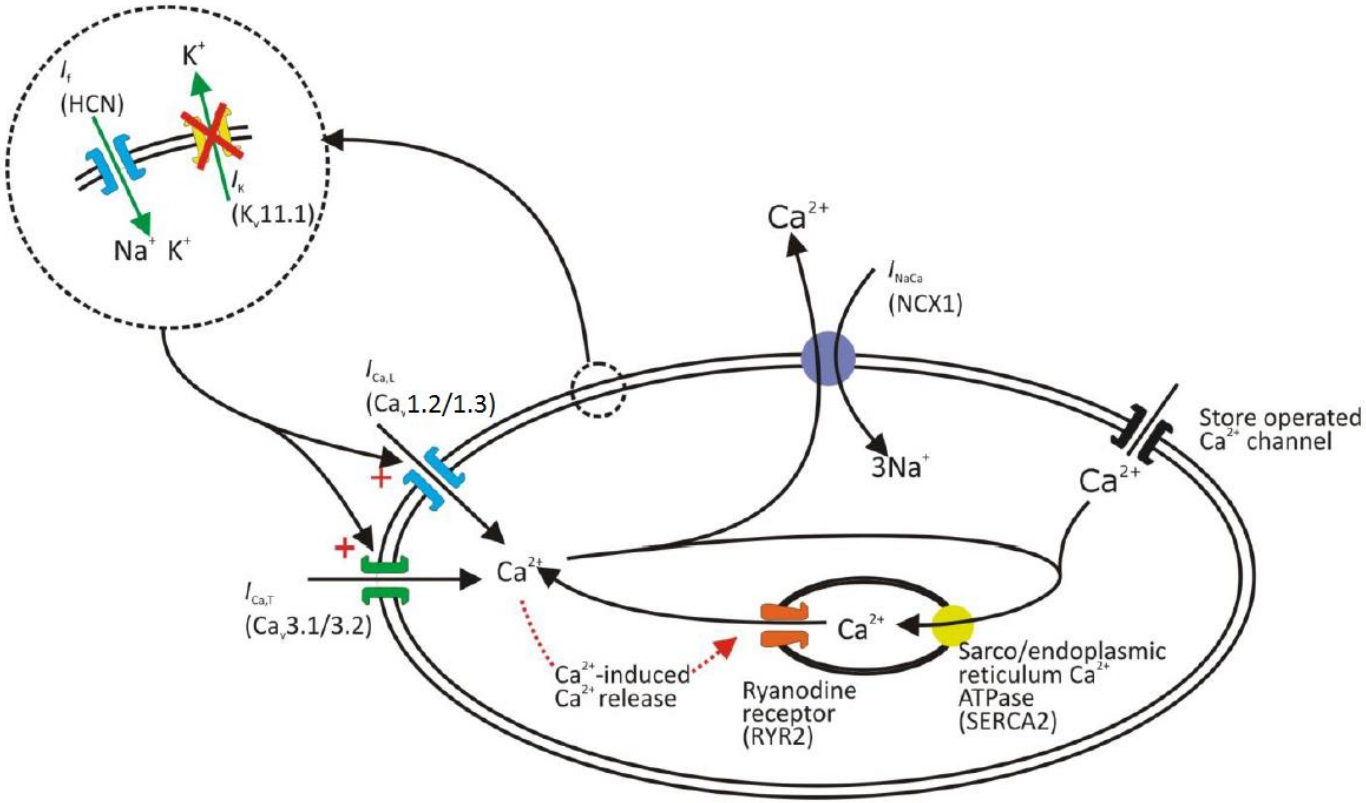

Figure 7. Diagrammatic representation of the ionic currents involved in the membrane and Ca^{2+} clocks of SAN pacemaking

A cell diagram highlighting aspects of Ca^{2+} cycling within pacemaker cells and the interaction of HCN and K^+ channels in the membrane clock (dotted circle). From Morris, 2010.[95]

Blocking it in the rabbit using Ni^{2+} reduces pacing rate, whilst knocking it out in mice results in bradycardia and a prolonged SAN recovery time.[88, 96]

The effect of $I_{Ca,T}$ blockade might be larger than expected considering the small amount it would contribute to membrane depolarization directly. This is because small increases in intracellular Ca^{2+} stimulates Ca^{2+} release from the cell's SR Ca^{2+} store through high conductance Ca^{2+} channels on the SR membrane called ryanodine receptors (RYRs). RYR2 is the particular isoform found in cardiac cells. This process of Ca^{2+} conductance through RYR2 in response to increasing cytosolic Ca^{2+} concentration is termed Ca^{2+}-induced Ca^{2+} release (CICR).[97] Blockade of $I_{Ca,T}$ in the cat using Ni^{2+} decreases DD, slows pacemaking and suppresses Ca^{2+} release from the SR.[89] It is therefore suggested that the role of $I_{Ca,T}$ in pacemaking is to trigger diastolic SR Ca^{2+} release from inside the cell via RYR2.

1.3.1.2.2 SR Ca^{2+} cycling and Ca^{2+} sparks via RYR2

In working myocardial cells SR Ca^{2+} cycling mainly plays a role in excitation-contraction coupling, which starts when membrane depolarization triggers influx of Ca^{2+} through L-type Ca^{2+} channels inside t-tubules that penetrate the cell. CICR stimulates a wave of SR Ca^{2+} release via RYR2 to pass through the cell (the Ca^{2+} transient) and cytosolic Ca^{2+} binds to myofibrils leading to cell contraction.[98] Without stimulation working myocytes remain quiescent and the SR remains mostly inactive in terms of Ca^{2+} release.[99]

SAN cells contain relatively fewer t-tubules, myofibrils and less SR but they still exhibit Ca^{2+} transients during each beat.[23, 25, 100] In contrast to working myocytes however, SAN cells demonstrate cyclical SR Ca^{2+} release during the diastolic phase of the AP, and this is critical to the Ca^{2+} clock.[100] Initial suspicion of the importance of SR Ca^{2+} release to pacemaking came in the late 1980s, when blockade of SR Ca^{2+} release using the plant alkaloid ryanodine caused a reduction in the slope of late DD specifically and slowed pacemaking in cat pacemaker cells.[101]

In the early 1990s, laser scanning confocal microscopy and the use of a Ca^{2+} sensitive fluorescent probe allowed visualisation of spontaneous Ca^{2+} release events from the SR through RYR2 in resting rat ventricular myocytes. These were termed local Ca^{2+} releases (LCRs) or 'Ca^{2+} sparks'.[102, 103] SAN cells demonstrate Ca^{2+} sparks under basal conditions more readily than ventricular cells and this is thought to be due to higher levels of cAMP and therefore increased protein kinase A driven phosphorylation of phospholamban and other Ca^{2+} cycling proteins.[104] This provides an avenue for the autonomic nervous system to regulate heart rate.

Ca^{2+} sparks were observed at low voltages during diastole in isolated cat and toad pacemaker cells, greatly increasing in frequency in the period just before each beat.[89, 105] Ca^{2+} sparks were also demonstrated in rabbit SAN cells that were either permeabilized or voltage clamped at potentials where no inward current would occur (-10 mV), suggesting that LCRs have their own intrinsic rhythmicity in the absence of membrane depolarization which could independently set the timing of beating cells.[106] Rising intracellular Ca^{2+} as a result of increasingly frequent Ca^{2+} sparks activates another Ca^{2+} dependent depolarizing membrane current, I_{NCX}, which finally brings the cell membrane potential up to the threshold for the next beat.

1.3.1.2.3 Na^{+}-Ca^{2+} exchanger

I_{NCX} is driven by the Na^{+}-Ca^{2+} exchanger (NCX), which exchanges one Ca^{2+} ion out of the cell for three Na^{+} ions in with a net depolarizing effect.[100] In SAN cells, Ca^{2+} spark generating RYR2 channels on the SR are located peripherally and are closely co-localized with NCX on the membrane, so NCX is quickly activated by exposure to LCRs.[107, 108] NCX is an exchanger rather than an ion channel and as such has no time dependent or voltage-gating mechanism.[109] Therefore, in contrast to I_f which gradually inactivates with increasing DD, NCX does not. Rise in NCX magnitude continues to accelerate with increasing intracellular Ca^{2+} between membrane potentials of about -60 to -30 mV, until the threshold potential for the next beat is reached.[100]

The critical value of NCX to pacemaking is revealed when blockade of this channel with Li^+ abolishes pacemaking altogether.[100] NCX knock-out in mouse embryos is lethal, whereas atrial specific knock-out causes failure of SAN pacemaking.[110-112]

1.3.1.2.4 SR Ca^{2+} replenishment

At the end of phase 4 when the threshold for the next beat is reached, L-type Ca^{2+} channels on the membrane open to initiate large scale phase 0 depolarization. CICR then triggers a large Ca^{2+} transient to sweep across the cell and causes the cell to contract which empties the SR of Ca^{2+}. Replenishment of SR Ca^{2+} load is performed by sarcoplasmic-endoplasmic reticulum calcium adenosine triphosphatase (SERCA) on the SR membrane.[113] The SR Ca^{2+} load can determine the speed of Ca^{2+} released by RYR2 during DD.[99] The rate of Ca^{2+} replenishment through SERCA is regulated by cAMP-mediated protein kinase A driven phospholamban phosphorylation.[113] In this way SERCA can influence the cycle length of the Ca^{2+} clock.[113, 114] Inhibition of SERCA using cyclopiazoic acid reduces spontaneous SAN firing by around 50% in the guinea-pig and rabbit.[113, 115] The SERCA2a subtype can be found specifically localised within the core of the SAN when immunolabelled.[107] The level of cytosolic Ca^{2+} available to SERCA may be regulated in part by store-operated Ca^{2+} channels (SOCC) on the cell membrane which act to replenish intracellular Ca^{2+}.[116] Blockade of these channels slows pacing rate in mice, however the precise mechanism is not certain.[117]

1.3.2 Gap junctions

Cell-to-cell coupling is achieved by 'gap junctions', proteins which form conduits between membranes of neighbouring cells and allow ungated transfer of electrical current. This allows propagation of depolarizing current away from spontaneously beating cells and through the heart. Gap junctions are a family of proteins called Connexins (Cx), each Cx named by its molecular weight in kilodaltons, for example Cx43.[118] Generally, gap junctions are made up of six subunits forming four transmembrane domains, two extracellular loops and an intracellular loop.[119] Conduction velocity through different

areas of the heart can depend upon the subtype of Cx expressed in that area. Phosphorylation of C-termini may also play a role.[120]

Cx40 and Cx43 are fast conducting subtypes found in atrial working myocardium which allow rapid propagation of electrical impulses. Cx43 is absent and Cx40 sparse in the centre of the SAN and instead the slower conducting Cx45 is present.[47, 54] The reduced electrical coupling that results in the SAN centre serves to protect pacemaker cells from being suppressed by surrounding hyperpolarized atrial cells.[121] The conduction velocity is slower within the SAN (~0.03 – 0.05 m/s) compared to atrial muscle (~1 m/s).[31, 54, 122]

As discussed above (section 1.2), the periphery of the SAN has intermediate features between the core SAN and atrial muscle. Both Cx43 and Cx45 are both expressed in the SAN periphery and this may gradually match the SAN to atrial muscle and propagate impulses.[121] This is supported by experiments in transgenic mice with Cx40 and Cx43 knocked out which demonstrated bradycardia due to SAN exit block, increased SAN recovery time, reduced SAN conduction time, slow conduction velocity outside the SAN, morphogenic abnormalities and propensity for atrial and ventricular arrhythmias. [123-125]

1.3.3 Phase 0 depolarization

The SAN AP has a slow phase 0 upstroke of around 10 V/s, whereas the working myocardial AP has a fast phase 0 upstroke of around 100 V/s.[42] The fast AP upstroke of working myocardium is caused by the strong inward Na^+ current (I_{Na}) via the voltage-gated $Na_v1.5$ membrane channel.[46, 126] The slower upstroke of the SAN AP is carried by the L-type Ca^{2+} current, $I_{Ca,L}$, primarily through the $Ca_v1.3$ channel, containing the α_{1D} pore forming subunit.[46, 55] The SAN lacks $Na_v1.5$ channels at its core, though it must be noted that Na^+ channels still play an important role in SAN function.[127] Disabling these channels can still lead to bradycardia and pauses like that seen in SND. This can be seen in knockout mice or in human mutations of the *Scn5a* gene coding for the $Na_v1.5$ channel.[128, 129] Absent from the central SAN, this channel can be detected at the periphery and may have a role in propagation of the AP into surrounding atrial muscle.[130, 131]

$Ca_v1.3$ channels in the SAN activate at thresholds around -50 mV peaking at -10 mV.[132] Therefore, $I_{Ca,L}$ in the SAN is triggered by the rising membrane potential late in phase 4 caused by NCX.[100, 132] Blockade of $I_{Ca,L}$ with nifedipine abolishes pacemaking from the central SAN but not the periphery.[133] Isolated cells from $Ca_v1.3$ knock-out transgenic mice display bradycardia, irregular rhythms and prolonged AP duration.[132, 134]

1.4 Subsidiary atrial pacemaker tissue

Although the SAN is the primary leading source of automatic electrical activity in the heart, 'nodal-like' cells exist in the AVN and tissues outside of the CCS that retain the capability of automaticity.[135] Subsidiary atrial pacemaker (SAP) tissues are often a source of ectopic beats which can lead to arrhythmias, or they can take over as leading pacemakers in cases of SND.[136, 137] This provides backup pacing meaning that the heart rarely ever stops beating completely due to SND alone providing added layers of robustness to the vital function of pacemaking (figure 8).

Early work on SAP tissue in the 1970s used SAN-excised dogs.[138] Initially these animals displayed junctional rhythms from around the AVN but after several days leading pacemakers shifted to bradycardic SAP tissue.[138] In 80% of these animals the SAP was mapped to the inferior RA at the junction of the IVC. During isoprotenerol infusion leading pacemakers shifted to the interatrial region in 70% of animals.[138] Studies have demonstrated SAP tissue in the inferior RA adjacent to the IVC and interatrial region in cats and dogs.[139, 140] Nodal-like cells exist in the interatrial groove and AV ring bundle around the tricuspid valve in rats.[22] A 'retroaortic' node in the interatrial septum has been described in guinea-pigs.[141] In the human, tachyarrhythmia have been mapped to the CT, coronary sinus, atrial appendages, interatrial septum, left atrium, mitral valve annulus and pulmonary sleeves.[142-148]

In the dog, SAP tissue adjacent to the IVC is bradycardic and has been seen to be more sensitive to cholinergic stimulation and more suppressible by overdrive pacing.[149] APs recorded from SAP cells exhibited prominent DD, a less negative MDP, a slower upstroke velocity and a lower amplitude compared to surrounding atrial muscle.[139]

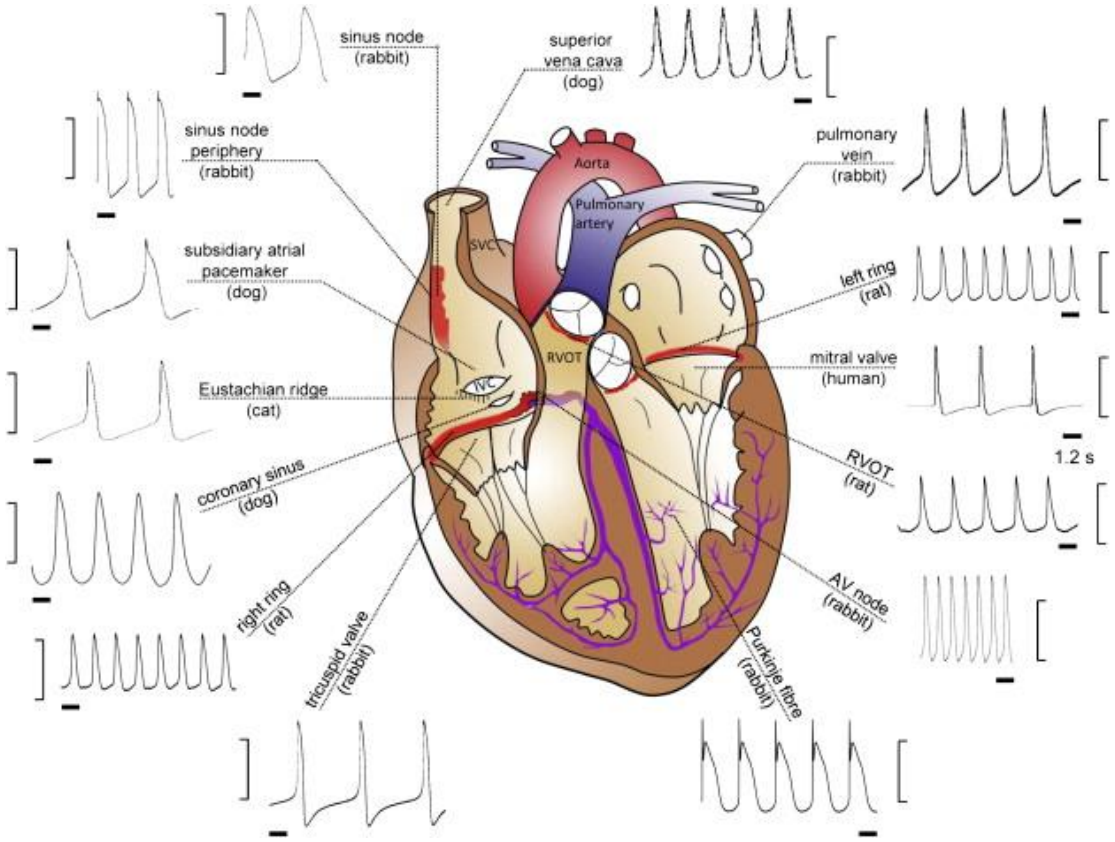

Figure 8. Diagram illustrating the numerous locations capable of spontaneous pacemaking and their action potentials

AP morphology of spontaneous pacemaker activity recorded from different regions of the heart illustrating the extent of pacemaker tissue outside of the SAN and the variation in their function. Taken from Dobrzynski et al, 2013.[135]

In the cat, SAP beating rate is slowed by blockade of RyRs, SERCA and NCX as well as I_f, suggesting elements of both Ca^{2+} and membrane clocks contribute to pacemaking.[101, 150, 151] The molecular character of this SAP tissue is intermediate between SAN and atrial tissue. Compared to the SAN, the SAP has a lower expression of HCN4 in the rat and concordantly I_f has a long activation time and smaller amplitude in the cat.[152, 153] However, the rat SAP displays similar levels of Tbx3, $K_{ir}2.1$, $Na_v1.5$ and HCN1 to the SAN.[152]

1.5 Sinus node dysfunction in humans

SND in humans manifests clinically with bradycardia and episodic asystole. Symptoms can occur if the heart rate drops too low (e.g. <40 beats per minute (bpm)) or with long pauses (e.g. >3 seconds). Symptoms can include dizziness, syncope, collapse, confusion, chest pain, breathlessness or peripheral oedema due to reduced cardiac output. Those with early SND without significant haemodynamic compromise may be asymptomatic. The only effective treatment for SND is implantation of an electronic pacemaker. According to the most recent UK audit in 2014, just under 40,000 new pacemakers were implanted, 20% of them for SND.[6] The overall prevalence of SND in the UK is 0.03% affecting young and old, but it is much more common in the elderly.[5]

SND can be intrinsic within the SAN or caused by extrinsic factors or both. An Austrian study of 277 patients with compromising bradycardia showed that 51% of cases were caused by an extrinsic factor such as an adverse drug effect, electrolyte disturbance or heart attack. The rest were idiopathic and assumed to be due to intrinsic SND.[154]

The pathophysiology of 'idiopathic' SND remains unclear. Historically it is attributed to fibrosis and cell senescence.[155, 156] Contemporary evidence suggests that remodelling of membrane ion channels and intracellular Ca^{2+} cycling are important factors in SND.[157]

Bradycardia and pauses may be due to reduced SAN automaticity or SAN exit block. Electrophysiology studies are not routinely performed in SND but are sometimes done in equivocal cases. Overdrive atrial pacing can be used to measure the corrected sinus node

recovery time (cSNRT) and sinoatrial conduction time (SACT). These parameters will both be prolonged in 64% of SND cases, and 88% of all cases with prolonged cSNRT and SACT are specific to SND.[158] cSNRT is the length of time between the last paced beat and the next spontaneous beat, minus the spontaneous cycle length.[159] A short recovery time is important for the SAN to remain robust against ectopic electrical activity. A prolonged cSNRT may therefore suggest SND in the form of decreased intrinsic automaticity.

SND is also characterised by conduction delay along the CT, a more unicentric and caudal shift to leading pacemaker activity within the SAN, and areas of low voltage within the RA.[160] Table 1 and figure 9 summarise the processes and remodelling that are likely to be taking place to account for these electrophysiological changes. The evidence is discussed below.

1.5.1 'Idiopathic' sinus node dysfunction

'Idiopathic' SND is more common in the elderly.[161] For a long time fibrosis and atrophy of the SAN has been suggested as the cause. This was seen by studies in the 1970s in patients diagnosed with SND.[155, 156] However, the same studies also reported cases of SND associated with normal histology as well as cases of severe fibrosis associated with normal SAN function.[155, 156] Complicating matters further, SAN atrophy and fatty infiltration have been associated with ageing in general.[162] Therefore it cannot automatically be assumed that fibrosis and atrophy are directly causing or the only cause of SND.

Ageing causes electrical remodelling in the atria and the SAN, changing expression of key ion channels. $Na_v1.5$ is a Na^+ channel required to improve electrical coupling of the SAN to the surrounding RA myocardium.[163] Ageing rats demonstrated a reduction in $Na_v1.5$ around the SAN periphery, which may cause SAN exit block by interfering with SAN to RA coupling.[164] The gap junction Cx43 may also play a role in coupling cells at the SAN periphery, and ageing has been associated with reduced levels of Cx43 in the SAN periphery along with conduction slowing.[165]

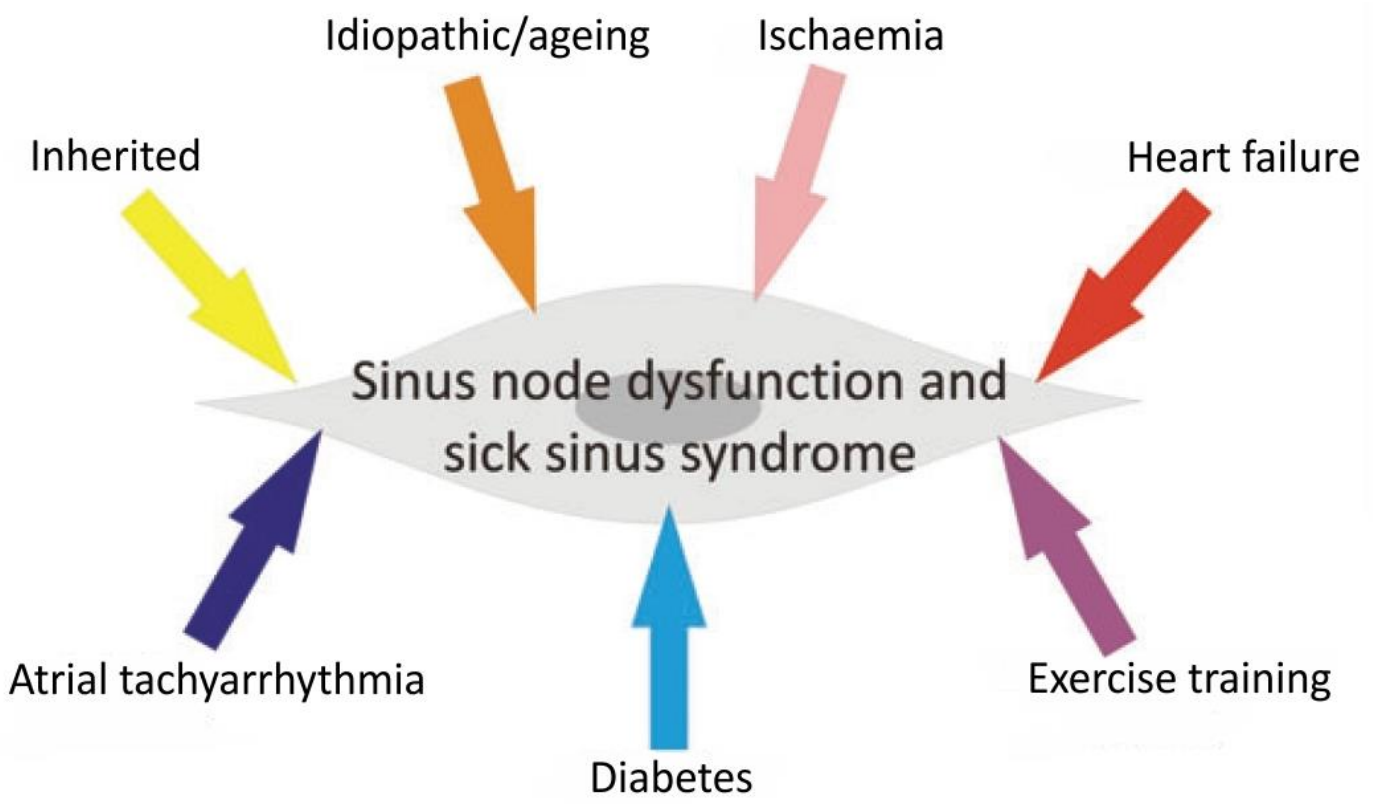

Figure 9. Diagrammatic summary of the various causes of SND

There are several causes of SND the most common being idiopathic as a result of ageing, however the others are all well recognised in association with SND. Inherited channelopathies leading to SND provide interesting insights into the precise mechanisms that can lead to SND which could also be relevant to idiopathic forms. Taken from Monfredi et al, 2010.[41]

Causes of SND	Ion channels and genes involved
Idiopathic/ageing	↓$Na_v1.5$,[164] ↓Cx43,[165] ↓$Ca_v1.2$,[166] ↓RYR2,[167] ↓HCN1,[167, 168] ↓HCN4,[168] ↓NCX1[168]
Atrial tachyarrhythmia	↓HCN2,[169] ↓HCN4[169]
Inherited	HCN4,[85-87, 170, 171] Scn5a ($Na_v1.5$),[172] RYR2,[173] CASQ2,[173, 174] AnkB[175]
Exercise training	↓HCN4,[176] ↓Tbx3[176]
Heart failure	↓HCN4[177]

Table 1. Summary of the genes and electrical remodelling involved in some causes of SND

The inherited genes are mutations seen in human families with SND, whereas in other types of SND electrical remodelling was seen in animal models. Downward arrows signify downregulation. From Choudhury et al, 2015.[178]

$Ca_v1.2$ is an L-type Ca^{2+} channel important in the phase 0 upstroke of the SAN AP.[55] Ageing guinea-pigs demonstrated a decline in $Ca_v1.2$ progressing from the SAN centre outwards, increasing sensitivity to the Ca^{2+} blocker nifedipine and reducing spontaneous SAN activity.[166] Ageing rats showed decreased levels of RYR2 and HCN1, lower intrinsic heart rate, prolonged APD and prolonged cSNRT.[167] Lastly, ageing mice demonstrated bradycardia and prolonged SACT associated with reduced expression of HCN1, HCN4, $Na_v1.5$ and many other K^+ and Ca^{2+} channels.[168]

In summary ageing is associated with remodelling of both structural and molecular features and so the cause of idiopathic SND in the elderly is probably a combination of many factors.

1.5.2 Sinus node dysfunction and tachyarrhythmia

Paroxysmal atrial tachyarrhythmia such as atrial fibrillation (AF) are often seen in association with SND. This can result in excessively fast as well as slow heart rates and therefore termed 'tachy-brady syndrome'. Some patients with SND demonstrate atrial remodelling including atrial enlargement, increased refractoriness and prolonged conduction times, predisposing to re-entrant circuit formation and increasing risk of AF.[160] SND could therefore be a prodrome of AF.

Conversely, chronic AF may predispose to SND. Patients with tachy-brady syndrome who flip between a fast AF rhythm and sinus bradycardia have demonstrated a caudal shift in the leading SAN pacemaker and reduced sensitivity to β-adrenergic stimulation.[36] A common treatment for persistent AF is electrical cardioversion, passing a short burst of DC current through the heart using a defibrillator to try to restore sinus rhythm. Once reverted these patients often demonstrate bradycardia and prolonged cSNRT.[179] Furthermore, the degree of post-cardioversion SNRT is thought to indicate the level of atrial remodelling and therefore predict the likelihood of AF recurrence.[180] Over time following cardioversion, SAN function can return to normal which suggests reversibility of AF-induced SAN remodelling.[181] This remodelling may involve changes in expression of

HCN channels. In a canine model of atrial tachycardia where dogs were artificially paced at 400 bpm, HCN2 and HCN4 were downregulated in the SAN by >50%, and I_f density was reduced by 48%.[169] 20 Hz atrial pacing in dogs has also been shown to lead to prolonged SNRT and bradycardia, reducing maximal and intrinsic heart rate.[182]

1.5.3 Familial sinus node dysfunction

Genotyping rare cases of familial SND has led to the discovery of specific gene mutations and associated channelopathies, allowing insight into their role in normal SAN function. DNA sequencing was used to screen patients with bradycardic phenotypes focusing on several candidate pacemaker genes.

Several families with inherited bradycardia were screened for point mutations or deletions within the *Hcn4* gene.[85-87, 170, 171] One patient with idiopathic SND was found to have a heterozygous single base deletion within *Hcn4* leading to a truncated C-terminus.[85] This mutant *Hcn4* gene was then transduced *in vitro* in COS-7 cells which demonstrated I_f insensitive to increased cAMP levels.[85] Three other families each exhibited three different *Hcn4* mutations that when transduced *in vitro* expressed HCN4 channels with more negative MDPs.[86, 87, 170] A group of Moroccan-Jewish patients exhibited a novel *Hcn4* point mutation that also led to HCN4 channels with more negative MDPs.[171] Many of these studies suggested an autosomal-dominant inheritance pattern. Each mutation changed HCN channel structure in a unique way, highlighting how numerous anomalies can lead to incorrect channel functionality and affect heart rate.

Scn5a gene mutations lead to dysfunction of the $Na_v1.5$ channel, known to be associated with many cardiac diseases including long QT syndrome, Brugada syndrome, dilated cardiomyopathy, atrial fibrillation in addition to SND.[172] $Na_v1.5$ exists in many different areas of the heart which is why patients with *Scn5a* mutations can present with a syndrome of multiple phenotypes.[172] Since $Na_v1.5$ exists at the SAN periphery rather than its centre, dysfunction of this channel can lead to conduction slowing into the surrounding atrium, SAN exit block and sinus arrest.[172, 183] Several different types of *Scn5a*

mutation are associated with SND with a suggested autosomal-recessive pattern of inheritance.[172]

Catecholaminergic polymorphic ventricular tachycardia (CPVT) is an inherited condition associated with sudden death in young patients as it causes stress-induced ventricular tachycardia leading to syncope and cardiac arrest. Two gene mutations are implicated, those for RYR2 and calsequestrin 2 (CASQ2), both involved with intracellular Ca^{2+} cycling. Patients exhibit sinus bradycardia with otherwise normal ECGs.[173, 174] Bradycardia is thought to be due to dysfunctional SR Ca^{2+} release and disruption of the Ca^{2+} clock.[174] Inherited RYR2 mutations show an autosomal-dominant pattern of inheritance, whereas most cases of CASQ2 mutations are autosomal-recessive.[174]

Ankyrin-B (AnkB) is a protein involved in anchoring certain ion channels to the cell membrane such as Na^+/K^+-ATPase, NCX and inositol triphosphate receptor 3 (IP3) and can therefore be implicated in dysfunction of these channels.[184] Mutations are associated with CPVT, long QT-syndrome and SND.[184] One study reports on two families demonstrating long QT intervals, histories of sudden death, AF and pacemaker implantation due to severe bradycardia.[175] Heterozygous AnkB mutations in transgenic mice were linked to severe SND associated with abnormal localisation and reduced expression of NCX1, Na^+/K^+-ATPase, IP3 and $Ca_v1.3$.[175]

1.5.4 Athletes and sinus node dysfunction

Endurance athletes often exhibit significant bradycardia as a result of exercise training, with one of the lowest resting heart rates belonging to five-time Tour de France winner Miguel Indurian recorded at 28 bpm. Other notable bradycardic athletes include Mo Farah, Usain Bolt, Sir Bradley Wiggins, Sir Chris Hoy and Sir Steve Redgrave all with resting rates in their 30s. A slow resting heart rate is therefore associated with fitness however some athletes have been known to go on to need pacemaker implantation later in life suggesting that this bradycardia is not merely compensating for increased cardiac output.[185] There is also a higher incidence of AF in athletes.[186] Bradycardia in athletes is

normally put down to high vagal tone i.e. is thought to be neurally mediated. However 'intrinsic heart rate', revealed by full autonomic pharmacologic blockade, has been shown to be lower in exercise trained individuals implicating electrical remodelling of the SAN.[187]

Heart rate was monitored in trained versus sedentary rats and mice demonstrating intrinsic bradycardia in response to exercise.[176] Trained animals also showed downregulation of HCN4 and Tbx3 compared to controls.[176] This study demonstrated for the first time that exercise training induces electrical remodelling in the SAN and that downregulation of HCN channels could be a direct cause of bradycardia.

1.5.5 Ischaemia and sinus node dysfunction

Acute myocardial ischaemia can lead to bradycardia, but this is often due to abnormal autonomic tone or injury to SAN tissue through lack of perfusion rather than intrinsic SAN dysfunction.[188, 189] Chronic ischaemia from coronary artery disease as a cause of SND is more controversial. The prevalence of both coronary artery disease and SND increase with age and so patients may well have the two concomitantly. Studies looking at the correlation in more detail show mixed results.

Angiography has been used to assess sinus node artery patency in patients with and without SND. One study showed reduced sinus node artery filling in only 20% of patients with SND and no significant obstruction in any patient.[190] Another study showed significantly lower intrinsic heart rates, prolonged cSNRTs and prolonged SACTs in cases of severe sinus node artery stenosis (>75%) versus moderate to no stenosis (<75%).[191] Other patients with SND had no sinus node artery disease and patients with normal SAN function were found to have severe sinus node artery disease.[156, 192] It therefore remains unclear whether a causal association between chronic ischaemia and SND actually exists.

1.6 Progress in biopacemaking

The concept of 'biopacemaking' evolved following the advent of new technologies that are capable of modifying cells on a molecular level, allowing us to either create ectopic

pacemaker tissue or repair dysfunctional pacemaker tissue. Multiple groups have taken up the challenge to find the best method to create biopacemakers that are as robust and reliable, deliver physiological beating rates, are autonomically sensitive, remain persistent over time and can be delivered safely. The ideal biopacemaker would aim to recapitulate the complex nature of the SAN as closely as possible. However, biopacemaker research is still in its infant stages, with more to learn about the most effective gene targets, methods of delivery, locations of delivery and safety. So far several strategies have been tried, focusing on either gene transfer using viral vectors or cell-based therapies using stem cells or engineered cells.

1.6.1 Gene therapy

One of the first ideas was to upregulate β-adrenergic receptors in the SAN by injecting a naked plasmid incorporating the β_2-receptor gene into the hearts of pigs and mice. This increased basal heart rate and sensitivity to sympathetic stimulation.[193, 194] The drawback to this strategy was that over-stimulation of the β-adrenergic pathway can promote arrhythmias. It also assumes that there would be healthy pacemaker cells left to stimulate which may not be the case in SND. Although naked plasmids are low in toxicity and are non-infectious, they are also relatively inefficient at transfecting cells and expressing the gene of interest.[195]

Recombinant adenoviruses (RAds) have been used in gene therapy effectively for several decades. One of the first applications in biopacemaking was to downregulate $I_{K,1}$ in the guinea pig LV *in vivo*. A dysfunctional, dominant-negative K_{ir}2.1AAA construct was overexpressed using a viral vector, which reduced $I_{K,1}$ by 50-90%, prolonged APD, reduced the speed of repolarization and left a more positive MDP. It was successful in producing slow ectopic pacemaker activity in the LV, originating from cells exhibiting DD.[52] However, there were concerns that prolonged repolarization could be associated with ventricular tachycardia and sudden death, since this is known to occur in an inherited form of $I_{K,1}$ suppression called Andersen syndrome.[196]

Focus shifted to upregulation of HCN channels to enhance the pacemaker current, I_f, without prolonging APD. Overexpression of HCN2 in neonatal rat myocytes resulted in robust pacemaker activity.[197] Following this, HCN2-expressing adenovirus was injected into the left atria of dogs creating a site of spontaneous activity when the SAN was inhibited by vagal stimulation. There was also some vagal responsiveness to the new left atrial pacemaker.[198] The same group overexpressed HCN2 in the canine left bundle branch, giving rise to stable albeit slow pacemaker activity from the injection site when the SAN and AVN were inhibited by vagal stimulation or complete heart block was induced by radiofrequency ablation of the AVN. This new activity was sensitive to sympathetic stimulation.[199]

Since HCN2 only gave rise to relatively slow pacing rates, a chimeric HCN212 channel was developed, combining the transmembrane pore-forming portion of HCN1 for superior channel kinetics, and the extracellular and intracellular portions of HCN2 for superior autonomic sensitivity. However, when transduced into the canine left bundle branch it overshot in terms of rate, resulting in episodic ventricular tachycardia that was responsive to I_f block with ivabradine.[200]

Another strategy to speed up pacing from HCN2 overexpression was to try to combine it with adenylyl cyclase (AC1) overexpression.[201] When stimulated by Ca^{2+}, AC1 acts downstream within the β-adrenergic pathway to increase levels of cAMP. This amongst cAMP's other mechanisms of increasing heart rate leads to increased HCN2 activity. Recombinant adenovirus expressing HCN2 and AC1 either singularly or in combination were injected into the left bundle branch of dogs with induced complete heart block. Dogs that received AC1 alone or HCN2-AC1 combined showed a robust increase in basal heart rate and reduced dependence on backup electronic pacing. However, the HCN2-AC1 group overshot to develop ivabradine-sensitive ventricular tachycardia upto 250 bpm. In fact AC1 alone provided the best results overall with basal rates of 60-90 bpm, reduced overdrive suppression and improved autonomic sensitivity versus HCN2 alone.[201]

The same group followed this up by combining HCN2 with the skeletal muscle Na^+ channel (SkM1) with even better results than AC1. SkM1 has a faster inactivation curve than cardiac $Na_v1.5$ and effectively lowers the threshold potential for phase 0 depolarization. Physiological beating rates, high autonomic sensitivity and very low dependence on backup pacing were achieved.[202]

Transcription factors involved in the development of the SAN are interesting targets in biopacemaking as they are known to activate multiple pacemaker mechanisms. The most successful of these has been Tbx18, which is involved in early SAN development. It was used to directly reprogramme ventricular myocytes morphologically and functionally into pacemaker cells *ex vivo* as well as *in vivo* within 48 hours of transduction.[203] When *ex vivo* isolated neonatal rat ventricular myocytes (NRVMs) were infected with Tbx18-expressing adenovirus both membrane and Ca^{2+} clocks were affected with upregulation of HCN4 and increased intracellular Ca^{2+} release events from the SR. When the ventricular apex of guinea pigs was injected *in vivo* with the same virus, an ectopic pacemaker developed at the site of injection within 2-4 days. Cells subsequently isolated from this site had developed SAN-like spindle-shaped morphology, exhibited beating rates comparable to isolated SAN myocytes and were autonomically sensitive.[203]

The group went on to overexpress Tbx18 in pigs with induced complete heart block.[204] This large animal model was needed as a step towards prospective human translation. Tbx18-expressing adenovirus was injected into the right ventricular septum of these pigs. They maintained physiological heart rates between 75-80 bpm from day 2 to day 14, and relied on backup pacing <1% of the time between day 5 and 11. As in their previous work on smaller animals, spindle-shaped transduced cardiomyocytes were isolated from the injection site, mRNA levels for $K_{ir}2.1$, Nkx2-5, $Na_v1.5$ and Cx43 were downregulated and HCN4 mRNA levels were upregulated.[204]

Tbx3 is another key transcription factor involved in SAN development, directly repressing the atrial gene programme and indirectly promoting the pacemaker gene programme.[16] This made it a logical target for biopacemaking. Tamoxifen induced overexpression of

Tbx3 in transgenic mice demonstrated efficient repression of the working myocardial genes Cx40, Cx43, $K_{ir}2.1$ and $Na_v1.5$.[205] However HCN4 was not upregulated rather it was downregulated in the ventricle and HCN1 was upregulated in the atrium. Furthermore, I_f was not recordable from isolated atrial cardiomyocytes. The group went on to overexpress Tbx3 using a lentiviral vector in NRVM monolayers, observing spontaneous activity based on DD, conduction slowing, reduced $I_{K,1}$ and I_{Na} in 25% of transduced cells, but again I_f was absent.[205]

1.6.2 Cell-based therapies

Cell-based therapy is an alternative method for delivering a biopacemaker to the heart. Pacemaker cells can be grown or engineered *in vitro* and then transplanted. Human embryonic stem cells have been used for this purpose. The cells were forced to develop into cardiac tissue using transcription factors and then a sub-population of these cells, that gave rise to pacemaker activity, were taken and implanted into pig ventricles with induced complete heart block.[206] These cells were reported to show strong I_f and weak $I_{K,1,}$ demonstrating DD and continuing to support ventricular contractions for up to three months. Interestingly, Na^+ current rather than L-type Ca^{2+} current was responsible for the phase 0 upstroke.[207] There are ethical concerns however with using human embryos.

Foetal and neonatal cells that have already differentiated into pacemaker cells have been grafted into the ventricles of pigs with complete heart block. They also produced an idioventricular rhythm originating from the cell injection site that was much faster than the ventricular escape rhythm in the controls, with added sensitivity to sympathetic stimulation.[208, 209] Foetal SAN cardiomyocytes have also been transplanted in dogs with AV block with similar success.[210] However, cell survival has been an issue as well as the need for immunosuppression to avoid cell rejection.

Fibroblasts taken from guinea pig lungs were engineered to incorporate HCN1 channels and fused to ventricular myocytes of the same animal. Autologous transplantation would

be an advantage eliminating cell rejection. Ectopic pacemaker activity from the injection site was demonstrated, sensitive to β-adrenergic stimulation.[211]

Adult human mesenchymal stem cells (hMSCs) show strong expression of Cx43 and Cx40 and therefore can couple with cardiac myocytes. They also show protection against rejection in human to human transplantation. They have been used as biopacemakers by loading them with HCN2 channels via electroporation and implanting them into canine ventricles. When vagal stimulation blocked SAN activity and AVN conduction, ectopic pacemaker activity emanated from the injection site, continuing for at least six weeks.[212]

Induced pluripotent stem cells (iPSCs) are fibroblasts obtained from skin or hair that have been dedifferentiated to become pluripotent through the use of transcription factors.[213] Then, like embryonic stem cells, they can become pacemaker cells if led down that lineage. They do not have the ethical concerns of obtaining stem cells from human embryos and can be autologous so therefore avoid the need for immunosuppression. iPSC-derived cardiomyocytes have been studied *in vitro* demonstrating spontaneous beating over 15 days as well as β-adrenergic sensitivity.[214] There is ongoing work *in vivo* in dogs with induced complete heart block in which iPSC-derived cardiomyocytes have been injected with success.[215]

Cell-based therapies suffer from a few problems. Xenotransplantation leads to rejection and the need for immunosuppression. There can be heavy cell loss through apoptosis. Stem cells may also migrate or differentiate into non-functional or malignant forms.[114]

1.6.3 Future challenges for biopacemaking

There are still several challenges to overcome before biopacemakers can compete with the electronic pacemaker. The ideal biopacemaker needs to be permanent, reliable and responsive to changing physiologic demands. They would also need to of course be safe, cost effective and suitable for clinical trials in humans.

The ideal molecular target to modulate still needs to be identified. Reducing $I_{K,1}$ revealed pacemaking activity but also prolonged repolarization which could lead to ventricular arrhythmias.[52, 196] Use of HCN channels, including the chimeric HCN212 channel, provided proof of concept that biopacemaking can produce an ectopic pacemaker responsive to autonomic stimulation and I_f blocking drugs like ivabradine. However, HCN2 expressed alone in ventricular tissue was too slow whilst HCN212 overcompensated and led to ventricular tachycardia.[200] Strategies involving AC1 and SkM1 have produced results closest to physiological parameters so far, and Tbx18 also looks very promising.[201-203] Certainly, reproducing the complexity of the SAN will not be straight forward and we have only scratched the surface. Further work on Ca^{2+} clock components would also prove interesting.

The ideal location for a biopacemaker needs to be carefully considered. Delivering it to the right ventricle might emulate an electronic pacemaker but the working myocardial substrate seems to limit its function.[216] Chronic RV apical pacing may also be detrimental to cardiac function.[7] Purkinje fibres have properties that are more suited to sustaining automaticity, but they are known to have a relatively high sensitivity to overdrive suppression, meaning they could develop prolonged pauses in the presence of a rapid competing impulse or arrhythmia.[217] Restoring a physiologically normal system sounds attractive targeting the dysfunctional SAN itself or nearby SAP tissue. This would provide a more supportive substrate being already capable of pacemaking and sensitive to autonomic control. However, those with concurrent AVN dysfunction would still need added intervention. SAP tissue is yet to be fully explored as a potential location for delivery of a biopacemaker.[95]

The current methods for delivering biopacemakers to the heart have their drawbacks. Adenoviruses can be used experimentally but only express the target gene transiently in episomal DNA and so would not provide a long-lasting effect.[218] Adeno-associated virus displays longer lasting expression but it is unclear whether this expression is episomal or truly genomic, and it also has a smaller packaging capacity for inserting target genes.[218]

Biopacemaking strategy	Outcomes/advantages	Drawbacks
VIRAL VECTOR-BASED		
β2-receptor[193, 194]	Increased basal heart rate and sympathetic sensitivity	May promote arrhythmias
I_{K1} knockout[52, 196]	Produced slow ectopic activity	Prolonged QT, risk of arrhythmias
HCN2[197-199]	Robust pacemaker activity	Slow beating rate
HCN212 chimera[200]	Robust pacemaker activity	Excessive beating rate
HCN2 + AC1[201]	Robust pacemaker activity	Excessive beating rate
HCN2 + SkM1[202]	Physiological pacemaker activity	Short-term expression
Tbx18[203, 204]	Robust pacemaker activity, morphological changes	Temporary expression
Tbx3[205]	Reduced atrial gene expression	No ectopic pacemaking or I_f current
CELL-BASED		
Human embryonic stem cells[206]	Ectopic pacemaker activity, strong I_f and weak $I_{K,1}$	Cell survival, need for immunosuppression and ethical considerations
Foetal SAN cells[208-210]	Ectopic pacemaker activity	Cell survival, need for immunosuppression and ethical considerations
Fibroblasts + HCN1[211]	Ectopic pacemaker activity, no ethical concerns and no cell rejection if autologous	No *in vivo* studies yet
hMSCs + HCN2[212]	Ectopic pacemaker activity, protected from rejection	Cell differentiation and migration
iPSC-derived cardiomyocytes[213-215]	Ectopic pacemaker activity, no ethical concerns and no cell rejection if autologous	Cell differentiation and migration

Table 2. Summary of biopacemaking strategies tried so far

Several biopacemaking strategies have been tried over more than 15 years. Above is a summary of these studies, their outcomes and their drawbacks.

Lentivirus is thought to be the better vector for stable genomic expression, but its long-term safety remains unclear being potentially oncogenic.[218] This is because there is no control over where the target gene is inserted into the host genome and it may lead to insertional mutagenesis. With cell-based therapies such as allogeneic stem cell or modified cell implantation, there is a risk of cell death, cell migration or rejection. Stem cells may transform into the wrong cell type or cause malignancy. Long-term immunosuppression might also be an unwanted necessity if these cells trigger a host immune response.[114] There are therefore still many problems that need to be solved before any option can be put forward as a viable strategy for human translation.

1.7 Summary of rationale for this project

This project will use an *in vitro* rat model of SND, which utilises a bradycardic leading pacemaker within SAP tissue located in the RA superiorly to the IVC and septal to the CT. SAP tissue shares many similarities with the dysfunctional SAN. Indeed there is evidence that in some forms of SND, the SAN develops an exit block and the leading pacemaker shifts to SAP tissue.[137] Various gene targets or transcription factors can then be used to modulate the function and molecular composition of this SAP tissue alone or in combination quickly, safely and cheaply, providing proof of concept of their effects.

The rat model was chosen due to physiological relevance with regards to pacemaker mechanisms relying on elements of both membrane and Ca^{2+} clocks which have been studied extensively in control animals creating a large body of data to compare to. There were also technical advantages such as appropriate tissue size and thickness for culture, electrical recording and viral injections.

The genes of interest for this study are Tbx18 due to its role in early morphogenesis of the SAN, Tbx3 due to its role in fine tuning the pacemaker phenotype in the CCS. In addition, NCX1 as it is a point of integration in both Ca^{2+} and membrane clocks thus making it an attractive target. We hypothesise that upregulating these genes of interest in SAP tissue using an adenoviral vector will individually improve function and change the molecular

attributes of the SAP leading pacemaker closer to that seen in the intact SAN, whilst maintaining characteristics of autonomic sensitivity and low overdrive suppression.

Although biopacemaking strategies using Tbx18 and Tbx3 have been studied in ventricular tissue and transgenic mice respectively,[16, 203-205] no-one has yet attempted to specifically upregulate these genes in SAP tissue. SAP tissue may hold certain advantages over ventricular tissue as a substrate since SAP tissue already exhibits regular pacemaking. Results of our study may provide insight into the feasibility of applying similar techniques to dysfunctional SAN tissue *in vivo* as a therapeutic strategy.

1.7.1 Specific objectives

Firstly, following on from previous work in the group, we aim to further characterise the molecular and functional nature of SAP tissue. We will try to visualise SAP tissue using immunohistochemistry. This will guide subsequent experiments to aid delivery of adenovirus to the right location. We will also assess change in SAP tissue function in response to I_f blockade, β-adrenergic stimulation and RYR blockade.

A custom tissue culture setup will be created to allow culture of isolated SAN and SAP preparations to keep them beating for several days whilst simultaneously recording continuous electrical signals from the tissue. Control SAN and SAP preparations will be compared to experimental SAP preparations injected with adenovirus expressing various genes of interest. We aim to upregulate Tbx18, Tbx3 and NCX1 individually in isolated SAP preparations. An additional control group will utilise SAP preparations injected with adenovirus expressing the inert protein GFP.

Each group will be characterised functionally to assess the properties important for normal SAN function; beating rates, response to pharmacology and overdrive suppression. Additionally, tissue samples from each preparation will be harvested following each experiment to measure mRNA levels of key pacemaker genes using RT-qPCR and key proteins/ion channels using immunohistochemistry.

1.7.2 List of hypotheses

1. HCN4-positive/Cx43-negative tissue similar to the SAN exists in the inferior RA near the inferior vena cava (SAP area).

2. SAN and SAP tissue will respond similarly to I_f blockade, β-adrenergic stimulation and RYR blockade.

3. RAd can be used to upregulate our genes of interest Tbx18, Tbx3 and NCX1 in SAP tissue.

4. Upregulating Tbx18 will cause an increase in beating rate in SAP tissue.

5. Upregulating Tbx3 will cause an increase in beating rate in SAP tissue.

6. Upregulating NCX1 will cause an increase in beating rate in SAP tissue.

7. Upregulating our genes of interest will individually reduce overdrive suppression in SAP tissue.

8. Upregulating Tbx18 will increase response to I_f blockade and β-adrenergic stimulation in SAP tissue.

9. Upregulating each gene of interest will alter expression of other genes or proteins related to pacemaking in SAP tissue.

2. METHODS

2.1 Sinoatrial node and subsidiary atrial pacemaker isolation

An *in vitro* model of SND has previously been developed within our group using SAP tissue isolated from the rat RA.[95, 152] Two-month-old male Wistar Hannover rats weighing 300-350g were humanely killed in accordance with Home Office regulations under the Animals (Scientific Procedures) Act 1986.[219] RA isolation was done in sterile Tyrode's solution pre-warmed to 37°C and bubbled with 5% CO_2 / 95% O_2 gas (appendix A1). The anterior wall was divided, opening the RA and revealing the endocardium vertically from the SVC to the tricuspid valve (TV), and horizontally from the interatrial septum to the right atrial appendage (RAA). On the endocardial posterior wall, the sinus node artery was visualised under a light microscope and used as a marker for the central SAN. The association between sinus node artery and the SAN has been described before.[21, 47]

The SND model, or 'SAP preparation', was formed by dividing the isolated RA preparation horizontally at the level of the fossa ovalis thus isolating the central SAN in the superior section from SAP tissue in the inferior section. The AVN and coronary sinus were also removed by dissecting up from the TV into the IVC orifice and then across from the IVC to the interatrial septum (figure 10). In the remaining inferior section a new bradycardic leading pacemaker has been shown to take over just above the IVC in the absence of the SAN and AVN (figure 11).[95] The superior section was utilised for control SAN recordings. Beating rates of superior sections were validated against whole RA preparations in order to ensure that removing the inferior portion did not affect SAN function.

2.2 Recombinant adenoviruses

RAds expressing various genes were acquired. Ad-Tbx18 and Ad-Tbx3 for expression in rat tissue were purchased (ABMGood) at a titre of $1x10^6$ plaque forming units per millilitre (pfu/ml). These were amplified and purified before administration into the SAP preparation (see method below). Ad-NCX1-GFP was kindly donated to us by Professor Godfrey Smith (University of Glasgow) at a titre of $1.5x10^{10}$ pfu/ml. This was also

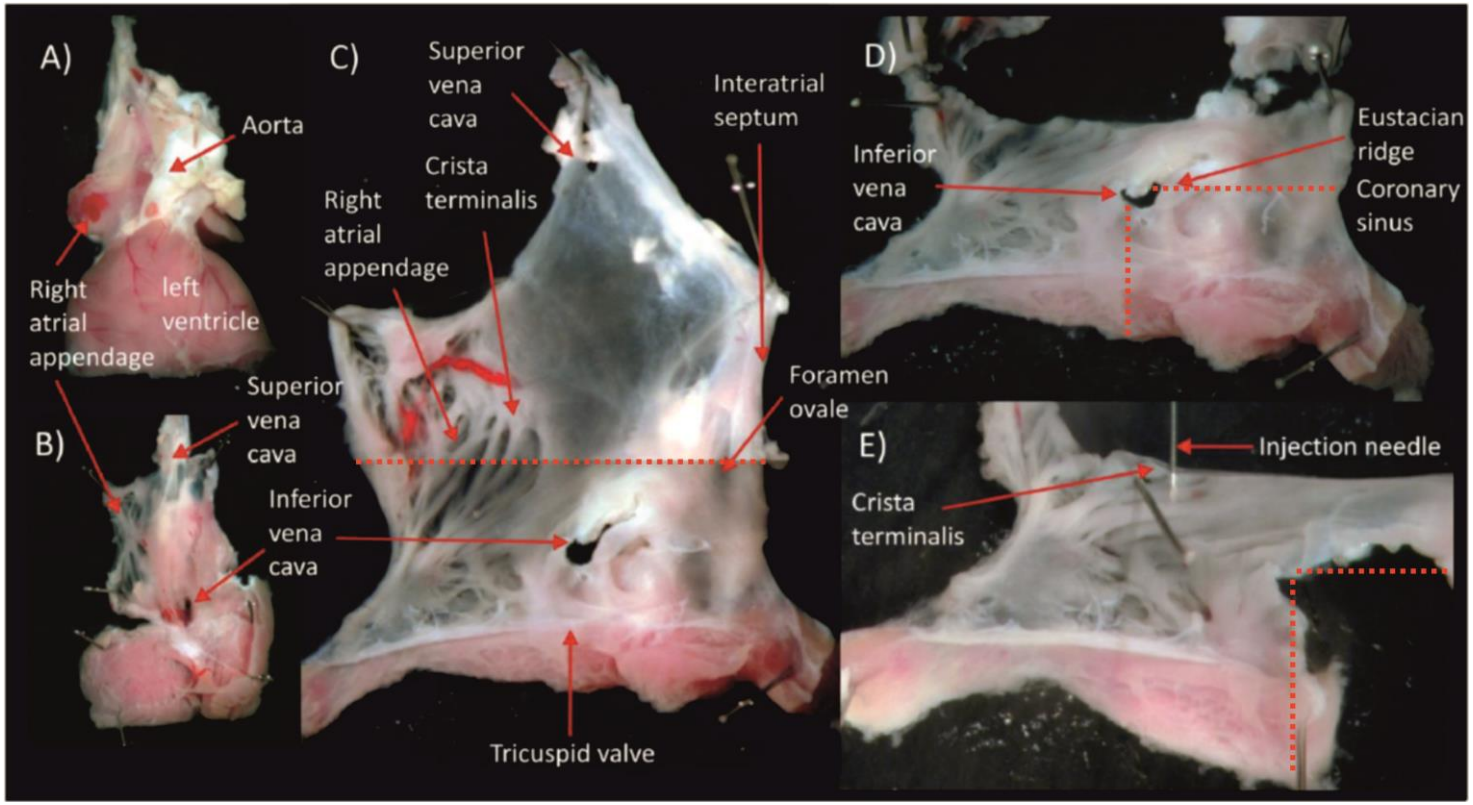

Figure 10. Preparation of the SND model

(A-C) The whole heart is removed from the thorax of the rat and the RA is isolated. The anterior wall is dissected to form the SAN preparation. (D,E) The preparation is hemisected at the level of the fossa ovalis and the AVN is removed by dissecting down and across from the IVC (red dotted lines). The remaining tissue harbours bradycardic SAP tissue which forms the basis of the SND model. Adapted from Morris, 2010.[95]

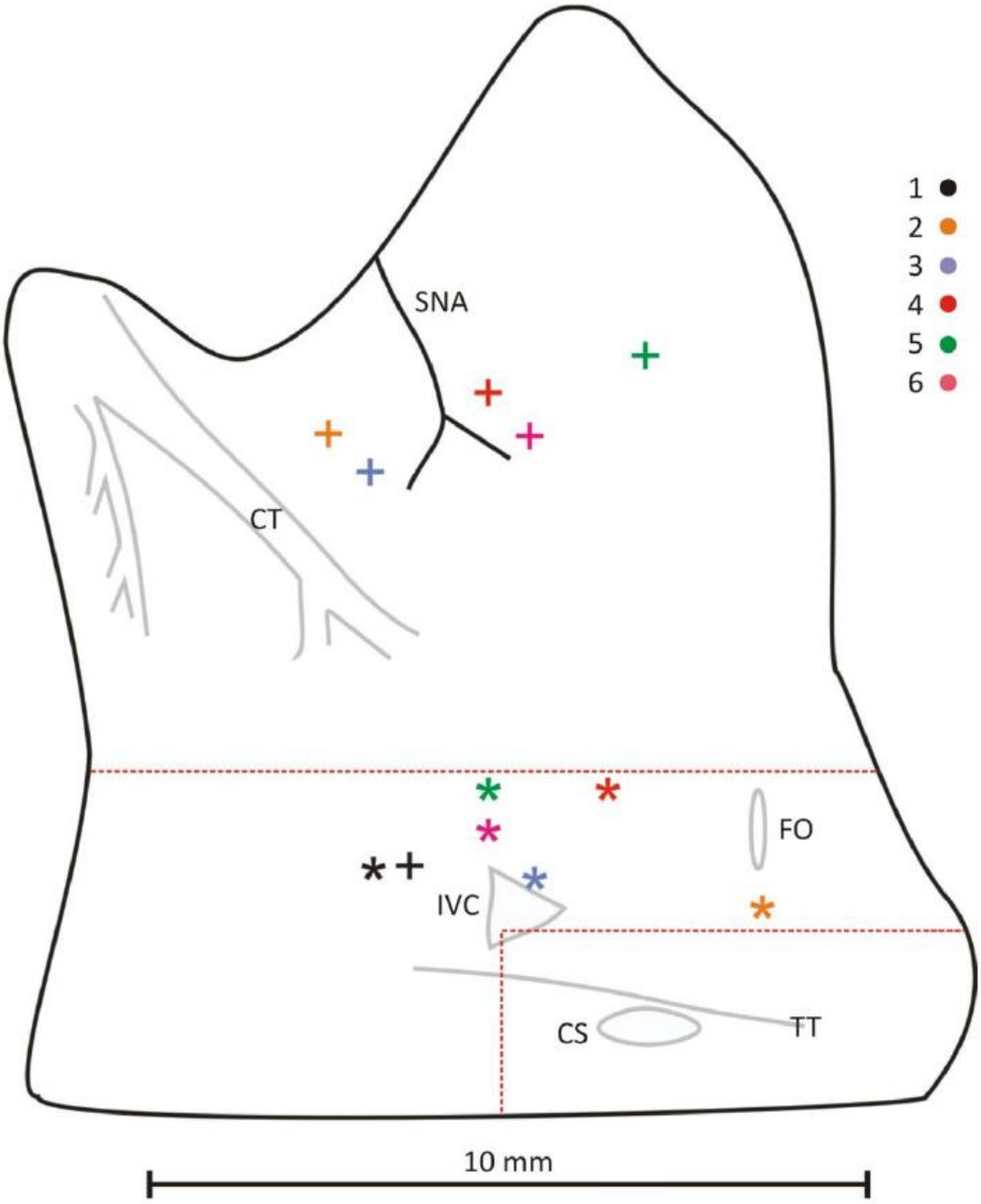

Figure 11. Leading pacemaker site mapping in SAN and SAP preparations

Diagram showing leading pacemaker sites mapped in SAN (crosses) and SAP preparations (asterisks). The red dotted lines represent approximate sites of division to create the SAP preparation. Mapping was performed using two sets of bipolar electrodes to determine the site of earliest activation. SNA, sinus node artery; CT, crista terminalis; IVC, inferior vena cava; FO, fossa ovalis; CS, coronary sinus; TT, tendon of todaro. From Morris, 2010.[95]

amplified and purified in order to maximise stock. Also already available to the group were Ad-GFP and Ad-LacZ at $1x10^{10}$ pfu/ml.

These RAds have been engineered to lack the E1 and E3 genes normally present in wild-type adenoviruses which they need to replicate.[220] This is a safety feature to ensure accidental exposure to the virus will not result in widespread infection. The amplification process therefore starts by growing Ad293 cells (Stratagene), human embryonic kidney cells which are specifically developed to grow easily in culture and contain the E1 gene so that viruses can replicate when the cells are infected by them. The timing of infection of the cells is crucial so that the cells are in their 'log phase' or fastest phase of growth and are of sufficient number. This is usually when the bottom of the flask is about 70-80% confluent with healthy looking cells seen under inverted phase contrast microscopy.[221, 222]

2.2.1 Amplification of viruses

The amplification protocol was as follows. All steps were performed in a strictly sterile manner within a laminar flow hood as per university 'genetically-modified organism' guidelines. First $1x10^6$ of stock Ad293 cells were recovered from liquid N_2 storage and thawed quickly in a 37°C waterbath. The cell suspension was transferred to a 15 ml tube, centrifuged at 300 g for 5 minutes and the freezing medium (appendix A1) supernatant was discarded. The cell pellet was resuspended in fresh pre-warmed 293 growth medium (appendix A1), transferred to a standard 75 cm^2 culture flask (labelled "flask one") and topped up to 15 ml of 293 medium. An even spread of cells was achieved by gently swirling the flask before placing it in a 37°C / 5% CO_2 incubator. Every time a flask was placed back into the incubator it was critical to ensure the cap was open slightly or had filtered holes to allow CO_2 into the flask or the cells would die. Cells were inspected each day under an inverted phase contrast microscope to check that they were adhering to the base of the flask and growing well.

On day 2, a second 75 cm^2 flask (labelled "flask two") of Ad293 cells was initiated in the exactly the same way as above for use later in the process.

On day 3, flask one was inspected to make sure it was 70-80% confluent and then 'passaged'. Passaging involved gently removing the medium from the flask without disturbing the cells and adding 10 ml pre-warmed phosphate buffered saline (PBS) (Life Technologies). The PBS was gently swirled within the flask and then removed. 1.5 ml of 0.25% trypsin solution was added to the flask and left at 37°C for 10-15 minutes to cause cells to detach from the base. The detached cells were easily resuspended in 8 ml fresh 293 medium within the flask by agitation and tituration. 2 ml of the cell suspension was transferred to another 75 cm^2 flask and topped up to 15 ml 293 medium. This meant that 1 in 4 cells were transferred. The new flask was then put back into the incubator.

On day 4, flask two was inspected to ensure cells were 70-80% confluent. The same passaging method as above was used to split all the cells equally into 10 x 175 cm^2 flasks and topping each one up to 20 ml of 293 medium. Flasks were returned to the incubator.

On day 5, flask one, having been passaged once on day 3, was inspected to ensure it was 70-80% confluent and then infected with the RAd of choice at a multiplicity of infection (MOI) of around 1-10, meaning 1-10 pfu of virus per cell. This was calculated using estimated 293 cell monolayer densities (appendix A2) and known viral titres. After gently removing the old medium from the flask, 100-200 µl of stock virus was added to 15 ml of fresh 293 medium and gently added to the flask, before returning it to the incubator.

On day 7 all flasks were inspected again. The 175 cm^2 flasks were all around 60-70% confluent by this stage. The infected 75 cm^2 flask demonstrated 'cytopathological effect' (CPE) in 90-95% of cells, that is they had all rounded up in shape and almost detached from the base of the flask as a result of being infected (figure 12). Care was taken not to let this process go on too long to cause all the cells to completely detach as this would reduce viral titre. The infected cells were suspended using the medium already in the flask by agitation and tituration, and then mixed with 200 ml of fresh 293 medium in a separate sterile bottle. Old medium from all the 175 cm^2 flasks was removed gently and the infected bottle of medium was split equally across the 175 cm^2 flasks to provide each with roughly 20 ml of infected medium. The flasks were returned to the incubator.

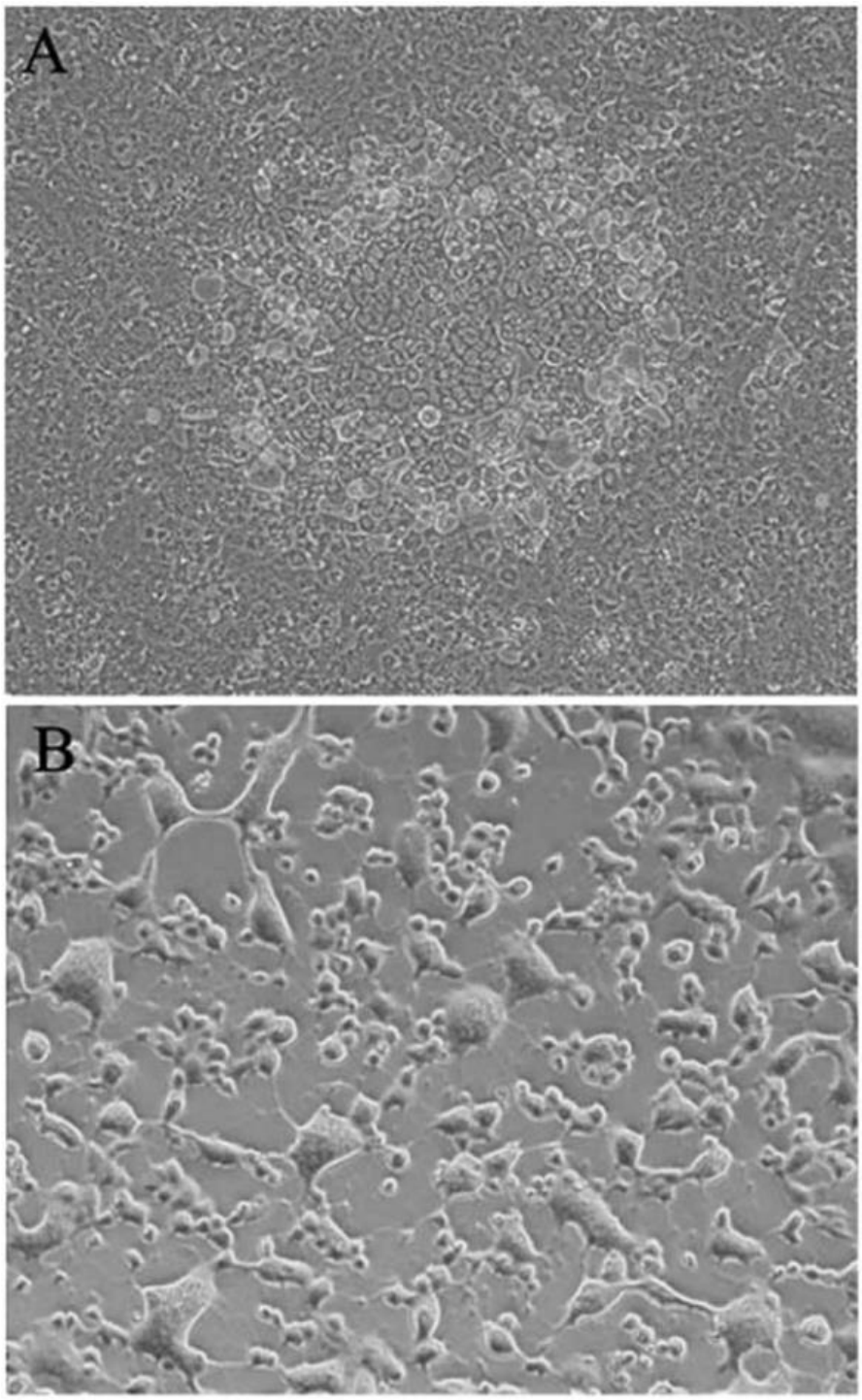

Figure 12. Inverted phase contrast microscopy showing cytopathological effect

(A) Uninfected 293 cells at 100% confluency and (B) cytopathological effect (CPE) referring to cells that show signs of viral infection. During CPE cells round up in shape and start detaching from the base of the flask. This occurs when viral titres are at their highest and this is the best time to commence viral purification. Taken from Zhang et al, 2013.[223]

By day 10-11 all the 175 cm^2 flasks showed 90-95% CPE and cells were ready to be harvested for virus purification.

2.2.2 Purification of amplified viruses

Purification of the virus involved using the "AdEasy Virus Purification" kit (Agilent Technologies) for a 200 ml preparation. The kit uses filters, which bind specifically to virus particles based on charge and size. The harvested solution was transferred to four 50 ml tubes and centrifuged at 3,500 g for 15 minutes to pellet intact virus containing cells. All but 10 ml of supernatant in each tube was decanted and stored at 4°C, and the cells resuspended within the remaining 10 ml. These were freeze-thawed three times using liquid N_2 and a 37°C waterbath to rupture cells and release viruses, and then centrifuged at 3,500 g for 15 minutes to sediment the cell debris. The supernatant, now containing viruses, was mixed with the decanted solution stored earlier and 12.5 U/ml of Benzonase nuclease (Merck Chemicals) was added, then left at 37°C for 30 minutes to break down unwanted nucleic acids. Then the entire solution was loaded onto the filters to bind the virus, washed through and viruses eluted as per the protocol described in the kit manual, taking care especially not to pass solution too quickly through the filters or introduce air bubbles. The viral eluate was concentrated further using a special filtered-centrifuge tube provided with the kit, centrifuging at 3,000 g for 20 minutes to leave no less than 1 ml above the filter. 4 ml of freezing buffer solution (appendix A1) was added and the mixture was centrifuged again at 3,000 g for 11 minutes to again leave no less than 1 ml above the filter. This was recovered and split into 10 µl aliquots in Eppendorf tubes before storage at -80°C.

2.2.3 Titre of amplified viruses

Titre of the amplified virus was done using the "AdEasy Virus Titre" kit (Agilent Technologies). First $1x10^6$ of stock Ad293 cells were spread evenly across 10 wells of a 24 well plate topped up to 1 ml of 293 medium in each well. 10 µl from the amplified stock was diluted by a factor of 100 by topping it up to 1 ml with 293 medium. It was then serially diluted four more times by a factor of 10 each time by taking 100 µl of the last

solution and topping it up to 1 ml for each dilution in turn. This created five dilution factors from 10^{-2} through to 10^{-6}. 50 µl of each dilution was added drop-wise to two of the 10 wells with 293 cells loaded earlier creating five duplicates. The plate was left in a 37°C / 5% CO_2 incubator for 48 hours to give the virus time to express the adenoviral genome.

Following this the AdEasy kit was used to perform an immunohistochemistry protocol as per the manual, to label hexon proteins specific to virus-infected cells. Infected cells stained a dark brown/black colour and counted under an inverted phase contrast microscope (figure 13). The total number of infected cells in a well was calculated from the average number of labelled cells seen within a single field of view (using the ratio between the field of view area and the total well area). Dividing this by the dilution factor and volume of virus used for that well extrapolated the total number of 'plaque forming units' per millilitre (pfu/ml) for the original amplified stock. In summary:

$$\text{Viral tire (pfu/ml)} = \frac{\text{(Average number of positive cells/field) x (Fields/well)}}{\text{(Volume of diluted virus used in ml) x (Dilution factor)}}$$

2.2.4 Validation of amplified viruses

Validation of the stock virus was done by the lab creating the virus using gene sequencing (appendix A3). Validation of the amplified viruses was performed using immunocytochemistry and qPCR.

2.2.4.1 Immunocytochemistry

For immunocytochemistry, $1x10^6$ Ad293 cells were spread evenly into 4 wells of a 6 well plate, which each had collagen coated cover slips placed at the bottom, topping up to 2 ml of 293 medium for each well. The plate was placed in a 37°C / 5% CO_2 incubator for 24 hours. The next day 10 µl of amplified virus was added to 8 ml of fresh pre-warmed 293 medium. Then the old medium was replaced in 2 wells with 2 ml of the infected 293 medium, and in 2 wells with 2 ml of fresh uninfected 293 medium. The plate was

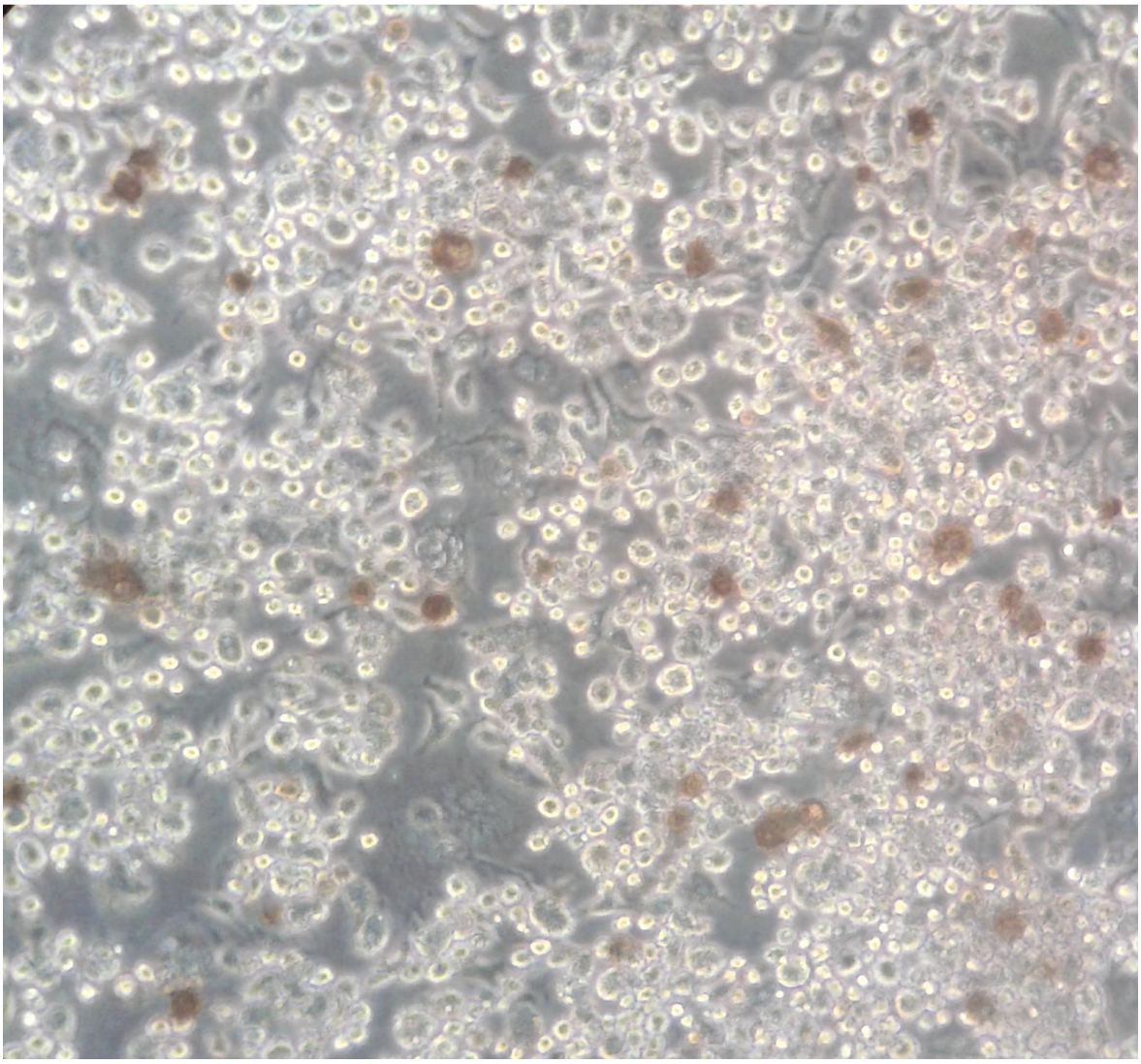

Figure 13. Immunolabelling of viral hexon protein to estimate viral titre

Photograph of inverted phase contrast microscopy showing adenovirus infected 293 cells demonstrating CPE, immunolabelled using the AdEasy virus titre kit. Cells displaying a brown colour were those that were positively labelled for the viral hexon protein indicating cell infection. This allowed easy counting of infected cells and thus extrapolation of the estimated titre within the stock viral suspension used to infect the cells, measured in plaque forming units per ml (pfu/ml).

returned to the incubator for a further 48 hours. Subsequently the following immunocytochemistry protocol was performed to stain the cells for the protein of interest depending on the virus used. Initially old medium in each well was replaced by ice cold methanol for 30 minutes. This was then removed and the wells were washed with PBS three times for 5 minutes each. Next 1% bovine serum albumin (BSA) was added to each well and left for 60 minutes. Following this, 20 µl of rabbit primary antibody against the gene of interest was diluted 1:100 in 1% BSA and used to replace the BSA already in the well. The plate was left overnight at 4°C. The next day the primary antibody was aspirated and each well was washed with PBS three times. Then 2 ml of donkey anti-rabbit secondary antibody conjugated to the green fluophore FITC was added at a dilution of 1:100, then left for 2 hours. Subsequently the secondary antibody was aspirated and each well was washed with PBS three times. Cover slips were then carefully lifted from each well and placed upside down onto slides with a drop of hardset Vectashield (Vector Labs) in between. The slides were then examined under a laser confocal microscope to look for immune staining of the protein of interest.

2.2.4.2 qPCR

For qPCR, $1x10^6$ Ad293 cells were cultured in a 25 cm^2 flask as previously described. After 24 hours the cells were infected with 10 µl of amplified virus in 5 ml of fresh 293 medium. Another 48 hours later, the cells were inspected under an inverted phase contrast microscope to ensure the majority of cells demonstrated CPE. Cells were harvested by agitation and tituration using the medium within the flask and collected into a 15 ml tube. A small scale DNA purification protocol was then performed as follows. The cells were centrifuged at 3000 g for 10 minutes, supernatant discarded and the pellet resuspended in 500 µl PBS. It was centrifuged again at 1,000 g for 5 minutes, supernatant discarded and the pellet resuspended in 360 µl of 1x Tris-EDTA pH8 buffer, then transferred to a 1.5 ml microcentrifuge tube. 25 µl of sodium dodecyl sulphate (Sigma Aldrich), 8 µl of 0.5 M EDTA and 4 µl of 20 mg/ml Proteinase K was added and the tube incubated at 37°C for 2 hours. After this 100 µl of 5 M NaCl was added and the tube kept on ice overnight. The next day the tube was centrifuged at 15,000 g for 1 hour at 4°C. A friable gelatinous pellet formed and the supernatant containing DNA was harvested taking care not to disturb the

pellet, and transferred to a new 1.5 ml microcentrifuge tube. DNA was extracted by adding phenol:chloroform:isoamylalcohol (25:24:1) at an equal volume to the harvested supernatant and the tube was mixed gently. Two phases were seen to the mixture now and the upper phase was transferred to a new microcentrifuge tube. Extracted DNA was precipitated by first adding 2 volumes of 95% ethanol and leaving it at room temperature for 10 minutes. The tube was centrifuged at 15,000 g for 20 minutes creating a very tiny white pellet. The ethanol was discarded and the pellet resuspended in 100 µl of 70% ethanol before centrifuging again at 15,000 g for 20 minutes. The ethanol was again discarded and the cap left open to aid drying before resuspending the pellet gently in 50 µl of distilled water containing 0.1 mg/ml of RNase.

The resulting solution of viral DNA was then processed by qPCR as follows. First 1 µl of the solution was loaded onto a 'Nanodrop' spectrophotometer to measure DNA content in ng/µl. The solution was diluted 1:100 with distilled water so that the nucleic acid concentration was between 5-50 ng/µl. For full details of the qPCR protocol used see section 2.7. In brief, 1 µl of the diluted viral DNA solution was added to 5 µl of 2x SYBR Green Master Mix (Life Technologies), 1 µl of 10x primer assay for the gene of interest (Qiagen) and 3 µl of distilled water in one well of a PCR plate and this was repeated in triplicate. The plate was loaded onto an ABI 7900HT Real-Time PCR machine (Applied Biosciences) to run a standard thermocycling protocol overnight. The threshold cycle (C_t) value was obtained as well as a dissociation curve (see section 2.7 for further explanation of these terms).

2.2.4.3 Gel electrophoresis

Amplified DNA from the qPCR step was run on an agarose gel to check that the molecular weight of the amplicon matched the expected weight quoted in the primer documentation. 2% agarose in Tris-acetate-EDTA (TAE) buffer was boiled and cooled in the microwave, 15 µl of Safeview nucleic acid stain (NBS Biologicals) was added to both this and a further 100 ml of TAE buffer. The agarose was loaded onto the electrophoresis tray and left for 30 minutes to solidify into a gel with a comb sitting above to form wells and then covered with the rest of the TAE buffer. 10 µl of 100 base pair (bp) Hyperladder

(Bioline) was loaded into the first and fifth wells for reference. 10 µl of each of the three amplified DNA solutions was mixed with 5 µl of 5x sample loading buffer (Bioline) before being loaded into the second, third and fourth wells. 150 mV was then passed through the gel for 30 minutes, checking the progress of the visible front to ensure it did not run too far. The gel was then visualised under a UV transilluminator and photographed. The bp of the amplicon was estimated.

2.2.5 Adenovirus injection into subsidiary atrial pacemaker tissue

Adenoviruses were used as vectors for delivery of genes of interest into SAP tissue. These include genes encoding for Tbx18, Tbx3, NCX1, GFP and *LacZ*. As described above, viruses capable of transducing these genes were amplified and purified to allow adequate concentrations of virus to be injected in very small volumes. Viruses were injected into the superior cut edge of SAP preparations at the CT where the tissue was thickest. Injection of more than 1-2 µl was not possible without potentially causing damage by excessively stretching the tissue. Experiments would utilise one adenovirus type at a time.

Injection of virus into SAP tissue was achieved using a 'nanofil' 35G needle, 'nanofil' syringe (World Precision Instruments), a micromanipulator (Narishige) with a custom holder for the syringe and a stereo dissection microscope. Dissected SAP tissue was positioned in the same Tyrode's solution it was dissected in at the edge of the petri dish to allow an easier trajectory for manipulation of the needle into the tissue. The cut edge of the SAP tissue was pinned with a slight stretch so the needle could pierce the tissue more easily.

The syringe and needle were first flushed repeatedly with Tyrode's solution. 5-10 µl of the RAd of choice was warmed to room temperature, drawn up into the syringe and 1-2 µl flushed through the 35G needle to get rid of air bubbles. The needle and syringe were then mounted onto the micromanipulator and the needle carefully advanced into the SAP preparation under the dissection microscope, piercing the cut edge of the CT by at least 2 mm. Occasionally the tissue had to be gently coaxed onto the needle using forceps. Once

the needle was visually within the tissue, 1-2 µl of virus was then injected ensuring that a small bleb of fluid accumulated at the injection site. If it was seen that volume was not immediately accumulating for example because the needle had gone through the tissue, then it was repositioned before trying again. Once a satisfactory injection was achieved the needle was left in place for 2 minutes to ensure the solution did not leak back out of the perforation straight away and also to aid diffusion of the virus into the tissue. After this the needle was removed and the preparation was transferred to a pre-prepared superfusion setup to be cultured and monitored using the methods described below (section 2.3).

2.2.6 β-galactosidase expression and X-Gal assay

In order to get a sense of the area of gene expression after adenovirus injection, Ad-LacZ was injected into SAP tissue. Expression of the *LacZ* gene produces the enzyme β-galactosidase. Once produced, this enzyme can be used as part of an 'X-gal assay' which produces blue discolouration in any tissue expressing the enzyme, providing visual recognition of the tissue area transduced as a result of the injection. The virus was provided by Paul Kingston (University of Manchester). The titre of this virus was known to be $1x10^{10}$ pfu/ml. Using the same method for injection that was used for biopacemaking, 1 µl of the virus ($1x10^{7}$ pfu) was injected into the SAP area. The tissue was then cultured using the method described below (section 2.3) for 24 hours. After this the preparation was moved from the culture chamber to a petri dish and washed with PBS twice. It was then soaked in 4% paraformaldehyde for 20 minutes. The preparation was washed with PBS three times and then permeabilized in 0.1% Triton solution for 15 minutes. After a further three washes in PBS, the preparation was immersed in freshly prepared X-Gal staining solution (Sigma Aldrich) (appendix A1) for several hours at 37 °C in the dark until enough blue discolouration had developed. A final wash in PBS was done before the preparation was air dried to be photographed.

2.3 Tissue culture and rate recording

2.3.1 Superfusion setup

A custom superfusion setup was developed to enable sterile culture of two tissue preparations simultaneously whilst recording extracellular potentials to monitor beating rates (figure 14). All equipment was initially sterilised by autoclave and solutions sterilised using bottle top vacuum filters (Steritop 0.2 µm pore, Scientific Laboratory Supplies). Preparations were placed in custom glass tissue chambers (internal glass blowing service, University of Manchester) each with two ports to pump tissue culture medium (appendix A1) in and out of and a 2 mm Sylgard (Sigma-Aldrich) silicone layer added at the base to pin the tissue to using small insect pins. Each chamber was designed to hold ~10 ml of fluid during circulation, regulated by the dimensions of the chamber and the height of the efflux port (figure 15). The system would continuously circulate medium to the chambers at ~10 ml/minute (maximum pump speed), each via two circuits (influx and efflux) travelling to and from a 500 ml reservoir, via a peristaltic pump (Gilson) and through standard silicone tubing (Scientific Laboratory Supplies). Calibrated silicone Gilson pump tubing (Scientific Laboratory Supplies) was necessary for use with the pump head and connected to the standard tubing using barbed connectors (Biorad). The use of a larger bore of tubing in the pump head for the efflux circuit (2.8 mm internal diameter) than the influx circuit (2 mm internal diameter) ensured the chamber never overfilled, and the outgoing chamber port was made higher than the incoming port to make sure a minimum level of medium was always maintained. Also within both the efflux and influx circuit a blood transfusion giving set (Biological Services Facility, University of Manchester) was added to drip medium through a filter, trapping debris and isolating the chamber from electrical noise coming from the pump to improve recording signal.

The chamber and reservoir sat inside a 37°C / 5% CO_2 incubator to maintain a stable solution temperature of 37°C and pH of 7.4 (for validation see section 4.2.1.2). However, it was not possible to keep the peristaltic pump inside the incubator as this led to an uncontrolled rise in temperature. It was therefore necessary to keep the pump outside the incubator with tubes temporarily passing out of the incubator to the pump and back.

Since this would cool circulating medium, the length of tubing outside the incubator was kept to a minimum, the length of tubing inside the incubator between the pump and culture dish was always long enough to allow time for rewarming and the internal incubator temperature was set 1-2 degrees warmer than 37°C, adjusted to the tenth of a degree to ensure culture medium in the tissue chamber was always at 37°C.

2.3.2 Rate recording via measurement of electrical potentials

Custom recording electrodes for recording extracellular potentials were fashioned from shielded two-core cables (Maplin) soldered to 0.22 mm stainless steel acupuncture needles (Sharp/The Journal of Chinese Medicine). Two needles were soldered to the two cores for recording and the other was soldered to the cable shielding for earthing. At the other end the cable was attached to an 8-pin DIN plug which would connect to a 'Powerlab' system (AD Instruments), soldering the wires and shielding to the respective 'input (+)', 'input (-)' and 'input (+) ref' pins as per guidance from the Powerlab manual (figure 16). The Powerlab would act as an amplifier, digital filter and recording device storing data on a personal laptop via Labchart software (AD Instruments). Direct connection from tissue to Powerlab using custom electrodes was necessary to reduce noise that was previously experienced by the group using an intermediate 'Neurolog' analog amplifier and filter setup.

Monophasic APs were recorded for up to 48 hours while preparations were cultured (figure 17). This time period was chosen in accordance with the time course for potential observable effects to become apparent from RAd-mediated transcription factor expression based on previous work as well as limitations in the reliability of our method of culture and recording after 48 hours.[152, 203] Raw signal was filtered (10-500 Hz band-pass filter) and analysed (ensuring individual beats detected by manually setting a threshold for deviation from baseline signal) by Labchart software providing beating rate data and mean rate for any time frame required (e.g. 1, 30 or 60 s). The statistical difference in mean rate between experimental groups was calculated via SigmaPlot software using paired t-test or one-way ANOVA where appropriate.

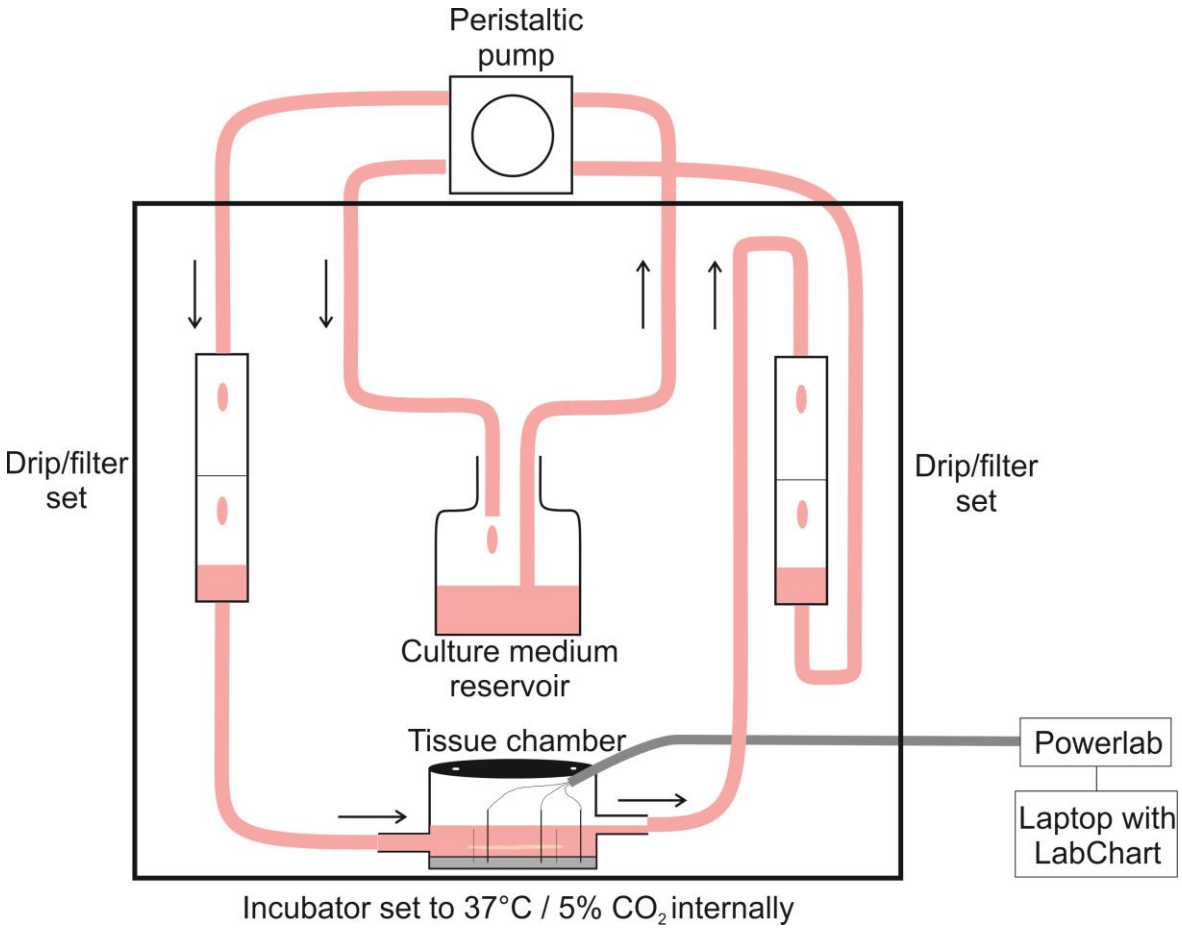

Figure 14. Diagrammatic representation of the superfusion setup used for tissue culture and rate recording

A significant amount of time was spent designing and testing a tissue superfusion setup to ensure reliability and consistent results. Two circuits were used to pump culture medium to and from each tissue chamber via a reservoir. Drip/filter sets electrically isolated the chamber from the pump reducing noise whilst trapping debris that would gradually build up in the circulating medium. Maintaining up to two tissue chambers in parallel was feasible for each setup. Stability in temperature and pH was validated carefully before data collection began (see section 4.2.1.2).

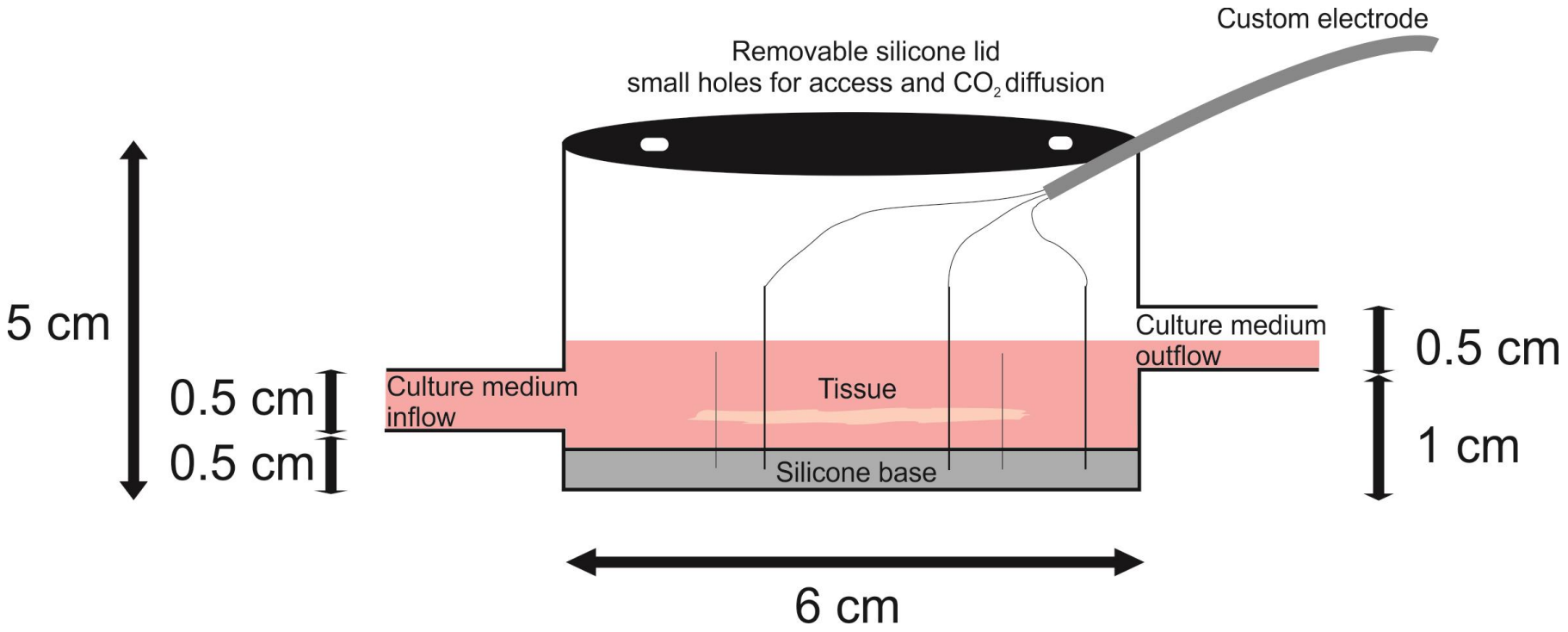

Figure 15. Custom tissue chamber dimensions

Custom tissue chambers were made to specification by the glass blowing service available at the University of Manchester. Precise dimensions were needed in order to provide a relatively small circulating volume within the tissue chamber so that volume exchange was quick and a low level of culture medium was maintained just enough to submerge the tissue. Lower levels of medium allowed for greater signal amplitude which made signal analysis over the whole 48 hours more reliable.

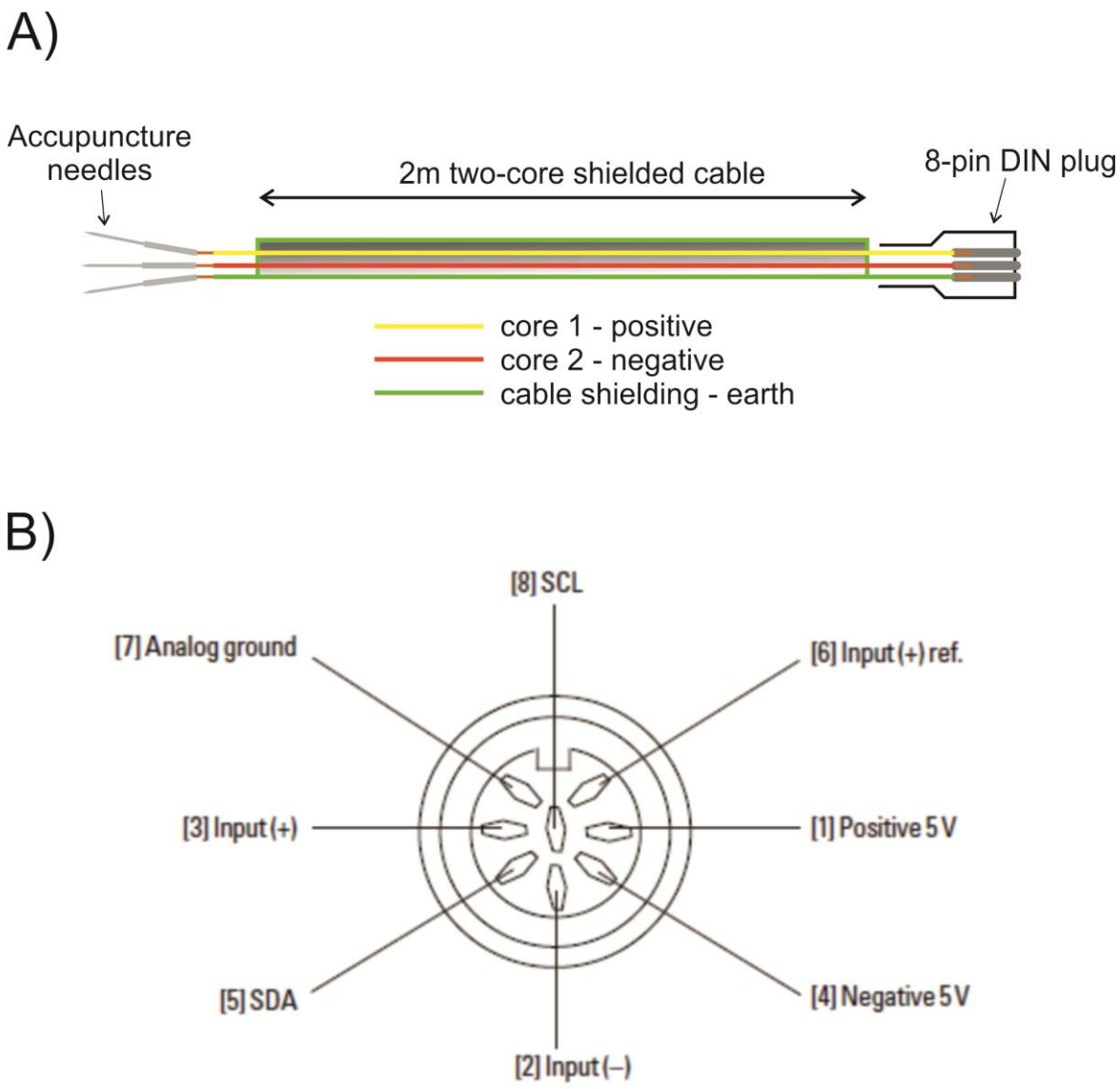

Figure 16. Custom cable and Powerlab DIN port pin assignments

(A) Custom electrodes were designed and soldered in-house. Three electrodes in the form of acupuncture needles were pinned into the tissue chamber - positive and negative electrodes into the tissue and an earthing electrode pinned into the chamber away from the tissue to reduce noise. These signals were conducted through a shielded two-core cable (the earth signal through the shielding) directly to the DIN port of a Powerlab transducer/amplifier. (B) The positive signal was delivered to '[3] Input (+)', the negative signal to '[2] Input (-)' and the earth signal to '[6] Input (+) ref.' The other inputs were not used. Taken from ADIntruments Powerlab manual.

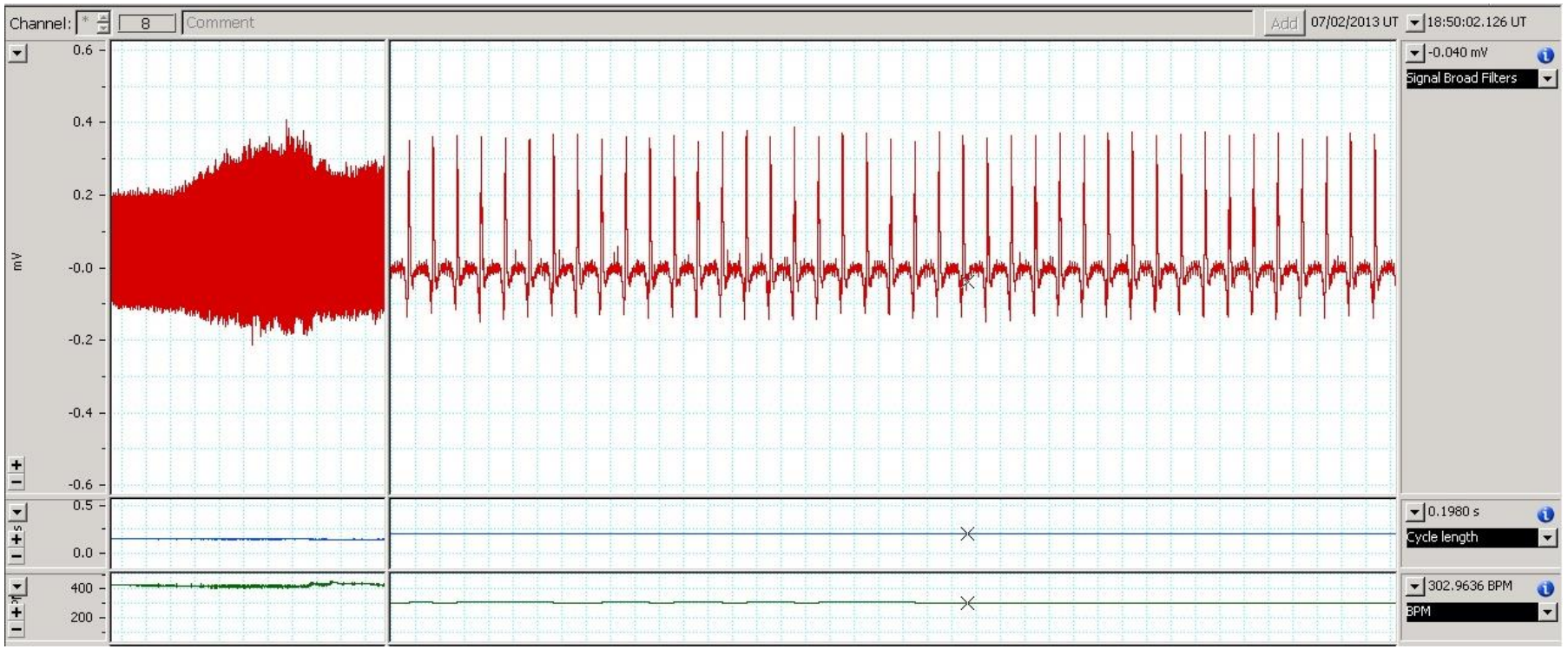

Figure 17. Example of the signal recordable from cultured SAN preparations using LabChart software

LabChart software was capable of displaying spontaneous electrical signal from multiple tissue chambers simultaneously. Signals were amplified by the Powerlab system and frequencies filtered (10-500 Hz band-pass filter) by the LabChart software to provide the strongest and cleanest signal. The reliability of this was crucial in order to leave experiements running for 48 hours without needing to interfere which would have destabilised temperature and pH.

2.4 Overdrive pacing

Overdrive pacing is a technique that involves electrically stimulating cardiac tissue at a faster rate than its spontaneous rate. Artificial pacing suppresses spontaneous pacemaker activity during stimulation. On cessation of artificial pacing there is a brief period in addition to the spontaneous cycle length before spontaneous pacemaking can resume termed the recovery time. Recovery time can be used as a measure of the suppressibility of spontaneous pacemaking i.e. how easily it is inhibited by ectopic electrical activity. For example, the SAN is known to have a very short recovery time making it more robust. Suppressibility of our biopacemaker in comparison will be an important measure.

After 48 hours of tissue culture, an overdrive pacing protocol was applied using the output function of the Powerlab in different experimental groups. The Powerlab was connected to a constant voltage isolated stimulator (Digitimer), which would pace the tissue via a small coaxial stimulator electrode set (Harvard Apparatus) mounted on a ball-joint manipulator to enable flexible placement and firm contact with the tissue.

Overdrive pacing protocols were formulated based on previous protocols used on rat RA tissue. Two studies used pulse trains at 50 – 80% of the spontaneous cycle length for 2 minutes.[224, 225] Pulse width was 2 ms and amplitude was 1.2 – 5 times capture threshold.

Once the stimulator electrode was placed onto the tissue, the incubator door was closed and time was allowed for environmental conditions to stabilise and for the preparation to equilibrate. Labchart software was used to control pacing frequency whilst recording continued. 3 x 2 minute pulse trains were delivered to the tissue at 75% of the spontaneous cycle length measured at the time just before each train. On the stimulator module, pulse width was set to 2 ms and voltage amplitude was gradually adjusted to 1.5 times the threshold for capture, observed live on the recording traces (figure 18).

Corrected recovery time (cRT) was calculated as the difference between the recovery time (the time from the last paced beat to the next spontaneous beat) and the spontaneous cycle length measured before each train. Statistical differences in mean cRT between experimental groups were calculated by unpaired t-test.

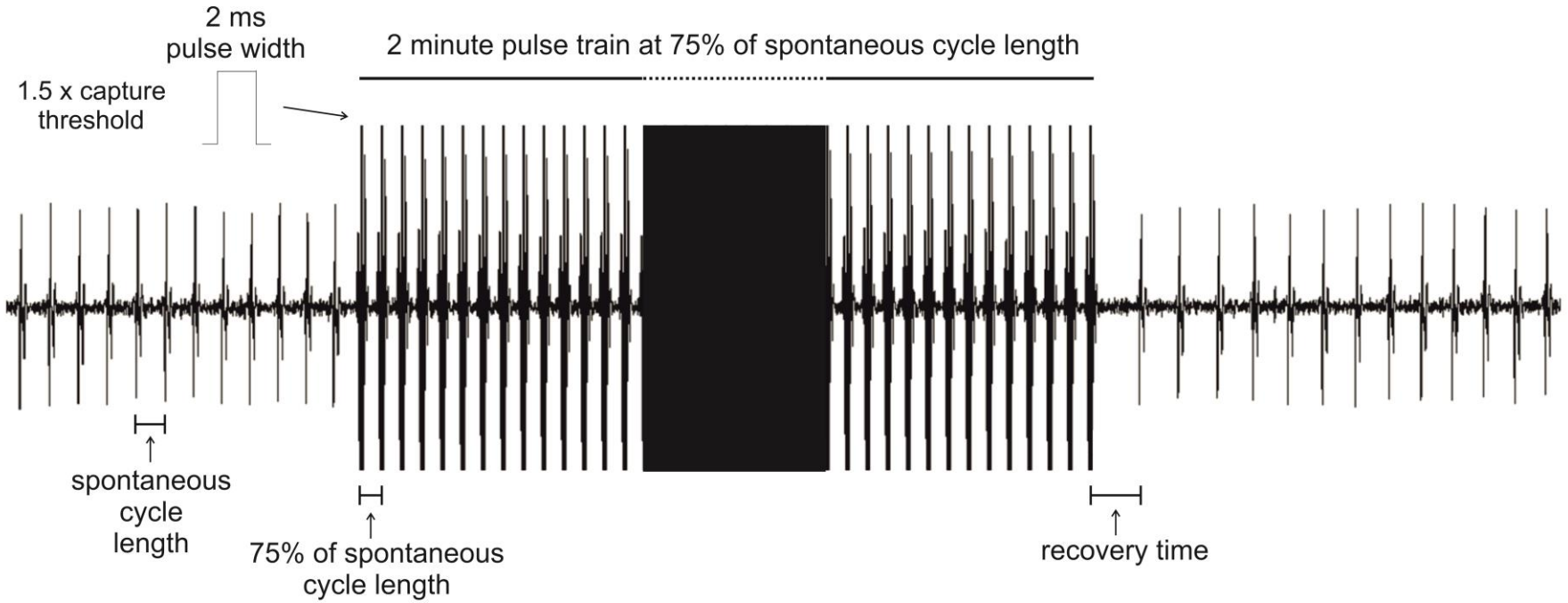

Figure 18. Example signal recording during overdrive pacing protocols

A representation of spontaneous signals from cultured tissue being interrupted by overdrive pacing at 75% of the spontaneous cycle length. Pulse trains lasted for 2 minutes. The time from the last paced beat to the first spontaneous beat (recovery time) was measured. The corrected recovery time (recovery time minus spontaneous cycle length) was calculated from recordings.

2.5 Pharmacology

2.5.1 Post-culture

Following tissue culture and pacing, beating rate was recorded in the presence of CsCl (Sigma-Aldrich) and isoprenaline (ISO) (Sigma-Aldrich) individually, to measure the sensitivity of different experimental groups to I_f blockade and β-adrenergic stimulation respectively. One disadvantage of using CsCl for I_f blockade is that it can also non-specifically block K^+ channels. Nonetheless it was chosen over ivabradine mainly due to the advantage of CsCl being easily washable from preparations allowing subsequent testing of ISO on the same preparation thus saving a lot of time and conserving animal use. Furthermore ivabradine has previously been used by the group and observed similar reductions in beating rate in SAN and SAP preparations with both CsCl and ivabradine.[152]

First, the culture medium in the tissue chamber was gradually replaced with normal Tyrode's solution (appendix A1) bubbled with 95% O_2 / 5% CO_2 gas mixture, in order to be more comparable to similar work done in fresh uncultured tissue. This was achieved by exchanging culture medium for Tyrode's solution at the reservoir and setting the pump speed very low while solution exchange gradually took place within the chamber, before increasing it back to normal speed. Thus a gradual change in perfusion from culture medium to Tyrode's solution was achieved, avoiding damage to the tissue by any sudden shifts in conditions e.g. osmolality. Subsequently similar beating rates were maintained. Permanent bradycardia was potentially inducible by exchanging solutions too rapidly.

200 ml of 2 mM CsCl solution and 200 ml of 0.05 µM ISO solution were pre-made in fresh Tyrode's and left earlier in the incubator to allow adequate equilibration of temperature and pH. After at least 10 minutes of tissue superfusion with Tyrode's solution to ensure stability of the tissue preparation, the Tyrode's solution was replaced with the CsCl solution at the reservoir and this was superfused over 20 minutes. CsCl was then washed off by replacing it with normal Tyrode's solution again at the reservoir, superfusing for another 10 minutes. Once beating rates were back to baseline and steady, Tyrode's was this time replaced by the ISO solution at the reservoir and superfused over 20 minutes.

Mean rates were measured before and 10 minutes after application of CsCl, and also before and 10 minutes after application of ISO. Statistical differences were measured by unpaired t-test or two-way ANOVA where appropriate.

2.5.2 Uncultured preparations

In addition to cultured preparations, a separate set of fresh uncultured SAN and SAP preparations were superfused with ivabradine (Sigma-Aldrich) to assess blockade of I_f, ISO (Sigma-Aldrich) to stimulate the β-adrenergic system and ryanodine (Abcam Biochemicals) to block RYRs and inhibit the Ca^{2+} clock. The preparations were placed in a tissue bath and continuously superfused from the start with 37°C normal Tyrode's solution bubbled with 95% O_2 / 5% CO_2 gas mixture. The preparations were left to stabilise within the bath for 10-15 minutes. Rates were then recorded for 10-20 minutes before the drug was added. Each drug was tested in separate experiments as none of them wash off well. 200 ml of 3 µM ivabradine, 0.05 µM ISO and 2 µM ryanodine were superfused individually over 20 minutes before a wash period, recording continuously throughout. The mean beating rates before and 10 minutes after each drug were statistically analysed by unpaired t-test.

2.6 Immunohistochemistry

2.6.1 Right atrial serial sections before tissue culture

In order to further localise the extent of SAP tissue and guide adenovirus injections into SAP tissue, immunohistochemistry was used to fluorescently label proteins related to pacemaking and assess the distribution of pacemaker tissue in the RA as a whole. To achieve this, the RA was dissected from the rat in Tyrode's solution as described above. In one preparation the anterior wall was left intact to allow horizontal sections that would be easier to interpret in terms of anatomy. The dissected RA was frozen in optimum cutting temperature (OCT) compound using liquid N_2, injecting OCT compound within the lumen of the RA in the case of the intact preparation to maintain an open shape as much as possible. Later these frozen preparations were cryosectioned using a cryostat (Leica)

onto glass slides at a thickness of 20-30 µm. Horizontal sections were saved every 0.5 – 1 mm from the level of the SVC to just below the IVC. These sections were labelled for HCN4, Cx43 and Caveolin-3 (Cav3).

The immunohistochemistry protocol was as follows. Sections were placed in ice cold 100% methanol for 30 minutes and then washed with PBS three times for 10 minutes. PBS was removed from the sections and then drawn around using a hydrophobic ink pen (Pap Pen). 1% bovine serum albumin (BSA) (Sigma -Aldrich) was gently pipetted onto sections and left for 60 minutes to block non-specific antibody labelling. Then primary antibody to the protein of interest was diluted in 1% BSA. Primary antibodies were used either individually or two together to allow double labelling as long as they were raised in different animals. These included rabbit anti-HCN4 (Alomone) at 1:50 dilution, rabbit anti-HCN1 (Alomone) at 1:100 dilution, mouse anti-Cx43 (Alomone) at 1:100 dilution and mouse anti-Cav3 (Alomone) at 1:100 dilution. BSA was removed from the sections and 100 µl of the diluted primary antibody was applied to them. They were then incubated overnight at 4 °C. The next day the sections were washed in PBS three times and then incubated in the appropriate secondary antibody for 60-120 minutes to label the primary antibody with a fluorescent probe. Donkey anti-mouse attached to the Fluor probe (Abcam) at 1:100 dilution was used to label mouse primary antibodies with green fluorescence, and donkey anti-rabbit attached to the Cy3 probe (Abcam) at 1:400 dilution was used to label rabbit primary antibodies with red fluorescence. After washing in PBS a final three times, the sections were mounted in H-1400 hardset Vectashield (Vector Laboratories) and covered with a glass coverslip. Sections were then either scanned onto a PC using confocal microscopy or a mercury lamp scanner (Faculty of Life Sciences, University of Manchester) and further analysed. Qualitative data was extracted in the form of labelling location.

2.6.2 Cultured tissue

Ad-Tbx18 injected SAP preparations after 48 hours of tissue culture were frozen whole in OCT compound for cryosectioning and immunohistochemistry using the same protocol as above. This was to confirm Tbx18 protein expression, and expression of other proteins

related to pacemaking, following Ad-Tbx18 infection. Individual sections were immunolabelled for Tbx18, Cx43, Cav3, HCN4 and HCN1. The same primary and secondary antibodies as above were used with the addition of rabbit anti-Tbx18 (Sigma Aldrich) at 1:50 dilution and rabbit anti-HCN1 (Alomone) at 1:50 dilution.

2.7 RT-qPCR

In order to confirm gene of interest expression following each experiment and any effect on other pacemaker genes, mRNA abundance was measured using RT-qPCR. This enabled quantitative comparison of the relative levels of mRNA for several molecular targets between experimental groups. 2 mm samples were dissected from all preparations from SAN, SAP or RA tissue where present after 48 hours of tissue culture. Samples were placed in a flat bottomed microcentrifuge tube (to allow easier homogenisation of the tissue during later steps), immediately snap frozen by immersing the tube in liquid N_2 and stored in a -80°C freezer.

Once ready to process, RNA was extracted using the 'MirVana' kit (Life Technologies) and DNA eradicated using 'Turbo DNase' (Life Technologies) as per manufacturer instructions. Following this, RNA quantity and quality was measured using a 'Nanodrop' spectrophotometer. Reverse transcription of total extracted RNA to cDNA was performed using the 'SuperScript VILO Master Mix' kit (Life Technologies) (containing multiple combinations of nucleotides and reverse transcriptases) as per manufacturer instructions. Extracted RNA concentrations measured by Nanodrop earlier were used to calculate dilutions of each sample, normalising RNA levels in all 20 µl reverse transcription reactions to the sample with the lowest RNA concentration.

The final qPCR reactions were performed in 96-well plates using a SYBR Green fluorescent probe assay with 10 µl reaction mixtures per well. SYBR Green probes produce measurable fluorescence once bound to DNA and so can be used to accurately quantify gene amplification in qPCR. Gene amplification is performed using primer assays which contain DNA sequences specifically complementary to part of the gene of interest along

with nucleotides and DNA polymerases. Plates were thermocycled through a denaturation step of 95°C for 10 min, and 40 cycles through steps of 95°C for 30 s, 60°C for 30 s and 72°C for 1 min. When cycled through these temperatures double stranded DNA will separate, the primer will bind to the gene of interest and the DNA polymerase will complete complimentary DNA strands from the primer binding site. Each cycle should double the number of copies (amplicons) of the gene of interest (assuming 100% reaction efficiency) and these copies will therefore increase exponentially. The threshold cycle (C_t) is the cycle number at which a gene has undergone exponential amplification and has reached a pre-defined level of fluorescence from the SYBR Green probe normally set above background fluorescence and somewhere within the exponential phase.

Each reaction was performed in triplicate in order to account for experimental error such as pipetting or user error. This would allow an outlier analysis to be performed to exclude reactions producing wildly anomalous results (see below for detail). Initially 5.25 µl of 2x SYBR Green Master Mix (Life Technologies), 1.05 µl of 10x primer assay (Qiagen) specific to the gene of interest and 3.15 µl of nuclease free water, all multiplied by the number of reactions being processed in the batch, was mixed well in a separate Eppendorf tube. These volumes accounted for a 5% pipetting error. 9 µl of this mixture and 1 µl of sample cDNA was added to each well and mixed well by pipetting up and down repeatedly. Care was taken when adding sample cDNA to use a separate pipette tip for each well to avoid contamination.

Genes of interest included Tbx18, Tbx3, HCN1, HCN2, HCN4, $Na_v1.5$, Cx43, Cx45, NCX1, RYR2, $K_{ir}2.1$, $K_v1.5$, $Ca_v1.2$ and $Ca_v3.1$ and were measured for every sample, chosen for their relevance to pacemaking. The housekeeper gene 18S was also measured for every sample to allow normalisation to a gene that was consistent in all samples. 18S was selected for this purpose as it had been used successfully by the group previously for samples taken from the rat SAN, SAP and RA.[152, 176] Reaction mixtures were thermocycled in an ABI Prism 7900 HT Sequence Detection System (Applied Biosystems) controlled by 'SDS software' through the following conditions: a denaturation step at 95°C for 10 minutes, then 40 cycles through steps of 95°C for 30 s, 60°C for 30 s and 72°C for 1

minute. A dissociation curve was measured by the machine by cycling through the steps: 95°C for 15 s, 60°C for 15 s and 95°C for 15 s.

The dissociation curve for each reaction was checked to ensure a single peak change in fluorescence where SYBR Green dissociated from DNA, indicating specific binding to the gene of interest, rather than primer dimers or genomic DNA. The C_t and maximal efficiency for each reaction was automatically analysed by the SDS software. The mean C_t value for 18S within a triplicate was used for all calculations for samples within that triplicate. Absolute mRNA abundance was calculated in terms of copies needed to reach threshold fluorescence using the formula: efficiency^C_t. Lower numbers therefore indicate a higher starting mRNA abundance. The ratio of mRNA abundance between the gene of interest and 18S (relative mRNA abundance) was then calculated for each reaction: efficiency^C_t for 18S/efficiency^C_t for gene of interest. Mean relative mRNA abundance for each gene of interest within a tissue was calculated from all reactions in that experimental group after applying an outlier analysis based on the median absolute deviation method regularly used by the group to remove statistical outliers caused by experimental error.[176, 226] Different gene targets, sample locations and experimental groups were compared. Statistical differences between relative mRNA abundances were analysed using unpaired t-test.

3. RESULTS

3.1 Characterisation of subsidiary atrial pacemaker tissue

3.1.1 Introduction

SAP tissue in the inferior RA adjacent to the IVC has been characterised before in the rat.[152] This tissue is bradycardic compared to the SAN and shares several but not all molecular features of the SAN. For example, both SAP and SAN showed similar mRNA levels for Tbx3, HCN1, $Na_v1.5$ and $K_{ir}2.1$, but a lower level of HCN4 and higher level of Cx43 in SAP tissue. Histology showed similar small 'nodal-like' cells in both SAP and SAN, but immunohistochemistry failed to show any HCN4-positive/Cx43-negative tissue characteristic of SAN tissue. The leading pacemaker in isolated SAP tissue was mapped in most cases septal to the CT and just superior to the IVC (figure 11).[152]

Further unpublished work was done on SAP tissue in the goat using histology and immunohistochemistry.[227] SAP tissue harboured a mix of nodal and atrial cells, HCN4 and NCX1 signal was seen in SAP tissue at similar levels to the SAN, however Cx43 was also seen within SAP tissue at a similar level to surrounding RA.[227] This intermediate character of SAP tissue may account for its bradycardic nature. It may also account for the lack of HCN4 immunolabelling seen in previous rat work if by chance selected sections only contained atrial cells.

We therefore opted to do further immunohistochemistry of serial RA cryosections to look again for any HCN4-positive pacemaker tissue in the inferior RA of the rat. This would increase confidence that adenoviral gene transduction would overlap with SAP tissue. We also isolated SAP tissue *in vitro* to characterise pharmacological response to I_f blockade, RyR blockade and β-adrenergic stimulation.

3.1.2 Immunohistochemistry before tissue culture

Serial sections of freshly dissected rat RA were subject to immunohistochemistry protocols to label HCN4, Cx43 and Cav3 proteins (n=2). The first animal horizontal sections taken superiorly through the SAN demonstrated 12 strips of tissue with extensive and discrete HCN4 signal, localised around the sinus node artery (figure 19). Higher magnification images show that HCN4 signal was localised to cell membranes. Cx43 signal was not present within this HCN4-positive tissue, but was extensive in all other tissue with an intercellular distribution.

Sections taken inferiorly around the level of the IVC demonstrated similar HCN4-positive tissue but this was sparse in comparison to SAN sections and inconsistent even in adjacent sections. This HCN4-positive tissue was again Cx43-negative with all other areas being HCN4-negative and Cx43-positive.

In the second animal the RA had been dissected so that the anterior wall was left intact to make it easier to interpret anatomy, therefore horizontal sections demonstrated rings of tissue with a central lumen. Sections taken superiorly through the SAN again demonstrated extensive HCN4-positive/Cx43-negative tissue with a discrete border surrounding the sinus node artery (figure 20). Sections labelled with both HCN4 and Cav3 showed Cav3 signal throughout the tissue and co-localised with HCN4 signal in cell membranes (figure 21).

This time, inferior sections around the IVC in this animal demonstrated a larger area of HCN4-positive/Cx43-negative tissue adjacent to the IVC (figure 20). HCN4 signal was co-localised with Cav3 signal (figure 21). HCN4-positive cells were smaller in size than neighbouring HCN4-negative cells when visualised at higher magnification but were not specifically measured (figure 21c).This tissue was consistently visualised in adjacent sections around the IVC, however was not continuous with the SAN (figure 22).

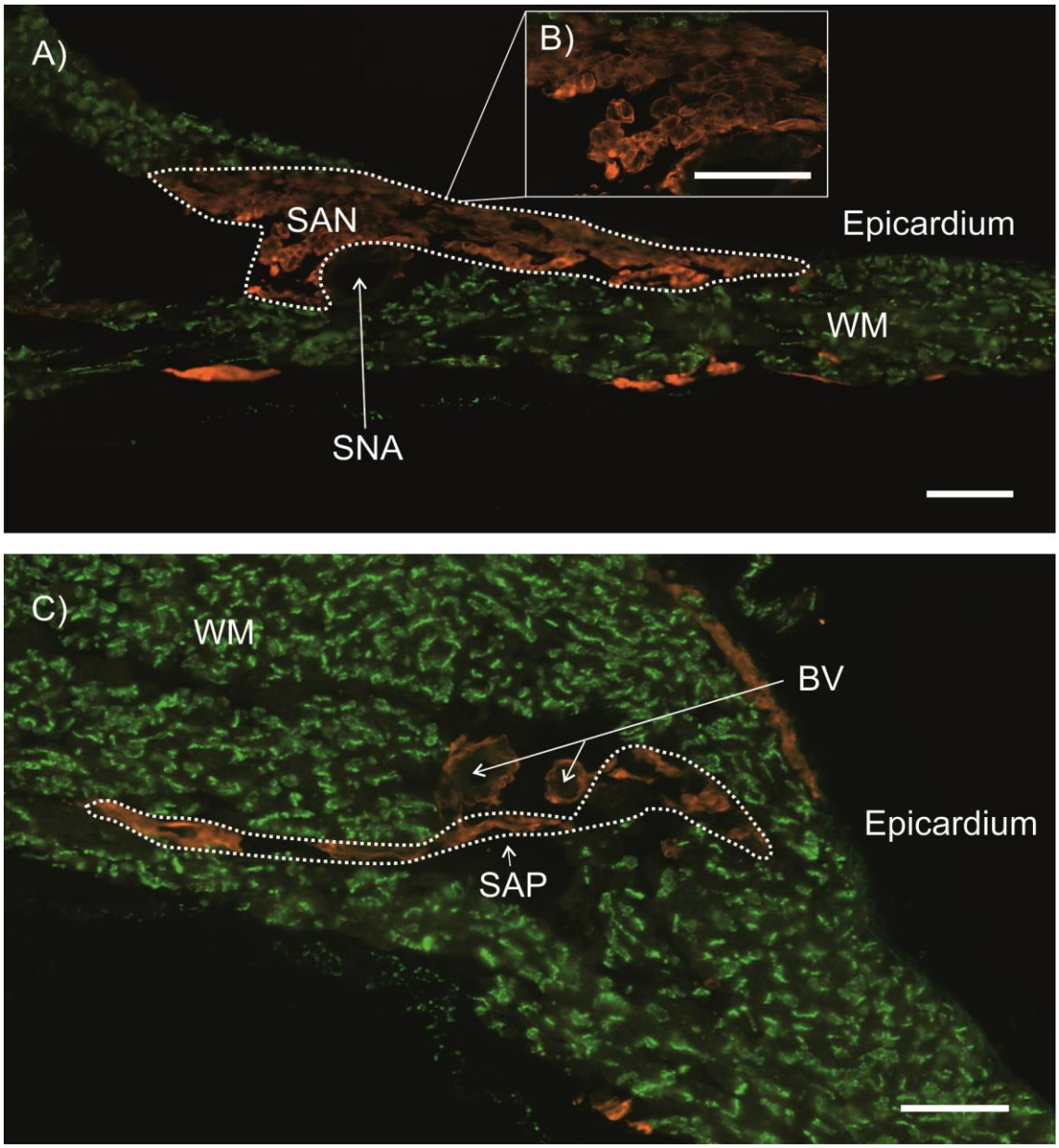

Figure 19. HCN4 and Cx43 immunostaining in horizontal sections of rat sinoatrial node and subsidiary atrial pacemaker tissue

20 µm horizontal cryosections at 1 mm intervals of (A,B) SAN and (C) SAP tissue were immunostained for HCN4 (orange) and Cx43 (green). 12 superior sections showed extensive HCN4-positive/Cx43-negative signal representing the SAN, whilst 5 inferior sections demonstrated this signal from SAP tissue within a smaller area of each section. Panel B shows a higher magnification image of the SAN demonstrating a cell membrane pattern of HCN4 signal. SAN, sinoatrial node; SAP, subsidiary atrial pacemaker; SNA, sinus node artery; WM, working myocardium; BV, blood vessel. Scale bars represent 100 µm.

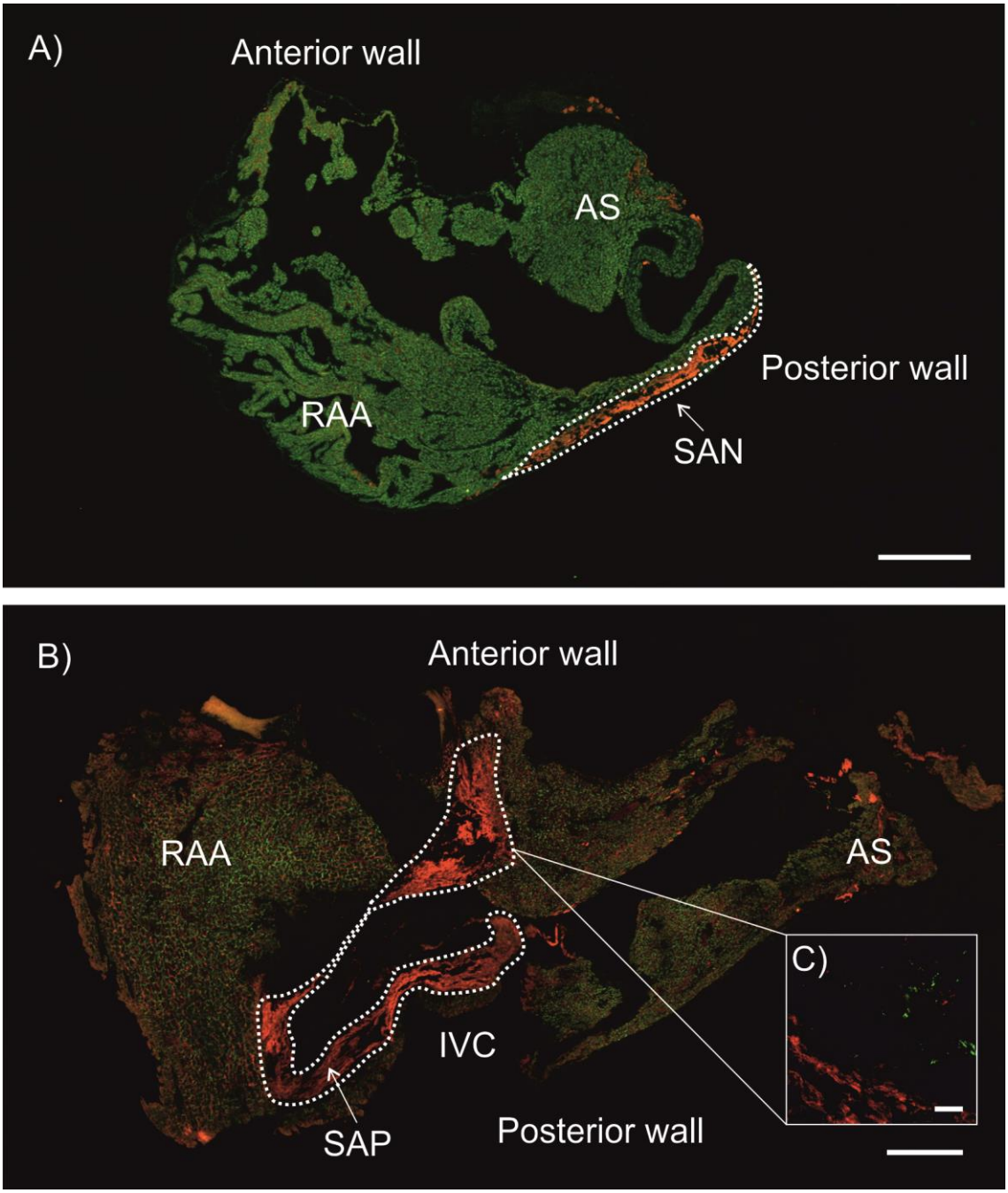

Figure 20. HCN4 and Cx43 immunostaining in serial sections of intact right atrial tissue

20 µm horizontal cryosections were taken from an intact RA preparation at 0.5 mm intervals and immunostained for HCN4 (orange) and Cx43 (green). (A) Extensive HCN4-positive/Cx43-negative tissue was seen in the SAN area. (B) A large amount of this tissue was also seen in the SAP area just above the IVC. (C) High magnification confocal microscopy of the SAP/atrial border shows mutually exclusive labelling of HCN4 and Cx43. RAA, right atrial appendage; IVC, inferior vena cava; AS, atrial septum. Scale bars in panels A and B are 500 µm. Scale bar in panel C is 20 µm.

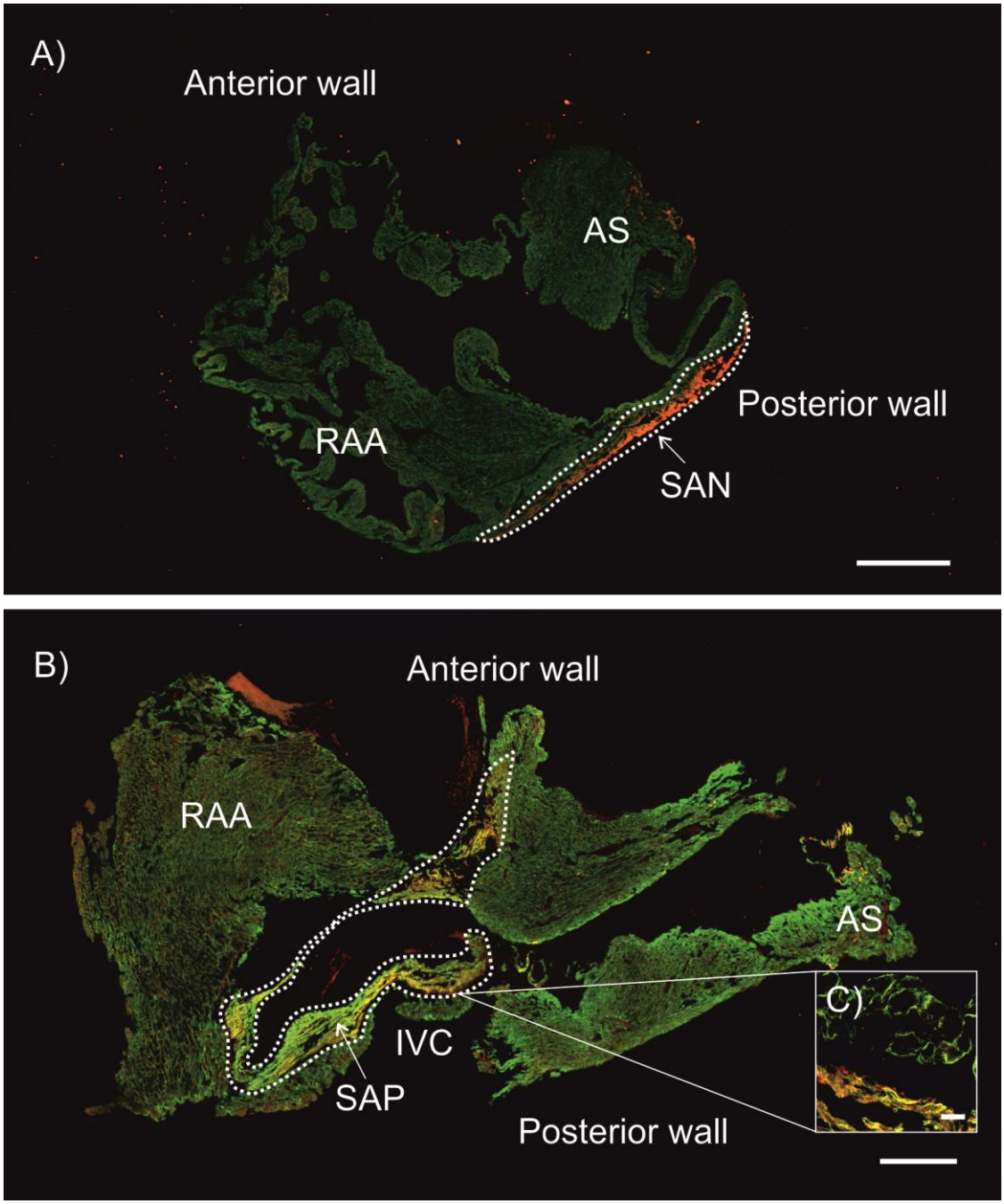

Figure 21. HCN4 and Cav3 immunostaining in serial sections of intact right atrial tissue

20 µm horizontal cryosections were taken from an intact RA preparation at 0.5 mm intervals and labelled for HCN4 (orange) and Cav3 (green). HCN4 signal was seen in (A) SAN and (B) SAP areas, colocalised (yellow) with Cav3 suggesting these cells were cardiomyocytes. (C) High magnification confocal microscopy showed that HCN4 colocalised with Cav3. These cells were smaller and spindle-shaped compared to atrial cells. RAA, right atrial appendage; IVC, inferior vena cava; AS, atrial septum. Scale bars in panels A and B are 500 µm. Scale bar in panel C is 20 µm.

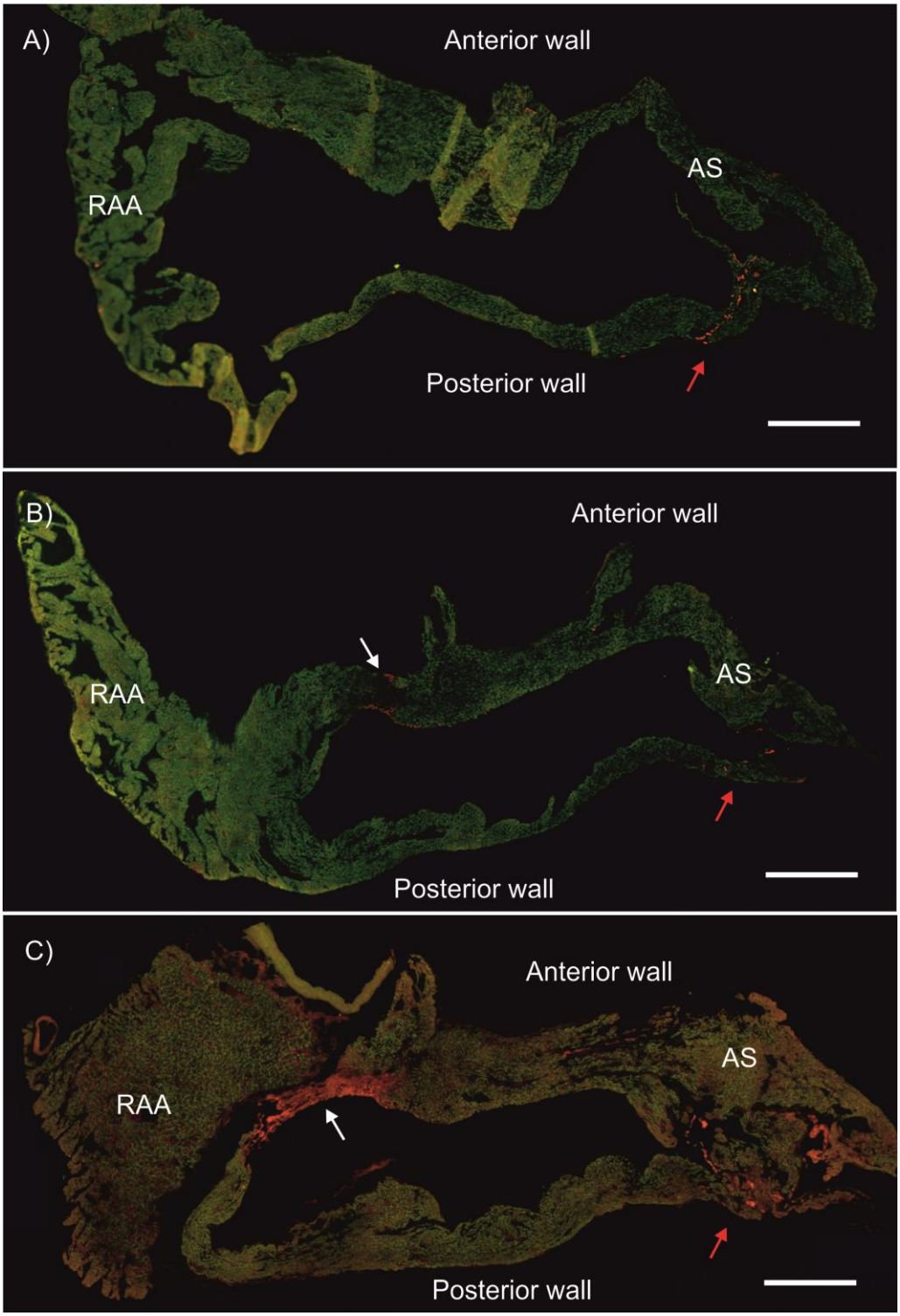

Figure 22. Intermediate sections between SAN and SAP tissue

(A-C) Descending 20 µm horizontal sections taken from an intact RA preparation at levels midway between superior SAN and inferior SAP signals. Red arrows indicate the SAN tail and white arrows indicate the superior SAP which were not continuous with each other. RAA; right atrial appendage; AS, atrial septum. Scale bars are 1000 µm.

3.1.3 Pharmacology before tissue culture

SAN and SAP preparations were freshly isolated from rat RA as described, superfused with physiologic Tyrode's solution and had extracellular potentials recorded from them to continuously measure beating rate. Tyrode's solution containing ivabradine (to block I_f) (n=5), ISO (as a β-agonist) (n=5) and ryanodine (to block RYRs) (n=7) were then individually superfused and mean 60 s beating rates and change in beating rate were analysed (figure 23). Unpaired t-testing was used to compare groups.

Using ivabradine, the mean beating rate of control SAN preparations was 328 ± 13 bpm reducing to 194 ± 9 bpm post application of ivabradine ($p<0.001$), demonstrating a 40.4 ± 3.7 % change in rate. The mean beating rate of control SAP preparations was 260 ± 34 bpm reducing to 165 ± 11 bpm post ivabradine ($p<0.05$), demonstrating a 33.0 ± 6.3 % change in rate.

Using ISO, the mean beating rate of control SAN preparations was 277 ± 16 bpm increasing to 427 ± 24 bpm post application of ISO ($p<0.001$), demonstrating a 55.1 ± 7.7 % change in rate. The mean beating rate of control SAP preparations was 238 ± 13 bpm increasing to 311 ± 10 bpm post ISO ($p<0.01$), demonstrating a 32.3 ± 8.2 % change in rate.

Using ryanodine, the mean beating rate of control SAN preparations was 309 ± 14 bpm reducing to 237 ± 22 bpm post application of ryanodine ($p<0.05$), demonstrating a 23.6 ± 6.6 % change in rate. The mean beating rate of control SAP preparations was 282 ± 11 bpm reducing to 234 ± 13 bpm post ryanodine ($p<0.05$), demonstrating a 16.9 ± 4.0 % change in rate.

The change in rate of SAN versus SAP preparations was not statistically significant using any of the pharmacological agents used.

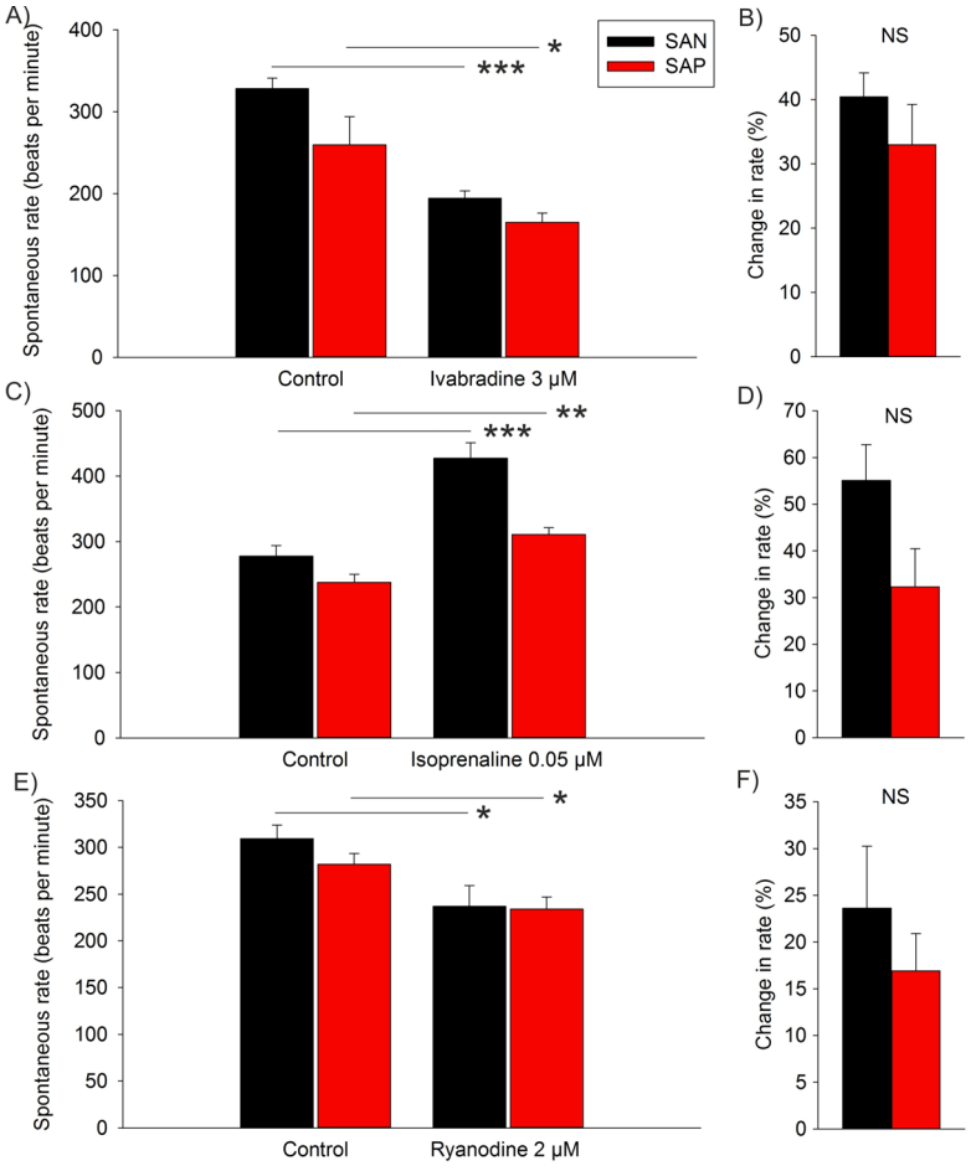

Figure 23. Effect of ivabradine, isoprenaline and ryanodine on SAN and SAP tissue beating rates

Isolated SAN and SAP preparations were exposed individually to (A,B) ivabradine (3 µM; n=5), (C,D) isoprenaline (0.05 µM; n=5) and (E,F) ryanodine (2 µM; n=7) and beating rates were measured. All three drugs had a similar effect in SAN and SAP tissues, suggesting that I_f, β-adrenergic and intracellular Ca^{2+} components play a similar role in both. Mean beating rates ± SEM shown. *p<0.05; **p<0.01; ***p<0.001; NS=not significant (unpaired t-test).

3.2 Recombinant adenovirus

3.2.1 Introduction

RAds are engineered adenoviruses that recombine the human serotype 5 adenoviral genome with a number of other genes including a high efficiency 'promotor' gene, in this case based on the cytomegalovirus (CMV). The virus' replication genes E1 and E3 are removed rendering it replication deficient for increased safety while providing capacity to insert of a gene of interest.[220] Thus instead of the virus infecting a host cell to deliver its own genes for replication, it delivers the gene of interest, which goes on to be expressed by the cell. Adenoviruses have a large capacity (upto 8 kilobases (Kb)) for a very wide range of genes of interest and so the catalogue of genes potentially available for expression is extensive. Adenoviruses are also capable of infecting a wide range of host cells from most tissue types in most mammalian species thanks to the ubiquity of the coxsackie/adenovirus receptor (CAR) on host cell membranes. Cells are normally viable post-infection with low levels of apoptosis.[220]

In order for RAds to replicate for the purposes of amplification, infection of 293 cells is necessary. 293 cells harbour the E1 and E3 genes needed for adenovirus replication. As a result of rapidly increasing levels of virus, 293 cells eventually rupture releasing large numbers of replicated virus that go on to infect surrounding cells. After most 293 cells have been used the amplified viral mixture can be purified and concentrated further. There is a small chance that wild-type viruses can be recreated by incorporation of the E1 and E3 genes back into replicating viruses, and so large-scale amplification should undergo regular testing for wild-type viruses. Amplification was needed to achieve titres high enough (at least $1x10^9$ pfu/ml) to ensure effective gene transduction from small volume injections (e.g. 1 µl).

Our genes of interest included Tbx18 for its role in early SAN morphogenesis, Tbx3 for its role in fine tuning the CCS and NCX1 for its integral role in membrane and Ca^{2+} clocks. In addition genes for GFP and LacZ would be used as controls. Adenoviruses used therefore included Ad-Tbx18, Ad-Tbx3, Ad-NCX1-GFP, Ad-GFP and Ad-LacZ. Amplification of Ad-

Tbx18, Ad-Tbx3 and Ad-NCX1-GFP was required whilst Ad-GFP and Ad-LacZ were available to the group at high titres already.

3.2.2 Amplification and titres

3.2.2.1 Ad-Tbx18

Stock Ad-Tbx18 virus was purchased (ABMGood) with a titre of at least $1x10^6$ pfu/ml. In order to attain a titre high enough to ensure effective transduction using small 1-2 µl injections (at least $1x10^9$ pfu/ml), this stock was amplified by infecting 293 cells (Stratagene). A total of three amplification cycles were necessary to bring the titre up to a satisfactory level. The final titre was measured at $9.4x10^8$ pfu/ml. This was the maximum titre obtained.

3.2.2.2 Ad-Tbx3

As above, stock Ad-Tbx3 virus was purchased (ABMGood) with a titre of at least $1x10^6$ pfu/ml. This was amplified using 293 cells (Stratagene). One amplification cycle was needed to ensure an adequate titre for small volume injections with a final titre measured at $9.4x10^{10}$ pfu/ml.

3.2.2.3 Ad-NCX1-GFP

Stock Ad-NCX1-GFP virus was kindly donated to us by Professor Godfrey Smith's lab (University of Glasgow) with a quoted titre of $1.5x10^{10}$ pfu/ml. Amplification was necessary to create a higher volume of stock virus rather than achieve a higher titre. After one cycle of amplification viral titre was measured at $2.5x10^{10}$ pfu/ml.

3.2.3 Validation

3.2.3.1 Ad-Tbx18

3.2.3.1.1 Immunohistochemistry

To validate expression of Tbx18 protein following infection with our amplified Ad-Tbx18 virus, immunohistochemistry was performed on 293 cells (n=2) and sections of injected SAP tissue after 48 hours of tissue culture (n=4).

In 293 cells, Ad-Tbx18 infection consistently resulted in positive immunolabelling of Tbx18 protein with a well-defined nuclear pattern and also defined nucleoli which showed no signal (figure 24). At high magnification a speckled cytosolic signal was also seen in some cells possibly representing ribosomes. Uninfected 293 cells demonstrated no Tbx18 signal at all.

In SAP tissue, results from immunohistochemistry were generally inconsistent. Only 2 of 4 preparations infected with Ad-Tbx18 virus analysed post-culture demonstrated detectable Tbx18 protein signal, examples of which can be seen in figure 24 and appendix A4. In the two positively stained preparations, Tbx18 signal was seen in individual cells distributed sporadically throughout the width of the tissue. High magnification images of these cells showed a solid, possibly nuclear pattern within each cell. Uninfected preparations never demonstrated any Tbx18 signal.

Immunolabelling of Cx43, Cav3 and HCN1 in Ad-Tbx18 infected SAP tissue was attempted but was inconsistent. Cx43 labelling was very patchy even in large areas of atrial tissue and therefore absence of signal would not necessarily suggest absence of Cx43. HCN1 signal was not apparent in any section tested despite previous success with the same antibodies in uncultured inferior RA (unpublished data from our group). Cav3 was more consistent than Cx43 but did not label all cells. Examples of these attempts are therefore available in appendix A4.

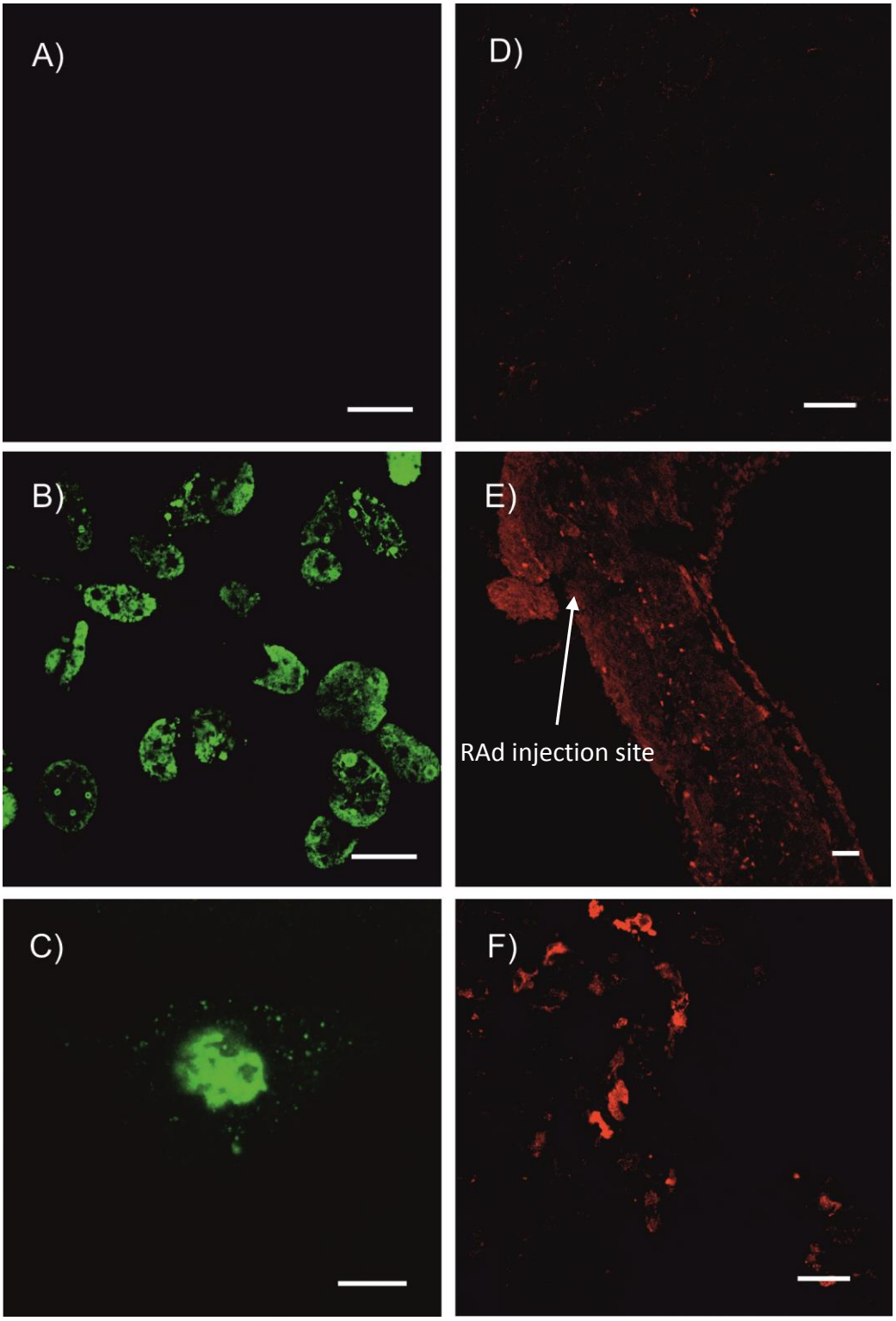

Figure 24. Cultured 293 cells and SAP tissue immunostained for Tbx18

Ad-Tbx18 infected 293 cells (n=2) and cultured SAP tissue (n=4) were immunostained for Tbx18 protein. (A) Uninfected and (B,C) Ad-Tbx18 infected 293 cells seen at low and high magnification. (D) Uninfected and (E,F) Ad-Tbx18 infected SAP tissue seen at low and high magnification. Scale bars represent 20 µm in panels A-C, and 50 µm in panels D-F.

3.2.3.1.2 qPCR

To validate Tbx18 expression, qPCR was performed on purified DNA extracted from 293 cells used for amplification of the virus (n=2) and RT-qPCR on total RNA isolated from SAP tissue following 48 hours of tissue culture (n=8).

In 293 cells, Ad-Tbx18 infected cells demonstrated consistent amplification of Tbx18 DNA with a mean C_t value in all samples of 15 and consistent peak dissociation at around 77.5°C (figure 25). The PCR end product was subject to gel electrophoresis to measure the molecular weight of the amplicon produced. This consistently resulted in a single band at around the quoted amplicon weight of 82 bp that Qiagen states should result from the Tbx18 primer used. In contrast, uninfected cells did not amplify any Tbx18 DNA.

In cultured SAP tissue, relative Tbx18 mRNA abundance was calculated in relation to the housekeeper gene 18S (figure 26). Ad-Tbx18 infection resulted in a 110-fold rise in Tbx18 mRNA compared to uninfected tissue (mean relative mRNA abundance of $4.1 \times 10^{-3} \pm 6.8 \times 10^{-4}$ arbitrary units in Ad-Tbx18 infected tissue versus $3.8 \times 10^{-5} \pm 4.8 \times 10^{-6}$ in uninfected tissue; $p<0.001$).

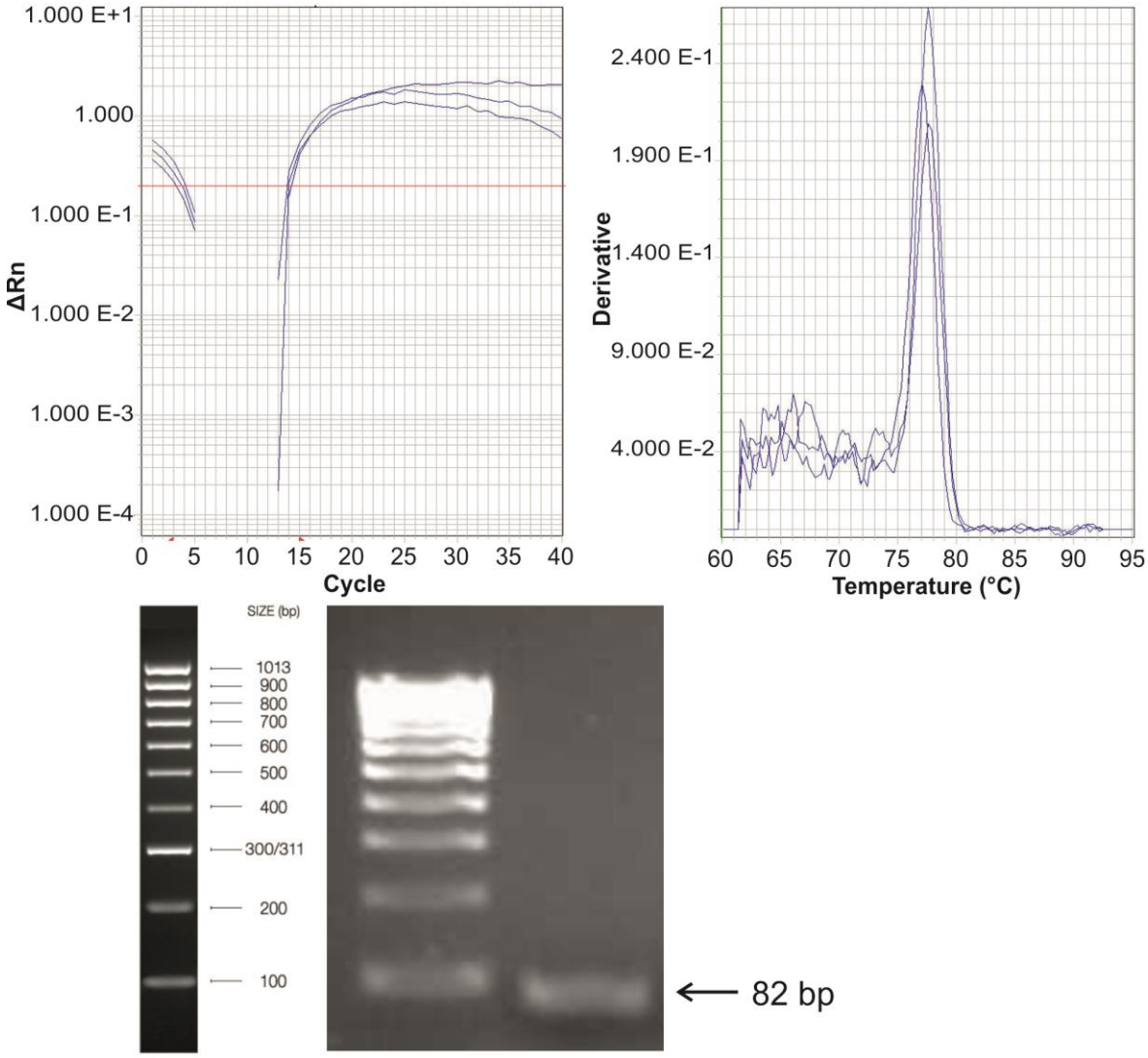

Figure 25. qPCR amplification plot, dissociation curve and gel electrophoresis for Tbx18 DNA isolated from Ad-Tbx18 infected 293 cells

DNA was purified from Ad-Tbx18 infected 293 cells and Tbx18 DNA was measured using qPCR (n=2). Consistent amplification of Tbx18 DNA was seen in every sample. The amplicon size measured using gel electrophoresis was as expected for the primer used.

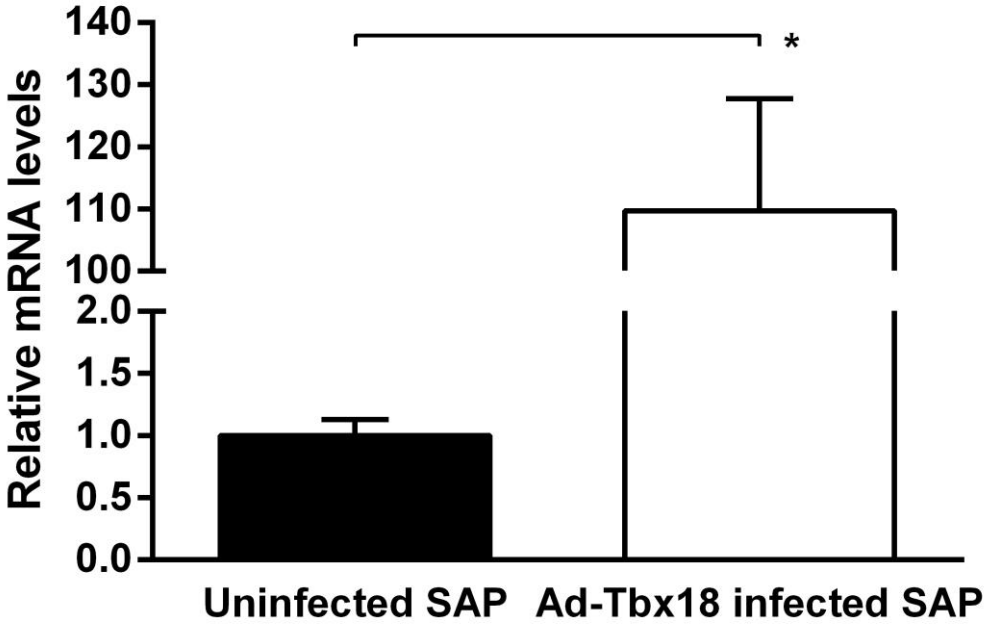

Figure 26. mRNA levels of Tbx18 measured by RT-qPCR in cultured SAP tissue with and without Ad-Tbx18 infection

RT-qPCR was used to measure relative levels of Tbx18 mRNA from Ad-Tbx18 infected (n=8) and uninfected SAP tissue (n=8). There was a 110-fold rise as a result of Ad-Tbx18 infection (*$p<0.001$).

3.2.3.2 Ad-Tbx3

3.2.3.2.1 RT-qPCR

In order to validate mRNA expression of Tbx3 following Ad-Tbx3 infection RT-qPCR was performed on SAP tissue following 48 hours of tissue culture (n=6).

Relative Tbx3 mRNA abundance was calculated in relation to the housekeeper gene 18S (figure 27). Ad-Tbx3 infection resulted in a 3.7-fold rise in Tbx3 mRNA compared to uninfected tissue (mean relative mRNA abundance of $4.5x10^{-5} \pm 1.2x10^{-5}$ arbitrary units in Ad-Tbx3 infected tissue versus $1.2x10^{-5} \pm 2.3x10^{-6}$ in uninfected tissue; $p<0.05$).

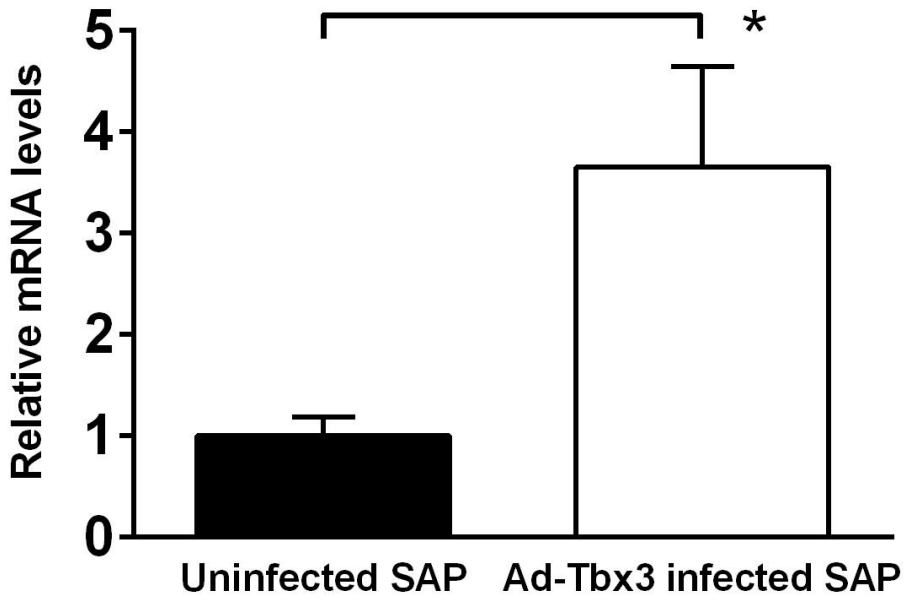

Figure 27. mRNA levels of Tbx3 measured by RT-qPCR in cultured SAP tissue with and without Ad-Tbx3 infection

RT-qPCR was used to measure relative levels of Tbx3 mRNA from Ad-Tbx3 infected (n=6) and uninfected SAP tissue (n=6). There was a 3.7-fold rise as a result of Ad-Tbx3 infection (*$p<0.05$).

3.2.3.3 Ad-NCX1-GFP

3.2.3.3.1 qPCR

To validate NCX1 DNA expression as a result of Ad-NCX1-GFP infection, qPCR was performed on purified DNA extracted from infected 293 cells following 48 hours of culture (n=1).

Ad-NCX1-GFP infected cells demonstrated amplification of NCX1 DNA with a mean C_t value of 11 and consistent peak dissociation. The PCR end product was subject to gel electrophoresis to measure the molecular weight of the amplicon produced. This resulted in a single band at around the quoted amplicon weight of 162 bp that Qiagen states should result from the NCX1 primer used (figure 28). In contrast, uninfected cells did not amplify any NCX1 DNA.

3.2.3.3.2 GFP signal

The Ad-NCX1-GFP virus was a bicistronic vector expressing both NCX1 and GFP, and so it was possible to visualise transduced cells within intact tissue directly under a confocal microscope. Therefore, both uninfected SAP tissue and SAP tissue infected with Ad-NCX1-GFP were visualised by microscopy under a mercury lamp and scanned with confocal microscopy after 48 hours of tissue culture (figure 29).

Ad-NCX1-GFP infected SAP tissue demonstrated extensive and bright GFP signal with a cell membrane pattern in all preparations (n=6). This GFP signal extended 3-4 mm in radius around the injection site and penetrated the full thickness of the tissue. Uninfected SAP tissue did not exhibit any GFP signal at all (n=6).

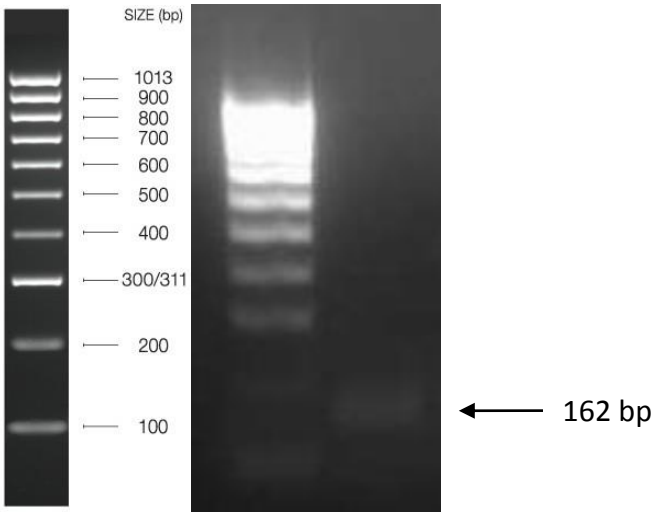

Figure 28. qPCR amplification and gel electrophoresis for NCX1 DNA isolated from Ad-NCX1-GFP infected 293 cells

DNA was purified from Ad-NCX1-GFP infected 293 cells and NCX1 DNA was measured using qPCR (n=1). Consistent levels of the NCX1 was seen in every sample. The amplicon size measured using gel electrophoresis was as expected for the primer used.

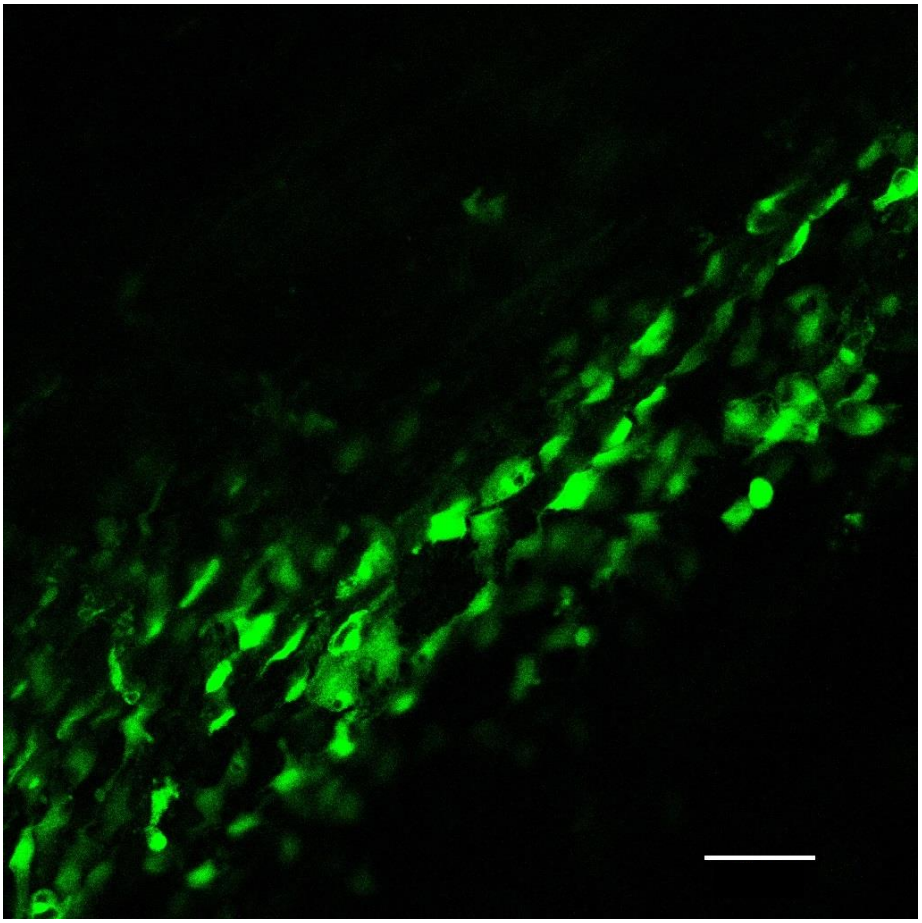

Figure 29. GFP signal seen by confocal microscopy in cultured SAP tissue following Ad-NCX1-GFP infection

Following 48 hours of tissue culture, Ad-NCX1-GFP infected SAP tissue was visualised under the confocal microscope. All preparations (n=6) demonstrated strong GFP signal from around the injection site with a cell membrane pattern. Scale bar represents 50 µm.

3.2.3.4 Ad-PREK-LacZ

By using the Ad-PREK-LacZ virus available to the lab, we could express the LacZ gene capable of producing a blue discolouration in successfully transduced tissue when subjected to an X-Gal assay protocol. We therefore injected the virus into SAP tissue using exactly the same methods as before to directly visualise the extent of transduction after 48 hours of tissue culture (n=1). This would provide an estimate of the area of tissue likely to be transduced by the other viruses of interest.

Blue discolouration was produced in Ad-PREK-LacZ infected tissue, which extended 2-3 mm in radius around the site of injection and penetrated the full thickness of the tissue (figure 30).

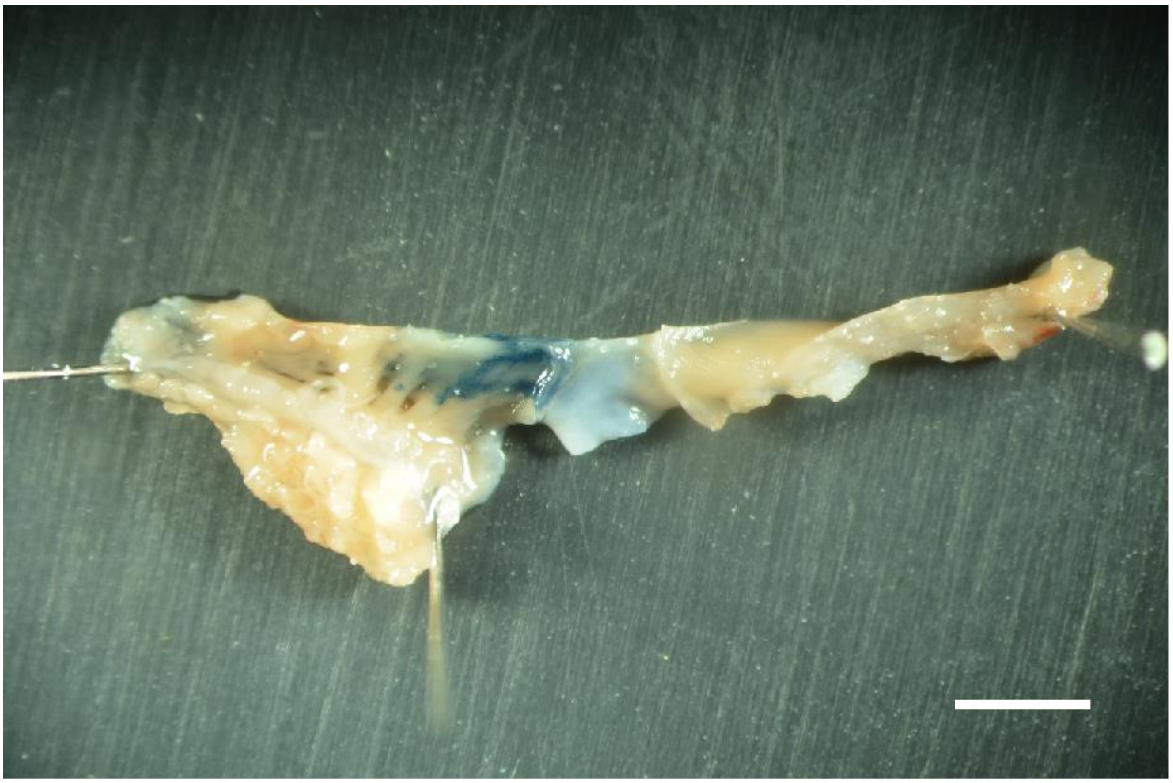

Figure 30. SAP tissue infected with Ad-LacZ and stained with an XGal assay

Ad-LacZ was injected into SAP tissue and cultured for 48 hours, then subject to an XGal assay. Blue discolouration was seen in tissue expressing LacZ as a result of viral transduction allowing direct visualisation of the extent of transduction from a single injection. Scale represents 2 mm.

3.3 Ad-Tbx18

3.3.1 Introduction

Tbx18 is a transcription factor normally present during the embryonic development of the SAN. It is seen in mice around day 9.5 within mesenchymal progenitor cells that persist at the caudal end of the developing heart tube.[19, 20] These cells go on to become the sinus horns where Tbx18 regulates the morphological development of the SAN head.[10, 20] Without Tbx18 the SAN head fails to develop.[20] Following birth Tbx18 is no longer seen in the neonatal or adult SAN.[203]

Tbx18 has been successfully used to reprogramme ventricular myocytes into pacemaker cells *ex vivo* in isolated NRVMs and *in vivo* in the ventricles of guinea pigs and pigs.[203, 204] The latest attempts in pigs with induced complete heart block created ectopic ventricular biological pacemakers at the site of adenoviral injection, with physiological beating rates, reduced corrected recovery time, abolition of backup electronic pacing and autonomic sensitivity.[204] Isolated cells demonstrated change in morphology from brick-like ventricular cells to a SAN-like spindle-shape.[203, 204] qPCR revealed downregulation in the atrial genes Cx43, $K_{ir}2.1$, Nkx2-5 and $Na_v1.5$, whereas HCN4 was upregulated.[203, 204] However, the functional effects of Tbx18 adenoviral injection were only seen to be temporary lasting around 14 days.[204]

Rather than use ventricular tissue which may harbour substrate that is inhibitory to pacemaker function, this work focused on bradycardic SAP tissue in the inferior RA since many molecular and functional features of the SAN are already seen to be present and this may aid biopacemaking.[152] SAP tissue could also be used as a model for SAN dysfunction and provide insight into the possible effects of injecting Tbx18-expressing adenovirus directly into a dysfunctional SAN for therapeutic purposes.

We therefore hypothesised that upregulating Tbx18 in SAP tissue would increase beating rates, reduce overdrive suppression, maintain autonomic sensitivity, upregulate pacemaker genes such as HCN4 and downregulate atrial genes.

3.3.2 Beating rates

Extracellular potentials were continuously recorded over 48 hours of tissue culture. Beating rate data from SAN preparations (n=15), uninfected SAP preparations (n=13) and SAP preparations infected with Ad-Tbx18 (n=8) were compared to one another. Raw beating rate data is shown in figures 31 - 33.

In all preparations regardless of type, beating rates rose at a steady rate over the first 20 hours and declined at a similar rate thereafter until the end of each experiment at 48 hours. This consistent pattern between all preparations made it possible to compare them at individual time points throughout the recording. In SAN preparations the mean beating rate over the first hour was 287 ± 8 bpm, rising to a maximum mean rate of 374 ± 9 bpm during hour 20 and falling to a minimum mean rate of 267 ± 14 bpm during the final hour. Uninfected SAP preparations were bradycardic compared to the SAN, demonstrating a mean first hour beating rate of 230 ± 8 bpm, a maximum of 277 ± 10 bpm during hour 17 and a minimum of 141 ± 9 bpm during the final hour. Ad-Tbx18 infected SAP preparations started during the first hour at 237 ± 17 bpm, rose to a maximum of 278 ± 20 bpm during hour 18 and fell to 215 ± 16 bpm during the final hour.

Further analysis was done looking at mean rates combining data every 4 hours from 20 – 48 hours of recording which allowed best comparison of beating rate data during the period in which Ad-Tbx18 would be predicted to have maximal effect (figure 34). During hours 17-20 when beating rates were generally at their maximum, SAN preparations showed a mean rate of 363 ± 9 bpm, uninfected SAP preparations 261 ± 16 bpm and Ad-Tbx18 infected preparations 277 ± 20 bpm. During the final 45-48 hours, SAN preparations showed a mean rate of 269 ± 12 bpm, uninfected SAP preparations 147 ± 9 bpm and Ad-Tbx18 infected preparations 211 ± 13 bpm.

Statistical analysis showed that SAN preparations were always significantly faster than both uninfected SAP preparations and Ad-Tbx18 infected SAP preparations ($p<0.001$). Meanwhile the difference between uninfected SAP preparations and Ad-Tbx18 infected

SAP preparations was not significant for the majority of the 48 hour recording. However, there was divergence of the curves from hour 20, which reached statistical significance between 45 – 48 hours ($p<0.01$) (figure 34).

3.3.3 RT-qPCR

After 48 hours of culture all preparations had 2 mm diameter samples taken from around the SAN or SAP, snap frozen and stored at -80°C. Once all samples had been acquired RT-qPCR was performed in order to analyse relative differences in mRNA expression focusing on 14 genes related to pacemaking between SAN (n=7), uninfected SAP (n=8) and Ad-Tbx18 infected SAP samples (n=8). The 14 genes measured were HCN1, HCN2, HCN4, Cx43, Cx45, $K_{ir}2.1$, $K_v1.5$, $Na_v1.5$, RYR2, NCX1, Tbx3, Tbx18, $Ca_v1.2$ and $Ca_v3.1$ (figures 35 and 36).

Comparing SAN to SAP tissue there was no significant difference between HCN1 and HCN2 levels, but significantly greater levels of HCN4 in the SAN versus the SAP tissue ($p<0.001$). Ad-Tbx18 infection demonstrated no significant difference in HCN1, but a significant rise in HCN2 and a significant fall in HCN4 versus uninfected SAP tissue ($p<0.01$).

There was significantly more Tbx3 and Tbx18 in the SAN versus SAP tissue ($p<0.05$ and $p<0.01$ respectively). Ad-Tbx18 infection showed no significant change in Tbx3 levels compared to uninfected SAP tissue. As reported in section 2.9.3.1.2 on validation of the Ad-Tbx18 virus, Tbx18 levels were 110-fold higher in Ad-Tbx18 infected SAP tissue compared to uninfected SAP tissue ($p<0.001$).

There were no significant differences in $Na_v1.5$, $K_{ir}2.1$, $K_v1.5$, Cx43, Cx45, NCX1, $Ca_v1.2$ and $Ca_v3.1$ between the groups. There was a significant rise in RYR2 in Ad-Tbx18 infected SAP tissue versus uninfected SAP tissue ($p<0.05$).

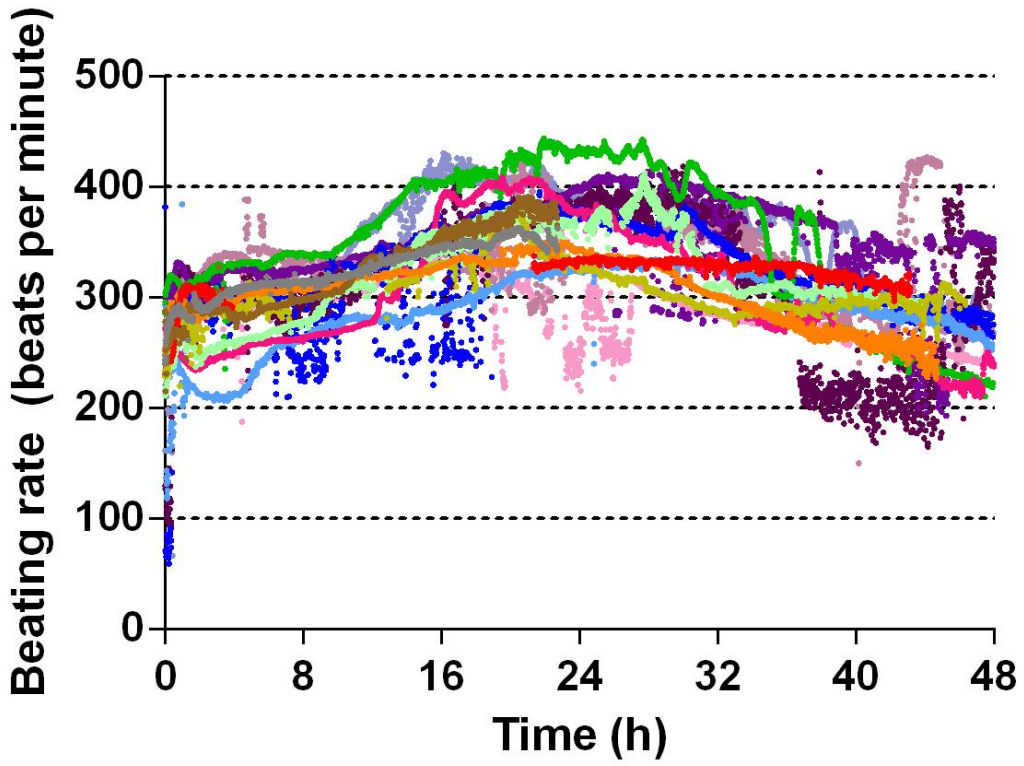

Figure 31. Raw beating rate data from SAN preparations

Beating rates were analysed from complete recordings by LabChart software as mean values at every 1 minute interval over the entire 48 hour culture period. All preparations were analysed. Different colours represent individual preparations (n=15). Dots represent 60 s mean beating rates.

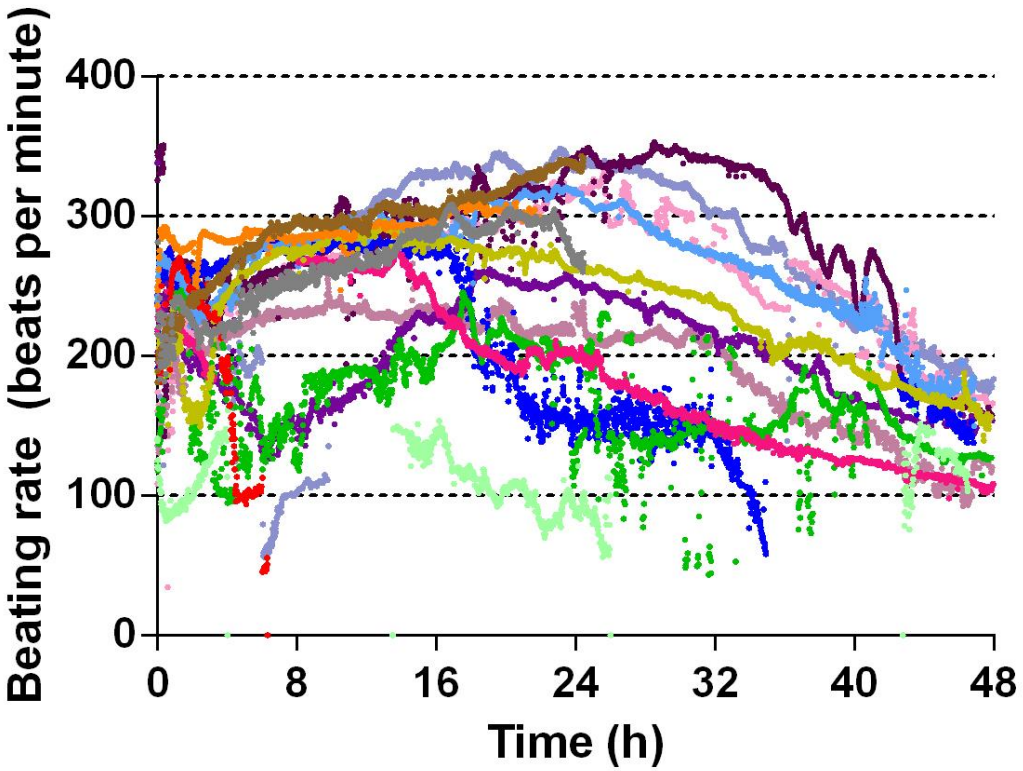

Figure 32. Raw beating rate data from uninfected SAP preparations

Beating rates were analysed from complete recordings by LabChart software as mean values at every 1 minute interval over the entire 48 hour culture period. All preparations were analysed. Different colours represent individual preparations (n=13). Dots represent 60 s mean beating rates.

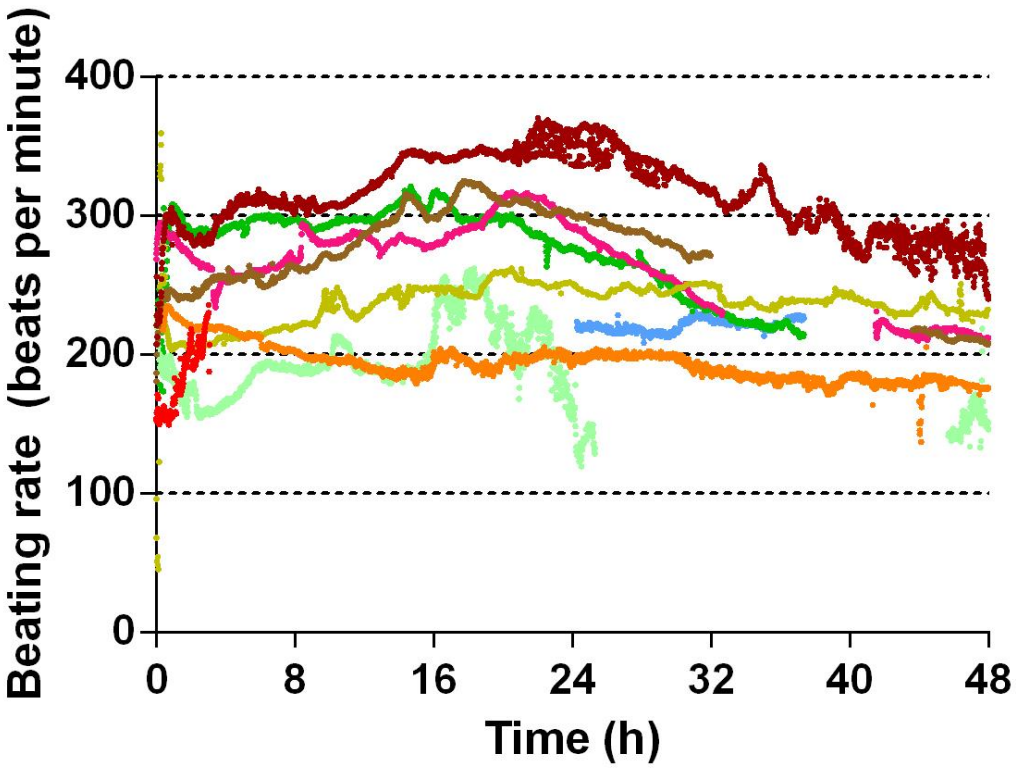

Figure 33. Raw beating rate data from Ad-Tbx18 infected SAP preparations

Beating rates were analysed from complete recordings by LabChart software as mean values at every 1 minute interval over the entire 48 hour culture period. All preparations were analysed. Different colours represent individual preparations (n=8). Dots represent 60 s mean beating rates.

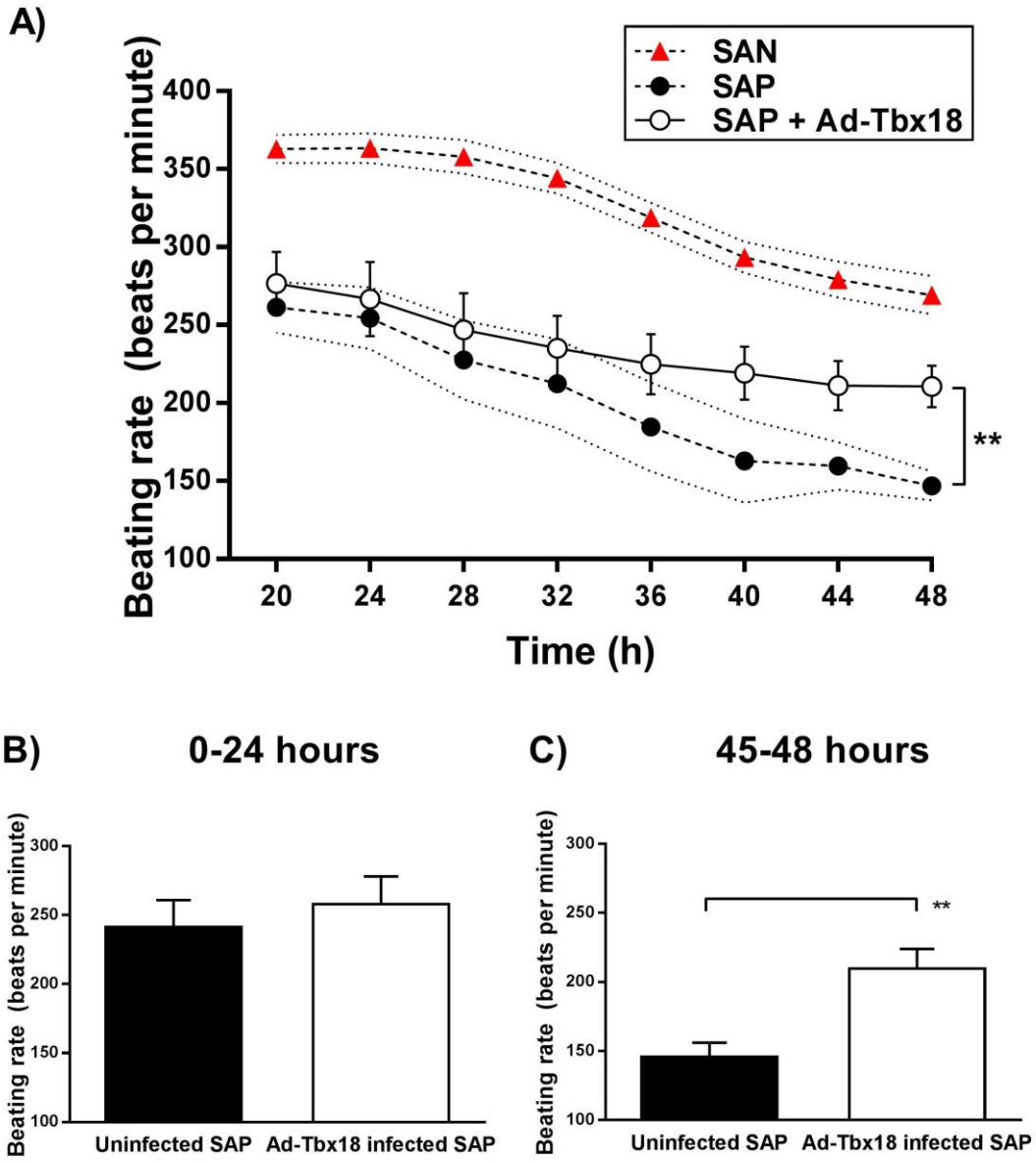

Figure 34. Beating rate data from SAN, uninfected SAP and Ad-Tbx18 infected SAP tissue

Ad-Tbx18 infected SAP tissue (n=8), uninfected SAP tissue (n=13) and SAN tissue (n=15) were cultured for 48 hours and beating rates were continuously measured. (A) Beating rates from Ad-Tbx18 infected tissue diverged from uninfected SAP tissue after 20 hours of culture, (B) with no significant difference between 0-24 hours, (C) Ad-Tbx18 infected SAP tissue becoming significantly faster than uninfected SAP tissue after 48 hours (**p<0.01).

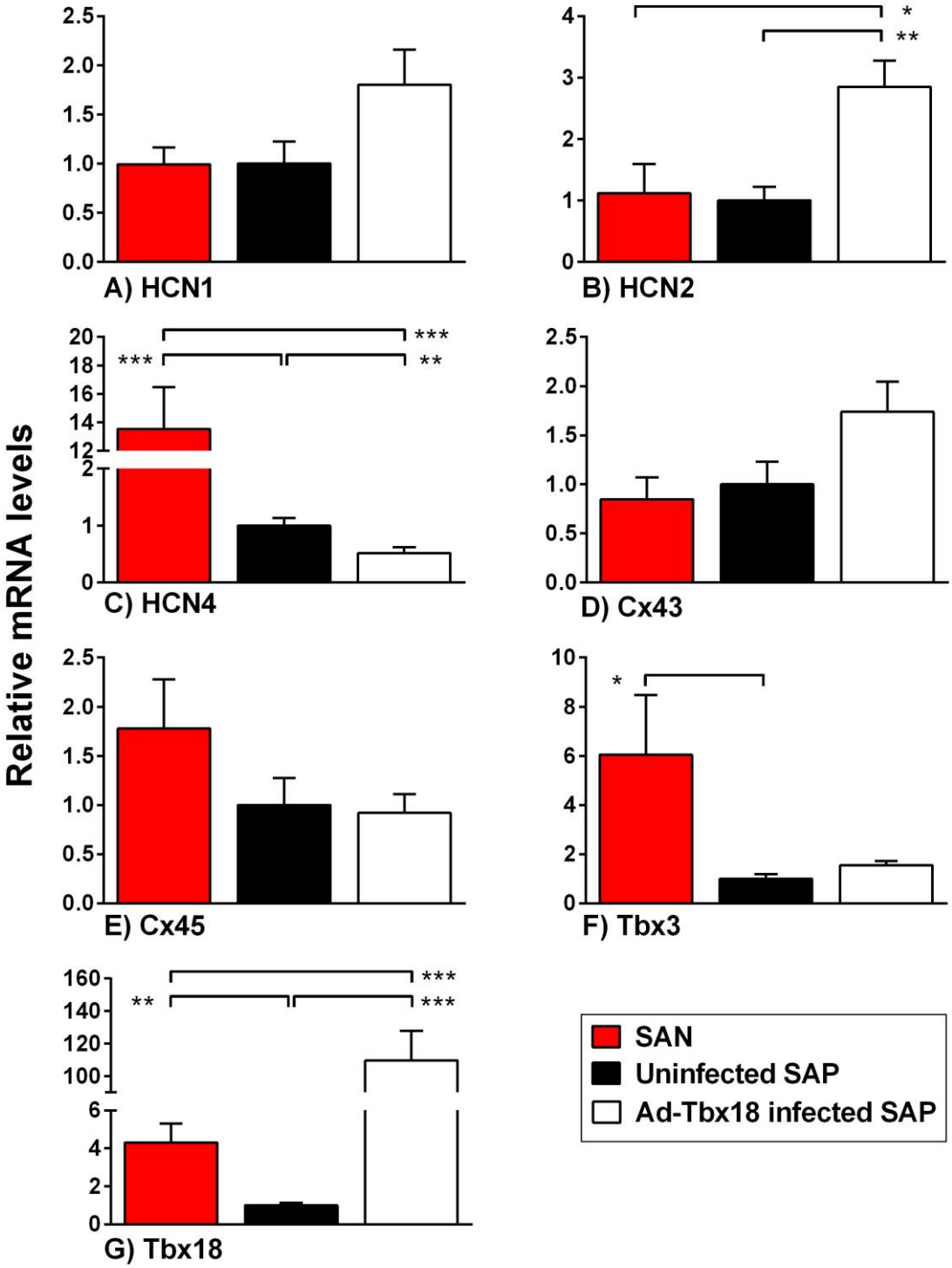

Figure 35. RT-qPCR data showing mRNA levels of pacemaker related genes comparing Ad-Tbx18 infected SAP tissue to SAN and uninfected SAP tissue

(A-G) Relative mRNA abundance of pacemaker related genes in SAN (n=8), uninfected SAP (n=8) and Ad-Tbx18 infected SAP tissue (n=8). *p<0.05; **p<0.01; ***p<0.001.

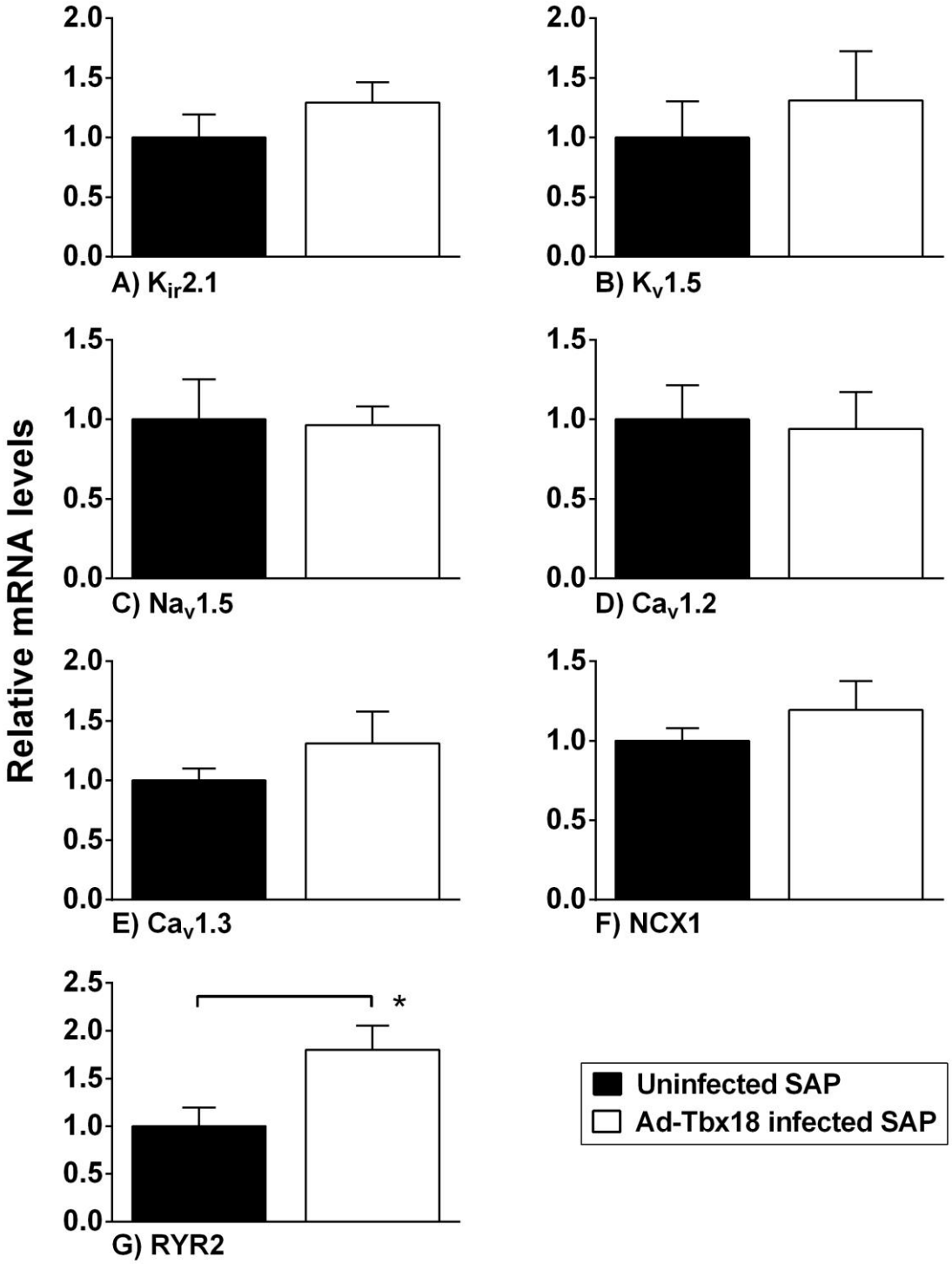

Figure 36. RT-qPCR data showing mRNA levels of atrial and Ca^{2+} handling genes comparing Ad-Tbx18 infected SAP tissue to uninfected SAP tissue

(A-G) Relative mRNA abundance of atrial and Ca^{2+} handling genes in uninfected SAP (n=8) and Ad-Tbx18 infected SAP tissue (n=8). SAN samples were excluded due to atrial contamination. *$p<0.05$.

3.3.4 Overdrive suppression

After 48 hours of tissue culture preparations were subject to an overdrive pacing protocol and cRT measured from Labchart recordings. cRT from SAN preparations (n=5), uninfected SAP preparations (n=6) and Ad-Tbx18 infected SAP preparations (n=5) were compared (figure 37).

SAN preparations demonstrated a cRT of 78 ± 9 ms. Uninfected SAP preparations showed a significantly slower cRT of 125 ± 10 ms compared to the SAN ($p<0.05$). Ad-Tbx18 infected SAP preparations exhibited a cRT of 140 ± 23 ms and therefore showed no significant difference compared to uninfected SAP preparations ($p>0.05$).

3.3.5 Response to I_f blockade and β-adrenergic stimulation

Following 48 hours of tissue culture preparations were superfused with solutions of CsCl and ISO individually in order to assess response to I_f blockade and β-adrenergic stimulation respectively. The SAN (CsCl, n=4; ISO n=5) was compared to uninfected SAP preparations (CsCl, n=5; ISO n=3) and Ad-Tbx18 infected SAP preparations (CsCl, n=4; ISO n=4) (figure 38).

CsCl induced a 33 ± 3% drop in SAN beating rate, a 37 ± 6% drop in uninfected SAP rate and a 31 ± 5% drop in Ad-Tbx18 infected SAP rate. There were therefore no significant differences between the three groups ($p>0.05$). ISO induced a 62 ± 12% rise in SAN beating rate, a 116 ± 34% rise in uninfected SAP rate and a 125 ± 56% rise in Ad-Tbx18 infected SAP rate. Statistically there were no differences between groups ($p>0.05$).

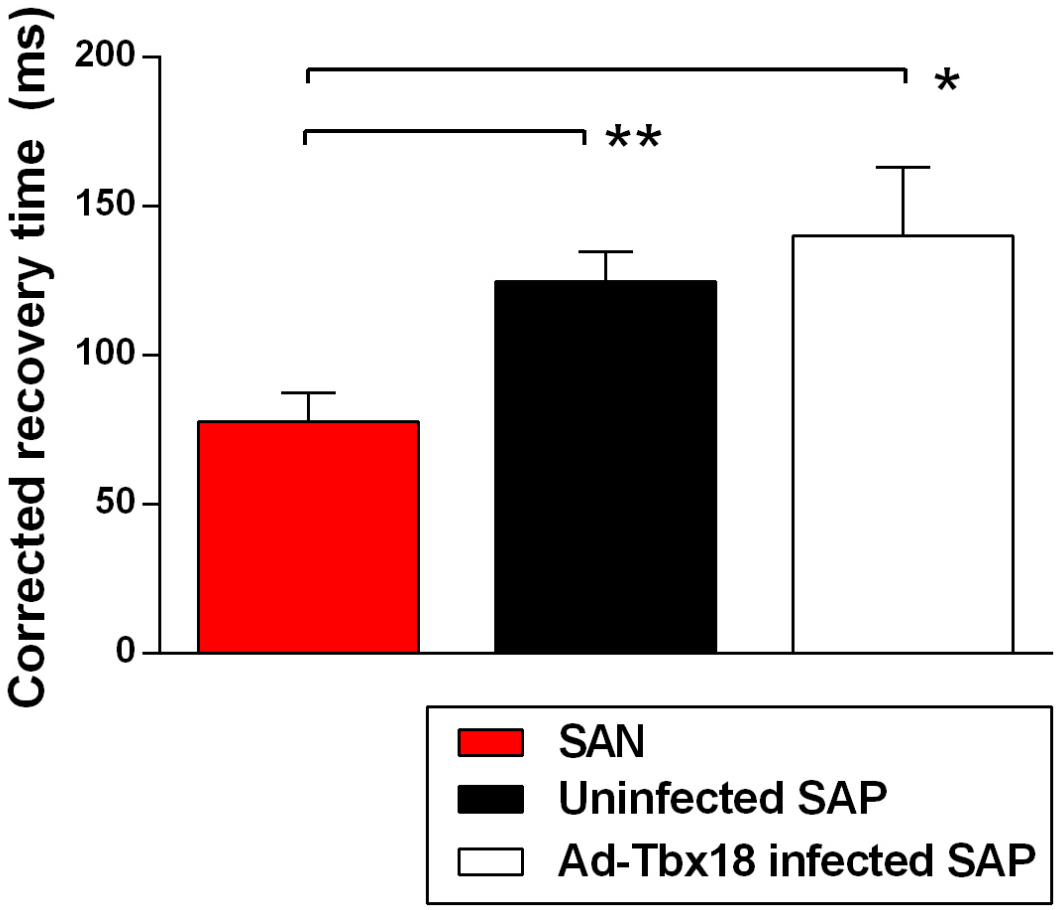

Figure 37. Corrected recovery times after overdrive pacing in SAN, uninfected SAP and Ad-Tbx18 infected SAP tissue

An overdrive pacing protocol was applied to SAN (n=5), uninfected SAP (n=6) and Ad-Tbx18 infected SAP tissue (n=5). No significant difference was found in corrected recovery times (cRT) between uninfected and Ad-Tbx18 infected SAP tissue. However, SAN tissue demonstrated a significantly shorter cRT than both uninfected and Ad-Tbx18 infected SAP tissue. *$p<0.05$; **$p<0.01$.

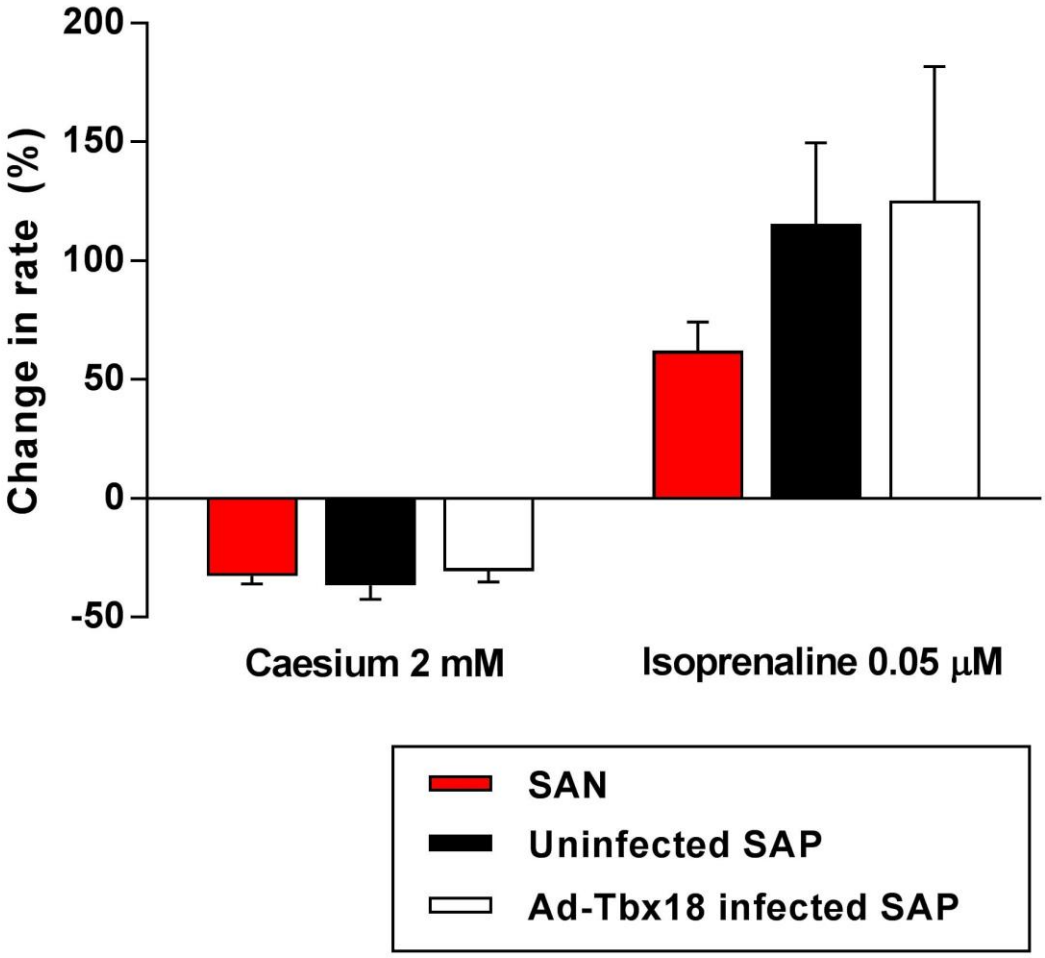

Figure 38. Effect of caesium and isoprenaline on SAN, uninfected SAP and Ad-Tbx18 infected SAP tissue

Cultured SAN, uninfected SAP and Ad-Tbx18 infected SAP tissues were exposed to caesium (2 mM) and isoprenaline (0.05 μM) solutions and change in beating rate was analysed. No significant differences were seen between groups ($p>0.05$).

3.4 Ad-Tbx3

3.4.1 Introduction

Tbx3 is a transcription factor involved in the embryonic development and maintenance of the CCS.[14 15] During embryogenesis Tbx3 acts as a repressor of the atrial phenotype inhibiting expression of genes, ion channels and gap junctions specific to working atrial myocardium such as *Nppa*, Cx40, Cx43, $Na_v1.5$ and $K_{ir}2.1$.[15, 16] Tbx3 may also lead to indirect promotion of pacemaker specific ion channels such as HCN and T-type Ca^{2+}channels.[16]

Tbx3 is an attractive target for biopacemaking. Previous work using transgenic mice has ectopically expressed Tbx3 using Tamoxifen in the adult heart.[205] It was successful in efficiently repressing the atrial genes Cx40, Cx43, $Na_v1.5$ and $K_{ir}2.1$, but HCN4 was downregulated in ventricular tissue and only HCN1 was upregulated in atrial tissue.[205] Furthermore, I_f was not recordable in this work.[205] Subsequent work using lentiviral expression of Tbx3 in NRVMs led to production of spontaneous pacemaking, conduction slowing, reduction of $I_{K,1}$ and I_{Na}, but again I_f was absent.[205]

We would again use SAP tissue in the inferior RA as our biopacemaking substrate, and since it already forms part of the CCS it may respond differently to Tbx3 upregulation than working myocardium. We hypothesised that adenoviral overexpression of Tbx3 in this tissue would improve pacemaker function in terms of beating rate, autonomic sensitivity and overdrive suppression and alter molecular features relating to pacemaking. However, Tbx3 is already expressed in SAP tissue and previous work has failed to significantly upregulate pacemaker ion channels like HCN4.[152, 205]

3.4.2 Beating rates

As with previous experiments, extracellular potentials were continuously recorded over 48 hours of tissue culture. Beating rate data from SAP preparations infected with Ad-Tbx3

(n=9) were compared to the previous SAN and uninfected SAP preparations. Raw beating rate data can be found in figure 39.

Ad-Tbx3 infected SAP tissue exhibited the same overall pattern of beating over 48 hours as SAN and uninfected SAP preparations, with a gradual rise in rate over the first 20 hours and a subsequent decline. However, the pattern was less consistent with marked acceleration and deceleration in 3 of 9 preparations over the 48 hours and much more variability between the different preparations, as seen in the raw data and highlighted by greater error margins. Figure 40 shows examples of raw traces from each of these groups to illustrate the increased variation seen in Ad-Tbx3 infected SAP tissue. This meant that mean rates for Ad-Tbx3 infected SAP preparations were generally lower than uninfected SAP preparations, but this never reached statistical significance.

For Ad-Tbx3 infected SAP preparations the mean rate over the first hour was 226 ± 17 bpm, compared to 287 ± 8 bpm for SAN and 230 ± 8 bpm for uninfected SAP preparations. The maximum mean beating rate for Ad-Tbx3 infected SAP preparations was 236 ± 32 bpm during hour 19, compared to maximum rates of 374 ± 9 bpm for SAN and 277 ± 10 bpm for uninfected SAP preparations. The minimum mean beating rate during the final hour of recording for Ad-Tbx3 infected SAP preparations was 117 ± 24 bpm, compared to 267 ± 14 bpm for SAN and 141 ± 9 bpm for uninfected SAP preparations.

When looking at 4 hourly mean rates during hours 17 – 48 during which adenoviral expression of Tbx3 was expected to have maximal effect, the maximum mean beating rate between 17 – 20 hours was 221 ± 39 bpm for Ad-Tbx3 infected SAP preparations, 363 ± 9 bpm for SAN and 261 ± 16 bpm for uninfected SAP preparations (figure 41). The final mean beating rate between 45 – 48 hours was 124 ± 23 bpm for Ad-Tbx3 infected SAP preparations, 269 ± 12 bpm for SAN and 147 ± 9 bpm for uninfected SAP preparations.

Statistical analysis showed no significant difference between the beating rates of Ad-Tbx3 infected SAP and uninfected SAP preparations at any time.

3.4.3 RT-qPCR

After 48 hours of culture, 2mm samples of each Ad-Tbx3 infected SAP preparation were taken from around the SAP area (n=6). RT-qPCR was then used to analyse relative mRNA levels of 11 genes related to pacemaking, including HCN1, HCN4, $K_{ir}2.1$, $Na_v1.5$, $K_v1.5$, Cx43, Cx45, RYR2, NCX1, Tbx3 and Tbx18. This data was compared to data from the previous uninfected SAP samples (figure 42).

Ad-Tbx3 infected SAP samples showed a significant downregulation of both HCN1 ($p<0.05$) and HCN4 ($p<0.01$) compared to uninfected SAP samples. There was a significant downregulation of $Na_v1.5$ ($p<0.05$) and $K_{ir}2.1$ ($p<0.01$) but no significant change in $K_v1.5$ versus uninfected SAP samples. Cx43 was upregulated ($p<0.05$) and Cx45 showed no significant change compared to uninfected SAP samples.

Ad-Tbx3 infected SAP samples demonstrated a 3.7-fold rise in Tbx3 compared to uninfected SAP samples ($p<0.05$). There was significant downregulation of Tbx18 in Ad-Tbx3 infected SAP compared to uninfected SAP samples although this was borderline ($p=0.048$). There was a significant downregulation of NCX1 ($p<0.01$) but no significant change in RYR2.

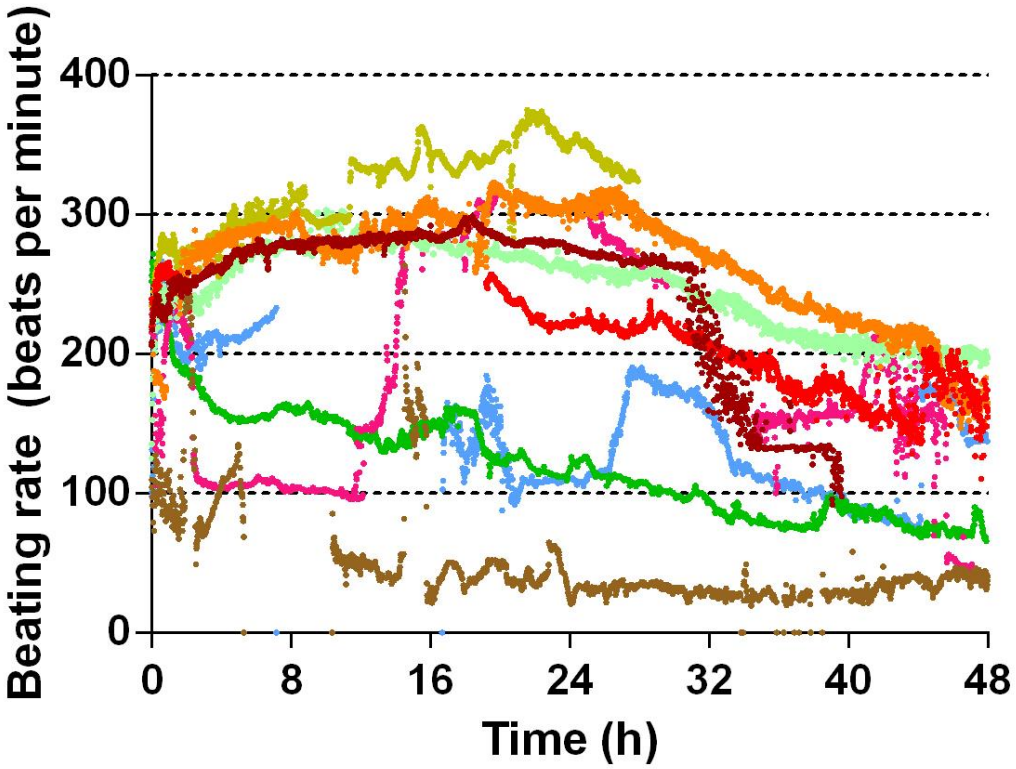

Figure 39. Raw beating rate data from Ad-Tbx3 infected SAP preparations

Beating rates were analysed from complete recordings by LabChart software as mean values at every 1 minute interval over the entire 48 hour culture period. All preparations were analysed. Different colours represent individual preparations (n=9). Dots represent 60 s mean beating rates.

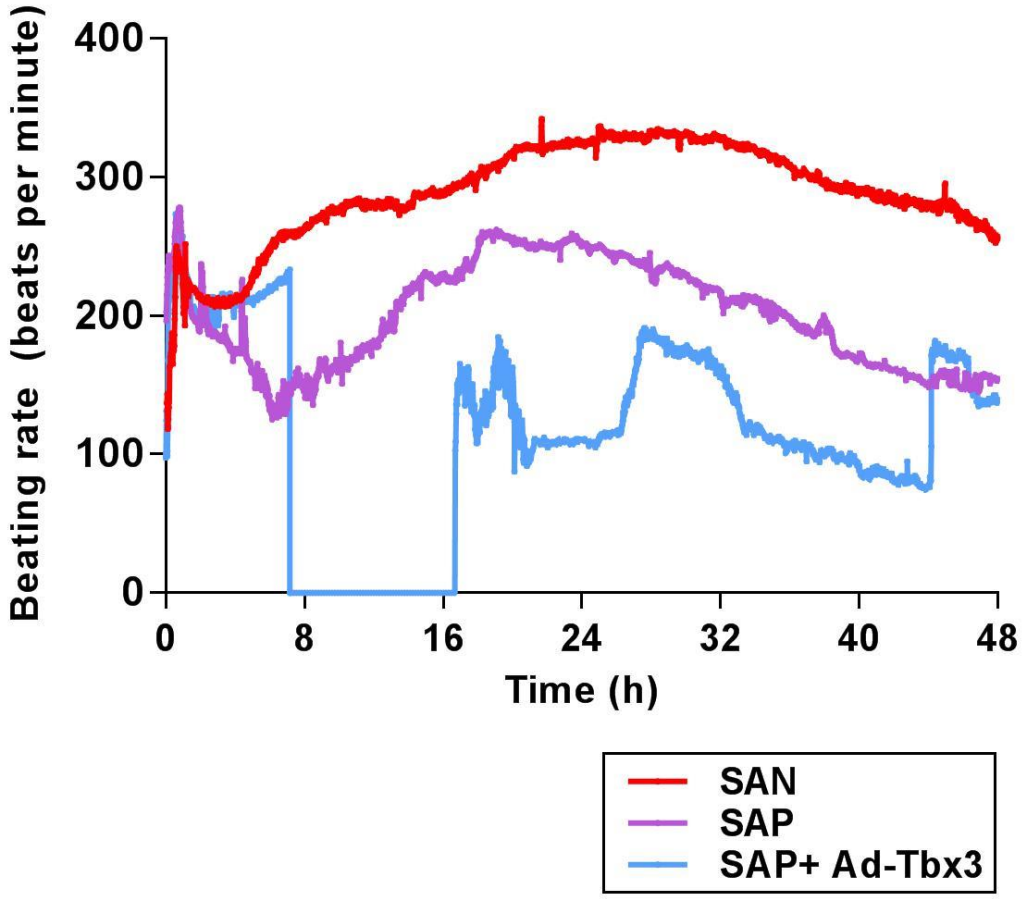

Figure 40. Example raw traces to illustrate variation seen during recordings

Raw data traces from single recordings comparing SAN, uninfected SAP and Ad-Tbx3 infected SAP tissue. Most SAN and SAP recordings varied little over the course of 48 hours, however 3 of 9 Ad-Tbx3 infected preparations demonstrated large variations such as those seen in the above example. Here the beating rate temporarily dropped to zero early on in the recording before recovering, but then demonstrating accelerations and decelerations. These variations were rarely seen in SAN and uninfected SAP tissue.

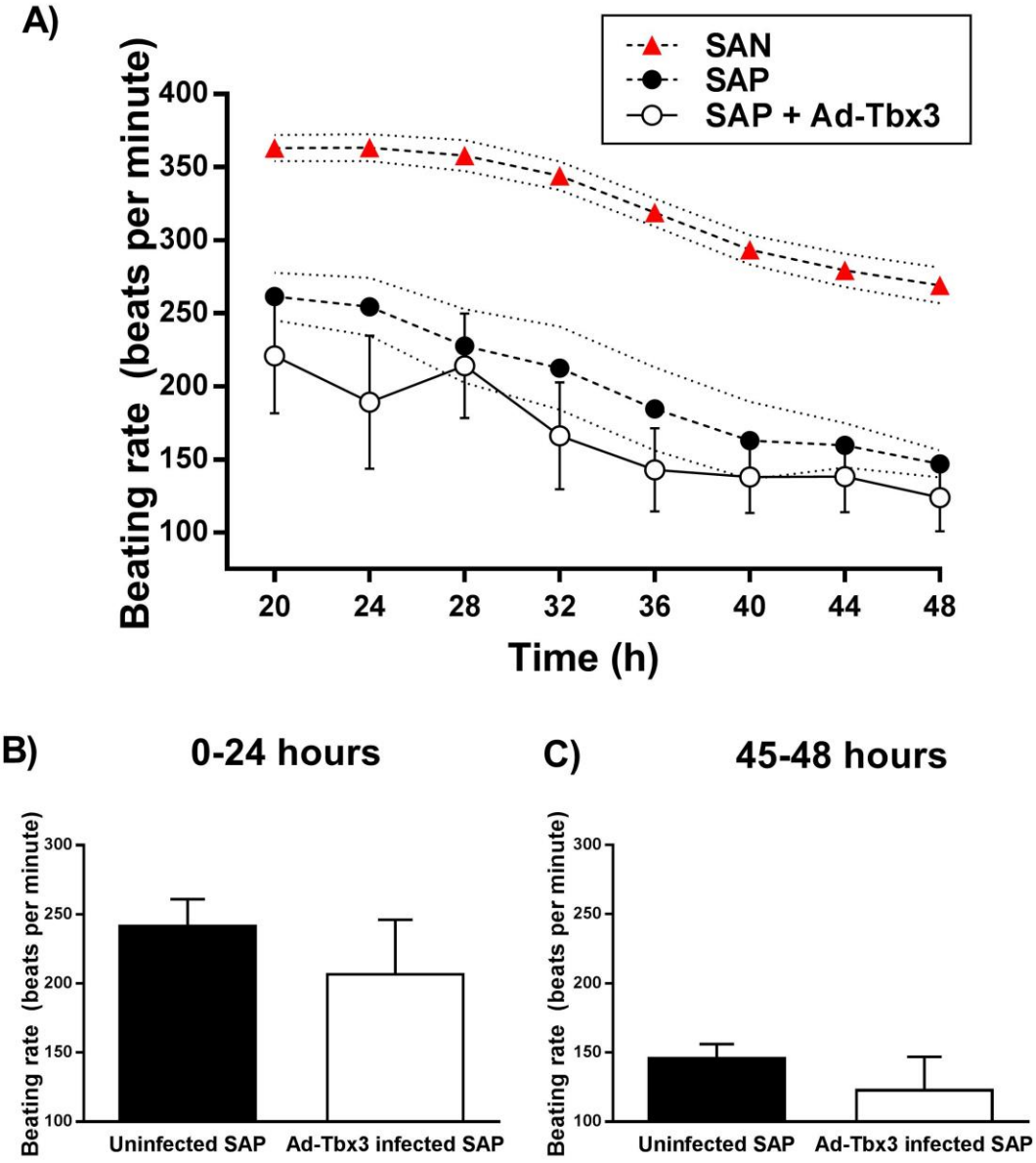

Figure 41. Beating rate data from SAN, uninfected SAP and Ad-Tbx3 infected SAP tissue

Ad-Tbx3 infected SAP tissue (n=9), uninfected SAP tissue (n=13) and SAN tissue (n=15) were cultured for 48 hours and beating rates were continuously measured. (A-C) Beating rates from Ad-Tbx3 infected SAP tissue were not significantly different than from uninfected SAP tissue throughout 48 hours of culture.

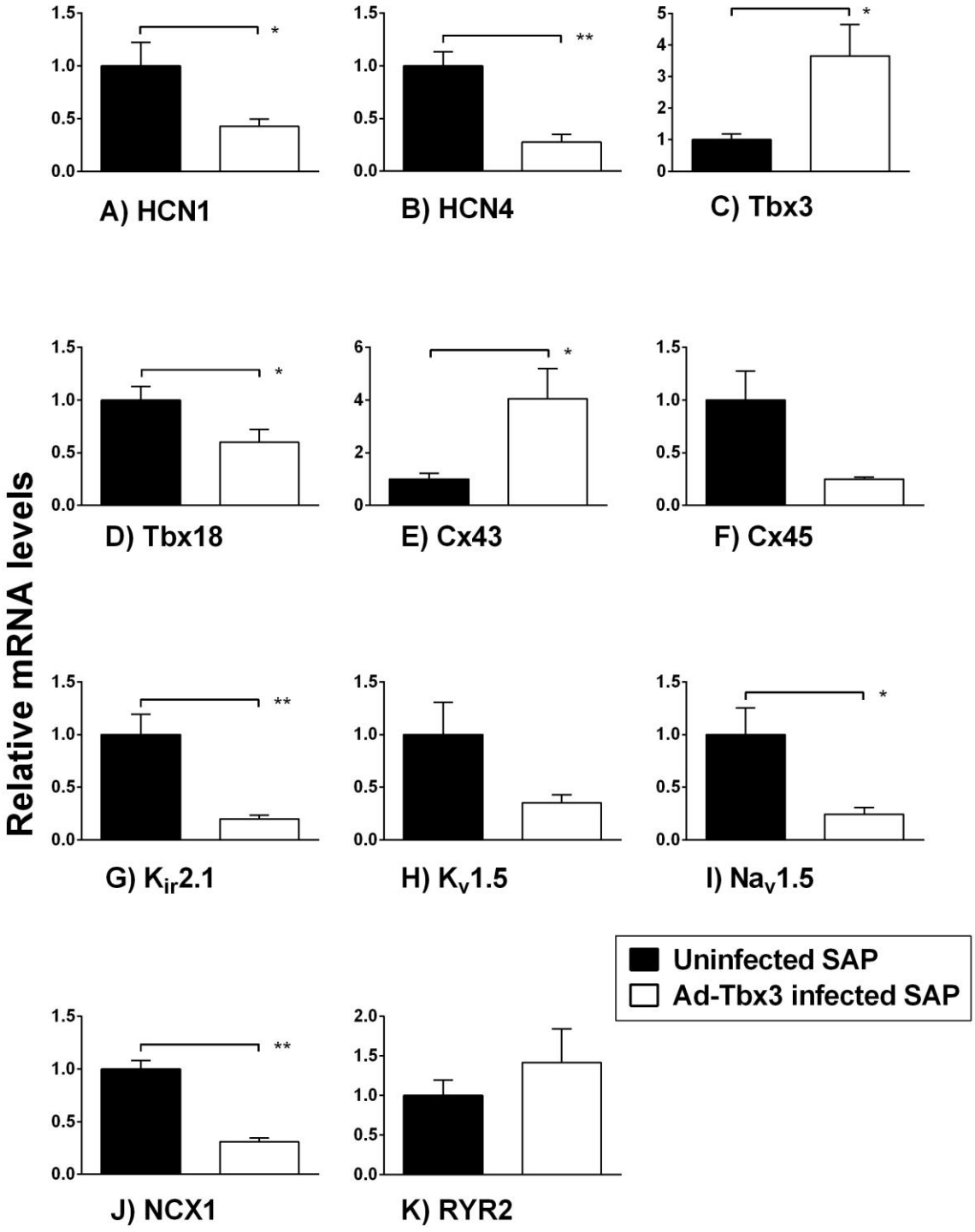

Figure 42. RT-qPCR data showing mRNA levels comparing Ad-Tbx3 infected SAP tissue to uninfected SAP tissue

(A-K) Relative mRNA abundance of pacemaker-related, atrial and Ca^{2+} handling genes in SAN (n=8), uninfected SAP (n=8) and Ad-Tbx3 infected SAP tissue (n=6). *p<0.05; **p<0.01.

3.5 Ad-NCX1-GFP

3.5.1 Introduction

NCX1 is a membrane channel which exchanges one Ca^{2+} ion out of the cell for three Na^{+} ions into the cell creating a net depolarizing effect.[100] In SAN cells NCX1 exchangers are closely co-localized with RYRs on the SR at the periphery of the cell.[107, 108] LCRs from the SR via RYRs stimulate NCX1 to exchange intracellular Ca^{2+} for extracellular Na^{+}.[100] NCX1 function accelerates as intracellular Ca^{2+} levels rise as a result of SR Ca^{2+} release, which contributes to membrane depolarization between -60 and -30 mV eventually reaching the threshold potential for SAN cells to beat.[100]

Modulation of the Ca^{2+} clock has not yet been investigated as a biopacemaker strategy. NCX1 already exists in SAP tissue.[227] Our hypothesis was that upregulating NCX1 in SAP tissue would increase beating rate, improve overdrive suppression and improve autonomic sensitivity.

3.5.2 Beating rates

Extracellular potentials were continuously recorded over 48 hours of tissue culture. Beating rate data from SAP preparations infected with Ad-NCX1-GFP (n=6) were compared to the previous SAN and uninfected SAP preparations. Raw beating rate data can be found in figure 43.

Ad-NCX1-GFP infected SAP preparations followed a similar pattern to uninfected SAP preparations over 48 hours with an initial rise in beating rate over the first 20 hours followed by a gradual decline. However, both the initial rise and the subsequent fall was less marked as seen by the raw data.

The mean beating rate during the first hour in Ad-NCX1-GFP infected SAP preparations was 247 ± 18 bpm, the maximal beating rate was 258 ± 22 bpm at 19 hours and the final rate was 174 ± 18 bpm after 48 hours. Maximal adenoviral expression of NCX1 was

expected to take place between around 12-16 hours, since previous work upregulating ion channels demonstrated this pattern.[152] At 16 hours Ad-NCX1-GFP infected preparations were beating at 254 ± 23 bpm whilst uninfected SAP preparations were beating at 272 ± 10 bpm, but the difference was not statistically significant ($p>0.05$).

The final beating rate in Ad-NCX1-GFP infected SAP preparations (174 ± 18) was higher than in uninfected SAP preparations (141 ± 9 bpm), but the difference in beating rates between the two groups never reached statistical significance at any point during the 48 hour culture period (figure 44).

3.5.3 Overdrive suppression

After 48 hours of tissue culture, preparations were subject to an overdrive pacing protocol and cRT measured from Labchart recordings. cRT measurements from Ad-NCX1-GFP infected SAP preparations (n=3) were compared to previous SAN (n=5) and uninfected SAP (n=6) preparations (figure 45).

Ad-NCX1-GFP infected preparations demonstrated a mean cRT of 85 ± 7 ms, while mean cRT in SAN preparations was 78 ± 9 ms and in uninfected SAP preparations was 125 ± 10 ms. Ad-NCX1-GFP infected preparations therefore showed a significant reduction in cRT compared to uninfected SAP preparations ($p<0.05$) and were not significantly different to SAN preparations.

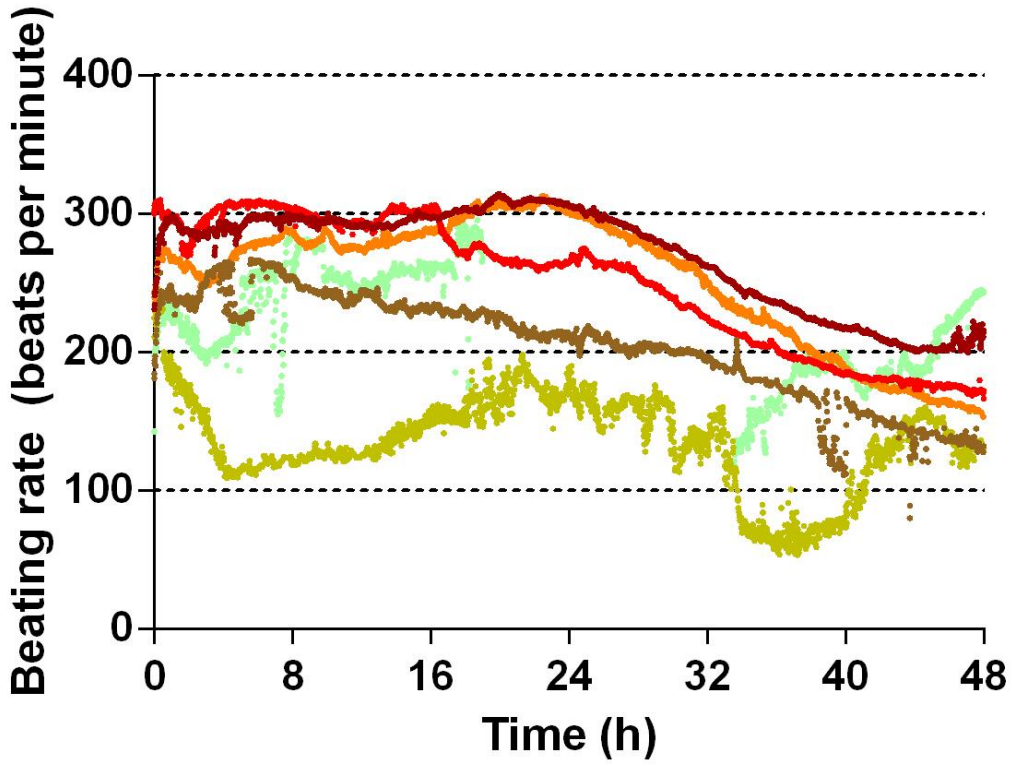

Figure 43. Raw beating rate data from Ad-NCX1-GFP infected SAP preparations

Beating rates were analysed from complete recordings by LabChart software as mean values at every 1 minute interval over the entire 48 hour culture period. All preparations were analysed. Different colours represent individual preparations (n=6). Dots represent 60 s mean beating rates.

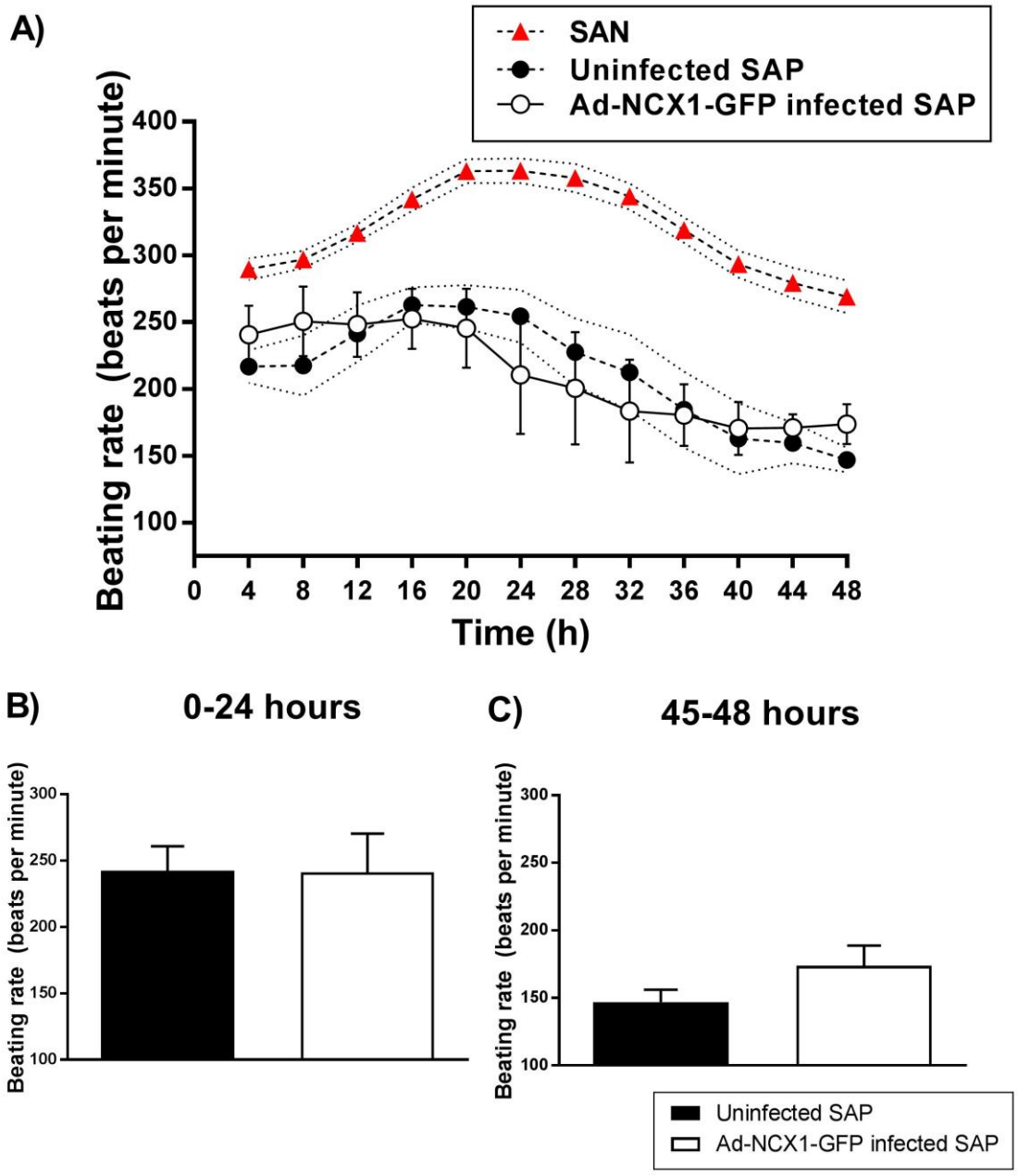

Figure 44. Beating rate data from Ad-NCX1-GFP infected SAP tissue

Ad-NCX1-GFP infected SAP tissue (n=9), uninfected SAP tissue (n=13) and SAN tissue (n=15) were cultured for 48 hours and beating rates were continuously measured. (A-C) Rates from Ad- NCX1-GFP infected SAP tissue were not significantly different than from uninfected SAP tissue throughout 48 hours of culture.

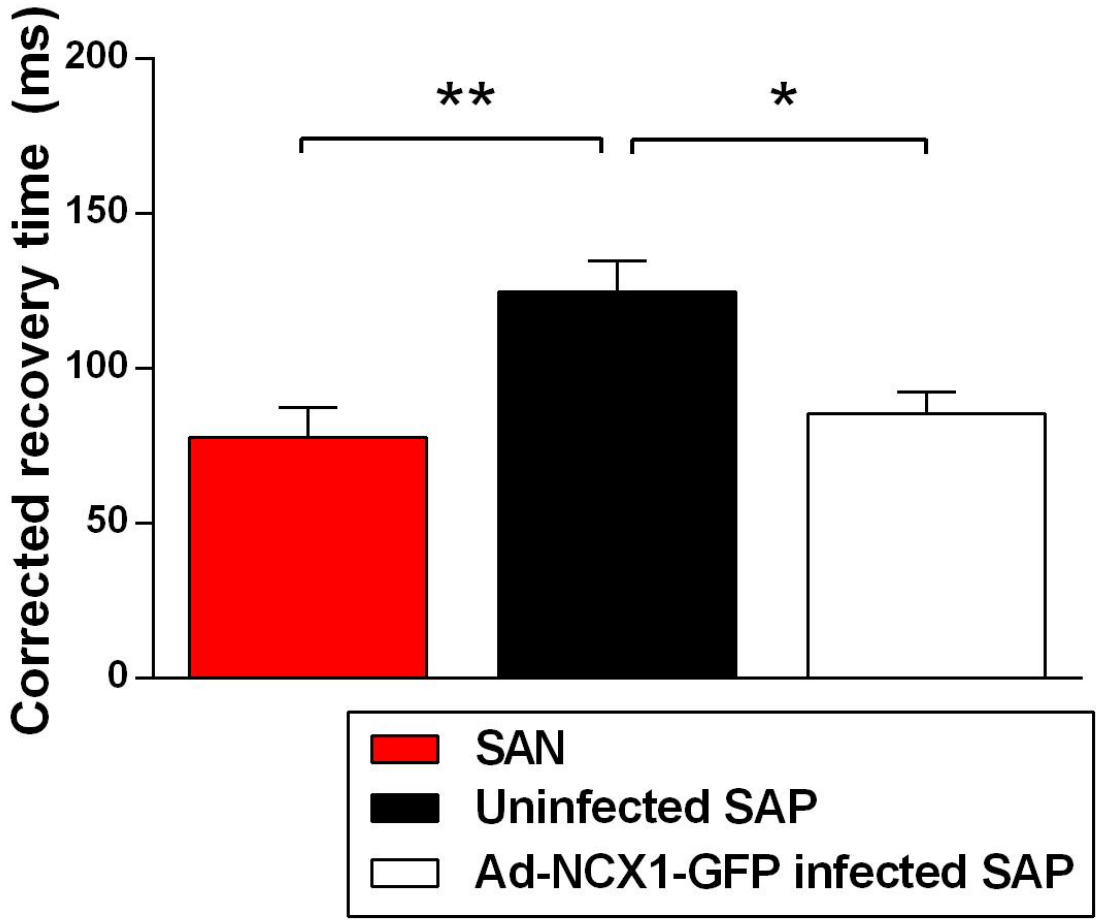

Figure 45. Corrected recovery times after overdrive pacing in Ad-NCX1-GFP infected SAP tissue

An overdrive pacing protocol was applied to SAN (n=5), uninfected SAP (n=6) and Ad-NCX1-GFP infected SAP tissue (n=3). A significant difference was found in corrected recovery times (cRT) between uninfected and Ad- NCX1-GFP infected SAP tissue. SAN tissue demonstrated a significantly faster cRT than both uninfected but not Ad-NCX1-GFP infected SAP tissue. *$p<0.05$; **$p<0.01$.

4. DISCUSSION

4.1 Summary introduction

Biopacemaking is an advancing field with only relatively recent progress in the last two decades alongside ongoing development of technologies such as gene therapy and stem cell transplantation. It promises ways of creating *de novo* pacemaker tissue from a wide range of other cell types or the repair of dysfunctional pacemaker tissue. It harbours several advantages over electronic pacemaker implantation most notably that pacemaking can be achieved without the need for indwelling hardware. Successful work has been done in large animal models using gene therapy and stem cell transplantation to create ectopic leading pacemakers with reliable, physiologic function. These studies are leading the way for prospective clinical translation for use in humans. However, many challenges lie ahead and many questions remain unanswered. What are the best gene targets for creating a biopacemaker with the most reliable function? How long can a biopacemaker continue to function? How safe would biopacemaking be for use in humans? What is the best location for a biopacemaker? No doubt a large body of work is yet needed and a number of avenues have yet to be explored before biopacemaking could ever be a feasible alternative to the electronic pacemaker in the clinic.

The data presented offers insight into the best gene targets for the use of biopacemaker technology in the treatment of SND. SAP tissue has many similarities to SAN tissue whilst also displaying many phenotypic features of SND (bradycardia and prolonged cSNRT). The following sections will discuss the success, failures and limitations of the techniques used during this work, how our results compare to data from other groups and how they might guide future work.

4.2 Validation of techniques used

4.2.1 Tissue culture and recording

4.2.1.1 Duration of tissue culture

Tissue culture was required to keep isolated RA tissue from the rat alive *ex vivo* and beating long enough to give adenoviral gene transduction the potential for effect. Depending on the particular gene the time for effect would vary. Time would need to be allowed for transduction of the gene into cell nuclei, translation of the gene into protein and interaction of the protein with cell function. Transduction of genes for transcription factors such as Tbx18 or Tbx3 will take longer as the transcription factor would subsequently need to modulate other pacemaker genes before an effect was seen, whereas transduction of genes for ion channels would depend on time for ion channel trafficking to the cell membrane.

Previous work guided the duration of tissue culture used for this work, the most relevant being that already done by this group. Adenoviral expression of HCN channels in isolated SAP tissue from the rat was seen to cause a significant rise in beating rate between 12 – 20 hours of tissue culture following adenoviral infection.[152] On the other hand, adenoviral expression of Tbx18 in isolated NRVM monolayers *in vitro* showed a significant effect after 36 – 48 hours of culture.[203] Thus, we first focused on being able to maintain reliable beating rate data from isolated SAN and SAP tissue preparations over at least 48 hours.

4.2.1.2 Reliability and stability of tissue culture environment

It was important to develop a reliable system for continuous superfusion of culture medium around isolated rat RA tissue with the ability to maintain a stable temperature and pH, as beating rates measured from SAN and SAP preparations are very sensitive to small changes in these parameters. A custom setup involved continuously pumping culture medium from a 500 ml reservoir to a tissue bath and back again within a 37°C / 5% CO_2 incubator. Temperature and pH were measured in a repeat series of initial

experiments to ensure the system maintained constant levels throughout the 48 hour culture period. Figure 46 shows a typical example of temperature readings being constantly measured over a 20 hour period overnight. Figure 47 demonstrates the difference in beating rate that can occur as a result of small variations in pH. Finally, figure 48 shows raw beating rate data acquired from SAN preparations illustrating the consistency of beating behaviour from repeat experiments and thus reliability of the system. This consistency would also make comparison of data between experimental groups and controls much easier.

4.2.1.3 Sinoatrial node and subsidiary atrial pacemaker beating patterns

During 48 hours of tissue culture a pattern emerged from all preparations whereby beating rates gradually accelerated in the first 20 hours and subsequently decelerated over the rest of each experiment. Previous work in the group showed the same pattern of beating from SAN and SAP tissue during tissue culture.[95] The same pattern was seen despite the use of a technique needing daily exchange of culture medium, suggesting that changes within the culture medium over the course of each experiment were not to blame. Beating rate was also seen to accelerate once again after 50 hours of culture up to 12 days later suggesting that the decline in rate between 20 – 50 hours may be due to other factors than tissue death or exhaustion of energy metabolites (figure 49). In fact this work demonstrated that cellular apoptosis semi-quantitatively measured by immunohistochemistry was not significantly increased in RA tissue after 48 hours of tissue culture.[95] The precise cause of this phenomenon therefore remains unclear. Figure 50 compares mean, first, maximum and minimum beating rates of all experimental groups.

4.2.2 Adenoviral gene expression

Validation of adenoviral gene expression was important to ensure that viral infection of SAP tissue led to gene expression and resulted in protein expression. This would increase confidence that any measured effect seen as a result of viral infection, such as an increase in beating rate for example, could be due to expression of the gene of interest.

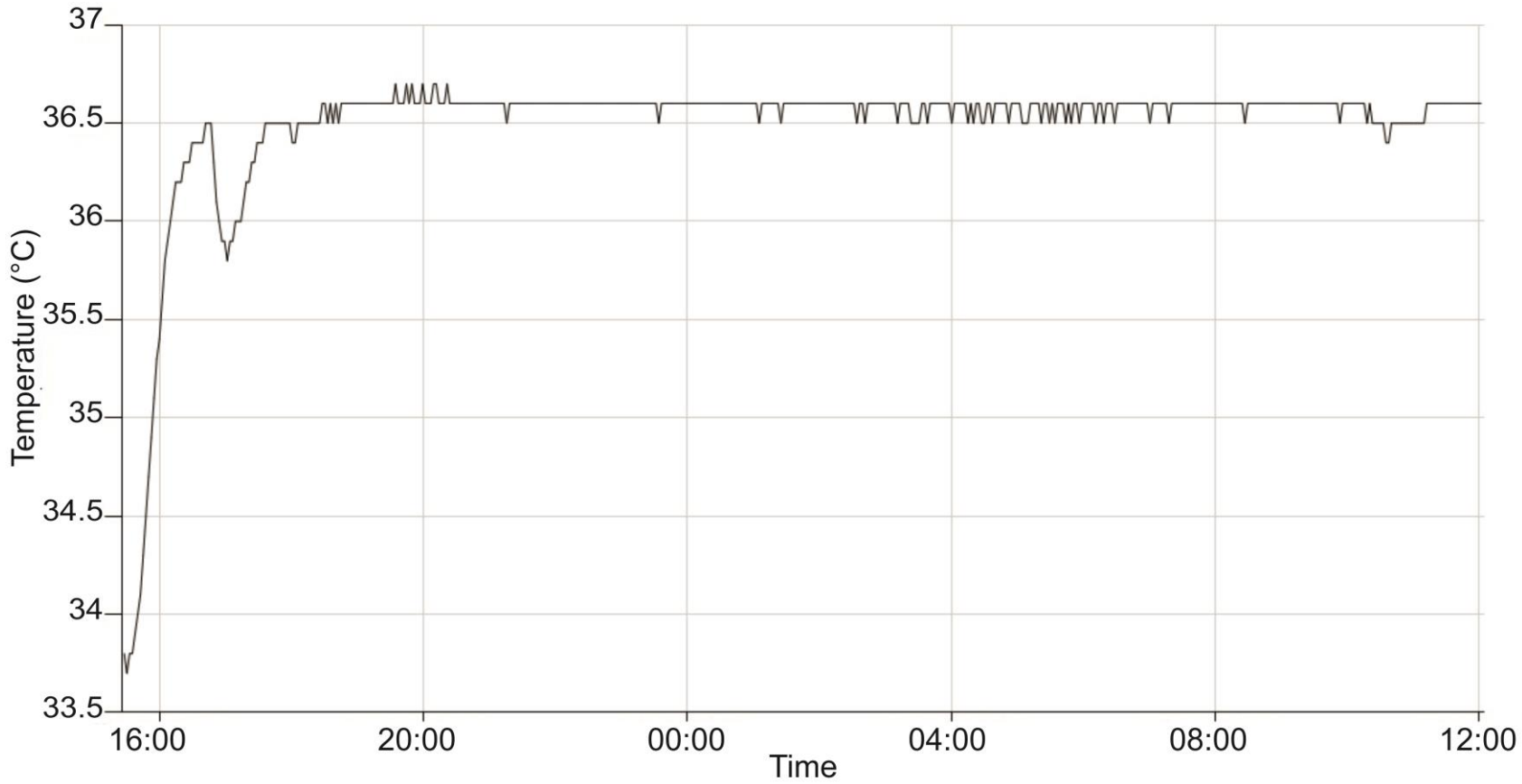

Figure 46. Typical tissue chamber temperature readings using the custom superfusion setup

Initial validation of the custom superfusion setup for tissue culture involved continuous temperature monitoring to ensure stability and reliability. Above is a typical example of temperatures recorded during 24 hours of tissue culture.

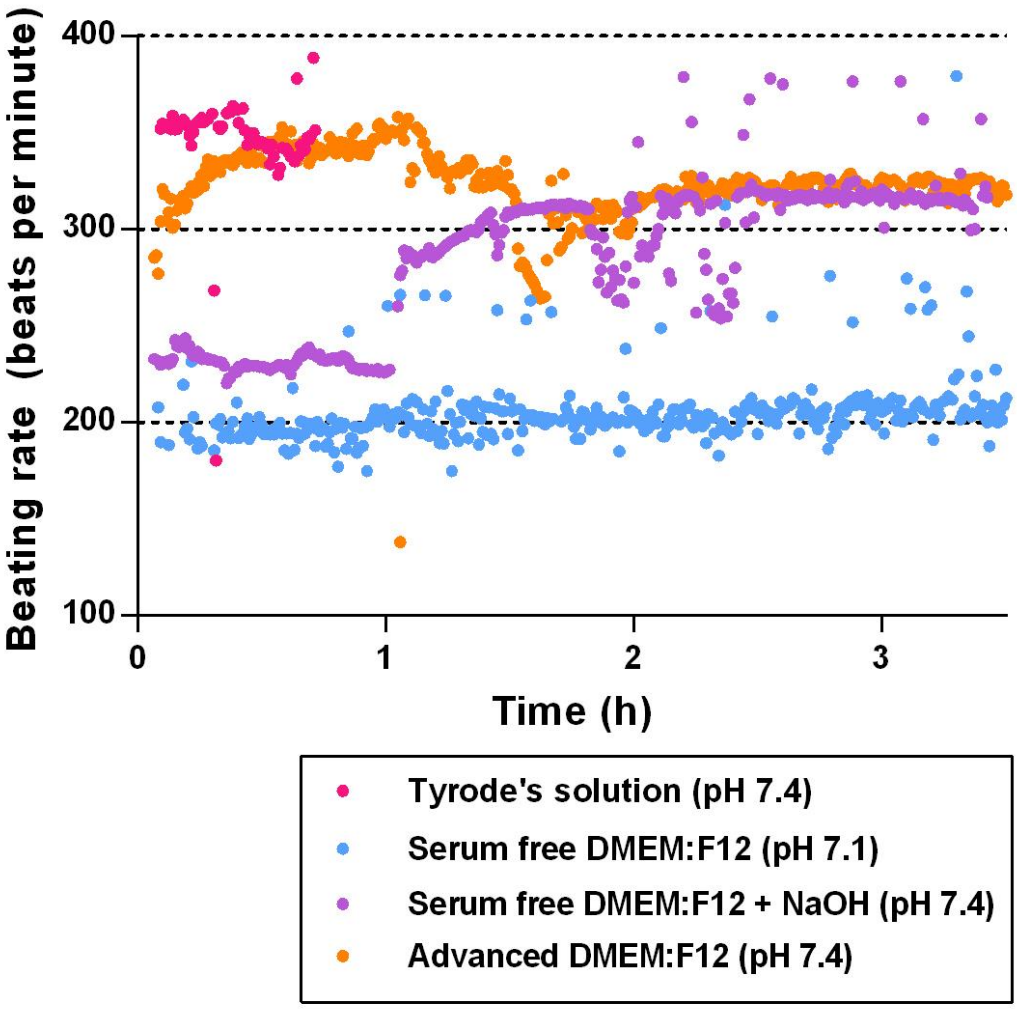

Figure 47. Raw beating rate behaviour from SAN preparations in different media and solutions

Beating rates were sensitive to the pH of the solution used for superfusion with even small changes in pH causing large shifts in rate. The first type of culture medium used (serum free DMEM:F-12) demonstrated lower pH readings of around 7.1 and this was associated with lower beating rates. When this was changed to the medium eventually used for all experiments (Advanced DMEM:F-12), pH readings of 7.4 were seen, which maintained beating rates in keeping with previous work. Furthermore, when the first type of medium was used but with the pH increased to 7.4 with the addition of NaOH solution, beating rates improved. Initial beating rates were also similar using physiologic Tyrode's solution. Each dot represents mean beating rate over 30 s.

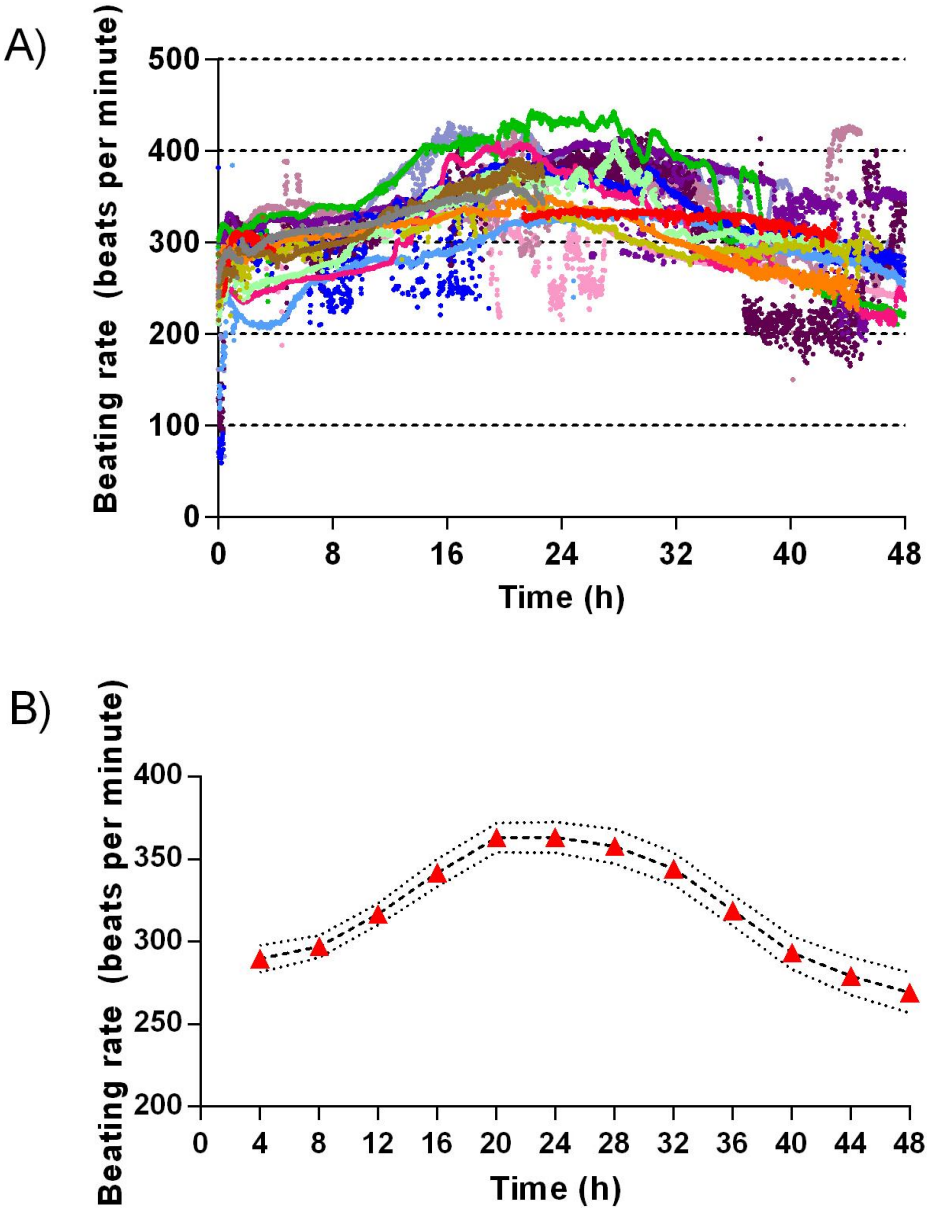

Figure 48. SAN beating rate data highlighting consistency

Beating rates from different SAN preparations cultured for 48 hours were consistent as demonstrated by (A) the raw data and (B) the fact that the SEM for each hourly mean rate was small. This highlighted the stability of the culture environment and the reliability of the system. Dots in panel A represent 60 s mean beating rates.

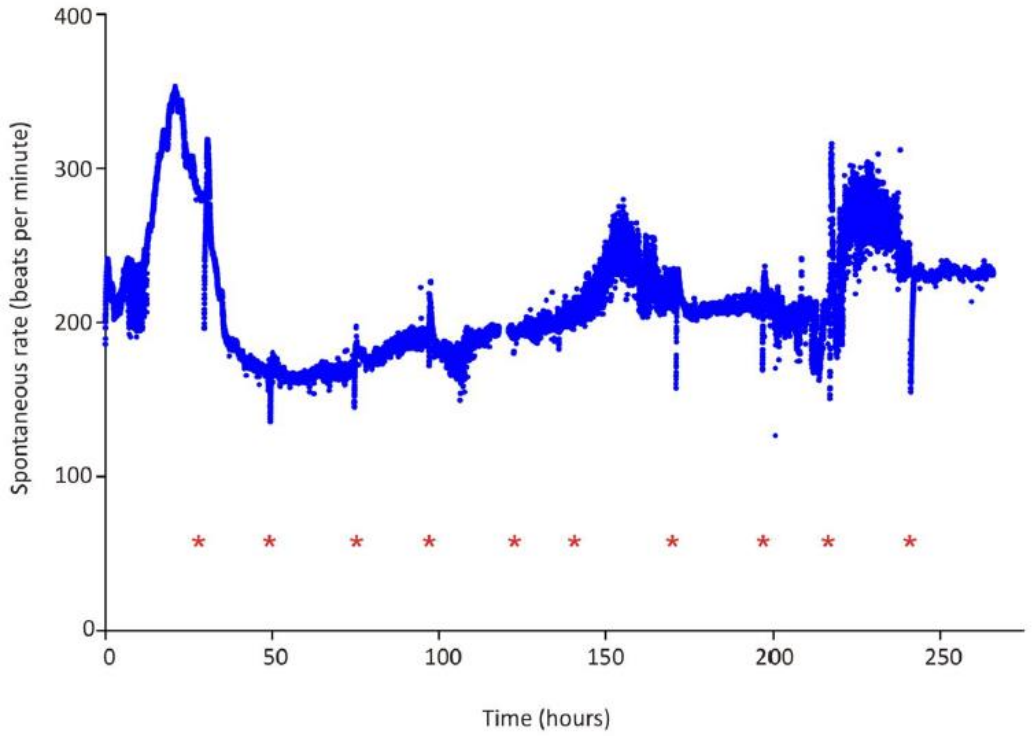

Figure 49. Beating rate measured from a cultured SAN preparation over a prolonged duration

Raw beating rate data showing the beating pattern of a SAN preparation in tissue culture over 11 days. The initial 48 hours of culture demonstrated a typical rising and falling pattern also seen in the work presented here, however preparations can continue beating for several days after highlighting that initial variations in beating rate are not due to degradation of the tissue or circadian rhythm. Taken from Morris, 2010.[95]

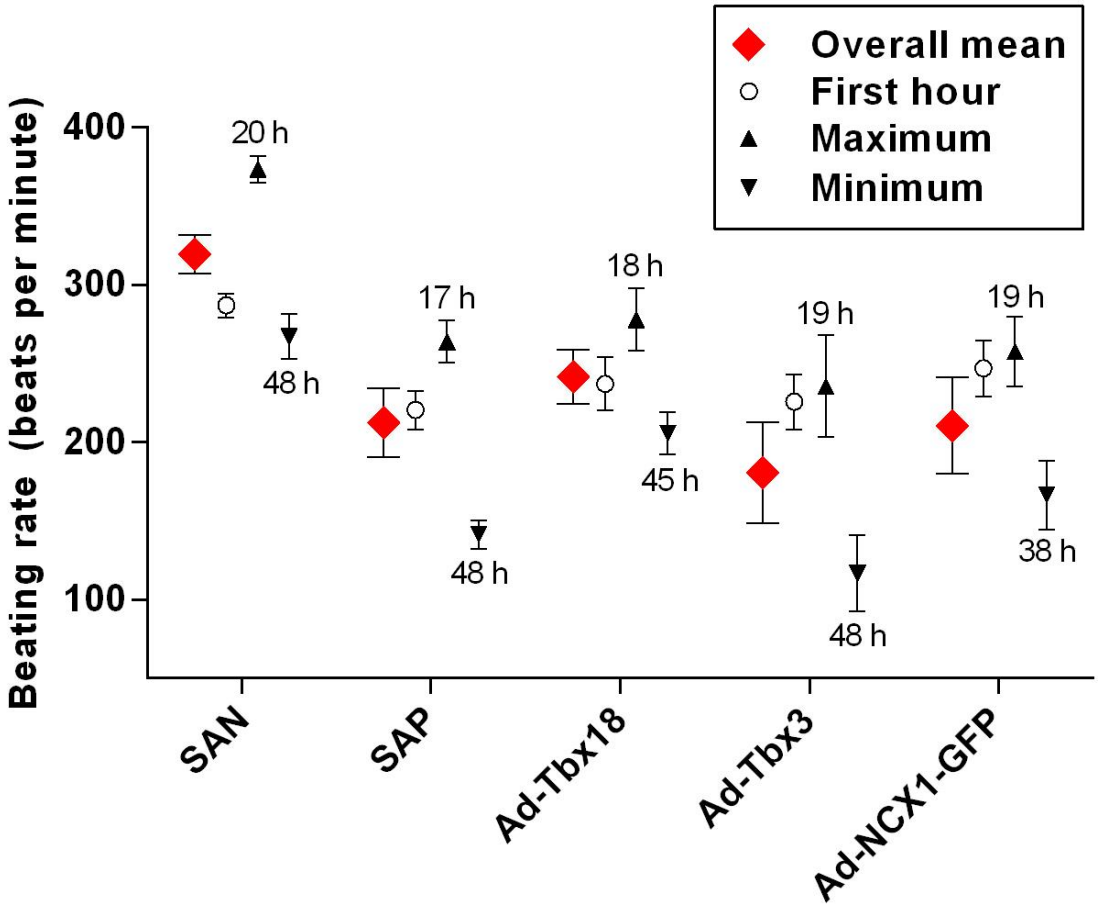

Figure 50. Comparison of beating patterns between experimental groups

The beating rates of all preparations followed similar patterns, rising over the first 20 hours and then falling to a minimum by the end of 48 hours. Mean, first hour, maximum and minimum beating rates are shown above ± SEM for SAN, uninfected SAP and virus infected SAP tissue. The hour in which maximum and minimum beating rates occurred are annotated.

Validation was achieved using several different methods including qPCR and immunolabelling in both SAP tissue and the 293 cells being used for amplification of each virus. Direct visualisation of GFP fluorescence was possible in the case of Ad-NCX1-GFP. LacZ expression was also a useful tool and enabled direct visualisation of blue colouration in successfully transduced tissue giving an indication of the area of adenoviral gene expression in SAP, which was 2-3 mm in radius around the injection site (figure 30).

Previous work has demonstrated that immunolabelling of cultured tissue can be problematic. HCN4 and Cx43 staining has been inconsistent in cultured SAP tissue in our group before.[95] Furthermore, after adenoviral expression of Tbx18 in pigs authors report unsuccessful attempts to visualise HCN4 channels using immunolabelling despite increased levels of HCN4 mRNA seen using PCR.[204] Similar issues were encountered in our work and an example of patchy Cx43 immunolabelling in cultured RA tissue can be found in appendix A4. For these reasons immunolabelling was not used extensively following tissue culture.

4.2.2.1 Ad-Tbx18

Expression of Tbx18 using Ad-Tbx18 was validated using qPCR and immunolabelling. qPCR detected Tbx18 DNA within total DNA purified from Ad-Tbx18 infected 293 cells whereas it did not in uninfected 293 cells. The amplicon detected from Ad-Tbx18 infected samples was also of the correct size (82 bp) as measured by gel electrophoresis, based on documentation for the Tbx18 primer used (figure 25). RT-qPCR revealed that mRNA levels of Tbx18 were 110-fold higher in Ad-Tbx18 infected SAP tissue than in uninfected SAP tissue (figure 26).

Immunolabelling of Tbx18 protein in 293 cells infected with Ad-Tbx18 revealed a signal localised to cell nuclei, which did not occur in uninfected 293 cells. Unfortunately, immunolabelling of SAP tissue after 48 hours of tissue culture did not yield consistent results. Nonetheless 2 of 4 SAP preparations infected with Ad-Tbx18 showed sporadic Tbx18 signal localised to the injection sites (figure 24).

4.2.2.2 Ad-Tbx3

Expression of Tbx3 using Ad-Tbx3 was validated using RT-qPCR in SAP tissue after 48 hours of tissue culture. Tbx3 mRNA levels were 3.7-fold higher in Ad-Tbx3 infected SAP tissue compared to uninfected SAP tissue (figure 27). Ad-Tbx3 therefore was not as effective at increasing levels of Tbx3 as Ad-Tbx18 was at increasing levels of Tbx18. This might be explained by the fact that Tbx3 would be expected to already be present in uninfected SAP tissue whereas Tbx18 would not.

Attempts to detect Tbx3 DNA in total purified DNA from Ad-Tbx3 infected 293 cells were unsuccessful. Immunolabelling was not attempted because of the limitations of this technique in cultured tissue as explained above. There was a significant rise in Tbx3 mRNA levels in Ad-Tbx3 infected SAP tissue indicating that the Ad-Tbx3 virus was capable of upregulating Tbx3 in SAP tissue.

4.2.2.3 Ad-NCX1-GFP

Expression of NCX1 using Ad-NCX1-GFP was validated using qPCR and direct visualisation of GFP signal in SAP tissue. qPCR detected NCX1 DNA in total DNA purified from Ad-NCX1-GFP infected 293 cells but did not in uninfected 293 cells. The amplicon detected from Ad-NCX1-GFP infected samples was also of the correct size (162 bp) as measured by gel electrophoresis, based on documentation for the NCX1 primer used (figure 28).

After 48 hours of tissue culture, SAP tissue infected with Ad-NCX1-GFP exhibited a strong GFP signal directly visualised by microscopy under a mercury lamp and scanned using confocal microscopy. This signal extended 3-4 mm in radius around the injection site and was not seen in the periphery of infected SAP tissue or at all in uninfected SAP tissue (figure 29).

The above shows that the virus successfully transduced SAP tissue. Although GFP signal was seen and the virus should bicistronically co-express NCX1 also, it was not directly proven that NCX1 was expressed in SAP tissue.

4.3 Analysis of results

4.3.1 Characterisation of subsidiary atrial pacemaker tissue

4.3.1.1 Immunohistochemistry revealed pacemaker cells in the inferior right atrium

Uninfected SAP tissue was characterised using immunohistochemistry, extracellular recordings and pharmacology experiments. Previous work did not elucidate any HCN4-positive/Cx43-negative tissue in the rat SAP. Study of the goat SAP tissue demonstrated HCN4-positive/Cx43-negative tissue that was not present in all sections, suspected to be as a result of a mixed atrial and nodal phenotype.[227] It was therefore possible that further study in the rat could also show this pattern.

In one preparation, extensive HCN4-positive/Cx43-negative signal was detected within SAN tissue in superior sections, whereas few tissue sections taken from above the level of the IVC showed HCN4-positive/Cx43-negative signal. Also the signal was exhibited in a small area within the centre of the tissue and surrounded a small blood vessel. It is possible that it may have represented a neurovascular bundle rather than SAP tissue(figure 19). A significant amount of HCN4-positive/Cx43-negative signal was also seen in the septal region, in keeping with previous reports of pacemaker tissue and pacemaker activity in the interatrial region.[22, 138, 141, 144]

In a second attempt, HCN4-positive/Cx43-negative signal was detected again in superior sections demonstrating the extensive nature of the SAN, taking a subepicardial position and its tail extending to midway down the length of the CT. Extensive HCN4-positive/Cx43-negative signal was seen in inferior sections (figure 20). This was a discrete signal from the tail of the SAN with an endocardial position adjacent to the IVC and extending 0.5 mm superiorly and inferiorly to the IVC (figure 22). This signal was present in most inferior sections studied, raising the possibility that it may have extended further with the potential for connection with the inferior nodal extension of the AVN, however this was not specifically investigated.

HCN4-positive tissue co-localised with Cav3 staining suggesting that this type of tissue seen near the IVC was comprised of cardiomyocytes rather than neurovascular tissue. High magnification images also revealed that these cells were smaller and spindle-shaped compared to HCN4-negative atrial cells (figure 21).

The HCN4-positive/Cx43-negative signal near the IVC shown here has not been demonstrated previously. Although only two preparations were studied as part of preliminary work, in the context of previous work it does suggest however that not only can pacemaker tissue in the SAP region be of mixed atrial and nodal phenotype, it may also vary in size between different animals. This may also account for variations in function between SAP preparations e.g. beating rate and reliability of pacemaking seen between SAP preparations in functional experiments in this work and previous.[95]

4.3.1.2 No difference in response to pharmacology was seen between sinoatrial node and subsidiary atrial pacemaker tissue

SAN and SAP preparations were isolated and superfused with physiologic Tyrode's solution while extracellular potentials were measured to allow monitoring of beating rate. Change of beating rate with the addition of ivabradine for I_f blockade, ISO for β-adrenergic stimulation and ryanodine for inhibition of RYRs allowed further characterisation of pacemaking from these two tissues. All three agents produced significant changes in mean beating rate but there was no significant difference in response between SAN and SAP tissue in any case (figure 23). This signifies that both SAN and SAP pacemaking are similarly reliant on membrane and Ca^{2+} clocks. Both show similar sensitivity to pharmacological assessment of autonomic modulation. However, the degree of autonomic innervation may differ between the two sites and this has not been investigated.

The functional and molecular similarities demonstrated between SAN and SAP tissue, along with the bradycardic nature of SAP pacemaking supports the use of SAP tissue as a model of SAN dysfunction. Moreover, SAP tissue becomes an interesting substrate for biopacemaking, firstly to assess the receptiveness of tissue already capable of

pacemaking and secondly to give insight into how effective biopacemaking might be if used to repair dysfunctional SAN tissue in SND.

4.3.2 Ad-Tbx18

4.3.2.1 Tbx18 was successfully transduced and increased beating rate

Ad-Tbx18 infection of SAP tissue led to a 110-fold increase in Tbx18 mRNA compared to uninfected SAP tissue and further validation showed successful transduction and expression of Tbx18 within single cells and SAP tissue at the gene and protein level. The mean beating rate of Ad-Tbx18 infected SAP preparations was significantly higher than uninfected SAP preparations after 48 hours of tissue culture (figure 34). Both infected and uninfected preparations followed a very similar pattern of beating over the first 24 hours. Between 24 – 48 hours gradual divergence of mean beating rate occurred, the difference becoming significant between 45 – 48 hours. Ad-Tbx18 infected beating rates approached rates seen in SAN preparations however 48 hours were not enough to see Ad-Tbx18 preparations accelerate all the way to SAN levels.

The timing of our observed effect is in keeping with previous work using Ad-Tbx18 to infect NRVM monolayers, guinea pig ventricles and the right ventricular tissue of pigs, where significant changes in beating rates were initially seen between 36 – 48 hours after infection and beyond.[203, 204] It is therefore possible that the difference in beating rates between Ad-Tbx18 and uninfected SAP tissue in our work would have continued to diverge after 48 hours of culture. The effect Tbx18 has of increasing beating rate in pigs was seen to last for at least 14 days before trending back down towards levels seen in Ad-GFP infected pigs.[204]

4.3.2.2 Ad-Tbx18 infection was associated with alteration of pacemaker genes

RT-qPCR data showed several differences in mRNA levels of key pacemaker genes between Ad-Tbx18 infected and uninfected SAP tissue. Tbx18 upregulation was associated with upregulation of HCN2 ($p<0.01$) and RYR2 ($p<0.05$) but downregulation of

HCN4 ($p<0.05$). No significant change was seen in levels of HCN1, $K_v1.5$, $K_{ir}2.1$, $Na_v1.5$, Cx43, Cx45, $Ca_v1.2$, $Ca_v3.1$, NCX1 or Tbx3 (figures 35 and 36). Previous work using Ad-Tbx18 in the ventricular tissue of pigs showed upregulation of HCN4 and downregulation of $K_{ir}2.1$, $Na_v1.5$ and Cx43 when compared to samples of LV epicardium remote from the injection site.[204] Cx45 was not significantly changed.[204] There are of course several differences in methodology between this work and ours. Discrepancies may be explained for example by differences in animal model (pig versus rat), tissue type (ventricular rather than SAP tissue) or time before samples were taken (14 days in their work versus 2 days in ours). Table 3 summarises the gene changes described by our work compared to others.

SAP tissue already harbours relatively more HCN1 and HCN2 than HCN4, shown here (figure 35) and in previous work.[152] We could speculate that there may be an isoform switch between SAN and SAP tissue regulated by transcriptional gene silencing. This could also explain the differences in effect from Tbx18 in ventricular tissue and SAP tissue (figure 35).[204] HCN2 upregulation was more pronounced than HCN4 downregulation, which could explain a net increase in beating rate, due to an overall increase in tissue I_f. HCN2 is also known to be more sensitive to cAMP driven autonomic pathways and have faster activation kinetics compared to HCN4.[200, 228]

4.3.2.3 Immunohistochemistry seemed unreliable post culture

We had limited success with immunohistochemistry after culture. Even with abundant atrial genes which usually stain very easily such as Cx43, signal remained patchy following 48 hours of tissue culture. Our attempts to stain HCN4 and HCN1 in Ad-Tbx18 infected SAP tissue were unsuccessful. Difficulty immunostaining following tissue culture was

Gene	Rat SAP Ad-Tbx18 (this study)	Porcine LV Ad-Tbx18[204]
HCN1	→	
HCN2	↑	
HCN4	↓	↑
Tbx3	→	
Tbx18	↑	↑
$K_v1.5$	→	
$K_{ir}2.1$	→	↓
$Na_v1.5$	→	↓
NCX1	→	
RYR2	↑	
Cx43	→	↓
Cx45	→	
$Ca_v1.2$	→	
$Ca_v3.1$	→	

Table 3. Comparison of gene changes as a result of Tbx18 upregulation in this study versus others

Upregulation of Tbx18 in the SAP tissue of rats altered several genes related to pacemaking. Previous work has upregulated Tbx18 in the left ventricles of pigs and differences were seen in how pacemaking genes were affected, which may reflect significant differences in methodology such as animal model, tissue type and time before tissue sampling. ↑ = upregulated; ↓ = downregulated; → = no change; blank = not tested.

experienced before by our group and others have also experienced limited success staining HCN channels following adenoviral expression of Tbx18.[95, 204] We therefore considered immunohistochemistry as unreliable post adenoviral infection and culture in our experiments. These results can be viewed in the appendix A4.

4.3.2.4 Overdrive suppression was no different following Ad-Tbx18 infection

There was no significant difference in cRT between Ad-Tbx18 infected and uninfected SAP tissue, which goes against our hypothesis. Both preparations had significantly longer cRTs than SAN tissue (figure 37). Previously cRT has been measured in freshly isolated SAN tissue with a mean of 33 ± 4 ms when subject to a 2 minute train of pulses at 80% cycle length, which is comparable to a cRT of 78 ± 9 ms measured from cultured SAN tissue in our work subject to a 2 minute train at 75% cycle length.[224] A significant drop in cRT has been seen as a result of Ad-Tbx18 infection in ventricular tissue from pigs, where electronic pacing was used 7 days after infection at 120 bpm (around 65% cycle length) for 1 minute.[204] This led to a mean cRT of around 300 ms which was quoted as 10-fold lower than ventricles infected with Ad-GFP which exhibited a mean cRT of approximately 3.2 s.[204] Again, differences in timing (pacing at 2 days in our work versus 7 days in the work quoted above) or tissue type (ventricular versus SAP tissue) may explain the lack of an effect on overdrive suppression in our work.

Overdrive suppression is thought to be related to both Na^+ and Ca^{2+}-based mechanisms.[54, 217, 229] In one early study on canine Purkinje fibres, short trains of overdrive pacing produced less suppression in low Ca^{2+} solutions and more suppression in high Ca^{2+} solutions, long trains led to similar levels of suppression in both low and high Ca^{2+} solutions, and low Na^+ solutions also led to a reduction in overdrive suppression.[230] The implication was that the Na^+-Ca^{2+} exchanger NCX might be involved. It also suggested greater suppression was associated with higher intracellular Ca^{2+}, increased K^+ conductance and increased hyperpolarization.[230] cRT was affected in another study by ryanodine showing greater overdrive suppression in the context of 0.1 µM ryanodine and a reduction in SR function.[224]

Ad-Tbx18 infection in our work did not reduce suppression or cause any change in Na^+ channels, K^+ channels or NCX, whereas reduction in overdrive suppression in Ad-Tbx18 infected porcine ventricles was associated with a reduction in $Na_v1.5$ and $K_{ir}2.1$.[204] The same group also showed no change in NCX1 or RYR2 in Ad-Tbx18 infected NRVMs whereas our work showed a modest but significant rise in RYR2, but this may not have been enough to lead to a significant effect on suppression.[203] It is possible that a difference in overdrive suppression may have been seen in association with Ad-Tbx18 infection if experiments were allowed to go on longer.

4.3.2.5 No difference in response to pharmacology was seen in Ad-Tbx18 preparations

We did not see any significant difference in the effect of CsCl or ISO as a result of Ad-Tbx18 infection suggesting it had no impact on sensitivity to I_f blockade or β-adrenergic stimulation (figure 38). A change in response to I_f blockade was hypothesised from changes in HCN channels. Our work demonstrated an HCN isoform switch from HCN4 towards the faster activating HCN2, with a bigger increase in HCN2 than reduction in HCN4. As a result Ad-Tbx18 infected tissue may have been expected to be more sensitive to I_f blockade. However, one drawback of using Cs^+ is that it is not a specific I_f blocker but also has an effect on some K^+ channels and so any effect purely due to I_f blockade may be negated.[231-233] No studies have previously looked at I_f blockade using Cs^+ following Ad-Tbx18 infection.

Sensitivity to β-adrenergic stimulation depends on cAMP driven pathways which have links to both HCN channels and Ca^{2+}-clock mechanisms. An isoform switch from HCN4 to HCN2 should increase sensitivity to cAMP and therefore an increase in response to ISO was hypothesised. However, ISO produced inconsistent results. There was large variation in response and therefore large standard error. This may have been to do with differences in the amount of nodal tissue present, or due to inactivation of ISO in solution at 37°C as ISO is known to be sensitive to oxidisation. Additional numbers are required to increase statistical power and confidence. In porcine ventricles Ad-Tbx18 infection led to around an 11 % higher change in heart rate in response to ISO compared to Ad-GFP

infected animals although statistical significance was only quoted for absolute heart rate values.[204] This suggested that in ventricular tissue β-adrenergic sensitivity did increase in response to Ad-Tbx18 infection.

4.3.2.6 Tbx18 summary

Tbx18 is currently regarded as a promising target for clinical translation of biopacemaker technology.[9, 234, 235] Our work supports this consensus because we also observed acceleration of beating rates along with an increase in mRNA levels of pacemaker ion channels. Furthermore it suggests that Tbx18 has the potential to improve the function of SAP tissue such that it could promote physiological beating rates from SAP tissue in patients with SND or perhaps repair the dysfunctional SAN tissue itself. However Tbx18 preparations failed to demonstrate any change in overdrive suppression or response to pharmacology. Although our work only demonstrated a limited effect, looking at the peak response time in other studies being longer than 48 hours, this was highly likely to be down to the short culture time used and had our experiments gone on longer we may have seen a more pronounced effect.

4.3.3 Ad-Tbx3

4.3.3.1 Tbx3 transduction was limited and beating rates became erratic

Ad-Tbx3 infection of SAP tissue led to a 3.7-fold rise in Tbx3 mRNA compared to uninfected SAP tissue. There was no significant increase in SAP beating rate following Ad-Tbx3 infection compared to uninfected SAP tissue (figure 41). In fact beating patterns of several preparations became erratic, in two cases suddenly dropping to zero before recovering just as quickly several hours later. This phenomenon also occurred once in control SAP recordings, but was not seen in Tbx18, NCX1 or SAN preparations. This erratic behaviour led to greater error margins and a greater general spread in the data was also seen. After 48 hours of culture no individual Tbx3 preparation was significantly faster than any uninfected SAP preparation. The mechanism of the erratic behaviour seen is not

clear, however with rates dropping to zero before recovering to normal, this could suggest a mechanism similar to sinus pauses. Raw traces can be found in figure 39.

Previous work has used adult transgenic mice and tamoxifen induced Tbx3 upregulation.[205] In keeping with our work they were also unable to elicit any increase in beating rate.[205] They used lentiviral expression of Tbx3 in NRVMs and again found no difference in beating rates compared to lentiviral GFP expression.[205] They also found no measurable I_f in either adult transgenic mice or NRVMs and no upregulation of HCN4 levels in adult transgenic mice.[205] The same group were able to elicit ectopic pacemaker activity as a result of Tbx3 overexpression in early embryonic mice associated with HCN channel upregulation but this was not possible in late embryogenesis which suggested that prolonged exposure to Tbx3 was needed to trigger an indirect pathway in order to have a positive effect on HCN channels and pacemaker function.[16] It is therefore possible that our experiments may have exhibited an effect if allowed to continue for longer.

4.3.3.2 Ad-Tbx3 infection was associated with alteration of atrial genes

Ad-Tbx3 infection was associated with marked downregulation of HCN4, $K_{ir}2.1$, $Na_v1.5$ and NCX1 (figure 42). Comparison with previous work on the effect of Tbx3 on pacemaker genes has demonstrated downregulation of the atrial genes for $K_{ir}2.1$ and $Na_v1.5$, causing conduction slowing with reduced $I_{K,1}$ and I_{Na}.[16, 205] HCN channels were only upregulated by Tbx3 overexpression in early embryogenesis but not in late embryogenesis suggesting an indirect pathway.[16] Cx43 and Cx45 were both downregulated in early development but Cx43 was not affected in late development.[16] In general Tbx3 overexpression seems to mostly have a downregulating effect on the majority of genes measured which is in keeping with the assertion that Tbx3 is a transcriptional repressor.[15, 16, 205]

Our work is therefore consistent with this concept, in particular the downregulation of the atrial genes for $K_{ir}2.1$ and $Na_v1.5$, which is regarded as the most direct effect of Tbx3.[10] Discrepancies seen in HCN channel expression between our work and early embryonic mice could be explained by a relatively limited upregulation of Tbx3 and the short timeframe used in our work, which would limit the effect of Tbx3 especially on

indirect pathways that take longer to manifest. It is interesting to note that 5 days of Tbx3 overexpression in adult transgenic mice led to HCN4 downregulation in ventricular tissue, and in atrial tissue had no effect on HCN4 but upregulated HCN1.[205] The effect of Tbx3 on HCN channels is complex. Table 4 compares all the gene changes seen in our work versus others as a result of Tbx3 overexpression.

4.3.3.3 Tbx3 summary

Tbx3 was predicted to be a promising target for biopacemaking with its role as a transcriptional repressor of the atrial gene programme and fine tuning of the pacemaker phenotype in CCS tissue during embryogenesis. However, the most recent attempts have not led to robust and physiological pacemaker activity and some mechanisms involved in Tbx3 activity seem to be complex and indirect. The most consistent effect in both our work and in transgenic mice is the downregulation of $K_{ir}2.1$ and $Na_v1.5$. A reduction in these channels slows conduction time and disinhibits DD in keeping with the characteristics of pacemaker tissue. One of the first attempts at biopacemaking utilising $K_{ir}2.1$ downregulation was successful at producing slow ectopic pacemaker activity in the LV of guinea pigs but rates were not physiological and prolonged repolarization was seen which would promote ventricular arrhythmias.[52]

Tbx3 only upregulated HCN channels in the context of early embryogenesis but not in late embryogenesis or adulthood, and so further work is needed to reveal the conditions under which Tbx3 would have a more complete effect. Perhaps it would need more time to exhibit a knock on effect on other pacemaker genes or maybe use of Tbx3 in conjunction with other targets should be considered.

Gene	Rat SAP Ad-Tbx3 (this study)	Adult transgenic mouse[205] LA	Adult transgenic mouse[205] LV	Early embryonic mouse[16] LA	Late embryonic mouse[16] LA
HCN1	↓	↑	→	↑	
HCN2		→		↑	
HCN4	↓	→	↓	↑	→
Tbx3	↑	↑	↑	↑	↑
Tbx18	↓				
$K_v1.5$	↓			↓	
$K_{ir}2.1$	↓	↓		↓	
$Na_v1.5$	↓	↓	↓	↓	
NCX1	↓				
RYR2	→				
Cx43	→	↓	↓	↓	→
Cx45	↓	↓		↓	
$Ca_v1.2$					
$Ca_v3.1$		→		↑	

Table 4. Comparison of gene changes as a result of Tbx3 upregulation in this study versus others

Upregulation of Tbx3 in the SAP tissue of rats altered several genes related to pacemaking and there was some concordance with previous work upregulating Tbx3 in adult, early embryonic and late embryonic transgenic mice. These results are compared in the table above. ↑ = upregulated; ↓ = downregulated; → = no change; blank = not tested.

4.3.4 Ad-NCX1-GFP

4.3.4.1 NCX1 was successfully transduced but had no significant effect on beating rate

Ad-NCX1-GFP successfully transduced SAP tissue producing a strong GFP signal localised around the site of injection in every case. NCX1 was detected using qPCR in DNA purified from Ad-NCX1-GFP infected 293 cells but not from uninfected controls. NCX1 levels were not directly measured from infected SAP tissue due to time constraints. However, NCX1 was detected in 293 cells and there was a detectable physiological effect in SAP tissue transduced with Ad-NCX1-GFP in the form of altered cRT.

There was no significant difference in beating rate over 48 hours of tissue culture between Ad-NCX1-GFP infected and uninfected SAP tissue (figure 44). Both showed similar patterns of beating throughout. Maximal effect from NCX1 overexpression would have been expected between 12 – 20 hours following injection allowing time for transduction, gene transcription, NCX1 channel synthesis and trafficking to the cell membrane. This would be in line with previous experiments done by our group overexpressing HCN2 channels in SAP tissue where an effect on beating rate was seen during this timeframe.[152]

NCX1 has not directly been studied as a target for biopacemaking before. It has been overexpressed in other contexts such as in transgenic mice to look at its effect on heart failure, where it improved myocyte contractility and normalised Ca^{2+} transients.[236] NCX1 overexpression was predicted to increase beating rate by accelerating late phase 4 depolarization, playing its role in the final part of the Ca^{2+} clock. Our work showed no effect on beating rate, but we did not directly measure NCX1 mRNA or protein in infected SAP tissue and so cannot be completely sure NCX1 was expressed. Ca^{2+} homeostasis is also complex and accelerated extrusion of Ca^{2+} from the cell may deplete intracellular Ca^{2+} stores and inhibit pacemaking in the long term, similar to the way only temporary increases in intracellular Ca^{2+} via RYRs are seen in response to caffeine before SR Ca^{2+} stores are depleted.[237]

Ca^{2+} clock mechanisms were affected by Tbx18 overexpression which increased intracellular Ca^{2+} release events from the SR.[203] This would suggest that NCX1 may play a role in Tbx18 biopacemaking, however this was not directly demonstrated. The relevance of the Ca^{2+} clock to biopacemaking was also demonstrated by one study that accelerated rhythmic ectopic pacemaker activity from rabbit ventricular myocytes by increasing Ca^{2+} handling protein phosphorylation.[113]

4.3.4.2 Overdrive suppression was reduced in Ad-NCX1-GFP preparations

Our work showed that Ad-NCX1-GFP infected SAP tissue demonstrates significantly lower overdrive suppression than uninfected SAP tissue (figure 45).

As discussed in section 4.3.2.4 overdrive suppression is thought to be related to Na^{+} and Ca^{2+} mechanisms.[54, 217, 229] NCX1 overexpression would theoretically reduce intracellular Ca^{2+} and extracellular Na^{+} which have both been shown to reduce overdrive suppression.[230] Use of ryanodine to block SR Ca^{2+} release has also been shown to prolong overdrive suppression, again highlighting the influence of intracellular Ca^{2+} on this process.[224]

4.3.4.3 NCX1 summary

NCX1 could be a useful target for use in biopacemaking, theoretically accelerating late phase 4 depolarization. Ca^{2+} clock pacemaker mechanisms have not yet been directly studied in the context of creating a biological pacemaker. This is likely to be because it is already clear that single components of pacemaking are unlikely to faithfully recapitulate the complex and robust function of the SAN and focus has shifted to strategies that affect multiple factors such as transcription factors. However, NCX1 overexpression could still represent an interesting target if combined with other aspects of the Ca^{2+} clock. Any effect on beating rate through the use of NCX1 alone may have been buffered by the complexities of Ca^{2+} homeostasis. Its role in overdrive suppression is also very intriguing and would be a useful feature to engineer into a biopacemaker. For example, it may play a role in treating SND that manifests primarily as sinus pauses caused by suppression

from ectopic activity. The Ca^{2+} clock is clearly a major factor in pacemaking and it would not make sense for it to remain unexplored.

4.4 Limitations

4.4.1 Responders vs non-responders

During Ad-Tbx18 experiments it was observed that only a proportion of the experiments demonstrated any acceleration in beating rate. The rest of the experiments followed similar beating rate patterns to uninfected controls. This led to the assertion that only certain preparations were capable of demonstrating an effect while others were not and could therefore be split into two groups, responders and non-responders. All preparations were still included in the analysis regardless of whether they were responders or not. However, we considered why a particular experiment might not respond to adenoviral infection.

Firstly, preparations may undergo ischaemia from the moment an animal is sacrificed to the point the RA tissue is adequately perfused in pre-warmed and oxygenated Tyrode's solution. This may include the time it takes to dissect and open out the RA within the solution as up until this point the RA remains closed and only exposed to solution from the outside. Care was taken to ensure that this time was kept to a minimum and was usually around 5 minutes. In rare cases, preparations started off extremely bradycardic e.g. <50 bpm and stopped beating within hours of starting the experiment and therefore had to be abandoned.

Adenoviral injections were achieved using a 35G needle and 10 µl syringe. 2 µl of adenoviral solution was injected into SAP tissue and usually created a bleb of fluid within the tissue. However, results did vary sometimes leading to excessive tissue stretch localised to the bleb which may have led to trauma. This was again suspected if beating rates started excessively slowly and never recovered.

Conversely certain injections would not lead to a bleb of fluid rather leaking adenoviral solution back out around the needle. In these cases it was difficult to ascertain exactly how much of the injection volume remained in the tissue. A subsequent lack of observed effect may have been due to a low number of infecting viral particles. Again, all preparations were included in the analysis whether there was an observed effect or not.

Targeting SAP tissue was vital to see an effect from viral transduction. However, the extent of pacemaker tissue around the SAP area has been seen to be variable in size when labelling for HCN channels and may also vary depending on dissection technique. Care was taken to dissect consistently using the fossa ovalis as a landmark at which to make the horizontal cut dividing the superior and inferior sections. Injections were also limited to cross-sections of tissue that were thick enough to harbour the injecting needle, which would be the CT. Viruses would transfect SAP tissue only if viral solution was able to diffuse across from the CT. There were therefore several factors that could have contributed to a variable amount of transduced SAP tissue and affect response in terms of observed beating rate.

Lastly, as discussed earlier, the time needed in previous experiments to observe an effect from Tbx18 was after 36 hours and maximally after 2 days following infection. Therefore there may have been some preparations that did not produce an observed effect on beating rate until after 48 hours. A longer culture period may have been needed to observe an effect from these preparations.

4.4.2 Limitations of RT-qPCR results

RT-qPCR was a powerful tool for the measurement of changes in pacemaker related genes as a result of adenoviral gene overexpression in SAP tissue. The aim was to measure atrial and pacemaker genes within SAN, infected and uninfected SAP and RA tissue.

Atrial genes measured from SAN samples seemed to be too high. Genes such as those for $K_{ir}2.1$ and $Na_v1.5$ were expected to be low within the SAN as previously described.[47, 50, 127] SAN samples demonstrated $K_{ir}2.1$ and $Na_v1.5$ levels unexpectedly higher than other genes (figure 51). This was likely to be due to contamination of SAN tissue with surrounding atrial tissue. Indeed when sampling SAN tissue, 2mm biopsies represented a wide excision that would harvest as much SAN tissue as possible. Wider inclusion was also important for better quality and quantity of RNA during isolation as the intercaval area of the RA harbouring the SAN is very thin. Unfortunately this also allowed atrial tissue surrounding the SAN to be included. mRNA levels of atrial specific genes within SAN samples were therefore not reported and can be found in figure 51. SAN specific genes such as HCN4 which appeared at very high levels were reported though, as atrial contamination due to wide excision would not affect these results. In the future, the area of SAN samples must be judged more carefully perhaps through the use of histology guided laser dissection.

RA samples yielded relative mRNA levels that were generally much lower than samples from other areas. Absolute mRNA levels were related to levels of the housekeeper gene 18S. Since RA tissue was a thicker section of tissue than SAN and SAP samples, total RNA quantity isolated was also much higher. 18S levels were therefore also comparatively much higher than in SAN and SAP samples. As a result, relative mRNA levels of each gene of interest became significantly smaller. This made it extremely difficult to compare results from RA samples to those of SAN and SAP samples. Due to this variation it would therefore only really be possible to compare results within a certain tissue type. RA sample results were therefore not reported and can be found in figure 51.

It is important during RT-qPCR to process simultaneously all samples that are to be compared to one another. Due to the nature of tissue culture experiments over many months, it was necessary to process samples in batches to minimise storage of samples and consequent mRNA degradation. This meant that the PCR experiments could not all be performed simultaneously which would be the gold standard.

It would have been useful to compare a panel of housekeeper genes to see which was the most consistent between all samples and tissue types. For example it seemed that 18S was measurable at higher levels in RA samples than SAN samples which made the two tissue types difficult to compare. Other housekeeper genes that could have been used include GAPDH and 28S. 18S was chosen over the others as it had previously been successfully used by the group to compare SAN, SAP and RA samples.[152]

It is important during RT-qPCR to ensure good quality of isolated RNA.[238] In our work this was done using spectrophotometry. The ratio of absorption of wavelengths 260 nm and 280 nm allowed measurement of nucleic acid levels versus contaminants and we ensured that is was at least greater than 2 in all samples. Other methods of RNA quality measurement include agarose gel electrophoresis to ensure tight bands of reference genes and low levels of degraded RNA, microfluidics for more accurate assessment of RNA integrity expressed as a 'RIN' number (using an Agilent Bioanalyser) or use of fluorescent RNA-binding dye probes (e.g. a Qubit assay) for specific detection of RNA.

Microfluidics can also be used to perform the qPCR step itself. Custom 'TaqMan' array cards allow simultaneous measurement of a wide array of gene targets on a single chip. The advantage is easier sample loading leading to fewer inaccuracies caused by user and pipetting error. However, these cards are expensive and additional funding was not available .

4.4.3 I_f blockade – caesium versus ivabradine

I_f blockade was used to assess the contribution of HCN channel function within SAN, infected SAP and uninfected SAP tissue. CsCl solution and ivabradine were used for this purpose with similar effects, both resulting in between 30-40% reduction in beating rate in all preparations.

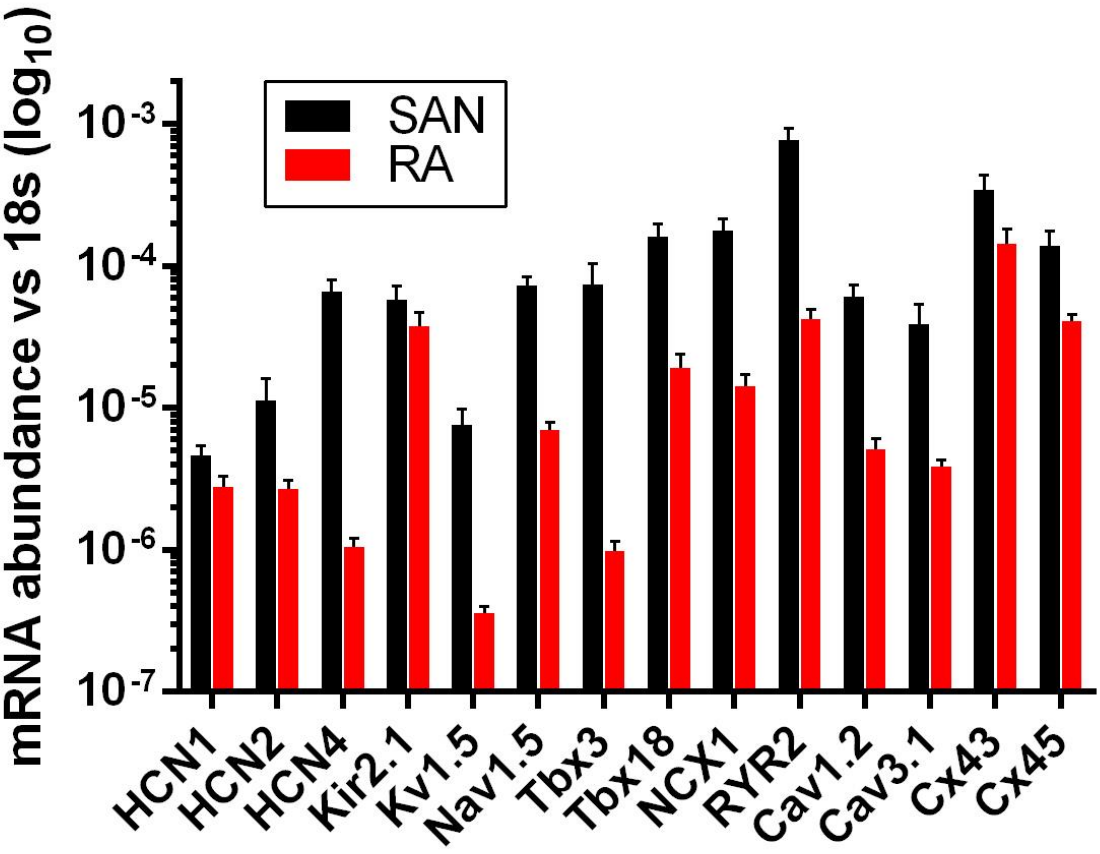

Figure 51. Excluded RT-qPCR data

mRNA abundance was measured by RT-qPCR against the housekeeper gene 18s for SAN and RA samples. Data for atrial genes from SAN tissue were excluded due to sampling being contaminated by atrial tissue leading to falsely high levels. RA data were excluded because 18s levels were much higher than in other tissues leading to disproportionately low mRNA abundance relative to 18s. Taking these discrepancies into account some interesting observations can still be made. A $\log_{10}$ scale is used in order to visualise low and high abundance genes more easily on the same axis.

The mechanism of action of Cs^+ is to enter the pore of HCN channels extracellularly in a voltage-dependent manner during hyperpolarization and blocks current flow. [231] Ivabradine on the other hand is more complex, entering HCN channels from the intracellular side and binding to a site within the channel in a current/use-dependent manner, meaning that even in a channel open state during hyperpolarization ivabradine mostly only inhibits channel function during current flow. In other words greater current flow from a higher the heart rate for example, leads to greater inhibition by ivabradine and vice versa.[84] In this study, differences in blocking mechanism between Cs^+ and ivabradine did not lead to a significant difference in rate reduction.

Criticism has been directed towards both Cs^+ and ivabradine regarding the specificity of each for HCN channel blockade. Cs^+ is also well known to block inward K^+ currents and was used for this purpose long before it was used for HCN channel blockade.[239] Ivabradine is thought to be more specific to HCN channels however at higher doses can also block hERG K^+ channels.[240] However our work has demonstrated similar effects of both ivabradine and Cs^+ on SAP tissue beating rates.

One particular advantage of using Cs^+ over ivabradine was that Cs^+ washed off easily within minutes after its application by superfusing normal Tyrode's solution. Beating rate would return to baseline and therefore it was possible to use a second agent directly afterwards with a similar effect to not having used Cs^+ beforehand. Being able to use two drugs on one preparation improved efficiency reducing use of animals and saved time. Ivabradine did not wash off easily with normal Tyrode's never returning to the baseline beating rate once applied despite extended periods of washing, and could therefore only be used on its own.

4.4.4 Viral cytotoxicity

A concern could be raised regarding the potential cytotoxicity of adenoviruses on cardiac tissue. Cell death may lead to an effect on beating rate. Importantly, RAds used in gene therapy are engineered to lack the ability to replicate and therefore once a virus infects a

cell it merely delivers the gene of interest to be transcribed by the cell's nuclear machinery rather than any genes for viral replication.[220] Newer generations of RAd also have genes deleted that can result in a strong host immune response and so in this way have lower cytotoxicity designed into them.[220] Cell death occurs in wild type viral infection when the cell is overwhelmed by replicated viruses within the cell triggering apoptosis or a host immune response that destroys the cell. In the absence of genes encoding replication and other viral genes that induce host immunity, each RAd infected cell should remain viable. Previous work was done by our group to detect cell apoptosis following RAd infection and suggested that no significant apoptosis occurred.[95] Therefore changes in beating rate were not suspected to be influenced by cell death as a result of viral infection, though this was not specifically measured.

4.4.5 Choice of virus type for gene therapy

RAds are DNA viruses effective at transducing cells with close to 100% efficiency as they can infect a large range of different cell types and do not require cells to be actively dividing.[220] They can be produced easily at high titres. They have a relatively large capacity for insertion of genes of interest at up to 7.5 kb.[220] Their safety profile is also good with most people having been exposed to adenoviruses before and already harbouring immunity, those that haven't only potentially developing mild cold-type symptoms.[220] Conversely, high immunity to adenoviruses also means that virus will be cleared more quickly and could therefore reduce efficacy. Even normal adenoviral gene transduction is transient lasting for 1-2 weeks before being cleared from the cell during replication, since the gene of interest is not integrated into any of the host cell's DNA.[220]

Adeno-associated virus (AAV) is an alternative DNA virus type which holds certain advantages over adenoviruses. They result in more stable and persistent gene transduction due to integration of the gene of interest into episomal DNA that lasts the life of cell.[241] They also harbour low pathogenicity towards host cells.[241] AAVs have a smaller capacity for gene insertion at 4.8 kb, however novel techniques are being developed to increase this to upto 9 kb.[241] Nonetheless there is considerable interest in AAVs in gene therapy for more persistent gene expression compared to adenoviruses.

Lentiviruses are another virus type being used for gene therapy. They are a subclass of RNA retrovirus that can only infect dividing cells and therefore have a lower transduction rate.[242] However, gene transduction is more persistent than AAVs as genes of interest are integrated into the host genome.[242] Unfortunately this integration can be at a random site and therefore carries the risk of disrupting genes responsible for programmed cell death which could theoretically lead to oncogenesis.[242]

Further work in biopacemaking looking at larger animal models and potentially translatable results for human studies are now considering AAVs or lentiviruses over adenoviruses due to their longer lasting effects.

4.5 Main summary

4.5.1 Original hypotheses addressed

1. **HCN4-positive/Cx43-negative tissue similar to the SAN exists in the inferior RA near the inferior vena cava (SAP area).** This hypothesis is supported most strongly by immunohistochemistry data obtained from cryosections of intact RA preparations, directly visualising HCN4-positive/Cx43-negative staining adjacent superiorly to the inferior vena cava.

2. **SAN and SAP tissue will respond similarly to I_f blockade, β-adrenergic stimulation and RYR blockade.** This hypothesis is supported by experiments superfusing ivabradine, ISO and ryanodine individually over freshly isolated SAN and SAP preparations whilst recording beating rates, demonstrating similar changes in beating rates with all three drugs between SAN and SAP preparations.

3. **RAd can be used to upregulate our genes of interest Tbx18, Tbx3 and NCX1 in SAP tissue.** This hypothesis is supported by immunohistochemistry and qPCR data on adenovirus infected 293 cells and cultured SAP tissue. In the case of NCX1 this was also validated by direct visualisation of GFP fluorescence.

4. **Upregulating Tbx18 will cause an increase in beating rate in SAP tissue.** This hypothesis is supported by beating rate data obtained from Ad-Tbx18 infected SAP preparations over 48 hours of culture, which demonstrated significantly faster rates than uninfected SAP preparations at 48 hours.

5. **Upregulating Tbx3 will cause an increase in beating rate in SAP tissue.** This hypothesis is refuted since Ad-Tbx3 infected SAP preparations never beat significantly faster than uninfected SAP preparations.

6. **Upregulating NCX1 will cause an increase in beating rate in SAP tissue.** This hypothesis is refuted since Ad-NCX1-GFP infected SAP preparations never beat significantly faster than uninfected SAP preparations.

7. **Upregulating our genes of interest will individually reduce overdrive suppression in SAP tissue.** This hypothesis was refuted for Ad-Tbx18 infected preparations, with overdrive pacing resulting in similar cRT values for both Ad-Tbx18 infected and uninfected SAP preparations. However, the hypothesis was supported for Ad-NCX1-GFP infected preparations with significantly lower cRT values seen in Ad-NCX1-GFP infected compared to uninfected SAP preparations.

8. **Upregulating Tbx18 will increase response to I_f blockade and β-adrenergic stimulation in SAP tissue.** This hypothesis is refuted with no significant difference in beating rates seen in response to caesium and ISO between Ad-Tbx18 infected and uninfected SAP preparations.

9. **Upregulating each gene of interest will alter expression of other genes or proteins related to pacemaking in SAP tissue.** This hypothesis is supported by upregulation of Tbx18 being associated with upregulation of HCN2 and RYR2, and downregulation of HCN4. Upregulation of Tbx3 was also associated with

downregulation of HCN1, HCN4, $Na_v1.5$, $K_{ir}2.1$, Tbx18 and NCX1, and upregulation of Cx43.

4.5.2 Main contribution to knowledge

The work presented here provides novel data regarding the effect of three transgenes Tbx18, Tbx3 and NCX1 on the functional and molecular character of SAP tissue in the isolated rat RA. The closest comparisons to this work are two studies, one successfully inducing ectopic pacemaking using adenovirus to upregulate Tbx18 but in the ventricular tissue of pigs,[204] the other accelerating bradycardic intrinsic pacemaker activity in isolated SAP tissue but rather through the use of adenovirus to upregulate a single HCN channel type.[152] The most interesting feature of this work is therefore the upregulation of Tbx18 in isolated SAP tissue, combining the ability of Tbx18 to alter several genes simultaneously and transform normally quiescent cells into SAN-like cells, with SAP tissue substrate which is potentially more amenable to biopacemaking than ventricular tissue as it is already capable of bradycardic pacemaking and harbours many similarities to SAN tissue. SAP tissue in this regard also represents a model of SAN dysfunction and our work provides insight into how these transgenes could directly affect a dysfunctional SAN in human disease. This has not been demonstrated before.

Out of the three transgenes used, Tbx18 was the only one to successfully increase beating rates in SAP tissue. This was associated with upregulation of HCN2 and RYR2, but a downregulation of HCN4. There was no effect on overdrive suppression or sensitivity to I_f blockade or β-adrenergic stimulation. Tbx3 did not significantly increase beating rate but actually seemed to increase the incidence of rate instability. Tbx3 upregulation was associated with downregulation of several genes including those for $K_{ir}2.1$ and $Na_v1.5$ but also HCN1, HCN4 and NCX1. Transduction of NCX1 did not significantly increase beating rate but it did reduce overdrive suppression. Tbx18 therefore shows the most promise as a biopacemaking target in SAP tissue and this reflects the current literature demonstrating successful application in ventricular tissue.[204] Since Tbx3 upregulation led to downregulation of atrial genes and NCX1 upregulation reduced overdrive suppression, these genes could be considered as secondary targets.

4.5.3 Future directions

Further work could focus on longer culture times, especially for transcription factors as other groups have suggested additional effect only after 48 hours. This would require modifications to the current superfusion and culture setup to ensure the reliability of circulating culture medium and prevention of infection. Additional characterisation of infected SAP tissue could be performed, including analysis of AP morphology using sharp microelectrode recording, activation mapping, quantitative protein analysis using western blot and analysis of a further panel of genes using RT-qPCR such as additional aspects of Ca^{2+} handling mechanisms like SERCA and phospholamban.

Faithfully replicating SAN function in a biopacemaker will require complex alterations to the substrate tissue. Several factors will have to be considered to recapitulate the intricate central and peripheral ultrastructure of the SAN as well as all aspects of both membrane and Ca^{2+} clocks. This may only be possible through the use of multiple transcription factors simultaneously. Perhaps the most effective strategy would be to reproduce the sequence of transcription factors seen in SAN embryogenesis which may therefore need to include Shox2, Tbx18 and Tbx3. Studies are currently ongoing in larger animals using longer lasting viral vectors with a view to translate findings into alternative therapies for human conduction system disorders.

Appendices

A1. Solutions and media

Tyrode's solution

Tyrode's solution was used for tissue dissection and electrophysiology experiments and consisted of 120 mM NaCl, 4 mM KCl, 2.6 mM $MgSO_4$, 1.2 mM NaH_2PO_4, 1.2 mM $CaCl_2$, 25.2 mM $NaHCO_3$ and 10 mM D-glucose in distilled H_2O. Solutions were filter-sterilised (Steritop 0.2 µm pore, Scientific Laboratory Supplies), pre-warmed to 37°C and bubbled with 5% CO_2 / 95% O_2 gas.

293 medium

293 cell culture utilised 500 ml minimum essential medium (MEM, Life Technologies) was supplemented with 50 ml foetal bovine serum (FBS, Life Technologies) and 5 ml L-glutamine-penicillin-streptomycin solution (200mM L-glutamine, 10000 units penicillin and 10 mg/ml streptomycin, Sigma-Aldrich) then stored at 4°C. Solutions were filter-sterilised (Steritop 0.2 µm pore, Scientific Laboratory Supplies).

Tissue culture medium

Tissue culture utilised 500 ml Advanced Dulbecco's modified Eagle's medium/Ham's F-12 (DMEM/F12, Life Technologies) was supplemented with 50 ml FBS (Life Technologies), and 5 ml L-glutamine-penicillin-streptomycin solution (200mM L-glutamine, 10000 units penicillin and 10 mg/ml streptomycin, Sigma-Aldrich) then stored at 4 °C. Solutions were filter-sterilised (Steritop 0.2 µm pore, Scientific Laboratory Supplies).

293 cell and virus freezing medium

Cells and viruses were suspended in freezing medium which was made using 9 ml Advanced DMEM/F12 (Life Technologies) supplemented with 1 ml Dimethyl Sulfoxide (DMSO, Sigma-Aldrich) and stored in cryotubes within a liquid N_2 sample storage container.

X-gal solution

20 ml X-Gal staining solution was prepared in 0.01 M PBS containing 42 mg $C_6N_6FeK_4$ (potassium ferrocyanide), 32 mg $C_6N_6FeK_3$ (potassium ferricyanide), 8 mg $MgCl_2$, 20 mg 5-Bromo-4-Chloro-3-Indolyl-D-Galactoside (X-Gal) dissolved in 500 µl DMSO.

Advanced DMEM/F-12 formulation

Components	Molecular Weight	Concentration (mg/L)	mM
Amino Acids			
Glycine	75.0	18.75	0.25
L-Alanine	89.0	4.45	0.049999997
L-Arginine hydrochloride	211.0	147.5	0.69905216
L-Asparagine-H_2O	150.0	7.5	0.05
L-Aspartic acid	133.0	6.65	0.05
L-Cysteine hydrochloride-H_2O	176.0	17.56	0.09977272
L-Cystine 2HCl	313.0	31.29	0.09996805
L-Glutamic Acid	147.0	7.35	0.05
L-Histidine hydrochloride-H_2O	210.0	31.48	0.14990476

Components	Molecular Weight	Concentration (mg/L)	mM
L-Isoleucine	131.0	54.47	0.41580153
L-Leucine	131.0	59.05	0.45076334
L-Lysine hydrochloride	183.0	91.25	0.4986339
L-Methionine	149.0	17.24	0.11570469
L-Phenylalanine	165.0	35.48	0.2150303
L-Proline	115.0	17.25	0.15
L-Serine	105.0	26.25	0.25
L-Threonine	119.0	53.45	0.44915968
L-Tryptophan	204.0	9.02	0.04421569
L-Tyrosine disodium salt dihydrate	261.0	55.79	0.21375479
L-Valine	117.0	52.85	0.4517094
Vitamins			
Ascorbic Acid phosphate	289.54	2.5	0.008634386

Components	Molecular Weight	Concentration (mg/L)	mM
Biotin	244.0	0.0035	1.4344263E-5
Choline chloride	140.0	8.98	0.06414285
D-Calcium pantothenate	477.0	2.24	0.0046960167
Folic Acid	441.0	2.65	0.0060090707
Niacinamide	122.0	2.02	0.016557377
Pyridoxine hydrochloride	206.0	2.0	0.009708738
Riboflavin	376.0	0.219	5.824468E-4
Thiamine hydrochloride	337.0	2.17	0.0064391694
Vitamin B12	1355.0	0.68	5.0184503E-4
i-Inositol	180.0	12.6	0.07
Inorganic Salts			
Calcium Chloride ($CaCl_2$) (anhyd.)	111.0	116.6	1.0504504
Cupric sulfate ($CuSO_4$-$5H_2O$)	250.0	0.0013	5.2E-6

Components	Molecular Weight	Concentration (mg/L)	mM
Ferric Nitrate ($Fe(NO_3)3"9H_2O$)	404.0	0.05	1.2376238E-4
Ferric sulfate ($FeSO_4$-$7H_2O$)	278.0	0.417	0.0015
Magnesium Chloride (anhydrous)	95.0	28.64	0.30147368
Magnesium Sulfate ($MgSO_4$) (anhyd.)	120.0	48.84	0.407
Potassium Chloride (KCl)	75.0	311.8	4.1573334
Sodium Bicarbonate ($NaHCO_3$)	84.0	2438.0	29.02381
Sodium Chloride (NaCl)	58.0	6995.5	120.61207
Sodium Phosphate dibasic (Na_2HPO_4) anhydrous	142.0	71.02	0.50014085
Sodium Phosphate monobasic (NaH_2PO_4-H_2O)	138.0	62.5	0.45289856
Zinc sulfate ($ZnSO_4$-$7H_2O$)	288.0	0.864	0.003
Proteins			
AlbuMAX® II		400.0	Infinity

Components	Molecular Weight	Concentration (mg/L)	mM
Human Transferrin (Holo)		7.5	Infinity
Insulin Recombinant Full Chain		10.0	Infinity
Reducing Agents			
Glutathione, monosodium	307.0	1.0	0.0032573289
Trace Elements			
Ammonium Metavanadate	116.98	3.0E-4	2.564541E-6
Manganous Chloride	198.0	5.0E-5	2.5252524E-7
Sodium Selenite	173.0	0.005	2.8901733E-5
Other Components			
D-Glucose (Dextrose)	180.0	3151.0	17.505556
Ethanolamine	97.54	1.9	0.019479187
Hypoxanthine Na	159.0	2.39	0.015031448
Linoleic Acid	280.0	0.042	1.4999999E-4

Components	Molecular Weight	Concentration (mg/L)	mM
Lipoic Acid	206.0	0.105	5.097087E-4
Phenol Red	376.4	8.1	0.021519661
Putrescine 2HCl	161.0	0.081	5.031056E-4
Sodium Pyruvate	110.0	110.0	1.0
Thymidine	242.0	0.365	0.0015082645

A2. Reference charts

	Surface Area (mm^2)	Seeding Density	Cells at Confluency[1]	Versene (ml of 0.53 mM EDTA)	Trypsin (ml of 0.05% trypsin, 0.53 mM EDTA)	Growth Medium (ml)
Dishes						
35 mm	962	0.3×10^6	1.2×10^6	1	1	2
60 mm	2,827	0.8×10^6	3.2×10^6	3	2	3
100 mm	7,854	2.2×10^6	8.8×10^6	5	3	10
150 mm	17,671	5.0×10^6	20.0×10^6	10	8	20
Cluster Plates						
6-well	962	0.3×10^6	1.2×10^6	2	2	3–5
12-well	401	0.1×10^6	0.4×10^6	1	1	1–2
24-well	200	0.05×10^6	0.2×10^6	0.5	0.5	0.5–1.0
Flasks						
T-25	2,500	0.7×10^6	2.8×10^6	3	3	3–5
T-75	7,500	2.1×10^6	8.4×10^6	5	5	8–15
T-160	16,000	4.6×10^6	18.4×10^6	10	10	15–30

[1] The number of cells on a confluent plate, dish, or flask will vary with cell type. For this table, HeLa cells were used.

Figure 52. Useful numbers for cell culture

Cells were seeded according to the size of flask or plate being used. This chart was helpful to decide how much medium to use, how many cells to seed and also estimate their number once they had reached confluency. Accessed at www.thermofisher.com.

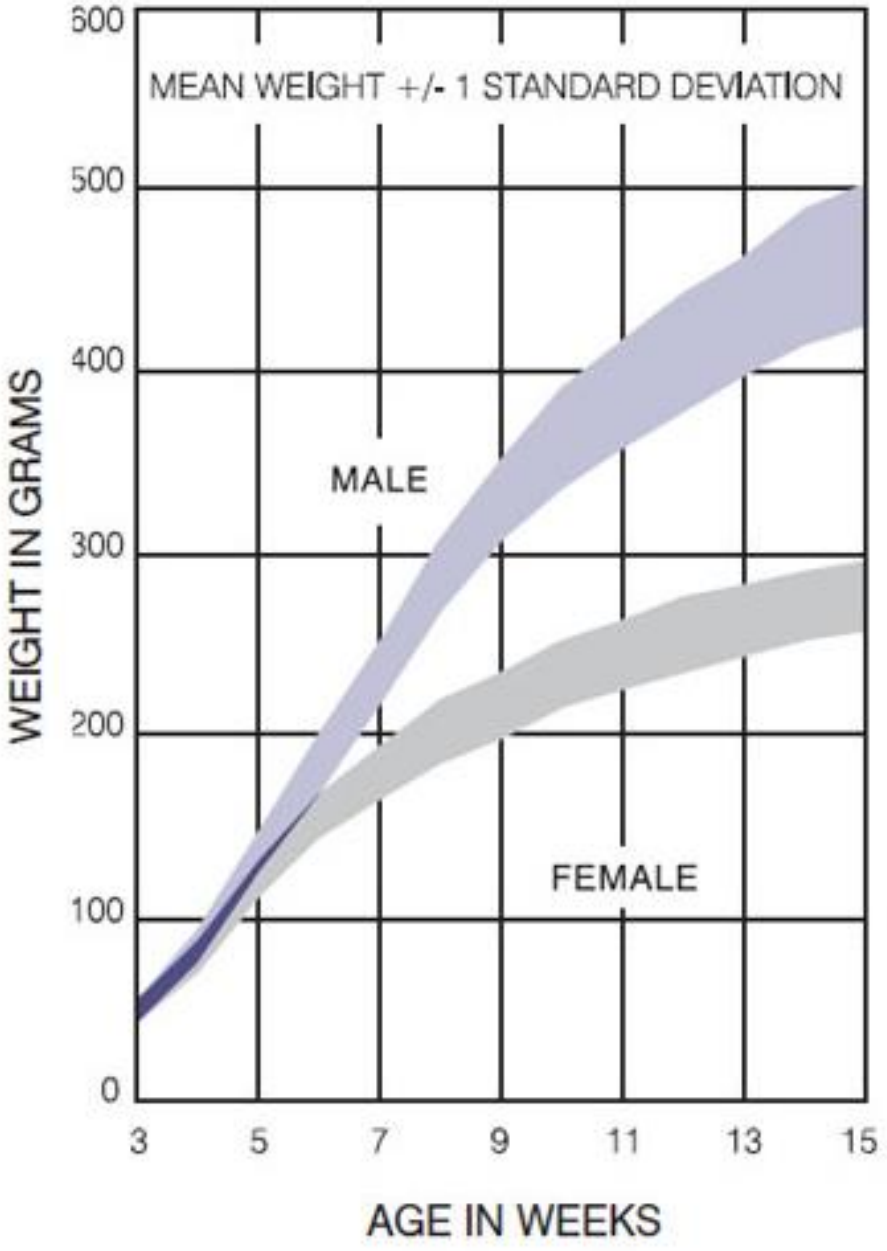

Figure 53. Charles River Wistar rat weight to age chart

Male Wistar rats supplied by Charles River were weighed before being culled to ensure they were all of a similar weight and age. This chart was used to estimate age from measured weight. Accessed at www.criver.com.

A3. Virus DNA sequencing

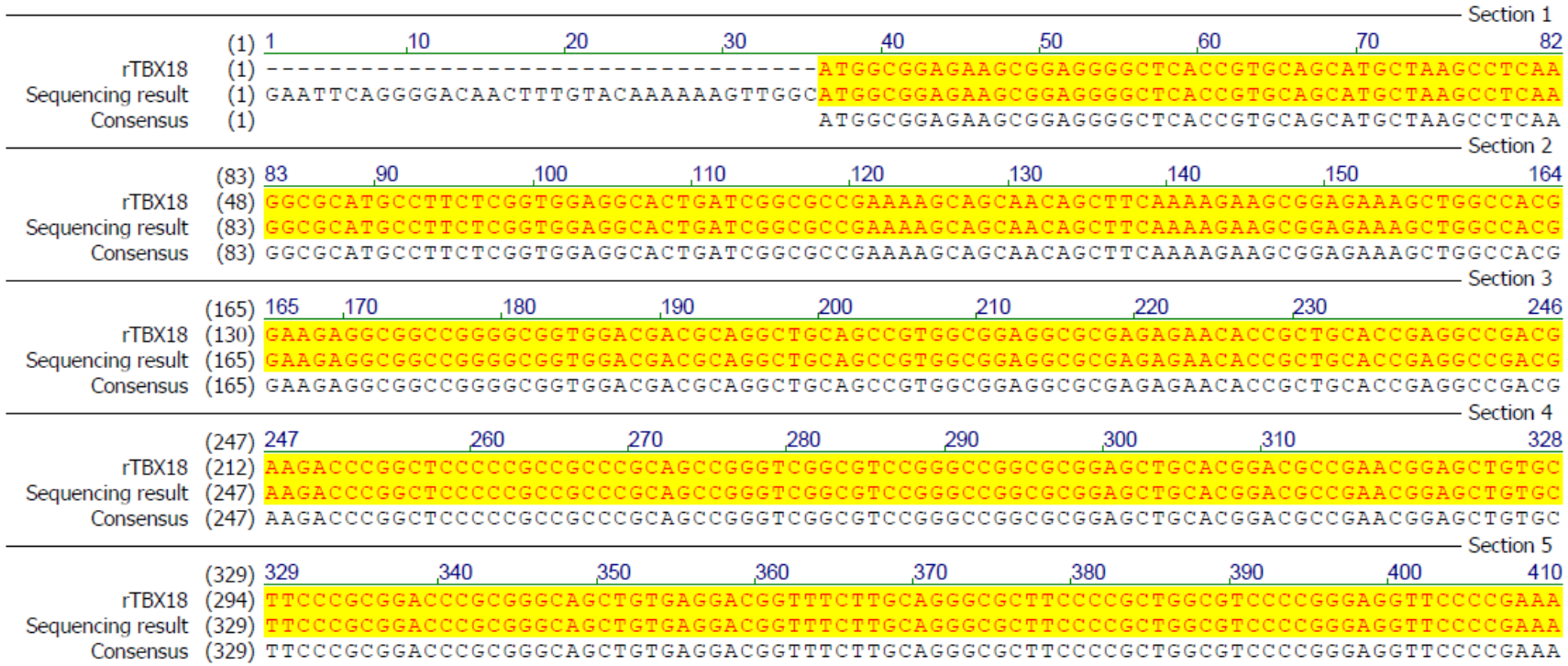

Figure 54. Ad-Tbx18 virus DNA sequencing

Ad-Tbx18 was purchased ready-made from ABMGood who manufactured the virus. The DNA sequencing of our Ad-Tbx18 was performed and provided by ABMGood before delivery to ensure quality of viral DNA and its consensus with the known sequence for Tbx18.

Figure 55. Ad-Tbx3 virus DNA sequencing

Ad-Tbx3 was purchased ready-made from ABMGood who manufactured the virus. The DNA sequencing above of our Ad-Tbx3 virus was performed and provided by ABMGood before delivery to ensure quality of viral DNA and its consensus with the known sequence for Tbx3.

A4. Supplementary data

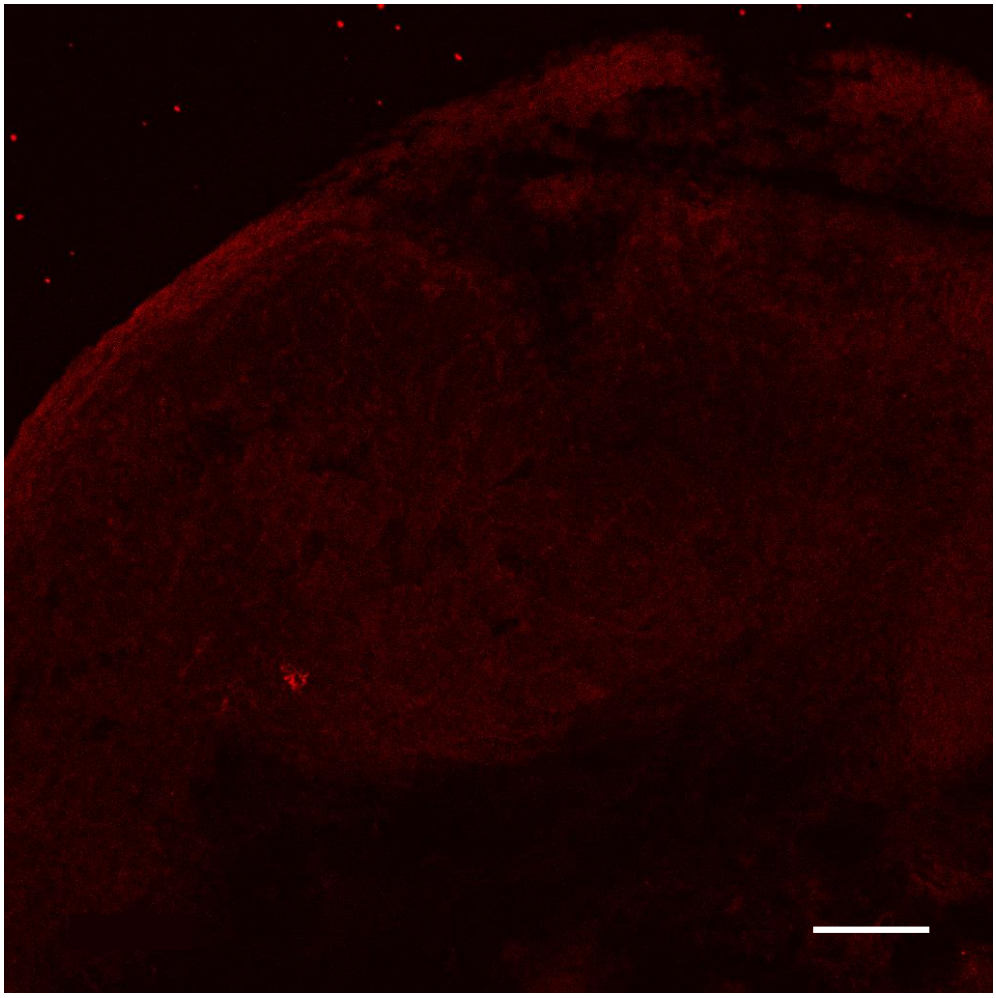

Figure 56. Attempted HCN1 immunostaining in cultured SAP preparations

Immunostaining HCN1 in SAP preparations following tissue culture was unsuccessful. No positive staining was seen. The HCN1 isoform is a relatively low abundance protein and the tissue culture process seemed to make immunostaining less effective as evidenced by patchy staining of even high abundance proteins like Cx43 following culture (see figure 58). Immunohistochemistry following tissue culture was therefore deemed unreliable. Scale bar represents 100 µm.

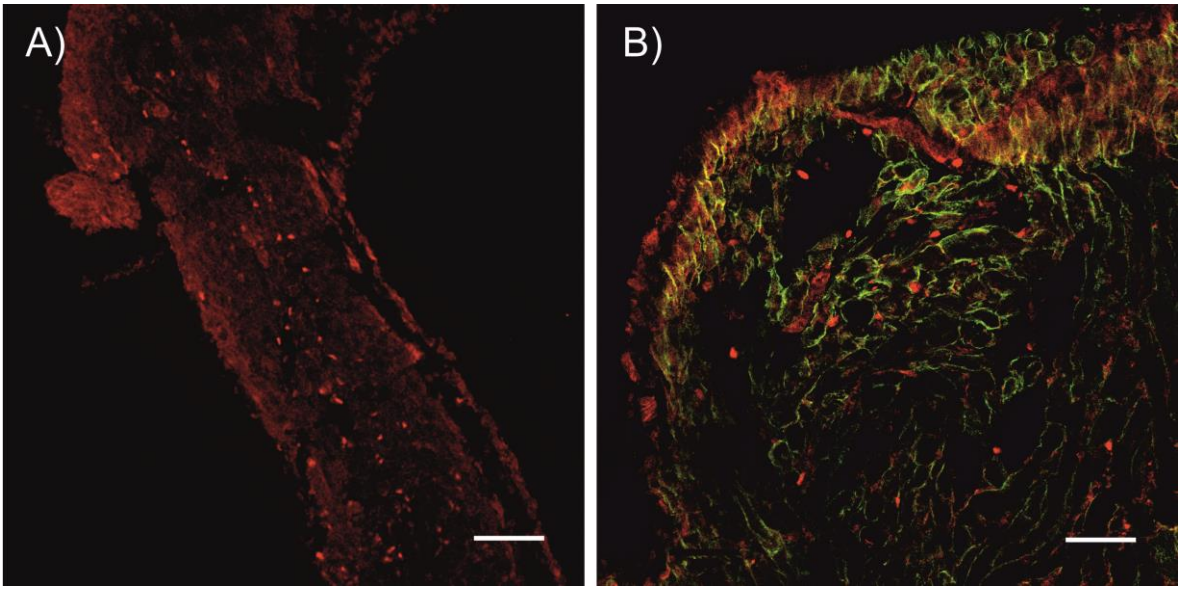

Figure 57. Tbx18 immunostaining in cultured SAP preparations

(A) Tbx18 immunostaining in Ad-Tbx18 infected SAP tissue following 48 hours of tissue culture was unreliable however 2 of 6 preparations did show sporadic Tbx18 signal at the site of injection. (B) Cav3 was co-stained in some sections of the same preparations which again showed sporadic Tbx18 signal but more often seen outside of cardiomyocyte membranes labelled with Cav3. Scale bars represent 100 µm in panel A and 50 µm in panel B.

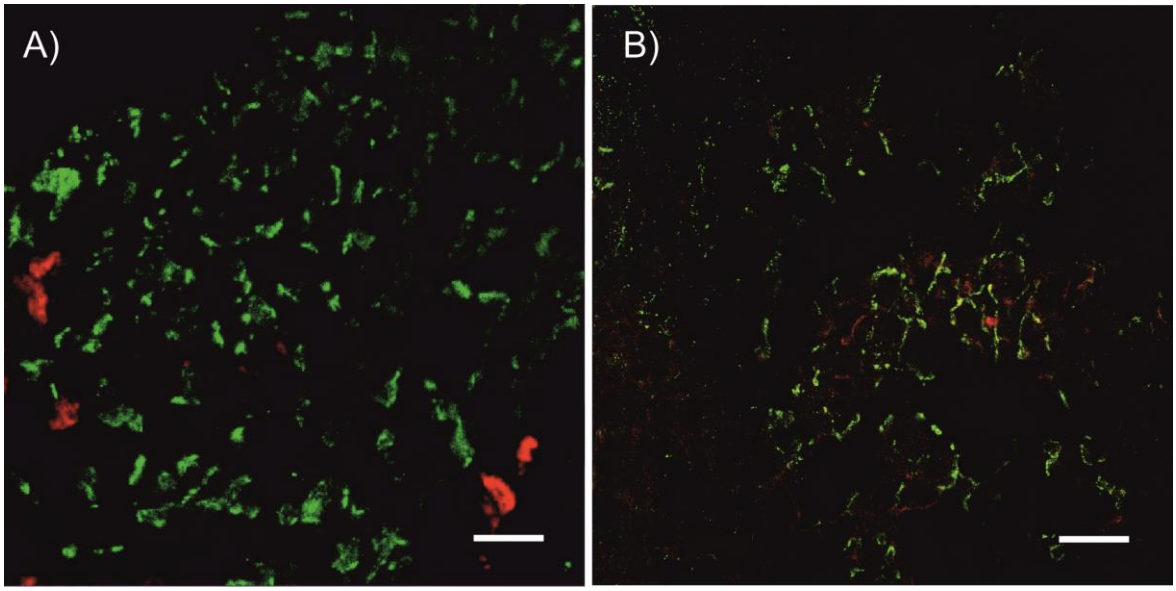

Figure 58. Patchy Cx43 immunostaining in cultured SAP tissue

Immunostaining following tissue culture was unreliable. (A) Cx43 is an abundant protein normally very easily labelled in fresh tissue. (B) After 48 hours of tissue culture, the same protocol led to patchy staining. Immunohistochemistry following tissue culture was therefore deemed unreliable. Scale bars represent 50 µm.

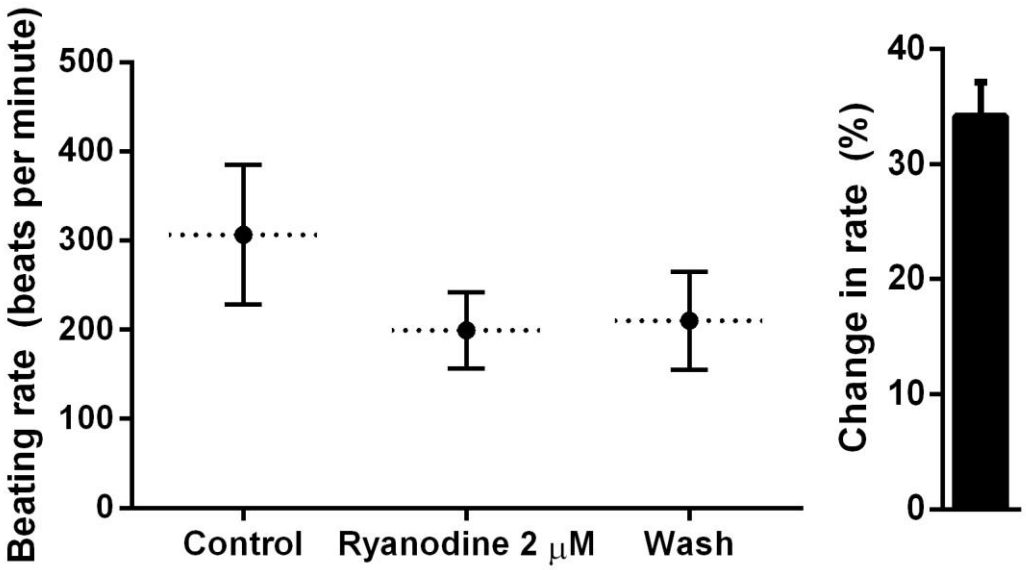

Figure 59. Effect of ryanodine on Ad-NCX1-GFP infected SAP tissue

Ad-NCX1-GFP infected SAP tissue (n=2) was exposed to ryanodine solution (2 μM) following 48 hours of tissue culture. Beating rates were reduced by 31% in one sample and 37% in the other. More samples are needed before data analysis can be performed.

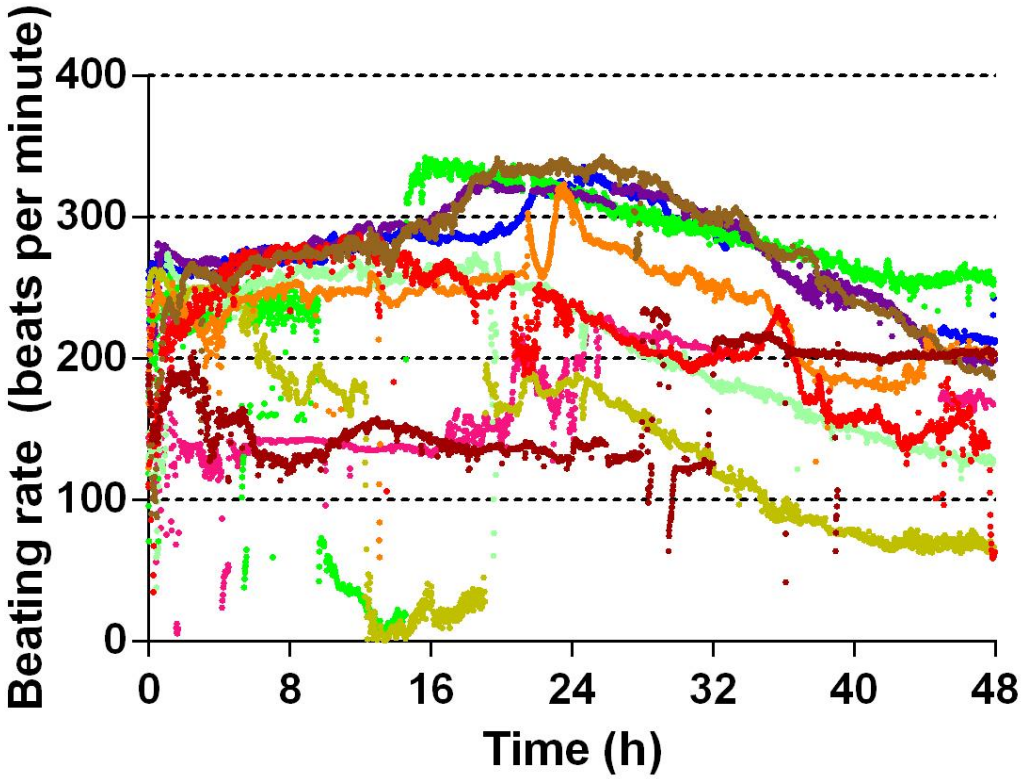

Figure 60. Raw beating rate data from Ad-GFP infected SAP tissue from two different batches of animals with different weights

Data from Ad-GFP infected SAP tissue was difficult to analyse and compare as initial experiments all exhibited beating rates that started much faster than they had ever been before. This was subsequently put down to a batch of animals that were underweight. A future batch of animals at the correct weight did exhibit lower beating rates in keeping with earlier data. A comparison was made of beating rates versus animal weight however unfortunately the data as a whole could not easily be compared to previous data and were therefore excluded. Dots represent 60 s mean beating rates.

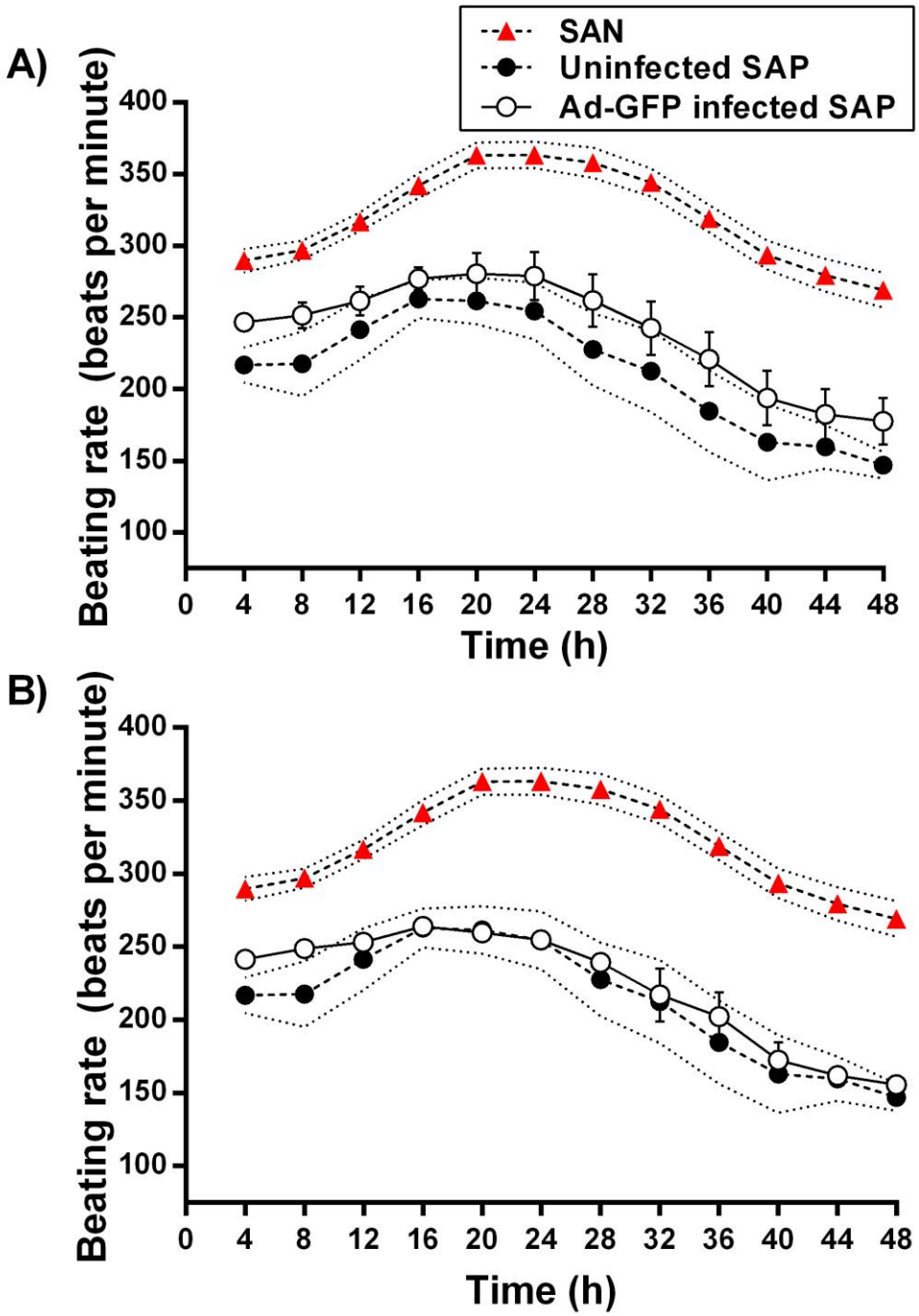

Figure 61. Mean beating rate data from Ad-GFP infected SAP tissue

Mean beating rate data taken from Ad-GFP infected SAP tissue preparations comparing (A) all preparations (n=10) and (B) data excluding underweight animals (n=6). Neither were significantly different to uninfected SAP preparations but including underweight animals increased error margins and increased mean beating rates throughout.

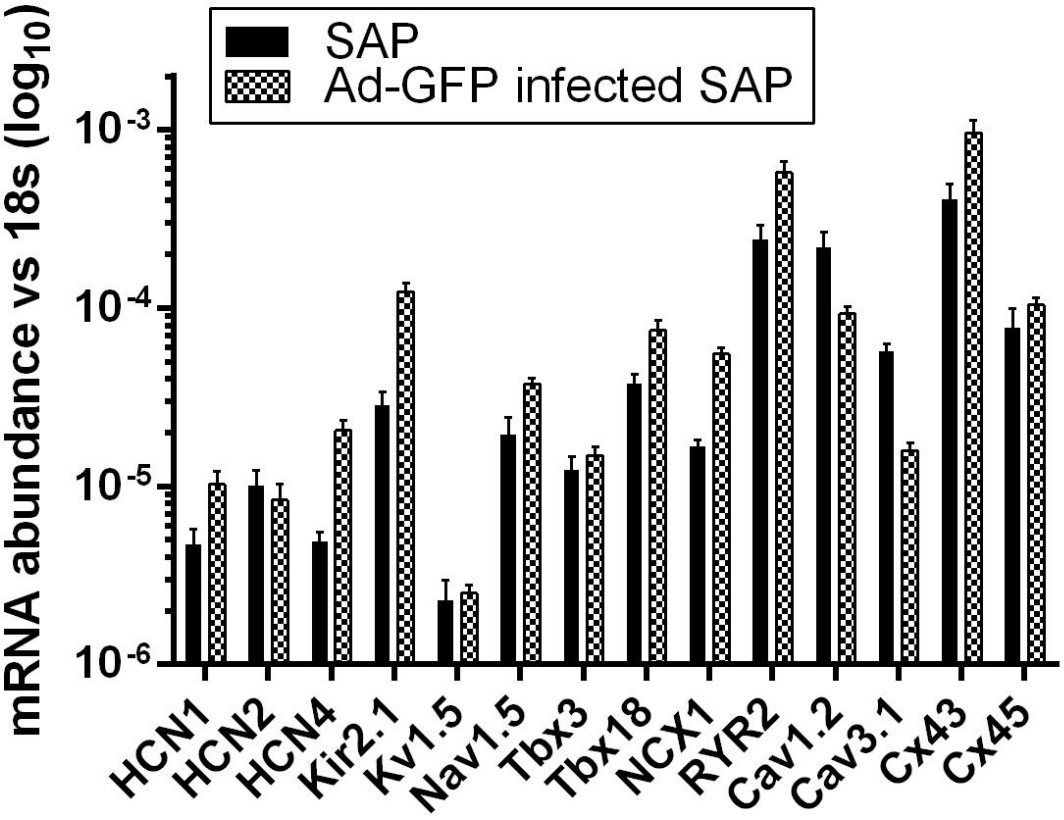

Figure 62. RT-qPCR data from Ad-GFP infected SAP tissue

mRNA abundance was measured by RT-qPCR against the housekeeper gene 18s for Ad-GFP infected SAP preparations. mRNA levels were similar to uninfected SAP preparations. However, data had to be excluded as it included animals that were underweight.

References

1. Silverman ME and Hollman A. Discovery of the sinus node by Keith and Flack: on the centennial of their 1907 publication. *Heart (British Cardiac Society)*. 2007;93:1184-7.

2. Silverman ME and Upshaw CB, Jr. Walter Gaskell and the understanding of atrioventricular conduction and block. *J Am Coll Cardiol*. 2002;39:1574-80.

3. Tawara S. Das Reizleitungssystem Des Säugetierherzens (The conduction system of the mammalian heart) Jena: Gustav Fischer. 1906;(Translated into English by Kozo Suma and Munehiro Shimada and published by Imperial College Press, London, 2000).

4. Keith A and Flack M. The form and nature of the muscular connections between the primary divisions of the vertebrate heart. *J Anat Physiol*. 1907;41:172-189.

5. National Institute for Clinical Excellence. Dual-chamber pacemakers for symptomatic bradycardia due to sick sinus syndrome and/or atrioventricular block. *NICE Technology Appraisal 88*. 2005.

6. Murgatroyd F, Linker N, Cunningham D, Cunningham M, Chadburn L, Gilbert S and de Lang A. National audit of cardiac rhythm management devices. *National Institute for Cardiovascular Outcomes Research*. 2014.

7. Sweeney MO and Hellkamp AS. Heart failure during cardiac pacing. *Circulation*. 2006;113:2082-8.

8. Rosen MR, Robinson RB, Brink PR and Cohen IS. The road to biological pacing. *Nat Rev Cardiol*. 2011;8:656-666.

9. Meyers JD, Jay PY and Rentschler S. Reprogramming the conduction system: Onward toward a biological pacemaker. *Trends in cardiovascular medicine*. 2016;26:14-20.

10. Christoffels VM, Smits GJ, Kispert A and Moorman AFM. Development of the pacemaker tissues of the heart. *Circ Res*. 2010;106:240-254.

11. van den Berg G, Abu-Issa R, de Boer BA, Hutson MR, de Boer PA, Soufan AT, Ruijter JM, Kirby ML, van den Hoff MJ and Moorman AF. A caudal proliferating growth center contributes to both poles of the forming heart tube. *Circ Res*. 2009;104:179 -188.

12. Moorman AFM and Christoffels VM. Cardiac chamber formation: development, genes and evolution. *Physiol Rev*. 2003; 83:1223-1267.

13. van Mierop LHS. Localization of pacemaker in chick embryo heart at the time of initiation of heartbeat. *Am J Physiol*. 1967;212:407- 415.

14. Mommersteeg MTM, Hoogaars WMH, Prall OWJ, de Gier-de Vries C, Wiese C, Clout DEW, Papaioannou VE, Brown NA, Harvey RP, Moorman AFM and Christoffels VM. Molecular pathway for the localized formation of the sinoatrial node. *Circ Res*. 2007;100:354 -362.

15. Hoogaars WMH, Tessari A, Moorman AFM, de Boer PAJ, Hagoort J, Soufan AT, Campione M and Christoffels VM. The transcriptional repressor Tbx3 delineates the developing central conduction system of the heart. *Cardiovasc Res*. 2004;62:489-499.

16. Hoogaars WM, Engel A, Brons JF, Verkerk AO, de Lange FJ, Wong LY, Bakker ML, Clout DE, Wakker V, Barnett P, Ravesloot JH, Moorman AF, Verheijck EE and Christoffels VM. Tbx3 controls the sinoatrial node gene program and imposes pacemaker function on the atria. *Genes Dev*. 2007;21:1098 -1112.

17. Blaschke RJ, Monaghan AP, Schiller S, Schechinger B, Rao E, Padilla-Nash H, Ried T and Rappold GA. SHOT, a SHOX-related homeobox gene, is implicated in craniofacial, brain, heart, and limb development. *Proceedings of the National Academy of Sciences of the United States of America*. 1998;95:2406-11.

18. Espinoza-Lewis RA, Yu L, He F, Liu H, Tang R, Shi J, Sun X, Martin JF, Wang D, Yang J and Chen Y. Shox2 is essential for the differentiation of cardiac pacemaker cells by repressing Nkx2-5. *Dev Biol*. 2009;327:376-85.

19. Christoffels VM, Mommersteeg MT, Trowe MO, Prall OW, de Gier-de Vries C, Soufan AT, Bussen M, Schuster-Gossler K, Harvey RP, Moorman AF and Kispert A. Formation of the venous pole of the heart from an Nkx2-5-negative precursor population requires Tbx18. *Circ Res*. 2006;98:1555-63.

20. Wiese C, Grieskamp T, Airik R, Mommersteeg MTM, Gardiwal A, de Gier-de Vries C, Schuster-Gossler K, Moorman AFM, Kispert A and Christoffels VM. Formation of the sinus node head and differentiation of sinus node myocardium are independently regulated by Tbx18 and Tbx3. *Circ Res*. 2009;104:388-397.

21. Sanchez-Quintana D, Cabrera JA, Farre J, Climent V, Anderson RH and Ho SY. Sinus node revisited in the era of electroanatomical mapping and catheter ablation. *Heart (British Cardiac Society)*. 2005;91:189-94.

22. Yamamoto M, Dobrzynski H, Tellez J, Niwa R, Billeter R, Honjo H, Kodama I and Boyett MR. Extended atrial conduction system characterized by the expression of the HCN4 channel and connexin45. *Cardiovasc Res*. 2006;72:271-281.

23. James TN, Sherf L, Fine G and Morales AR. Comparative ultrastructure of the sinus node in man and dog. *Circulation*. 1966;34:139-63.

24. Alings AM, Abbas RF and Bouman LN. Age-related changes in structure and relative collagen content of the human and feline sinoatrial node. A comparative study. *Eur Heart J*. 1995;16:1655-67.

25. Ayettey AS and Navaratnam V. The T-tubule system in the specialized and general myocardium of the rat. *Journal of anatomy*. 1978;127:125-40.

26. Dobrzynski H, Li J, Tellez J, Greener ID, Nikolski VP, Wright SE, Parson SH, Jones SA, Lancaster MK, Yamamoto M, Honjo H, Takagishi Y, Kodama I, Efimov IR, Billeter R and Boyett MR. Computer three-dimensional reconstruction of the sinoatrial node. *Circulation*. 2005;111:846-54.

27. Chandler N, Aslanidi O, Buckley D, Inada S, Birchall S, Atkinson A, Kirk D, Monfredi O, Molenaar P, Anderson R, Sharma V, Sigg D, Zhang H, Boyett M and Dobrzynski H. Computer three-dimensional anatomical reconstruction of the human sinus node and a novel paranodal area. *Anat Rec (Hoboken)*. 2011;294:970-9.

28. Bromberg BI, Hand DE, Schuessler RB and Boineau JP. Primary negativity does not predict dominant pacemaker location: implications for sinoatrial conduction. *Am J Physiol*. 1995;269:H877-87.

29. Fedorov VV, Glukhov AV, Chang R, Kostecki G, Aferol H, Hucker WJ, Wuskell JP, Loew LM, Schuessler RB, Moazami N and Efimov IR. Optical mapping of the isolated coronary-perfused human sinus node. *Journal of the American College of Cardiology*. 2010;56:1386-94.

30. Matsuyama TA, Inoue S, Kobayashi Y, Sakai T, Saito T, Katagiri T and Ota H. Anatomical diversity and age-related histological changes in the human right atrial posterolateral wall. *Europace*. 2004;6:307-315.

31. Bleeker WK, Mackaay AJ, Masson-Pevet M, Bouman LN and Becker AE. Functional and morphological organization of the rabbit sinus node. *Circ Res*. 1980;46:11-22.

32. Ramanathan C, Jia P, Ghanem R, Ryu K and Rudy Y. Activation and repolarization of the normal human heart under complete physiological conditions. *Proceedings of the National Academy of Sciences of the United States of America*. 2006;103:6309-14.

33. Lee RJ, Kalman JM, Fitzpatrick AP, Epstein LM, Fisher WG, Olgin JE, Lesh MD and Scheinman MM. Radiofrequency catheter modification of the sinus node for "inappropriate" sinus tachycardia. *Circulation*. 1995;92:2919-28.

34. Schuessler RB, Boineau JP and Bromberg BI. Origin of the sinus impulse. *Journal of cardiovascular electrophysiology*. 1996;7:263-74.

35. Shibata N, Inada S, Mitsui K, Honjo H, Yamamoto M, Niwa R, Boyett MR and Kodama I. Pacemaker shift in the rabbit sinoatrial node in response to vagal nerve stimulation. *Exp Physiol*. 2001;86:177-84.

36. Joung B, Hwang HJ, Pak HN, Lee MH, Shen C, Lin SF and Chen PS. Abnormal response of superior sinoatrial node to sympathetic stimulation is a

characteristic finding in patients with atrial fibrillation and symptomatic bradycardia/clinical perspective. *Circ Arrhythm Electrophysiol*. 2011;4:799 - 807.

37. Lewis T, Oppenheimer BS and Oppenheimer A. The site of origin of the mammalian heart beat: the pacemaker in the dog. *Heart (British Cardiac Society)*. 1910;2:147-169.

38. Wybauw R. Sur le point d'origine de la systole cardiaque dans l'oreillette droite. *Arch internat d Physiol*. 1910;10:78 -90.

39. Weidmann S. Membrane excitation in cardiac muscle. *Circulation*. 1961;24:499-505.

40. Noble D, Garny A and Noble PJ. How the Hodgkin-Huxley equations inspired the Cardiac Physiome Project. *The Journal of Physiology*. 2012;590 2613-2628. .

41. Monfredi O, Dobrzynski H, Mondal T, Boyett MR and Morris GM. The anatomy and physiology of the sinoatrial node--a contemporary review. *Pacing Clin Electrophysiol*. 2010;33:1392-406.

42. Boyett MR. 'And the beat goes on.' The cardiac conduction system: the wiring system of the heart. *Exp Physiol*. 2009;94:1035-49.

43. Zhang H, Holden AV, Kodama I, Honjo H, Lei M, Varghese T and Boyett MR. Mathematical models of action potentials in the periphery and center of the rabbit sinoatrial node. *American journal of physiology Heart and circulatory physiology*. 2000;279:H397-421.

44. West TC. Ultramicroelectrode recording from the cardiac pacemaker. *The Journal of pharmacology and experimental therapeutics*. 1955;115:283-90.

45. Lakatta EG and DiFrancesco D. What keeps us ticking: a funny current, a calcium clock, or both? *J Mol Cell Cardiol*. 2009;47:157-70. .

46. Harmar AJ, Hills RA, Rosser EM, Jones M, Buneman OP, Dunbar DR, Greenhill SD, Hale VA, Sharman JL, Bonner TI, Catterall WA, Davenport AP, Delagrange P, Dollery CT, Foord SM, Gutman GA, Laudet V, Neubig RR, Ohlstein EH, Olsen RW, Peters J, Pin JP, Ruffolo RR, Searls DB, Wright MW and Spedding M. IUPHAR-DB: the IUPHAR database of G protein-coupled receptors and ion channels. *Nucleic acids research*. 2009;37:D680-5.

47. Chandler NJ, Greener ID, Tellez JO, Inada S, Musa H, Molenaar P, Difrancesco D, Baruscotti M, Longhi R, Anderson RH, Billeter R, Sharma V, Sigg DC, Boyett MR and Dobrzynski H. Molecular architecture of the human sinus node: insights into the function of the cardiac pacemaker. *Circulation*. 2009;119:1562-1575.

48. Hibino H, Inanobe A, Furutani K, Murakami S, Findlay I and Kurachi Y. Inwardly rectifying potassium channels: their structure, function, and physiological roles. *Physiol Rev*. 2010;90:291-366.

49. Irisawa H, Brown HF and Giles W. Cardiac pacemaking in the sino-atrial node. *Physiol Rev*. 1993;73:197-227.

50. Dobrzynski H, Boyett MR and Anderson RH. New insights into pacemaker activity: promoting understanding of sick sinus syndrome. *Circulation*. 2007;115:1921-32.

51. Dobrzynski H, Billeter R, Greener ID, Tellez JO, Chandler NJ, Flagg TP, Nichols CG, Lopatin AN and Boyett MR. Expression of $K_{ir}2.1$ and $K_{ir}6.2$ transgenes under the control of the alpha-MHC promoter in the sinoatrial and atrioventricular nodes in transgenic mice. *J Mol Cell Cardiol*. 2006;41:855-67.

52. Miake J, Marban E and Nuss HB. Biological pacemaker created by gene transfer. *Nature*. 2002;419:132-3.

53. Lei M HH, Kodama I, Boyett MR. Heterogeneous expression of the delayed-rectifier K^+ currents $I_{K,r}$ and $I_{K,s}$ in rabbit sinoatrial node cells. *J Physiol*. 2001;535:703-714.

54. Boyett MR, Honjo H and Kodama I. The sinoatrial node, a heterogeneous pacemaker structure. *Cardiovasc Res*. 2000;47:658-87.

55. Tellez JO, Dobrzynski H, Greener ID, Graham GM, Laing E, Honjo H, Hubbard SJ, Boyett MR and Billeter R. Differential expression of ion channel transcripts in atrial muscle and sinoatrial node in rabbit. *Circ Res*. 2006;99:1384-93.

56. Kodama I, Boyett MR, Nikmaram MR, Yamamoto M, Honjo H and Niwa R. Regional differences in effects of E-4031 within the sinoatrial node. *Am J Physiol*. 1999;276:H793-802.

57. Noble D and Tsien RW. The kinetics and rectifier properties of the slow potassium current in cardiac Purkinje fibres. *J Physiol*. 1968;195:185-214.

58. Cohen I, Daut J and Noble D. The effects of potassium and temperature on the pace-maker current, I_{K2}, in Purkinje fibres. *J Physiol*. 1976;260:55-74.

59. Brown HF, DiFrancesco D and Noble SJ. How does adrenaline accelerate the heart? *Nature*. 1979;280:235-6.

60. DiFrancesco D. A new interpretation of the pace-maker current in calf Purkinje fibres. *J Physiol*. 1981;314:359-76.

61. DiFrancesco D. The role of the funny current in pacemaker activity. *Circ Res*. 2009;106:434-446.

62. DiFrancesco D. Characterization of single pacemaker channels in cardiac sino-atrial node cells. *Nature*. 1986;324:470-3.

63. Robinson RB and Siegelbaum SA. Hyperpolarization-activated cation currents: from molecules to physiological function. *Annu Rev Physiol*. 2003;65:453-480.

64. Wainger BJ, DeGennaro M, Santoro B, Siegelbaum SA and Tibbs GR. Molecular mechanism of cAMP modulation of HCN pacemaker channels. *Nature*. 2001;411:805-10.

65. DiFrancesco D and Tortora P. Direct activation of cardiac pacemaker channels by intracellular cyclic AMP. *Nature*. 1991;351:145-7.

66. DiFrancesco D, Ducouret P and Robinson RB. Muscarinic modulation of cardiac rate at low acetylcholine concentrations. *Science*. 1989;243:669-71.

67. Yu H, Wu J, Potapova I, Wymore RT, Holmes B, Zuckerman J, Pan Z, Wang H, Shi W, Robinson RB, El-Maghrabi MR, Benjamin W, Dixon J, McKinnon D, Cohen IS and Wymore R. MinK-related peptide 1: A beta subunit for the HCN ion channel subunit family enhances expression and speeds activation. *Circ Res*. 2001;88:E84-7.

68. Barbuti A, Gravante B, Riolfo M, Milanesi R, Terragni B and DiFrancesco D. Localization of pacemaker channels in lipid rafts regulates channel kinetics. *Circ Res*. 2004;94:1325-31.

69. Barbuti A, Terragni B, Brioschi C and DiFrancesco D. Localization of f-channels to caveolae mediates specific beta2-adrenergic receptor modulation of rate in sinoatrial myocytes. *J Mol Cell Cardiol*. 2007;42:71-8.

70. Pian P, Bucchi A, Robinson RB and Siegelbaum SA. Regulation of gating and rundown of HCN hyperpolarization-activated channels by exogenous and endogenous PIP2. *J Gen Physiol*. 2006;128:593-604.

71. Poolos NP, Bullis JB and Roth MK. Modulation of h-channels in hippocampal pyramidal neurons by p38 mitogen-activated protein kinase. *The Journal of neuroscience : the official journal of the Society for Neuroscience*. 2006;26:7995-8003.

72. Zong X, Eckert C, Yuan H, Wahl-Schott C, Abicht H, Fang L, Li R, Mistrik P, Gerstner A, Much B, Baumann L, Michalakis S, Zeng R, Chen Z and Biel M. A novel mechanism of modulation of hyperpolarization-activated cyclic nucleotide-gated channels by Src kinase. *The Journal of biological chemistry*. 2005;280:34224-32.

73. Moosmang S, Stieber J, Zong X, Biel M, Hofmann F and Ludwig A. Cellular expression and functional characterization of four hyperpolarization-activated pacemaker channels in cardiac and neuronal tissues. *European journal of biochemistry / FEBS*. 2001;268:1646-52.

74. Shi W, Wymore R, Yu H, Wu J, Wymore RT, Pan Z, Robinson RB, Dixon JE, McKinnon D and Cohen IS. Distribution and prevalence of hyperpolarization-activated cation channel (HCN) mRNA expression in cardiac tissues. *Circ Res*. 1999;85:e1-6.

75. Chen S, Wang J and Siegelbaum SA. Properties of hyperpolarization-activated pacemaker current defined by coassembly of HCN1 and HCN2 subunits and basal modulation by cyclic nucleotide. *J Gen Physiol*. 2001;117:491-504.

76. Ulens C and Tytgat J. Functional heteromerization of HCN1 and HCN2 pacemaker channels. *The Journal of biological chemistry*. 2001;276:6069-72.

77. Brioschi C, Micheloni S, Tellez JO, Pisoni G, Longhi R, Moroni P, Billeter R, Barbuti A, Dobrzynski H, Boyett MR, DiFrancesco D and Baruscotti M. Distribution of the pacemaker HCN4 channel mRNA and protein in the rabbit sinoatrial node. *J Mol Cell Cardiol*. 2009;47:221-7.

78. Robinson RB, Yu H, Chang F and Cohen IS. Developmental change in the voltage-dependence of the pacemaker current, I_f, in rat ventricle cells. *Pflugers Archiv : European journal of physiology*. 1997;433:533-5.

79. Yasui K, Liu W, Opthof T, Kada K, Lee JK, Kamiya K and Kodama I. I_f current and spontaneous activity in mouse embryonic ventricular myocytes. *Circ Res*. 2001;88:536-42.

80. Cerbai E, Pino R, Sartiani L and Mugelli A. Influence of postnatal-development on I_f occurrence and properties in neonatal rat ventricular myocytes. *Cardiovasc Res*. 1999;42:416-23.

81. DiFrancesco D and Camm JA. Heart rate lowering by specific and selective I_f current inhibition with ivabradine: a new therapeutic perspective in cardiovascular disease. *Drugs*. 2004;64:1757-65.

82. Fox K, Ford I, Steg PG, Tendera M, Ferrari R and Investigators B. Ivabradine for patients with stable coronary artery disease and left-ventricular systolic dysfunction (BEAUTIFUL): a randomised, double-blind, placebo-controlled trial. *Lancet*. 2008;372:807-16.

83. Tardif JC, Ponikowski P, Kahan T and Investigators AS. Efficacy of the I_f current inhibitor ivabradine in patients with chronic stable angina receiving beta-blocker therapy: a 4-month, randomized, placebo-controlled trial. *Eur Heart J*. 2009;30:540-8.

84. Bucchi A, Baruscotti M and DiFrancesco D. Current-dependent block of rabbit sino-atrial node I_f channels by ivabradine. *J Gen Physiol*. 2002;120:1-13.

85. Schulze-Bahr E, Neu A, Friederich P, Kaupp UB, Breithardt G, Pongs O and Isbrandt D. Pacemaker channel dysfunction in a patient with sinus node disease. *The Journal of clinical investigation*. 2003;111:1537-45.

86. Milanesi R, Baruscotti M, Gnecchi-Ruscone T and DiFrancesco D. Familial sinus bradycardia associated with a mutation in the cardiac pacemaker channel. *The New England journal of medicine*. 2006;354:151-7.

87. Nof E, Luria D, Brass D, Marek D, Lahat H, Reznik-Wolf H, Pras E, Dascal N, Eldar M and Glikson M. Point mutation in the HCN4 cardiac ion channel pore affecting synthesis, trafficking, and functional expression is associated with familial asymptomatic sinus bradycardia. *Circulation*. 2007;116:463-70.

88. Hagiwara N, Irisawa H and Kameyama M. Contribution of two types of calcium currents to the pacemaker potentials of rabbit sino-atrial node cells. *J Physiol*. 1988;395:233-253.

89. Huser J, Blatter LA and Lipsius SL. Intracellular Ca^{2+} release contributes to automaticity in cat atrial pacemaker cells. *J Physiol*. 2000;524 Pt 2:415-22.

90. Lacinova L. Voltage-dependent calcium channels. *General physiology and biophysics*. 2005;24 Suppl 1:1-78.

91. Dolphin AC, Page KM, Berrow NS, Stephens GJ and Canti C. Dissection of the calcium channel domains responsible for modulation of neuronal voltage-dependent calcium channels by G proteins. *Annals of the New York Academy of Sciences*. 1999;868:160-74.

92. Staes M, Talavera K, Klugbauer N, Prenen J, Lacinova L, Droogmans G, Hofmann F and Nilius B. The amino side of the C-terminus determines fast inactivation of the T-type calcium channel alpha1G. *J Physiol*. 2001;530:35-45.

93. Ono K and Iijima T. Pathophysiological significance of T-type Ca^{2+} channels: properties and functional roles of T-type Ca^{2+} channels in cardiac pacemaking. *Journal of pharmacological sciences*. 2005;99:197-204.

94. Monfredi O, Maltsev VA and Lakatta EG. Modern concepts concerning the origin of the heartbeat. *Physiology*. 2013;28:74-92.

95. Morris GM. *Characterisation of subsidiary pacemaker tissue in an ex vivo model of sick sinus syndrome and its utility for biopacemaking*: Thesis: University of Manchester, UK; 2010.

96. Mangoni ME, Traboulsie A, Leoni AL, Couette B, Marger L, Le Quang K, Kupfer E, Cohen-Solal A, Vilar J, Shin HS, Escande D, Charpentier F, Nargeot J and Lory P. Bradycardia and slowing of the atrioventricular conduction in mice lacking $Ca_v3.1/\alpha_{1G}$ T-type calcium channels. *Circ Res*. 2006;98:1422-1430.

97. Fabiato A. Calcium-induced release of calcium from the cardiac sarcoplasmic reticulum. *Am J Physiol*. 1983;245:C1-14.

98. Bers DM. Cardiac excitation-contraction coupling. *Nature*. 2002;415:198-205.

99. Diaz ME, Trafford AW, O'Neill SC and Eisner DA. Measurement of sarcoplasmic reticulum Ca^{2+} content and sarcolemmal Ca^{2+} fluxes in isolated rat ventricular myocytes during spontaneous Ca^{2+} release. *J Physiol*. 1997;501 (Pt 1):3-16.

100. Bogdanov KY, Vinogradova TM and Lakatta EG. Sinoatrial nodal cell ryanodine receptor and Na^{+}-Ca^{2+} exchanger: molecular partners in pacemaker regulation. *Circ Res*. 2001;88:1254 -1258.

101. Rubenstein DS and Lipsius SL. Mechanisms of automaticity in subsidiary pacemakers from cat right atrium. *Circ Res*. 1989;64:648-57.

102. Cheng H, Lederer WJ and Cannell MB. Calcium sparks: elementary events underlying excitation-contraction coupling in heart muscle. *Science*. 1993;262:740-4.

103. Stern MD, Kort AA, Bhatnagar GM and Lakatta EG. Scattered-light intensity fluctuations in diastolic rat cardiac muscle caused by spontaneous Ca^{2+}-dependent cellular mechanical oscillations. *J Gen Physiol*. 1983;82:119-53.

104. Vinogradova TM, Lyashkov AE, Zhu W, Ruknudin AM, Sirenko S, Yang D, Deo S, Barlow M, Johnson S, Caffrey JL, Zhou YY, Xiao RP, Cheng H, Stern MD, Maltsev VA and Lakatta EG. High basal protein kinase A-dependent phosphorylation drives rhythmic internal Ca^{2+} store oscillations and spontaneous beating of cardiac pacemaker cells. *Circ Res*. 2006;98:505-14.

105. Ju YK and Allen DG. The distribution of calcium in toad cardiac pacemaker cells during spontaneous firing. *Pflugers Archiv : European journal of physiology*. 2000;441:219-27.

106. Vinogradova TM, Zhou YY, Maltsev V, Lyashkov A, Stern M and Lakatta EG. Rhythmic ryanodine receptor Ca^{2+} releases during diastolic depolarization of sinoatrial pacemaker cells do not require membrane depolarization. *Circ Res*. 2004;94:802-9.

107. Lyashkov AE JM, Dobrzynski H, Vinogradova TM, Maltsev VA, Juhasz O, Spurgeon HA, Sollott SJ, Lakatta EG. Calcium cycling protein density and functional importance to automaticity of isolated sinoatrial nodal cells are independent of cell size. *Circ Res*. 2007 100:1723-31.

108. Li J, Qu J and Nathan RD. Ionic basis of ryanodine's negative chronotropic effect on pacemaker cells isolated from the sinoatrial node. *Am J Physiol*. 1997;273:H2481-9.

109. Shigekawa M and Iwamoto T. Cardiac Na^{+}-Ca^{2+} exchange: molecular and pharmacological aspects. *Circ Res*. 2001;88:864-76.

110. Koushik SV, Wang J, Rogers R, Moskophidis D, Lambert NA, Creazzo TL and Conway SJ. Targeted inactivation of the sodium-calcium exchanger (Ncx1) results in the lack of a heartbeat and abnormal myofibrillar organization. *FASEB journal : official publication of the Federation of American Societies for Experimental Biology*. 2001;15:1209-11.

111. Groenke S, Larson ED, Zhang R, Nakano H, Jordan MC, Roos KP, Nakano A, Proenza C, Philipson KD and Goldhaber JI. The Na^{+}-Ca^{2+} exchanger is required for sinoatrial node pacemaker activity in murine myocardium. *Biophys J*. 2011;100:247a.

112. Groenke S, Larson ED, Nakano H, Nakano A, Proenza C, Philipson KD and Goldhaber JI. Atrial-specific NCX KO mice reveal dependence of sinoatrial node pacemaker activity on sodium-calcium exchange. *Biophys J* 2012;102:663a.

113. Vinogradova TM, Brochet DX, Sirenko S, Li Y, Spurgeon H and Lakatta EG. Sarcoplasmic reticulum Ca^{2+} pumping kinetics regulates timing of local Ca^{2+} releases and spontaneous beating rate of rabbit sinoatrial node pacemaker cells. *Circ Res*. 2010 107:767-75.

114. Zipes DP and Jalife J. *Cardiac Electrophysiology: From Cell to Bedside*: Saunders 5th Ed; 2009.

115. Rigg L and Terrar DA. Possible role of calcium release from the sarcoplasmic reticulum in pacemaking in guinea-pig sino-atrial node. *Exp Physiol*. 1996;81:877-80.

116. Beech DJ, Xu SZ, McHugh D and Flemming R. TRPC1 store-operated cationic channel subunit. *Cell Calcium*. 2003;33:433-440.

117. Ju YK, Chu Y, Chaulet H, Lai D, Gervasio OL, Graham RM, Cannell MB and Allen DG. Store-Operated Ca^{2+} Influx and Expression of TRPC Genes in Mouse Sinoatrial Node. *Circ Res*. 2007;100:1605-1614.

118. Sohl G and Willecke K. Gap junctions and the connexin protein family. *Cardiovasc Res*. 2004;62:228-32.

119. Laird DW. Life cycle of connexins in health and disease. *The Biochemical journal*. 2006;394:527-43.

120. Solan JL and Lampe PD. Connexin43 phosphorylation: structural changes and biological effects. *The Biochemical journal*. 2009;419:261-72.

121. Boyett MR, Inada S, Yoo S, Li J, Liu J, Tellez J, Greener ID, Honjo H, Billeter R, Lei M, Zhang H, Efimov IR and Dobrzynski H. Connexins in the sinoatrial and atrioventricular nodes. *Advances in cardiology*. 2006;42:175-97.

122. Yamamoto M, Honjo H, Niwa R and Kodama I. Low-frequency extracellular potentials recorded from the sinoatrial node. *Cardiovasc Res*. 1998;39:360-72.

123. Hagendorff A, Schumacher B, Kirchhoff S, Luderitz B and Willecke K. Conduction disturbances and increased atrial vulnerability in Connexin40-deficient mice analyzed by transesophageal stimulation. *Circulation*. 1999;99:1508-15.

124. Kirchhoff S, Kim JS, Hagendorff A, Thonnissen E, Kruger O, Lamers WH and Willecke K. Abnormal cardiac conduction and morphogenesis in connexin40 and connexin43 double-deficient mice. *Circ Res*. 2000;87:399-405.

125. Kirchhoff S, Nelles E, Hagendorff A, Kruger O, Traub O and Willecke K. Reduced cardiac conduction velocity and predisposition to arrhythmias in connexin40-deficient mice. *Current biology : CB*. 1998;8:299-302.

126. Abriel H and Kass RS. Regulation of the voltage-gated cardiac sodium channel $Na_v1.5$ by interacting proteins. *Trends in cardiovascular medicine*. 2005;15:35-40.

127. Maier SK, Westenbroek RE, Yamanushi TT, Dobrzynski H, Boyett MR, Catterall WA and Scheuer T. An unexpected requirement for brain-type sodium channels for control of heart rate in the mouse sinoatrial node. *Proceedings of the National Academy of Sciences of the United States of America*. 2003;100:3507-12.

128. Benson DW, Wang DW, Dyment M, Knilans TK, Fish FA, Strieper MJ, Rhodes TH and George AL, Jr. Congenital sick sinus syndrome caused by recessive mutations in the cardiac sodium channel gene (SCN5A). *The Journal of clinical investigation*. 2003;112:1019-28.

129. Lei M, Goddard C, Liu J, Leoni AL, Royer A, Fung SS, Xiao G, Ma A, Zhang H, Charpentier F, Vandenberg JI, Colledge WH, Grace AA and Huang CL. Sinus node dysfunction following targeted disruption of the murine cardiac sodium channel gene Scn5a. *J Physiol*. 2005;567:387-400.

130. Honjo H BM, Kodama I, Toyama J. Correlation between electrical activity and the size of rabbit sinoatrial node cells. *J Physiol*. 1996;496:795- 808.

131. Lei M, Jones SA, Liu J, Lancaster MK, Fung SS, Dobrzynski H, Camelliti P, Maier SK, Noble D and Boyett MR. Requirement of neuronal- and cardiac-type sodium channels for murine sinoatrial node pacemaking. *J Physiol*. 2004;559:835-48.

132. Mangoni ME, Couette B, Bourinet E, Platzer J, Reimer D, Striessnig J and Nargeot J. Functional role of L-type $Ca_v1.3$ Ca^{2+} channels in cardiac pacemaker activity. *Proceedings of the National Academy of Sciences of the United States of America*. 2003;100:5543-8.

133. Kodama I, Nikmaram MR, Boyett MR, Suzuki R, Honjo H and Owen JM. Regional differences in the role of the Ca^{2+} and Na^{+} currents in pacemaker activity in the sinoatrial node. *Am J Physiol*. 1997;272:H2793-806.

134. Platzer J, Engel J, Schrott-Fischer A, Stephan K, Bova S, Chen H, Zheng H and Striessnig J. Congenital deafness and sinoatrial node dysfunction in mice lacking class D L-type Ca^{2+} channels. *Cell*. 2000;102:89-97.

135. Dobrzynski H, Anderson RH, Atkinson A, Borbas Z, D'Souza A, Fraser JF, Inada S, Logantha SJ, Monfredi O, Morris GM, Moorman AF, Nikolaidou T, Schneider H, Szuts V, Temple IP, Yanni J and Boyett MR. Structure, function and clinical relevance of the cardiac conduction system, including the atrioventricular ring and outflow tract tissues. *Pharmacol Ther*. 2013;139:260-88.

136. Boineau JP, Canavan TE, Schuessler RB, Cain ME, Corr PB and Cox JL. Demonstration of a widely distributed atrial pacemaker complex in the human heart. *Circulation*. 1988;77:1221-37.

137. Matsuo S, Yamane T, Date T and Yoshimura M. Spontaneously isolated sinus node activation in sick sinus syndrome as revealed by a three-dimensional mapping system. *Heart Rhythm*. 2010 7:856-7.

138. Jones SB, Euler DE, Hardie E, Randall WC and Brynjolfsson G. Comparison of SA nodal and subsidiary atrial pacemaker function and location in the dog. *Am J Physiol*. 1978;234:H471-6.

139. Rozanski GJ and Lipsius SL. Electrophysiology of functional subsidiary pacemakers in canine right atrium. *Am J Physiol*. 1985;249:H594-603.

140. Rubenstein DS, Fox LM, McNulty JA and Lipsius SL. Electrophysiology and ultrastructure of eustachian ridge from cat right atrium: a comparison with SA node. *J Mol Cell Cardiol*. 1987;19:965-76.

141. Yanni J, Boyett MR, Anderson RH and Dobrzynski H. The extent of the specialized atrioventricular ring tissues. *Heart Rhythm*. 2009a;6:672-680.

142. Kistler PM, Sanders P, Fynn SP, Stevenson IH, Hussin A, Vohra JK, Sparks PB and Kalman JM. Electrophysiological and electrocardiographic characteristics of focal atrial tachycardia originating from the pulmonary veins: acute and long-term outcomes of radiofrequency ablation. *Circulation*. 2003;108:1968-1975.

143. Hillock RJ, Singarayar S, Kalman JM and Sparks PB. Tale of two tails: The tip of the atrial appendages is an unusual site for focal atrial tachycardia. *Heart Rhythm*. 2006;3:467-469.

144. Marrouche NF, SippensGroenewegen A, Yang Y, Dibs S and Scheinman MM. Clinical and electrophysiologic characteristics of left septal atrial tachycardia. *Journal of the American College of Cardiology*. 2002;40:1133-1139.

145. Nakahara S, Seino M, Sakai Y and Takayanagi K. A unique iatrogenic organized left atrial tachycardia with a gap conduction in previously ablated lesions. *Journal of Cardiology*. 2010;55:139-142.

146. Kistler PM, Sanders P, Hussin A, Morton JB, Vohra JK, Sparks PB and Kalman JM. Focal atrial tachycardia arising from the mitral annulus: electrocardiographic and electrophysiologic characterization. *J Am Coll Cardiol*. 2003;41:2212-2219.

147. Kistler PM, Fynn SP, Haqqani H, Stevenson IH, Vohra JK, Morton JB, Sparks PB and Kalman JM. Focal atrial tachycardia from the ostium of the coronary sinus: electrocardiographic and electrophysiological characterization and radiofrequency ablation. *J Am Coll Cardiol*. 2005;45:1488-1493.

148. Kalman JM, Olgin JE, Karch MR, Hamdan M, Lee RJ and Lesh MD. "Cristal tachycardias": origin of right atrial tachycardias from the crista terminalis identified by intracardiac echocardiography. *J Am Coll Cardiol*. 1998;31:451-459.

149. Rozanski GJ, Lipsius SL and Randall WC. Functional characteristics of sinoatrial and subsidiary pacemaker activity in the canine right atrium. *Circulation*. 1983;67:1378-87.

150. Bassani RA, Bassani JW, Lipsius SL and Bers DM. Diastolic SR Ca efflux in atrial pacemaker cells and Ca-overloaded myocytes. *Am J Physiol*. 1997;273:H886-92.

151. Zhou Z and Lipsius SL. Na^{+}-Ca^{2+} exchange current in latent pacemaker cells isolated from cat right atrium. *J Physiol*. 1993;466:263-85.

152. Morris GM, D'Souza A, Dobrzynski H, Lei M, Choudhury M, Billeter R, Kryukova Y, Robinson RB, Kingston PA and Boyett MR. Characterization of a right atrial subsidiary pacemaker and acceleration of the pacing rate by HCN over-expression. *Cardiovasc Res*. 2013; 100:160-9.

153. Zhou Z and Lipsius SL. Properties of the pacemaker current I_f in latent pacemaker cells isolated from cat right atrium. *J Physiol*. 1992;453:503-23.

154. Sodeck GH, Domanovits H, MeronG, Rauscha F, Losert H, Thalmann M, Vlcek M and Laggner AN. Compromising bradycardia: management in the emergency department. *Resuscitation* 2007;73:96-102.

155. Thery C, Gosselin B, Lekieffre J and Warembourg H. Pathology of sinoatrial node. Correlations with electrocardiographic findings in 111 patients. *Am Heart J*. 1977;93:735-40.

156. Evans R and Shaw D. Pathological studies in sinoatrial disorder (sick sinus syndrome). *Br Heart J*. 1977;39:778-786.

157. Morris GM and Kalman JM. Fibrosis, electrics and genetics. Perspectives in sinoatrial node disease. *Circ J*. 2014;78:1272-82.

158. Guidelines for clinical intracardiac electrophysiologic studies. A report of the American College of Cardiology/American Heart Association Task Force on Assessment of Diagnostic and Therapeutic Cardiovascular Procedures (Subcommittee to Assess Clinical Intracardiac Electrophysiologic Studies). *J Am Coll Cardiol*. 14:182 -1842.

159. Alboni P, Malcarne C, Pedroni P, Masoni A and Narula OS. Electrophysiology of normal sinus node with and without autonomic blockade. *Circulation*. 1982;65:1236-42.

160. Sanders P, Morton JB, Kistler PM, Spence SJ, Davidson NC, Hussin A, Vohra JK, Sparks PB and Kalman JM. Electrophysiological and electroanatomic characterization of the atria in sinus node disease: evidence of diffuse atrial remodeling. *Circulation*. 2004;109:1514-22.

161. Lamas GA, Lee K, Sweeney M, Leon A, Yee R, Ellenbogen K, Greer S, Wilber D, Silverman R, Marinchak R, Bernstein R, Mittleman RS, Lieberman EH, Sullivan C, Zorn L, Flaker G, Schron E, Orav EJ and Goldman L. The mode selection trial (MOST) in sinus node dysfunction: Design, rationale, and baseline characteristics of the first 1000 patients. *Am Heart J*. 2000;140:541 - 551.

162. I Shiraishi, T Takamatsu, T Minamikawa, Z Onouchi and S Fujita. Quantitative histological analysis of the human sinoatrial node during growth and aging. *Circulation* 1992;85:2176-2184.

163. Lei M, Zhang H, Grace AA and Huang CL. SCN5A and sinoatrial node pacemaker function. *Cardiovasc Res*. 2007 74:356-65.

164. Yanni J, Tellez JO, Sutyagin PV, Boyett MR and Dobrzynski H. Structural remodelling of the sinoatrial node in obese old rats. *J Mol Cell Cardiol*. 2010;48:653-662.

165. Jones SA, Lancaster MK and Boyett MR. Ageing-related changes of connexins and conduction within the sinoatrial node. *J Physiol*. 2004;560:429-437.

166. Jones SA, Boyett MR and Lancaster MK. Declining into failure: the age-dependent loss of the L-type calcium channel within the sinoatrial node. *Circulation*. 2007;115:1183-1190.

167. Tellez JO, Mczewski M, Yanni J, Sutyagin P, Mackiewicz U, Atkinson A, Inada S, Beresewicz A, Billeter R, Dobrzynski H and Boyett MR. Ageing-dependent remodelling of ion channel and Ca^{2+} clock genes underlying sino-atrial node pacemaking. *Exp Physiol*. 2011;96:1163-78.

168. Hao X, Zhang Y, Zhang X, Nirmalan M, Davies L, Konstantinou D, Yin F, Dobrzynski H, Wang X, Grace A, Zhang H, Boyett M, Huang CL and Lei M. TGF-β1-mediated fibrosis and ion channel remodeling are key mechanisms in producing the sinus node dysfunction associated with SCN5A deficiency and aging. *Circ Arrhythm Electrophysiol*. 2011;4:397-406.

169. Yeh YH, Burstein B, Qi XY, Sakabe M, Chartier D, Comtois P, Wang Z, Kuo CT and Nattel S. Funny current downregulation and sinus node dysfunction associated with atrial tachyarrhythmia: a molecular basis for tachycardia-bradycardia syndrome. *Circulation*. 2009;119:1576-85. .

170. Duhme N, Schweizer PA, Thomas D, Becker R, Schröter J, Barends TR, Schlichting I, Draguhn A, Bruehl C, Katus HA and Koenen M. Altered HCN4 channel C-linker interaction is associated with familial tachycardia-bradycardia syndrome and atrial fibrillation. *Eur Heart J*. 2013;34:2768-75.

171. Laish-Farkash A, Glikson M, Brass D, Marek-Yagel D, Pras E, Dascal N, Antzelevitch C, Nof E, Reznik H, Eldar M and Luria D. A novel mutation in the HCN4 gene causes symptomatic sinus bradycardia in Moroccan Jews. *Journal of cardiovascular electrophysiology*. 2010;21:1365-72. .

172. Ruan Y, Liu N and Priori SG. Sodium channel mutations and arrhythmias. *Nat Rev Cardiol*. 2009;6:337-48.

173. Postma AV, Denjoy I, Kamblock J, Alders M, Lupoglazoff JM, Vaksmann G, Dubosq-Bidot L, Sebillon P, Mannens MM, Guicheney P and Wilde AA. Catecholaminergic polymorphic ventricular tachycardia: RYR2 mutations, bradycardia, and follow up of the patients. *J Med Genet*. 2005;42:863-70.

174. Postma AV, Denjoy I, Hoorntje TM, Lupoglazoff JM, Da Costa A, Sebillon P, Mannens MM, Wilde AA and Guicheney P. Absence of calsequestrin 2 causes severe forms of catecholaminergic polymorphic ventricular tachycardia. *Circ Res*. 2002;91:e21-6.

175. Le Scouarnec S, Bhasin N, Vieyres C, Hund TJ, Cunha SR, Koval O, Marionneau C, Chen B, Wu Y, Demolombe S, Song L, Le Marec H, Probst V, Schott J, Anderson ME and Mohler PJ. Dysfunction in ankyrin-B-dependent ion channel and transporter targeting causes human sinus node disease. *Proceedings of the National Academy of Sciences of the United States of America*. 2008;105:15617 - 15622.

176. D'Souza A, Bucchi A, Johnsen AB, Logantha SJ, Monfredi O, Yanni J, Prehar S, Hart G, Cartwright E, Wisloff U, Dobryznski H, DiFrancesco D, Morris GM and Boyett MR. Exercise training reduces resting heart rate via downregulation of the funny channel HCN4. *Nat Commun*. 2014;13:3775.

177. Zicha S, Fernandez-Velasco M, Lonardo G, L'Heureux N and Nattel S. Sinus node dysfunction and hyperpolarization-activated (HCN) channel subunit remodeling in a canine heart failure model. *Cardiovasc Res*. 2005;66:472 - 481.

178. Choudhury M, Boyett MR and Morris GM. Biology of the Sinus Node and its Disease. *Arrhythmia & Electrophysiology Review*. 2015;4:28–34.

179. Manios EG, Kanoupakis EM, Mavrakis HE, Kallergis EM, Dermitzaki DN and Vardas PE. Sinus pacemaker function after cardioversion of chronic atrial fibrillation: is sinus node remodeling related with recurrence? *Journal of cardiovascular electrophysiology*. 2001;12:800-6.

180. Park J, Shim J, Uhm JS, Joung B, Lee MH and Pak HN. Post-shock sinus node recovery time is an independent predictor of recurrence after catheter ablation of longstanding persistent atrial fibrillation. *Int J Cardiol*. 2013;168:1937-42.

181. Sparks PB, Jayaprakash S, Vohra JK and Kalman JM. Electrical remodeling of the atria associated with paroxysmal and chronic atrial flutter. *Circulation*. 2000;102:1807 - 1813.

182. Elvan A, Wylie K and Zipes DP. Pacing-induced chronic atrial fibrillation impairs sinus node function in dogs: Electrophysiological remodeling. *Circulation*. 1996;94:2953 - 2960.

183. Butters TD, Aslanidi OV, Inada S, Boyett MR, Hancox JC, Lei M and Zhang H. Mechanistic links between Na^+ channel (SCN5A) mutations and impaired cardiac pacemaking in sick sinus syndrome. *Circ Res*. 2010 107:126-37. .

184. Mohler PJ, Splawski I, Napolitano C, Bottelli G, Sharpe L, Timothy K, Priori SG, Keating MT and Bennett V. A cardiac arrhythmia syndrome caused by loss of ankyrin-B function. *Proceedings of the National Academy of Sciences of the United States of America*. 2004;101:9137-42.

185. Baldesberger S, Bauersfeld U, Candinas R, Seifert B, Zuber M, Ritter M, Jenni R, Oechslin E, Luthi P, Scharf C, Marti B and Attenhofer Jost CH. Sinus node disease and arrhythmias in the long-term follow-up of former professional cyclists. *Eur Heart J*. 2008;29:71-8.

186. Mont L, Sambola A, Brugada J, Vacca M, Marrugat J, Elosua R, Pare C, Azqueta M and Sanz G. Long-lasting sport practice and lone atrial fibrillation. *Eur Heart J*. 2002;23:477-82.

187. Boyett MR, D'Souza A, Zhang H, Morris GM, Dobrzynski H and Monfredi O. Viewpoint: is the resting bradycardia in athletes the result of remodeling of the sinoatrial node rather than high vagal tone? *J Appl Physiol*. 1985;114:1351-5. .

188. Rokseth R and Hatle L. Sinus arrest in acute myocardial infarction. *Br Heart J*. 1971;33:639-642.

189. Ando' G, Gaspardone A and Proietti I. Acute thrombosis of the sinus node artery: arrhythmological implications. *Heart Rhythm*. 2003;89:E5.

190. Shaw DB, Linker NJ, Heaver PA and Evans R. Chronic sinoatrial disorder (sick sinus syndrome): a possible result of cardiac ischaemia. *Br Heart J*. 1987;58:598-607.

191. Alboni P, Baggioni GF, Scarfò S, Cappato R, Percoco GF, Paparella N and Antonioli GE. Role of sinus node artery disease in sick sinus syndrome in inferior wall acute myocardial infarction. *Am J Cardiol*. 1991;67:1180-4.

192. Engel TR, Meister SG, Feitosa GS, Fischer HA and Frankl WS. Appraisal of sinus node artery disease. *Circulation*. 1975;52:286-91.

193. Edelberg JM, Aird WC and Rosenberg RD. Enhancement of murine cardiac chronotropy by the molecular transfer of the human beta2 adrenergic receptor cDNA. *The Journal of clinical investigation*. 1998;101:337-43.

194. Edelberg JM, Huang DT, Josephson ME and Rosenberg RD. Molecular enhancement of porcine cardiac chronotropy. *Heart (British Cardiac Society)*. 2001;86:559-62.

195. Gorecki DC. "Dressed-up" naked plasmids: emerging vectors for non-viral gene therapy. *Discovery medicine*. 2006;6:191-7.

196. Miake J, Marban E and Nuss HB. Functional role of inward rectifier current in heart probed by $K_{ir}2.1$ overexpression and dominant-negative suppression. *The Journal of clinical investigation*. 2003;111:1529-36.

197. Qu J, Barbuti A, Protas L, Santoro B, Cohen IS and Robinson RB. HCN2 overexpression in newborn and adult ventricular myocytes: distinct effects on gating and excitability. *Circ Res*. 2001;89:E8-14.

198. Qu J, Plotnikov AN, Danilo P, Jr., Shlapakova I, Cohen IS, Robinson RB and Rosen MR. Expression and function of a biological pacemaker in canine heart. *Circulation*. 2003;107:1106-9.

199. Plotnikov AN, Sosunov EA, Qu J, Shlapakova IN, Anyukhovsky EP, Liu L, Janse MJ, Brink PR, Cohen IS, Robinson RB, Danilo P Jr and Rosen MR. Biological pacemaker implanted in canine left bundle branch provides ventricular escape rhythms that have physiologically acceptable rates. *Circulation*. 2004;109:506-12.

200. Plotnikov AN, Bucchi A, Shlapakova I, Danilo P, Jr., Brink PR, Robinson RB, Cohen IS and Rosen MR. HCN212-channel biological pacemakers manifesting ventricular tachyarrhythmias are responsive to treatment with I_f blockade. *Heart Rhythm*. 2008;5:282-8.

201. Boink GJ, Nearing BD, Shlapakova IN, Duan L, Kryukova Y, Bobkov Y, Tan HL, Cohen IS, Danilo P Jr, Robinson RB, Verrier RL and Rosen MR. Ca^{2+}-stimulated adenylyl cyclase AC1 generates efficient biological pacing as single gene therapy and in combination with HCN2 *Circulation*. 2012 126:528-36.

202. Boink GJJ, Duan L, Nearing BD, Shlapakova IN, Sosunov EA, Anyukhovsky EP, Bobkov E, Kryukova Y, Ozgen N, Danilo Jr. P, Cohen IS, Verrier RL, Robinson RB and Rosen MR. HCN2/SkM1 gene transfer into canine left bundle branch induces stable, autonomically responsive biological pacing at physiological heart rates. *J Am Coll Cardiol*. 2013;61:1192–1201.

203. Kapoor N, Liang W, Marbán E and Cho HC. Direct conversion of quiescent cardiomyocytes to pacemaker cells by expression of Tbx18. *Nature biotechnology*. 2013;31:54-62.

204. Hu YF, Dawkins JF, Cho HC, Marbán E and Cingolani E. Biological pacemaker created by minimally invasive somatic reprogramming in pigs with complete heart block. *Sci Transl Med*. 2014;6:245ra94.

205. Bakker ML, Boink GJ, Boukens BJ, Verkerk AO, van den Boogaard M, den Haan AD, Hoogaars WM, Buermans HP, de Bakker JM, Seppen J, Tan HL, Moorman AF, 't Hoen PA and Christoffels VM. T-box transcription factor TBX3 reprogrammes mature cardiac myocytes into pacemaker-like cells. *Cardiovasc Res*. 2012;94:439-49.

206. Kehat I, Khimovich L, Caspi O, Gepstein A, Shofti R, Arbel G, Huber I, Satin J, Itskovitz-Eldor J and Gepstein L. Electromechanical integration of cardiomyocytes derived from human embryonic stem cells. *Nature biotechnology*. 2004;22:1282-9.

207. Satin J, Kehat I, Caspi O, Huber I, Arbel G, Itzhaki I, Magyar J, Schroder EA, Perlman I and Gepstein L. Mechanism of spontaneous excitability in human embryonic stem cell derived cardiomyocytes. *J Physiol*. 2004;559:479-96.

208. Cai J, Lin G, Jiang H, Yang B, Jiang X, Yu Q and Song J. Transplanted neonatal cardiomyocytes as a potential biological pacemaker in pigs with complete atrioventricular block. *Transplantation*. 2006 81:1022-6.

209. Lin G, Cai J, Jiang H, Shen H, Jiang X, Yu Q and Song J. Biological pacemaker created by fetal cardiomyocyte transplantation. *Journal of biomedical science*. 2005;12:513-9.

210. Ruhparwar A, Tebbenjohanns J, Niehaus M, Mengel M, Irtel T, Kofidis T, Pichlmaier AM and Haverich A. Transplanted fetal cardiomyocytes as cardiac pacemaker. *European journal of cardio-thoracic surgery : official journal of the European Association for Cardio-thoracic Surgery*. 2002;21:853-7.

211. Cho HC, Kashiwakura Y and Marbán E. Creation of a biological pacemaker by cell fusion. *Circ Res*. 2007;100:1112-5.

212. Plotnikov AN, Shlapakova I, Szabolcs MJ, Danilo P Jr, Lorell BH, Potapova IA, Lu Z, Rosen AB, Mathias RT, Brink PR, Robinson RB, Cohen IS and Rosen MR. Xenografted adult human mesenchymal stem cells provide a platform for sustained biological pacemaker function in canine heart. . *Circulation*. 2007 116:706-13.

213. Takahashi K and Yamanaka S. Induction of pluripotent stem cells from mouse embryonic and adult fibroblast cultures by defined factors. *Cell*. 2006;126:663-76.

214. Mandel Y, Weissman A, Schick R, Barad L, Novak A, Meiry G, Goldberg S, Lorber A, Rosen MR, Itskovitz-Eldor J and Binah O. Human embryonic and induced pluripotent stem cell-derived cardiomyocytes exhibit beat rate variability and power-law behavior. *Circulation*. 2012;125:883-93.

215. Chauveau S, Anyukhovsky Y, Potapova I, Binah O, Itskovitz-Eldor J, Naor S, Rahim T, Jiang Y, Danilo P and Cohen IS. Keratinocyte-derived cardiomyocytes provide in vivo biological pacemaker function. *European Heart Journal*. 2014;35:105.

216. Zhang H, David HL, Shlapakova I, Zhao X, Danilo P J, Robinson RB, Cohen IS, Qu D, Xu Z and Rosen MR. Implantation of sionatrial node cells into canine right ventricle: Biological pacing appears limited by the substrate *Cell Transplant*. 2011 20:1907-14.

217. Boyett MR and Fedida D. Changes in the electrical activity of dog cardiac Purkinje fibres at high heart rates. *J Physiol*. 1984;350:361-391.

218. Limberis MP. Phoenix rising: gene therapy makes a comeback. *Acta Biochim Biophys Sin*. 2012;44:632–640.

219. Animals (Scientific Procedures) Act 1986.Available at: http://www.legislation.gov.uk/ukpga/1986/14/contents.

220. Vorburger SA and Hunt KK. Adenoviral gene therapy. *Oncologist*. 2002;7:46-59.

221. Yamada K, Morishita N, Katsuda T, Kubo S, Gotoh A and Yamaji H. Adenovirus vector production using low-multiplicity infection of 293 cells. *Cytotechnology*. 2009;59:153-60.

222. Hofacre A, Wodarz D, Komarova NL and Fan H. Early infection and spread of a conditionally replicating adenovirus under conditions of plaque formation. *Virology*. 2012;423:89-96.

223. Zhang M, Zhang X, Han Z, Chen X, Yang L, Sheng Y and Wen J. Construction of a novel oncolytic adenoviral vector and its biological characteristics. *Oncol Rep*. 2013;29:798-804.

224. Bassani JW, Godoy CM and Bassani RA. Effect of ryanodine on sinus node recovery time determined in vitro. *Braz J Med Biol Res*. 1999;32:1039-43.

225. de Magalhaes Galvao K and de Godoy CM. A new strategy for direct measurement of sinus atrial conduction time by sinus node threshold determination in a rat-isolated atrium. *Physiol Meas*. 2007;28:105-15.

226. Atkinson AJ, Logantha SJ, Hao G, Yanni J, Fedorenko O, Sinha A, Gilbert SH, Benson AP, Buckley DL, Anderson RH, Boyett MR and Dobrzynski H. Functional, anatomical, and molecular investigation of the cardiac conduction system and

arrhythmogenic atrioventricular ring tissue in the rat heart. *J Am Heart Assoc*. 2013;2:e000246.

227. Borbas Z, Saeed Y, Caldwell J, Jawad F, Vohra A, Hoschtitzky A, Boyett M, Garratt C and Dobrzynski H. Novel Immunohistochemical and Structural Features of Subsidiary Atrial Pacemakers in the Goat; Relevance to Potential Sites for Biological Pacemakers. *Heart (British Cardiac Society)*. 2014;100:A92-A93.

228. Qu J, Altomare C, Bucchi A, DiFrancesco D and Robinson RB. Functional comparison of HCN isoforms expressed in ventricular and HEK 293 cells. *Pflugers Archiv : European journal of physiology*. 2002;444:597-601.

229. Watanabe EI, Honjo H, Boyett MR, Kodama I and Toyama J. Inactivation of the calcium current is involved in overdrive suppression of rabbit sinoatrial node cells. *Am J Physiol*. 1996;271:H2097-107.

230. Musso E and Vassalle M. The role of calcium in overdrive suppression of canine cardiac Purkinje fibers. *Circ Res*. 1982;51:167-80.

231. DiFrancesco D. Block and activation of the pace-maker channel in calf purkinje fibres: effects of potassium, caesium and rubidium. *J Physiol*. 1982;329:485-507.

232. Goldoni D, Zhao Y, Green BD, McDermott BJ and Collins A. Inward rectifier potassium channels in the HL-1 cardiomyocyte-derived cell line. *J Cell Physiol*. 2010;225:751-6.

233. Meier CF, Jr. and Katzung BG. Cesium blockade of delayed outward currents and electrically induced pacemaker activity in mammalian ventricular myocardium. *J Gen Physiol*. 1981;77:531-47.

234. Cho HC. Pacing the Heart with Genes: Recent Progress in Biological Pacing. *Curr Cardiol Rep*. 2015;17:65.

235. Boink GJ, Christoffels VM, Robinson RB and Tan HL. The past, present, and future of pacemaker therapies. *Trends in cardiovascular medicine*. 2015;25:661-73.

236. Wang J, Gao E, Chan TO, Zhang XQ, Song J, Shang X, Koch WJ, Feldman AM and Cheung JY. Induced overexpression of Na^+/Ca^{2+} exchanger does not aggravate myocardial dysfunction induced by transverse aortic constriction. *J Card Fail*. 2013;19:60-70.

237. Greensmith DJ, Galli GL, Trafford AW and Eisner DA. Direct measurements of SR free Ca reveal the mechanism underlying the transient effects of RyR potentiation under physiological conditions. *Cardiovasc Res*. 2014;103:554-63.

238. Bustin SA, Benes V, Garson JA, Hellemans J, Huggett J, Kubista M, Mueller R, Nolan T, Pfaffl MW, Shipley GL, Vandesompele J and Wittwer CT. The MIQE

guidelines: minimum information for publication of quantitative real-time PCR experiments. *Clin Chem*. 2009;55:611-22.

239. Adelman WJ, Jr. and French RJ. Blocking of the squid axon potassium channel by external caesium ions. *J Physiol*. 1978;276:13-25.

240. Melgari D, Brack KE, Zhang C, Zhang Y, El Harchi A, Mitcheson JS, Dempsey CE, Ng GA and Hancox JC. hERG potassium channel blockade by the HCN channel inhibitor bradycardic agent ivabradine. *J Am Heart Assoc*. 2015;4.

241. Daya S and Berns KI. Gene therapy using adeno-associated virus vectors. *Clin Microbiol Rev*. 2008;21:583-93.

242. Escors D and Breckpot K. Lentiviral vectors in gene therapy: their current status and future potential. *Arch Immunol Ther Exp (Warsz)*. 2010;58:107-19.